Control and optimization of ecosystems in bioreactors for bioenergy production

Pierre Masci

PhD THESIS

prepared at

INRIA Sophia Antipolis, COMORE team

and presented at the

UNIVERSITY OF NICE-SOPHIA ANTIPOLIS
Graduate School of Information and Communication Sciences

A dissertation submitted in partial fulfillment
of the requirements for the degree of

DOCTOR OF SCIENCE

Specialized in Control, Signal and Image Processing

Control and optimization of ecosystems in bioreactors for bioenergy production

Pierre MASCI

Thesis prepared in the COMORE team, INRIA Sophia Antipolis.
Directed by Olivier BERNARD and co-supervised by Frédéric GROGNARD

defended on the 9th of *Novembre 2010*

Jury :

M. Olivier BERNARD	DR, INRIA Sophia	Advisor
M. Alain VANDE WOUWER	Pr., Université de Mons	Reviewer
M. Frédéric MAZENC	CR, INRIA Saclay	Reviewer
M. Gonzalo ROBLEDO	Assistant Pr., Univ. de Chile	Examiner
M. Jean-Christophe POGGIALE	Pr., Université Aix-Marseille II	Examiner
M. Gaël BOUGARAN	CR, IFREMER Nantes	Examiner
Invited member : M. Frédéric GROGNARD	CR, INRIA Sophia	Advisor

UNIVERSITE DE NICE-SOPHIA ANTIPOLIS

ECOLE DOCTORALE STIC
SCIENCES ET TECHNOLOGIES DE L'INFORMATION ET DE LA COMMUNICATION

T H E S E

pour obtenir le titre de

Docteur en Sciences

de l'Université de Nice-Sophia Antipolis

Discipline: Automatique, Traitement du Signal et des Images

présentée et soutenue par

Pierre MASCI

Contrôle et optimisation d'écosystèmes en bioréacteurs pour la production de bioénergie

Thèse dirigée par O*livier BERNARD, co-supervisée par Frédéric GROGNARD*
et pr*éparée à l'INRIA Sophia-Antipolis, projet COMORE*

soutenue le 9 *Novembre 2010*

Jury :

M. Olivier BERNARD	DR, INRIA Sophia	Directeur
M. Alain VANDE WOUWER	Pr., Université de Mons	Rapporteur
M. Frédéric MAZENC	CR, INRIA Saclay	Rapporteur
M. Gonzalo ROBLEDO	Assistant Pr., Univ. de Chile	Examinateur
M. Jean-Christophe POGGIALE	Pr., Université Aix-Marseille II	Examinateur
M. Gaël BOUGARAN	CR, IFREMER Nantes	Examinateur
Invited member: M. Frédéric GROGNARD	CR, INRIA Sophia	Directeur

Contents

Thank you

Thank you to my two PhD supervisors, Olivier Bernard and Frédéric Grognard for being able to stay positive and constructive, and to listen to my hopes and pains all along these three years. I hope I brought you more happiness than pain in this adventure. Most of the work presented here was built by the complex and dynamical symbiose between the three of us, sometimes including more people. This symbiose was not modelled nor optimized rigourously during the thesis, but we kind of tried...

Thank you Jean-Luc Gouze for insightful scientific discussions, and without who I probably wouldn't have finished this thesis. Thank you Maryze Renaud and Thierry Vieville for that too, and for listening to me when it was just crucial.

Thank you to the jury members for their presence and encouraging remarks on my PhD defense day.

Thank you Éric Benoît, Francis Mairet, Andrei Akhmetzhanov, Antoine Sciandra, Thomas Lacour, Amélie Gelay, Mariem Mojaat Guemir, Bruno Sialve, Ludovic Mailleret, Jean-Phi Steyer, Eric Latrille, Jean-Baptiste Sorba, Serena Esposito, Christophe Mocquet, all the joyeux Nantais and other Shamashians for fructuous scientific discussions and research in common, often mixed with more general thoughts about life. And for all the people in Villefranche-sur-Mer who made the experiments possible.

Thanks again Tomtom for those interesting ethical and political discussions. Hope we'll have some of these again! And for letting me sleep in your couch several times, too.

Thank you Stephanie Sorres for always being here and ready for everything, let it be a need to speak about life or laugh, boring administrativities, or cooking some good good stuff (miam miam !!).

Thanks to all the COMORE team: I had some good time with you, good persons you are!

Thanks Sapnette for everyday mutual joy and support =o) Thanks Seb, Jeff and Cali for that too!

Thanks to my precious mum for reading and correcting this thesis, you have eagle eyes!

Thank you Daria, Cloé, Julia, Jenny and my maman-Romain for supporting my complains about everyday pains, and bringing some courage and hapinness on the way.

Merci merci merci aux Rikikibians (je vais pas commencer à vous lister les copains, vous êtes trop...et trop bons. Et puis vous avez transformé ma vie), Amarinians, Flayoscians, EdlNians, Sanghasians, Parizians (chabi, chabidhou et chabichette), Dolinians et les autres (Antibians, Nicians, ...), et tous les amis pour toujours être dans le coin quand j'ai besoin de vous...

... et à mes Sarlotteuh maman & Roberto & Edoudou et Patriste papa & Annie depuis bien plus longtemps encore.

Merci maman-Fernande et Georges-Tutur pour ça aussi: vous êtes jamais loin, vous, on dirait.

Bon courage et bon délire aux nouveaux venus! Kowanee, CharlèneJeremours, TildouSamours, PacoMamarinous et les autres à venir... Quel monde et quels coeurs vous laissera-t-on à notre tour?

Résumé

Des biocarburants alternatifs, utilisant des écosystèmes microbiens, sont actuellement étudiés dans le but de limiter la consommation non raisonnée de ressources énergétiques et le rejet de gaz à effet de serre, qui modifient le climat. Dans cette thèse, nous avons considéré des bioréacteurs à base de microalgues oléagineuses, et des écosystèmes bactériens anaérobies qui décomposent des déchets et produisent du méthane. Ces travaux avaient pour objectif de mieux comprendre ces procédés et d'en améliorer les performances. Nous avons tout d'abord modélisé et étudié des cultures de microalgues en photobioréacteurs, dans lesquels les pigments algaux induisent une forte atténuation lumineuse. Pour les écosystèmes bactériens, nous avons utilisé un modèle précédemment développé. A l'aide de ces modèles et de leur analyse mathématique rigoureuse, nous avons proposé des stratégies pour optimiser leur productivité. Ensuite, l'étude de la sélection naturelle entre plusieurs espèces de microorganismes dans ces deux écosystèmes a permis de prédire quelles espèces remportent la compétition. Et finalement nous avons montré comment il est possible, dans chaque écosystème, de contrôler la compétition pour diriger la sélection naturelle, de façon à avantager des espèces améliorant les performances du procédé.

Abstract

Some alternative biofuels, produced by microbial ecosystems, are presently studied with the aim of limiting the unreasoned resource consumption of energetic resources, and greenhouse gases emissions which modify the climate. In this thesis we have considered bioreactors based on oleaginous microalgae, and on anaerobic bacterial ecosystems which degrade wastes and produce methane. The aims of these works were to better understand these processes and to improve their performances. First we have developed and studied models of microalgal cultures in photobioreactors, in which algal pigments cause strong light attenuation. For anaerobic digestion we have used an existing model. By rigorous mathematical analysis of these models, we propose strategies for optimizing their productivity. Then the study of natural selection between several microbial species, in these two ecosystems, leads to the prediction of the species which wins the competition. And finally we showed how it is possible in each ecosystem to control competition and drive natural selection, in order to advantage species with efficient characteristics, inducing better performances.

Chapter 1

Introduction

The beginning of the 21th century is characterized by a large scale awareness that the way humankind is developing is no more sustainable [28]. The concept of ecological footprint [45] was proposed in order to compare human demand of resources with Earth's ecological capacity to regenerate them. It represents the amount of biologically productive land and sea area needed to regenerate the resources a human population consumes and to absorb and recycle the corresponding waste. To date, the ecological footprint of a French inhabitant is 5 global hectares [15] (a global hectare represents an average productive surface on Earth), which means that 2.5 Earth planets would be necessary to sustain a population of shortly 7 billion inhabitants. There are two ways of reducing our ecological footprint in order to pass a planet on to our children with a sustainable model in a world which may reach 9 billion inhabitants before the end of the century. The first approach consists in drastically decreasing our needs in order to save resources and decrease the generated pollution. The second approach, which must be carried out concomitantly, consists in improving the technologies we are using in order to minimize their impact. This second approach, towards more efficiency and less impacting technologies has a meaning only if it is led in parallel to a drastic decrease in consumption and waste production. This PhD thesis focuses on this technological approach in order to reduce the impact of transportation, which is responsible of more than 20% of the total greenhouse gas emissions. In order to decrease the impact of transportations and to limit the use of fossil fuel, alternative non-fossil biofuel production processes are investigated. In this thesis we focused on a new generation of biofuel based on microscopic photosynthetic organisms which harvest the solar energy with a better efficiency than terrestrial plants.

Light energy from the sun is the main source of energy on Earth, and it supports life on Earth. Plants are the very base of the alimentary chain, as they are the main organisms which can turn mineral molecules into organic molecules with higher energy content: this energy gain, gathered by photosynthesis, comes from light. Solar energy allows to transform, through photosynthesis, CO_2 together with various nutrients (nitrogen, phosphorus, potassium, ...) into organic matter. Except autotrophic organisms, all the other organisms (heterotrophic bacteria, yeasts, animal, ...) need to consume such organic molecules and use the energy they contain to live. The enzyme which is responsible for $C0_2$ fix-

ation is the Rubisco (Ribulose-1,5-bisphosphate carboxylase oxygenase), which intervenes in the Calvin cycle [16]. This enzyme is the most abundant enzyme on Earth [16], and it is also the most abundant protein on Earth which demonstrate the crucial role played by photosynthesis. The idea of producing biofuel consists in exploiting this capacity of plants to harvest light energy and to recover the energy stored in the plants. There are two possibilities to recover this energy. Either plants can be grown for their ability to store energy under some specific usable form (lipids, sugars) into dedicated organs. The energy is then recovered under the form of oil which can be transformed into biodiesel (or bioethanol if sugar reserves are used). The energy can also be recovered from wastes, after the plant has been used. In such a case, a community of anaerobic archae and bacteria can be grown on the remaining wastes, and methane (which is also a biofuel) can be produced. This second process can also be combined to the treatment of organic wastes in order, to both produce bioenergy, and process organic pollutants at the same time.

Phytoplankton (mainly composed of microalgae and cyanobacteria) are microscopic plants which can be found in most of the aquatic environments, from the ocean to lakes and rivers [24]. Some species can even develop in very extreme environments, in the ice, and other can be found in geysers or in very acid lakes. More than 30 000 species have been described, but there are probably more than 1 million species on Earth [7]. Figure 1.1 illustrates their broad diversity in size, shapes and colours. Phytoplankton is often refered to as microalgae, which is a slight abuse of language (since cyanobacteria are not, rigorously speaking, microalgae), but this term will be used in the manuscript.

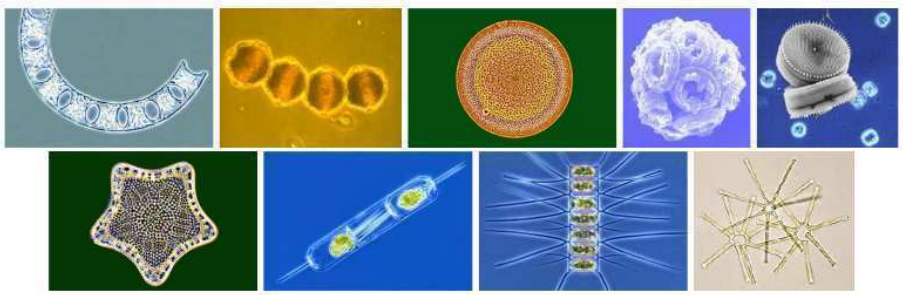

Figure 1.1: Microalgae can be found almost anywhere on the globe, approximately 30.000 species have been referenced.

In the last fifty years, several microalgal species have demonstrated attractive characteristics for biotechnological applications, from food and pharmaceutic productions [38, 42], to CO_2 fixation [3] and biofuel production [26, 8]. Their high actual photosynthetic yield compared to terrestrial plants (whose growth is limited by CO_2 availability) leads to large potential algal biomass productions of several order of magnitude higher than terrestrial plants [7]. This actual higher efficiency in recovering solar energy is the main reason why several projects have been initiated in the very begining of the century. Among them, the ANR-Shamash project was aiming at studying and optimising the potential of biofuel production from microalgae. Another ANR project (Symbiose) is considering the possibility of using microalgae to feed an anaerobic ecosystem in order to

produce methane and recycle nitrogen and phosphorus under the form of nitrate and phosphate. Such anaerobic ecosystem is rather complex since it can involve more than 300 bacterial species [11] in complex interactions. Anaerobic digestion can be observed in the sediment of lakes and rivers, where they degrade wastes and produce methane that will go back to the atmosphere, thus contributing to global warming. When the process is domesticated in a bioreactor (see Figure 1.2) the anaerobic ecosystem can both produce methane and process wastewater [2].

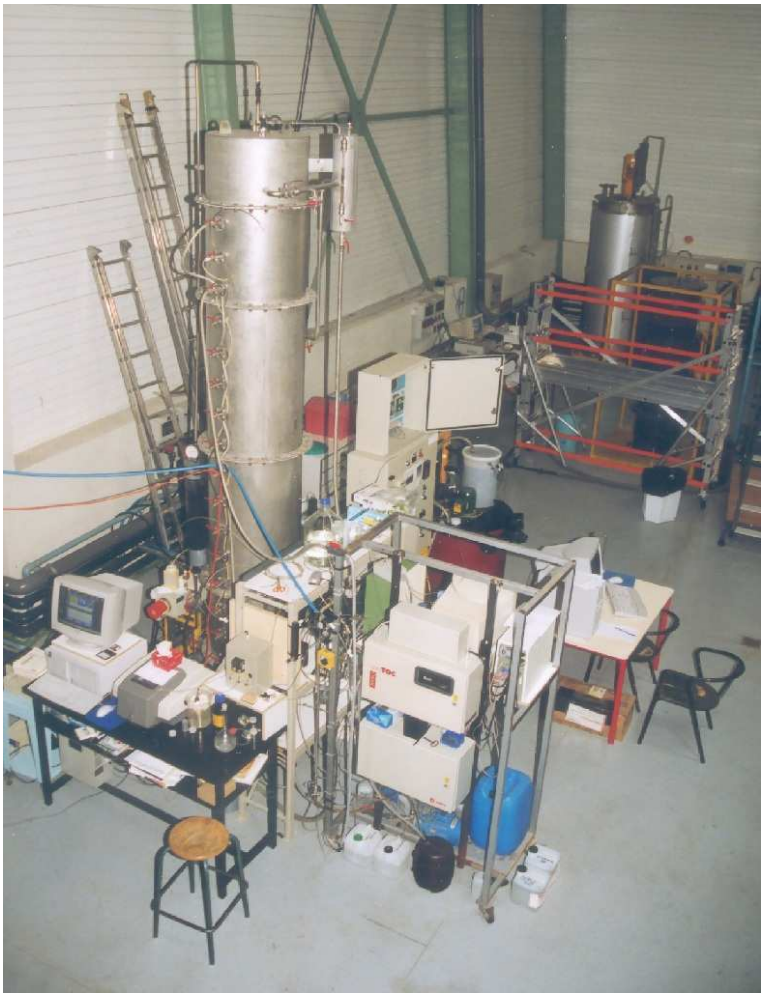

Figure 1.2: Anaerobic digester developed at the Laboratoire de Biotechnologie de l'Environnement, INRA, Narbonne, France.

Apart from their direct application in renewable energy, microbial ecosystems have also a strong interest for theoretical ecology [29]: experiments with microbial ecosystems can be monitored accurately, replicated easily, grow fast, the organisms can be archived by cryogenic processes, and their physiologi-

cal and genetic constituents are pretty well-characterized. These strengths are counterbalanced by some limitations: evolution is often fast so that interactions can change before researchers have completed their characterization; and finally, we are limited in our ability to extrapolate from microbial experimental systems to larger and often more complex systems. In particular in this thesis, the works concerning competition have conceptual implications that could also apply to non-microbial ecosystems.

Several obstacles must be considered to study microbial ecosystems: biological systems and environments are complex, measurements are often not accurate or at low sampling frequency, the systems often display non-linearities, such as threshold effect leading to sudden and stiff reactions. To limit the degree of complexity of such systems in order to have higher chances to develop models, it is often useful to first simplify them. In 1942, Monod [36] developed a tool for microbial dynamics study: the chemostat. This vessel is continuously filled with growth medium. To keep the same volume, a mixing of nutrients and microorganisms is removed at the same rate. Such a system allows to isolate the microorganisms from the possible environment variations (light, temperature, ...) and to accurately control the growth conditions. It also allows to accurately monitor the growth of the organisms, thanks to dedicated sensors. During this thesis, experiments were made in the continuous photobioreactors (chemostat) of the LOV (Laboratory of Oceanography of Villefranche-sur-Mer), see figure 1.3. Nutrients, light, temperature and pH where on-line measured and for some of them, regulated. Most of these experiments were done by Thomas Lacour in the context of his PhD thesis [30], dealing with the effect of environment on microalgal growth and lipid synthesis.

In order to study these bioenergy producing microbial processes on a quantitative point of view, we use mathematical models which are able to describe their dynamics. With such a model based on ordinary differential equations, we can explain, predict and control the ecosystem state and behaviour at every instant of its life. This model must account for the inherent complexity and the non-linearity of these biological systems. For example, when dealing with microalgae, the complex interactions with their environment must be taken into account: microalgal growth is influenced by nutrients and light availability, but at the same time microalgae absorb nutrients and attenuate light in the water column, thus changing their environment.

Modelling natural phenomena is the basis of physics, where empirical laws have been deduced from observations. However, on the contrary to physics, there does not exist any law in biology from which a model can be based with a reasonable degree of accuracy.

The models in the biological field are often the results of an iterative approach, which was described by Hardin [23]:

> *" From the model we make predictions; these we test against empirical data. When we find that a prediction is not verifiable we then set about modifying the model. There is no procedural rule to tell us which element of the model is best abandoned or changed. (...). Aesthetics plays a part in such decision. "*

Monod developed a pioneer model, where bacterial growth rate was directly dependent on nutrients availability in the medium. As phytoplankton has a

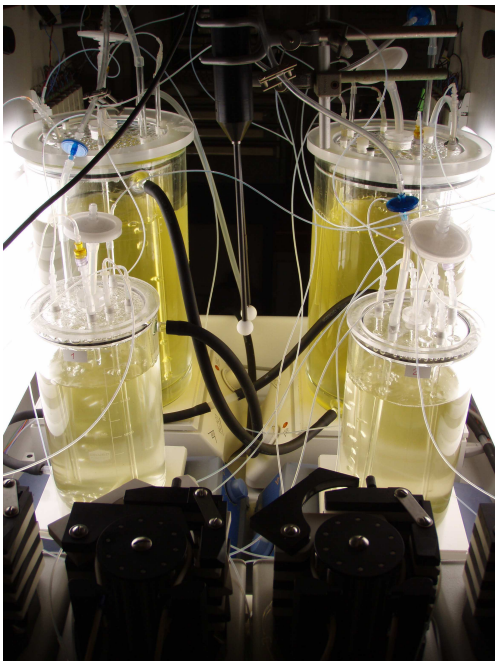

Figure 1.3: Photobioreactors at the LOV for carrying out experiments on lipid production with microalgae [30].

capacity to store nutrients and continue to grow on their nutrient storage when the medium is depleted, Droop [13] introduced a new model which represents this feature. The Droop model does not take light effects into account (it was mainly used for a constant experimental light). In this thesis we developed a new model, based on the Droop model, including light effect and light distribution in a photobioreactor with high microalgal biomass (chapter 2.1). We named our model "Droop Photobioreactor Model" (DPM). In order to study oil production we then added two variables to this model, to represent lipid and sugar synthesis (chapter 2.2).

The Monod (or Droop) chemostat model is however very simple and does not account for the biodiversity which can be found in the nature, or even in biofuel producing open microalgal ponds often faced to invasion by local endemic species. Even when considering anaerobic digestion, we used a variant of a previously developed model [6] which is basically a two stages Monod/Haldane model. Quite surprisingly, this complex ecosystem involving hundreds of bacterial species could be described by only two main phenomena. In a first step, acidogenic bacteria turn organic wastes into volatile fatty acids according to Monod model. In a second step volatile fatty acids are turned into methane by methanogenic bacteria, according to Haldane model. The Haldane model includes inhibition of growth by high nutrient concentration, whereas Monod growth function is increasing with respect to nutrient.

In order to go closer from real outdoor ecosystems (even if these ecosys-

tems are still simplified), and optimize the behaviour of exploited ecosystems, the interactions between microbial populations must be considered. One of the simplest interaction to be considered is competition for a limiting nutrient. Competition for a substrate between several species in an homogeneous medium is a topic of great interest to ecologists: "when and why is coexistence possible?", "can we explain the mosaic of observed spatial and temporal species distribution?", "can we predict in some cases which species will win a competition and exclude all the others from the environment?".

Theoreticians predicted competitive exclusion with several competing species represented by Monod models [1, 41], and then, later on, represented by Droop models [25]: in both cases only one species wins the competition and excludes all the others from the chemostat. From the theoretical result, it was possible to predict the outcome of competition from parameters derived from single species experiments.

These results were experimentally validated by Hansen and Hubbel [22], which demonstrated the power of using mathematical models. These authors experimented the competition outcome between two bacterial species, on the basis of single-species experiments which were used to characterize the species parameters. More surprisingly, they demonstrated that the outcome could be triggered by manipulating the dilution rate of the chemostat. Figure 1.8 shows the result of their experiments, where they could predict in two cases which species would win the competition, and where they could also force a coexistence between two species.

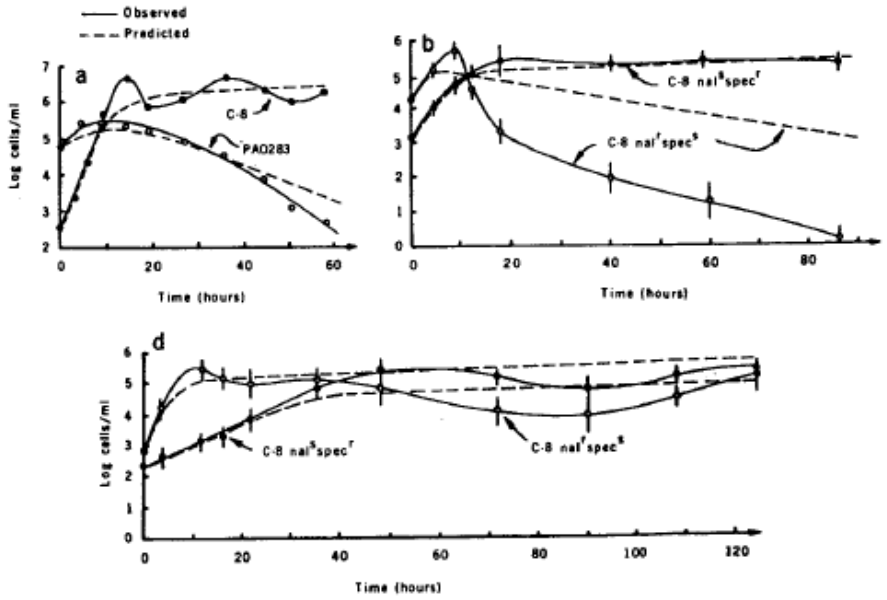

Figure 1.4: Validation of the theoretical competition results with bacteria. Hansen and Hubbel could make one bacteria or another win the competition, or make two species coexist.

But sometimes several species do not all exclude each other. For example the species represented by the Contois model [9] can coexist under some conditions [19, 31] which are less restrictive than to get coexistence from Monod type species [35]. In the Contois model, like in the Monod model, the population growth rate depends directly on the nutrient concentration in the medium. But in this model, the growth rate also depends on the biomass: the more biomass, the slower the population grows. This reflects *e.g.* intraspecific population competition for space (spatial heterogeneity, flocculation/deflocculation phenomena [32, 21]).

Thus with the Monod, Droop, and Contois models, we can represent three different types of behaviors of the species present in microbial ecosystems. The result of competition is not the same for each of the models: pure Monod or Droop competition models predict competitive exclusion [41, 25], whereas pure Contois competition models predict coexistence. In this thesis, we propose a generalized result for a competition between species represented by Monod, Droop or Contois models.

One way of optimising the efficiency of an exploited microbial ecosystem is to use the competition principle to make the more efficient species win the competition. This principle is a basis of the directed selection. Indeed, this technique can be used as an alternative to genetic engineering for identifying microorganisms with efficient characteristics, or for improving some species characteristics. Percival Zhang gives a review of techniques to improve a species characteristics [37]. He expresses quite clearly the interest of the "selection by competition" approach, against biotechnologist genetic rational design:

> *" The faith in the power of rational design relies on the belief that our current scientific knowledge is sufficient to predict function from structure. But such information of structures and mechanisms is not available for the vast majority of enzymes. [...] An exceedingly higher cell concentration of* 10^{12} *individual cells per litre and a longer cultivation time (generations) allow continuous culture to become a powerful selection system for the ultra-large size of the mutant library even when selective advantages are very small. "*

Several examples are given [14] where competitions in specific environments led to the selection of population with desired traits. The review of Zelder and Hauer [47] details some examples and industrial considerations.

The principle is the same as the one used in agriculture since the Neolithic to produce bigger vegetables, by using the seeds of the biggest individuals. Along the course of time and generations, this led to a progressive evolution from wild plants with small fruits or seeds, to the vegetables we know today: for example corn with big yellow grains, which did not exist seven thousands of years ago (before the Neolithic revolution).

In the spirit of maximizing exploited microbial ecosystems performances, two approaches can be deployed. In this thesis we considered these approaches focusing either on the individuals, or on the ecosystem.

First, the models can be used to derive control strategies which will be used to dynamically compute the input to be applied to the ecosystem (dilution rate, influent nutrient concentrations, ...) from the knowledge of its state. Based on a Pontryagin maximum principle, optimal controls are proposed which maximize

productivity. In this study we focus on microalgal biomass productivity optimization in a photobioreactor, under continuous light (chapter 3.1) or day-night cycles (chapter 3.2). For these studies, we use our previously developed DPM model (chapter 2.1).

Finally, species with efficient characteristics that increase productivity must be chosen, and the condition to drive the ecosystem in more efficient working mode can be found. We propose rigorous mathematical results based on the models, to predict and control the outcome of competition in both Monod and Droop models (chapter 4.2), as well as in the anaerobic ecosystem model (chapter 4.3). With these results it becomes possible to change the selection criteria in the ecosystem, in order to select species with new desired characteristics that should help to increase productivity, both for microalgal or bacterial ecosystems.

Introduction

Le début du 21ème siècle est caractérisé par une prise de conscience à grande échelle que la façon dont l'humanité se développe actuellement n'est pas durable [28]. Le concept de l'empreinte écologique
[45] a été proposé afin de comparer la demande humaine de ressources avec la capacité écologique de la Terre à les régénérer. Il représente la surface de terre biologiquement productive et la zone maritime nécessaires pour régénérer les ressources consommées par une population humaine et pour absorber et recycler les déchets correspondants. À ce jour, l'empreinte écologique moyenne d'un habitant français est de 5 hectares globaux [15] (un hectare global représente une surface moyenne de production sur terre), ce qui signifie que 2,5 planètes Terre seraient nécessaires pour soutenir une population de 7 milliards d'habitants vivant comme un habitant français moyen. Il y a deux façons de réduire notre empreinte écologique afin de laisser à nos enfants une planète avec un modèle durable dans un monde qui peut atteindre 9 milliards d'habitants avant la fin du siècle. La première approche consiste à réduire radicalement nos besoins afin d'économiser les ressources et diminuer la pollution générée. La seconde approche, qui doit être réalisée de façon concomitante, consiste à améliorer les technologies que nous utilisons afin de minimiser leur impact. Cette seconde approche, vers plus d'efficacité et moins d'impact des technologies, n'a de sens que si elle est menée en parallèle à une diminution drastique de la production, de la consommation et des déchets. Cette thèse met l'accent sur cette approche technologique afin de réduire l'impact du transport, qui est responsable de plus de 20 % du total des émissions de gaz à effet de serre. Afin de diminuer l'impact des transports et de limiter l'utilisation de combustibles fossiles, des processus de production de biocarburants non-fossiles sont étudiés. Dans cette thèse nous nous sommes concentrés sur une nouvelle génération de biocarburants produits pas des organismes photosynthétiques microscopiques qui capturent l'énergie solaire plus efficacement que les plantes terrestres.

L'énergie lumineuse du soleil est la principale source d'énergie sur Terre, dont elle soutient la vie. Les plantes sont la base même de la chaîne alimentaire, car elles sont les principaux organismes qui peuvent transformer des molécules minérales en molécules organiques dotées d'un contenu énergétique plus élevé : ce gain d'énergie, fruit de la photosynthèse, provient de la lumière. L'énergie solaire permet de transformer, grâce à la photosynthèse, le CO_2, avec les divers éléments nutritifs (azote, phosphore, potassium, ...) en matière organique. À part les organismes autotrophes, tous les autres organismes (bactéries hétérotrophes, levures, animaux, ...) ont besoin de consommer de telles molécules organiques et d'utiliser l'énergie qu'elles contiennent pour vivre. L'enzyme qui est respon-

sable de la fixation du $C0_2$ est la Rubisco (ribulose-1,5-bisphosphate carboxylase/oxygénase), qui intervient dans le cycle de Calvin [16]. Cette enzyme est l'enzyme la plus abondante sur Terre [16], et c'est aussi la protéine la plus abondante sur Terre, ce qui démontre le rôle crucial joué par la photosynthèse. L'idée de produire des biocarburants consiste à exploiter cette capacité des plantes à emmagasiner l'énergie lumineuse, pour récupérer ensuite l'énergie ainsi stockée. Il y a deux possibilités pour récupérer cette énergie. Soit les plantes peuvent être cultivées pour leur capacité à stocker l'énergie sous une forme utilisable spécifique (lipides, sucres) dans des organes spécialisés. L'énergie est alors récupérée sous forme d'huile qui peut être transformée en biodiesel (ou bioéthanol pour des réserves cellulaires de sucre). Soit l'énergie peut être récupérée à partir de déchets, après que la plante a été utilisée. Dans ce cas, une communauté d'archea-bactéries et de bactéries anaérobies peut être cultivée sur les déchets restants et du méthane (qui est aussi un biocarburant) peut être produit. Ce second procédé peut également être combiné au traitement de déchets organiques industriels et ménagers, dans le but de produire de la bioénergie et de traiter des polluants organiques en même temps.

Le phytoplancton est constitué de plantes microscopiques (microalgues et cyanobactéries) qui se trouvent dans la plupart des milieux aquatiques, que ce soit dans les océans, dans les lacs ou dans les rivières [24]. Certaines espèces peuvent même se développer dans des environnements extrêmes, comme la glace, et d'autres peuvent être trouvées dans des geysers ou dans des lacs très acides. Plus de 30 000 espèces ont été décrites, mais il y a probablement plus d'un million d'espèces sur Terre [7]. La Figure 1.5 illustre leur très grande diversité de tailles, de formes et de couleurs. Les organismes phytoplanctoniques sont souvent désignés par le terme "microalgues", ce qui est un abus de langage (puisque les cyanobactéries ne sont pas, rigoureusement parlant, des microalgues), mais ce terme sera utilisé dans le manuscrit.

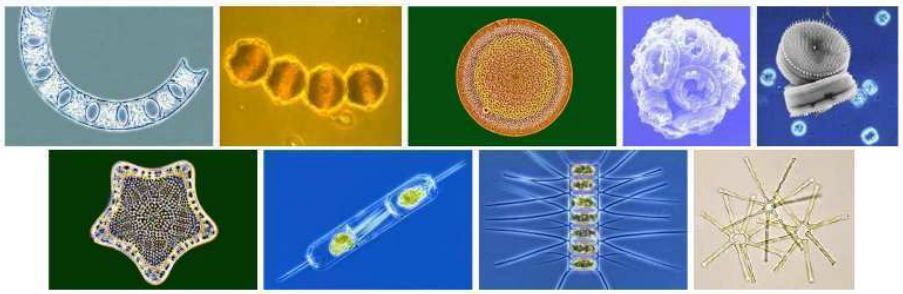

Figure 1.5: Les microalgues peuvent être rencontrées à peu près partout sur le globe, environ 30.000 espèces ont été référencées.

Dans les cinquante dernières années, plusieurs espèces de microalgues ont montré des caractéristiques intéressantes pour des applications biotechnologiques : de la production de nourriture aux productions pharmaceutiques [38, 42], à la fixation de CO_2 [3] et à la production de biocarburants [26, 8]. Leur haut rendement photosynthétique par rapport aux plantes terrestres (dont la croissance est limitée par la disponibilité en CO_2) permet de fortes productivités potentielles en biomasse, de plusieurs ordres de grandeur plus élevées que les plantes ter-

restres [7]. Cette plus grande efficacité dans la récupération de l'énergie solaire est la principale raison pour laquelle plusieurs projets ont été lancés au début de ce siècle. Parmi eux, le projet ANR-Shamash a pour but d'étudier et d'optimiser le potentiel de production de biocarburants à partir de microalgues. Un autre projet ANR (Symbiose) envisage la possibilité d'utiliser des microalgues pour nourrir un écosystème anaérobie, afin de produire du méthane et recycler l'azote et le phosphore sous forme de nitrate et de phosphate, dont une nouvelle culture de microalgues pourra alors se nourrir. Ces écosystèmes anaérobies sont assez complexes car ils peuvent impliquer plus de 300 espèces bactériennes [11] dans des interactions complexes. La digestion anaérobie peut être naturellement observée dans les sédiments des lacs et des rivières, où des déchets sont dégradés et du méthane produit. Ce méthane est ensuite libéré dans l'atmosphère, contribuant ainsi au réchauffement climatique. Lorsque le processus est domestiqué dans un bioréacteur (voir la figure 1.6) l'écosystème anaérobie peut à la fois produire du méthane (qui sera ensuite valorisé energétiquement) et traiter les eaux usées [2].

Indépendamment de leur application directe dans les énergies renouvelables, les écosystèmes microbiens ont également un fort intérêt pour l'écologie théorique [29] : les expériences avec des écosystèmes microbiens peuvent être suivies de très près, reproduites facilement, elles présentent une croissance rapide de la population, les organismes peuvent être archivés par des procédés cryogéniques, et leurs constituants physiologiques et génétiques sont assez bien caractérisés. Ces atouts sont contrebalancés par certaines limites : l'évolution est souvent rapide de telle sorte que les interactions peuvent changer avant que les chercheurs aient terminé leur caractérisation. Enfin, nous sommes limités dans notre capacité à extrapoler à partir de systèmes expérimentaux microbiens, vers des systèmes plus grands et souvent plus complexes. En particulier dans cette thèse, les travaux sur le fonctionnement de la compétition ont des implications conceptuelles qui pourraient également s'appliquer à des écosystèmes non microbiens.

Plusieurs obstacles doivent aussi être considérés dans l'étude des écosystèmes microbiens : les systèmes biologiques et les environnements sont complexes, les mesures sont souvent inexactes ou à faible fréquence d'échantillonnage, les systèmes présentent souvent des non-linéarités, telles que des effets de seuil conduisant à des réactions brusques et rapides. Pour limiter le degré de complexité de ces systèmes, afin d'accroitre les chances de développer des modèles, il est souvent utile de commencer par les simplifier. En 1942, Monod [36] a développé un outil pour étudier la dynamique microbienne : le chémostat. C'est un récipient dans lequel on injecte continument du milieu de croissance. Pour garder un volume constant dans le récipient, un mélange de nutriments et de micro-organismes est évacué à la même vitesse que le débit d'entrée. Un tel système permet d'isoler les micro-organismes des variations environnementales (lumière, température, ...) et ainsi de contrôler avec précision les conditions de croissance. Il permet également de surveiller précisément la croissance des organismes, grâce à des capteurs dédiés. Au cours de cette thèse, des expériences ont été faites dans les photobioréacteurs continus (cultures de microalgues en chémostats) du LOV (Laboratoire d'Océanographie de Villefranche-sur-Mer), que l'on peut voir à la Figure 1.7. Les éléments nutritifs, la lumière, la température et le pH étaient mesurés en ligne et pour certains d'entre eux, régulés. La plupart de ces expéri-

Figure 1.6: Fermenteur anaérobie du Laboratoire de Biotechnologie de l'Environnement, INRA, Narbonne.

ences ont été réalisées par Thomas Lacour dans le cadre de sa thèse de doctorat [30], traitant de l'effet de l'environnement sur la croissance des microalgues et sur la synthèse des lipides.

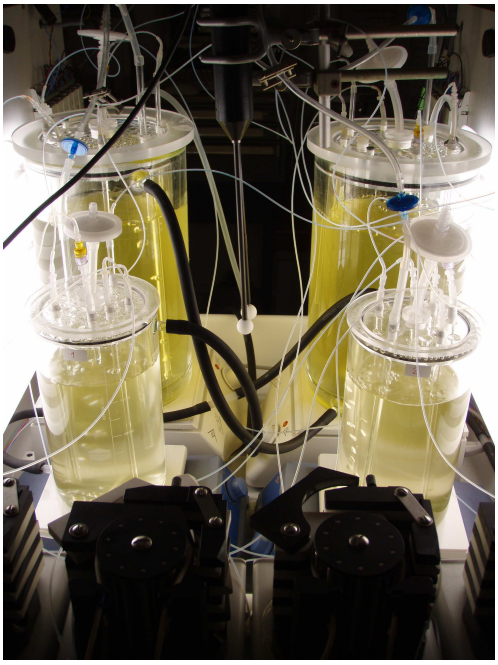

Figure 1.7: Photobioréacteurs du LOV, utilisés pour des expériences sur la production lipidique des microalgues [30]

Afin d'étudier ces processus microbiens de production de bioénergie d'un point de vue quantitatif, nous utilisons des modèles mathématiques qui sont en mesure de décrire leur dynamique. Avec de tels modèles basés sur des équations différentielles ordinaires, nous pouvons expliquer, prédire et contrôler l'état de l'écosystème et son comportement à chaque instant de sa vie. Le modèle doit prendre en compte la complexité inhérente et la non-linéarité des systèmes biologiques impliqués. Par exemple, lorsqu'il s'agit de microalgues, les interactions complexes avec leur environnement doivent être prises en compte : la croissance des microalgues est influencée par les éléments nutritifs et la disponibilité de la lumière, mais en même temps les microalgues absorbent des nutriments, et la lumière est atténuée dans la colonne d'eau, ce qui modifie leur environnement.

La modélisation des phénomènes naturels est également la base de la physique, où des lois empiriques ont été déduites des observations. Cependant, au contraire de la physique, il n'existe pas une loi de la biologie à partir de laquelle un modèle peut être construit avec un degré raisonnable d'exactitude.

Les modèles dans le domaine biologique sont souvent le résultat d'une approche itérative, qui a été décrite par Hardin [23] :

> *" À partir du modèle nous faisons des prédictions que nous comparons à des données empiriques. Lorsque nous constatons que la*

prédiction n'est pas vérifiée, nous modifions alors le modèle. Il n'y a pas de règle ni de procédure pour nous dire quels éléments du modèle devraient être abandonnés ou modifiés. (...). L' esthétique joue un rôle dans cette décision. "

Monod a développé un modèle pionnier, où le taux de croissance bactérien est directement lié à la disponibilité en éléments nutritifs dans le milieu. Comme le phytoplancton a une capacité à stocker des éléments nutritifs et à continuer à croître sur ses stocks d'éléments nutritifs lorsque le milieu est appauvri, Droop [13] a introduit un nouveau modèle qui représente ce processus. Le modèle de Droop ne prend pas en compte les effets de la lumière (il a été principalement utilisé pour une lumière expérimentale constante). Dans cette thèse nous avons développé un nouveau modèle, basé sur le modèle de Droop, comprenant les effets de la lumière et de la distribution de la lumière dans un photobioréacteur à forte biomasse de microalgues (chapitre 2.1). Nous avons nommé notre modèle "Droop Photobioreactor Model" (DPM). Afin d'étudier la production d'huile nous avons ensuite ajouté deux variables à ce modèle, pour représenter la synthèse des lipides et du sucre (chapitre 2.2).

Lorsque nous avons considéré la digestion anaérobie, nous avons utilisé une variante d'un modèle précédemment développé [6] qui est essentiellement un modèle Monod / Haldane à deux étapes. De manière étonnante, cet écosystème complexe impliquant des centaines d'espèces de bactéries peut être décrit par seulement deux réactions principales. Dans un premier temps, des bactéries acidogènes transforment les déchets organiques en acides gras volatils selon le modèle de Monod. Dans une deuxième étape ces acides gras volatils sont transformés en méthane par des bactéries méthanogènes, selon le modèle de Haldane. Le modèle de Haldane représente une inhibition de la croissance par les concentrations élevées en nutriments, alors que la fonction de croissance de Monod augmente toujours avec la concentration en éléments nutritifs.

Ce dernier modèle, ainsi que les modèles de chémostat de Monod et de Droop, sont très simples et ne tiennent pas compte de la diversité biologique qui se trouve dans la nature, ou même dans les étangs ouverts de culture de microalgues, qui sont souvent confrontés à l'invasion par des espèces compétitrices locales.

Pour se rapprocher des écosystèmes réels, en plein air (même si ces écosystèmes sont encore simplifiés), et optimiser le comportement de ces écosystèmes, les interactions entre différentes populations microbiennes doivent être considérées. L'une des interactions les plus simples à prendre en compte est la compétition pour un élément nutritif limitant. La compétition pour un substrat entre plusieurs espèces dans un milieu homogène est un sujet de grand intérêt pour les écologistes : "quand et pourquoi des situations de coexistence sont-elles possibles?", "Peut-on expliquer les mosaïques spatiales et temporelles de distribution des espèces?", "Peut-on prévoir dans certains cas quelle espèce gagne la compétition et va ainsi exclure toutes les autres de l'environnement?".

Dans le cas d'une compétition entre plusieurs espèces représentées par des modèles de Monod, la théorie prédit l'exclusion compétitive.
[1, 41]. Ce même résultat a ensuite été étendu à une compétition entre des espèces représentées par des modèles de Droop [25] : dans les deux cas une

seule espèce remporte la compétition et exclut toutes les autres du chémostat. Le résultat théorique permet même de prédire le résultat de la compétition, à partir des paramètres des espèces, ces derniers pouvant être obtenus par des expériences avec une seule espèce.

Ces résultats ont été validés expérimentalement par Hansen et Hubbel [22], qui ont démontré la puissance de l'utilisation des modèles mathématiques. Ces auteurs ont prédit le résultat de la compétition entre deux espèces bactériennes, sur la base d'expériences mono-spécifiques qui ont été utilisées pour caractériser les paramètres de ces espèces. Plus surprenant, ils ont vérifié expérimentalement que le résultat de la compétition pouvait être contrôlé en faisant varier le taux de dilution du chémostat. La Figure 1.8 montre le résultat de leurs expériences, où ils ont pu prédire dans deux cas l'espèce qui remporterait la compétition, et où ils ont également pu forcer la coexistence entre deux espèces.

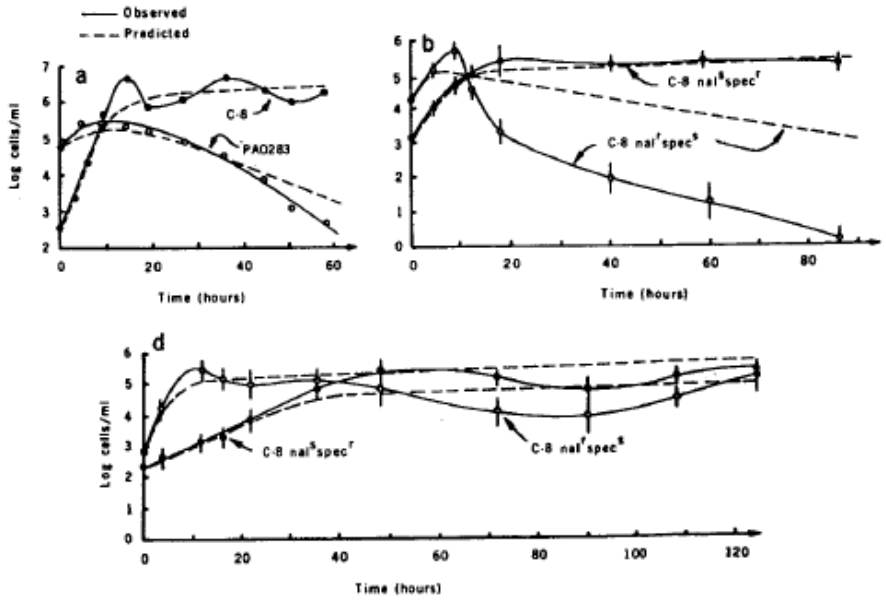

Figure 1.8: Validation des résultats théoriques de la compétition entre des espèces de bactéries. Hansen et Hubbel pouvaient faire gagner une espèce de bactéries, ou une autre, ou même faire coexister deux espèces.

Mais parfois plusieurs espèces ne s'excluent pas mutuellement. Par exemple, il a été démontré que des espèces représentées par le modèle Contois [9] peuvent coexister dans certaines conditions [19, 31] qui sont moins restrictives que pour obtenir la coexistence des espèces de type Monod [35]. Dans le modèle de Contois, comme dans le modèle de Monod, le taux de croissance de la population dépend directement de la concentration des nutriments dans le milieu. Mais dans ce modèle, le taux de croissance dépend aussi de la concentration de biomasse : plus il y a de biomasse, plus le taux de croissance est faible. Cela peut refléter par exemple une compétition intraspécifique des individus pour l'espace

(hétérogénéité spatiale, phénomènes de floculation / défloculation [32, 21]).

Ainsi, avec les modèles de Monod, Droop, et Contois, on peut représenter trois types de comportements différents d'espèces présentes dans les écosystèmes microbiens. Le résultat de la compétition n'est pas la même pour chacun des modèles : dans les modèles de compétition pure entre des espèces représentées par le modèle de Monod ou celui de Droop , la théorie prédit l'exclusion compétitive [41, 25], tandis que les modèles de compétition pure entre des espèces représentées par le modèle Contois prédisent la coexistence. Dans cette thèse, nous proposons une généralisation de ces résultats, en mettant en compétition mixte des espèces représentées par des modèles de Monod, Droop et Contois.

Une façon d'optimiser l'efficacité d'un écosystème microbien est d'utiliser le principe de compétition pour faire remporter la compétition à l'espèce la plus efficace. C'est le principe de base de la Sélection Dirigée. Cette technique peut être utilisée comme une alternative au génie génétique, pour identifier les micro-organismes ayant des caractéristiques efficaces, ou pour améliorer certaines caractéristiques d'une population donnée. Percival Zhang donne une vue d'ensemble des techniques permettant d'améliorer les caractéristiques d'une population [37]. Il exprime très clairement l'intérêt de l'approche de "sélection par compétition", par rapport au "genetic rational design" des biotechnologistes :

> *" La foi dans la puissance du "rational design" repose sur la conviction que nos connaissances scientifiques actuelles sont suffisantes pour prédire la fonction à partir de la structure. Mais de telles informations sur les structures et les mécanismes ne sont pas disponibles pour la grande majorité des enzymes. [...] Une concentration cellulaire extrêmement élevée d'environ 10^{12} cellules par litre et un long temps de culture (de l'ordre de dizaines ou centaines de générations) permettent à la culture continue de devenir un système de sélection puissant dans la bibliothèque immense des mutants, même lorsque les avantages sélectifs sont infimes. "*

Plusieurs exemples sont donnés [14] où des compétitions dans des environnements spécifiques ont conduit à la sélection d'une population ayant des caractéristiques souhaitées. La review de Zelder et Hauer [47] détaille quelques exemples et donne des considérations industrielles.

Le principe est le même que celui utilisé dans l'agriculture depuis le Néolithique pour produire de plus gros légumes, en utilisant les graines des plus gros individus. Au fil du temps et des générations, cela a conduit à une évolution progressive à partir de plantes sauvages à petits fruits ou graines, jusqu'aux légumes que nous connaissons aujourd'hui : par exemple le maïs avec de gros grains jaunes, qui n'existait pas il y a sept milliers d'années (avant la Révolution néolithique).

Dans l'esprit de maximiser les performances des écosystèmes microbiens contrôlés, deux approches peuvent être déployées. Dans cette thèse, nous avons étudié ces deux approches, centrées soit sur les individus, soit sur l'écosystème.

D'abord, les modèles peuvent être utilisés pour déterminer des stratégies de contrôle qui seront utilisées pour calculer à chaque instant l'entrée à appliquer à l'écosystème (taux de dilution, concentration en nutriments de l'influent, ...) à partir de la connaissance de son état. Basé sur le principe du maximum de

Pontryagin, nous proposons des stratégies de contrôle optimales qui permettent de maximiser la productivité. Dans cette étude, nous nous concentrons sur l'optimisation de la productivité de la biomasse de microalgues dans un photobioréacteur, sous une lumière continue (chapitre 3.1) ou sous des cycles jour-nuit (chapitre 3.2). Pour ces études, nous utilisons notre modèle "DPM" développé antérieurement (chapitre 2.1).

Enfin, les espèces ayant des caractéristiques efficaces qui augmentent la productivité doivent être choisies. Nous proposons des résultats mathématiques rigoureux basés sur les modèles, pour prévoir et contrôler le résultat de la compétition dans les modèles de Monod et de Droop (chapitre 4.2), ainsi que dans le modèle d'écosystème anaérobie (chapitre 4.3). Avec ces résultats, il devient possible de changer les critères de sélection dans l'écosystème, afin de sélectionner des espèces possédant de nouvelles caractéristiques souhaitées, qui devraient contribuer à accroître la productivité, tant pour les écosystèmes de microalgues que pour ceux de bactéries.

Chapter 2

Photobioreactor modelling

A first approach for studying microorganisms consists in growing them in "batch", *i.e.* with a predefined quantity of nutrients that they will consume. When the nutrients are depleted, the population stops growing. In general, in the two bioreactor types that we will consider (photobioreactor and anaerobic digester), only one nutrient will be limiting, and we denote this nutrient's concentration s (for "substrate"). To get closer to the conditions of natural environments where water and nutrients are renewed (sea, lakes, etc.), researchers began to change the nutritive medium after periodic time intervals [17]. This approach was improved by changing part of the medium continuously, which is achieved in a chemostat. Water continuously comes in, enriched with nutrients (with concentration s_{in}), and goes out together with microorganisms and the remaining nutrients. The flow of water leads to a dilution rate denoted D, which corresponds to the proportion of medium renewed each day. The main biological phenomena occurring in the chemostat are substrate absorption (ρ will be the absorption rate per population unit) and population growth, whose rate will be denoted μ. Thus, with x the microorganisms biomass concentration (*e.g.* in grams of carbon per liter), a chemostat model can be written:

$$\begin{cases} \text{nutrients concentration change} = & \text{nutrients input} - \text{nutrients output} \\ & -\text{nutrients absorption} \\ \text{microalgal biomass change} & = \text{growth} \\ & -\text{microalgae going out of the chemostat} \end{cases} \tag{2.1}$$

This model can also be written with mathematical symbols:

$$\begin{cases} \dot{s} &= Ds_{in} - Ds - \rho(.)x \\ \dot{x} &= \mu(.)x - Dx \end{cases} \tag{2.2}$$

This general chemostat model is presented in Figure 2.1.

Many variants of this chemostat model were developed, with different factors affecting absorption and growth rates. Monod model [36] states that the growth rate is proportional to the absorption rate :

$$\mu(.) = k\rho(.)$$

it means that microorganisms need a fixed amount of substrate for building one biomass unit. In this model also, the growth rate is a function of the output substrate concentration s.

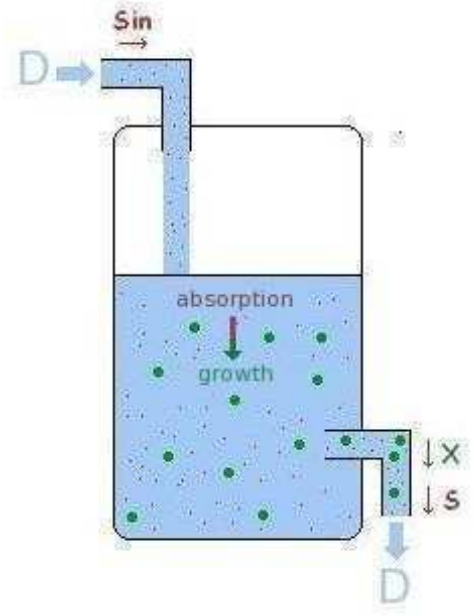

Figure 2.1: In the chemostat the main physical phenomena are influent medium with nutrients, and water output with both remaining nutrients and microorganisms. The main biological phenomena are nutrients absorption, and growth.

But it was observed that nutrients absorption and growth rate can be uncoupled for some microorganisms, and especially for microalgae. In a batch culture limited with nitrogen, microalgae will absorb all the nitrogen until the medium is depleted, and keep on growing (thus accumulating carbon by photosynthesis) for some time, by using the previously stored nitrogen. In this case the microalgal intracellular nitrogen/carbon ratio will vary along time. This phenomenon is represented in Droop model [13] where the nitrogen/carbon quota in the biomass is a new variable denoted q. Then, the growth rate does not depend on the extracellular substrate concentration s, but on the internal quota q. By denoting $Q = qx$ the total nitrogen in the biomass (grams of algal nitrogen per liter), the model writes:

$$\begin{cases} \dot{s} &= Ds_{in} - Ds - \rho(s)x \\ \dot{Q} &= \rho(s)x - DQ \\ \dot{x} &= \mu(q)x - Dx \end{cases} \tag{2.3}$$

By a simple computation $\left(\dot{q} = \frac{\dot{Q}}{x} - q\frac{\dot{x}}{x}\right)$ we obtain another formulation for this model:

$$\begin{cases} \dot{s} &= Ds_{in} - Ds - \rho(s)x \\ \dot{q} &= \rho(s) - \mu(q)q \\ \dot{x} &= \mu(q)x - Dx \end{cases} \tag{2.4}$$

This model is satisfactory when growth rate has no light dependence, but must be changed if light varies and if the microorganisms are affected by this light variation.

In order to produce energy from microalgae, since the light conversion yield is lower than 20% [7], electric energy cannot reasonably be used as a source of light. Thus, the sun is the only sustainable energy source to support microalgal growth. Since light varies along the day-night cycle, it will affect photosynthesis and thus microalgal growth. More precisely, when considering a photobioreactor or a raceway to grow outdoor microalgae, the following aspects must be taken into account:

- when biomass is high the light is attenuated by pigments (mainly chlorophyll);
- under this condition, respiration is not negligible and must be considered;
- high light intensities lead to a photoinhibition which decreases the growth rate;
- Microalgae photoacclimate to light intensity: they adapt their chlorophyll to the incident flux of photons. As a consequence, the chlorophyll/carbon ratio varies with light intensity in the photobioreactor, and is linked to the nitrogen/carbon ratio.

For the optimization works presented in this thesis (chapter 3), we needed a model that would take all these phenomena into account, while being simple enough to be validable, identifiable, and to allow a mathematical analysis. The photobioreactor models encountered in literature did not meet these criteria [40, 39], so we had to build our own model. In particular, the models developed in [34, 5] were too complex for identification and mathematical analysis. In the following we present a new photobioreactor model, based on Droop's formulation, and called Droop Photobioreactor Model (DPM). It contains the main Droop's ingredients, as well as the light effect, auto shading by the microalgal population and photoacclimation mechanisms.

Finally, we need a lipid synthesis model for assessing lipid productivity. This model, developped in cooperation with the biologists of the Laboratoire d'Océanographie de Villefranche-sur-mer, represents lipid and sugar synthesis, as well as a functionnal carbon pool. Its singularity is that lipids are accumulated during nitrate stresses (for example in the final stationnary phase of a batch culture), whereas the lipid/carbon quota decreases under nitrate limitation in a continuous culture at equilibrium. The sugar/carbon quota at equilibrium increases with increasing nitrate concentration in the medium. Finally, the functionnal carbon pool is constitued of all the remaining carbon. The variables of this model can be added to the Droop model, as presented in the paper, or to the DPM model.

Modelling planar photobioreactors in nitrogen limited conditions

Olivier Bernard[a,*], Francis Mairet[a], Pierre Masci[a], Antoine Sciandra[b]

[a] *COMORE-INRIA, BP93, 06902 Sophia-Antipolis Cedex, France*
[b] *LOV, UMR 7093, Station Zoologique, B.P. 28 06234, Villefranche-sur-mer, France*

Abstract

Oleaginous microalgae are seen as a potential major biofuel producer in the future since, under conditions of nitrogen deprivation, they can contain high amounts of lipids. In order to optimize productivity in a microalgal production system (including open raceways and closed photobioreactors), we develop a new model to predict biomass dynamics in conditions of nitrogen limitation and light gradient. On the basis of the Droop model, we represent light influence, and then we relate the chlorophyll content to the nitrogen cell quota, for a given photoacclimation light. In a second step, we compute the light distribution thanks to a Beer-Lambert law. It results in a model where biology (microalgal growth in nitrogen limited conditions) and physics (radiative transfer) are strongly coupled. Dynamical photoacclimation to light variation is the key biological phenomenon that couples these two aspects. The mathematical complexity is kept at a minimal level so that the model calibration is rather straightforward. The model is assessed with experimental data of *Isochrysis galbana* under light/dark cycles. This model shows that, when averaged along photobioreactor depth, the photoinhibition feature of a microalgal species may apparently disappear while photoinhibition reduces overall productivity. The proposed model can be the basis for research of working conditions which optimize biomass or lipid productivity.

Key words: Microalgae, modelling, photoacclimation, photoinhibition, nitrogen limitation, photobioreactor, biofuel

Autotrophic microalgae and cyanobacteria use photons as energy source to fix carbon dioxide (CO_2). These microorganisms have recently received a specific at-

*Olivier Bernard
BP93, 06902 Sophia-Antipolis, France
Tel:+33 492 387 785
Fax:+33 492 387 858
Email: olivier.bernard@inria.fr

tention in the framework of renewable energy. Their high actual photosynthetic yield compared to terrestrial plants (whose growth is limited by CO_2 availability) leads to large potential algal biomass productions of several tens of tons per hectare and per year (Chisti, 2007). After a nitrogen starvation, some oleaginous microalgal species can reach a very high lipid content (up to 80% of dry weight (Metting, 1996)). These possibilities have led some authors to consider that microalgae could be one of the main biofuel sources in the future (Huntley and Redalje, 2007; Chisti, 2007). Lipid can be extracted from the biomass to produce biodiesel (Huntley and Redalje, 2007), while anaerobic digestion of the residual biomass (Chisti, 2007; Sialve et al., 2009) can generate methane.

On top of this, the ability of microalgae to fix CO_2 in a controlled way has recently involved them in the race for mitigation systems (Benemann, 1997; Olaizola, 2003). Thus microalgal biofuel production systems could be associated to industrial power plants with a high CO_2 production. In the same spirit, microalgae could be used to consume inorganic nitrogen and phosphorus, and thus avoid expensive wastewater treatment plants.

These advantages put microalgae in a good position for renewable energy production at large scale (Chisti, 2007). This means that, in the coming years, there might be industrial plants to produce microalgae dedicated to energy production. However, the culture of algae is not straightforward and suffers from many limitations (Pulz, 2001; Carvalho et al., 2006). In this article we will consider planar microalgal production systems including open raceways and closed photobioreactors, which will be called photobioreactors (PBR) for sake of brevity. We will assume that microalgal growth is not limited by inorganic carbon availability, and thus that light and inorganic nitrogen are driving microalgal kinetics.

Extensive microalgae production in PBR is a complex process that should be strongly monitored and optimized through on-line control algorithms. In this objective, a model is a powerful tool to support an automatic control strategy. Several PBR models exist, especially to deal with light transfer properties in the culture medium (Suh and Lee, 2003; Pottier et al., 2005; Franco-Lara et al., 2006), but none of them considered the microalgal kinetics in condition of nutrient limitation and none of them deal with photoacclimation.

In the specific case of biodiesel production, nitrogen starvation is known to increase the lipid content of phytoplankton (Spoehr and Milner, 1949; Rodolfi et al., 2009; Pruvost et al., 2009). But, it also strongly affects the pigment composition and concentration (Turpin, 1991; Geider et al., 1996; Sciandra et al., 1997; Stramski et al., 2002; Geider et al., 1998), which modifies the radiative transfer properties in the culture medium (Stramski et al., 2002). The objective of our modelling approach is to propose a new model that can predict the behaviour of a PBR characterized by varying irradiance gradient and nitrogen availability, which

are both conditions susceptible of modifying pigment concentrations.

The targeted model must keep a level of complexity compatible with the requested mathematical analyses necessary for deriving optimal control algorithms. We will thus consider the simplest model that contains the elements to reproduce both the ability of microalgae to adapt their pigments to a given irradiance (photoacclimation) (Anning et al., 2000; MacIntyre et al., 2002) and the reduction of the cell pigment contents in case of nitrogen limitation (Laws and Bannister, 1980; Sciandra et al., 2000). The basis of our development is Droop model (Droop, 1968, 1983) which has been deeply investigated (Lange and Oyarzun, 1992; Bernard and Gouzé, 1995, 2002; Vatcheva et al., 2006) and proved to accurately reproduce situations of nitrogen limitations (Droop, 1983; Sciandra and Ramani, 1994; Bernard and Gouzé, 1999) in constant light conditions. A link between cellular nitrogen and chlorophyll will then be introduced, so that, for a planar geometry, a simplified irradiance distribution model within the reactor can be proposed.

The paper is organized as follows. In a first part, we recall Droop model. Then we introduce the light influence in this model. In a third part we propose a model to infer chlorophyll concentrations. Finally the radiative transfer is examined, and the photoacclimation equation is proposed. The model is then validated using data from *Isochrysis galbana* light/dark cultures.

1. Recall and presentation of Droop model

Droop model, initially established to represent the effect of B_{12} Vitamin internal quota on the growth rate of phytoplankton (Droop, 1968), has been shown appropriate to represent also the effect of macronutrients, such as nitrogen, on growth rate (Droop, 1983). Contrarily to Monod model in which the growth is related to the limiting substrate external concentration (s), Droop model considers that nutrient uptake and growth are uncoupled processes. Growth of the biomass (expressed in carbon and denoted x) is thus assumed to be related to the nitrogen cell concentration for nitrogen limited microalgae. The intracellular nitrogen cell concentration, or quota (q), is defined by the amount of limiting element per biomass unit. The model equations, in a chemostat with dilution rate D and influent inorganic nitrogen (nitrate or ammonium) concentration s_{in} writes:

$$\begin{cases} \dot{s} = Ds_{in} - \rho(s)x - Ds \\ \dot{q} = \rho(s) - \mu(q)q \\ \dot{x} = \mu(q)x - Dx \end{cases} \tag{1}$$

In this model the absorption rate $\rho(s)$ and the growth rate $\mu(q)$ are generally

taken as Michaelis-Menten and Droop functions:

$$\begin{aligned} \rho(s) &= \rho_m \frac{s}{s+K_s} \\ \mu(q) &= \bar{\mu}(1-\frac{Q_0}{q}) \end{aligned} \tag{2}$$

where K_s is the half saturation constant for substrate uptake, associated with the maximum uptake rate ρ_m. Parameter $\bar{\mu}$ is defined as the growth rate at hypothetical infinite quota, while Q_0 is the minimal nitrogen cell quota for which no algal growth can take place. This model is more accurate than Monod model for algal growth modelling (Vatcheva et al., 2006), but it is more complex and has been less studied from a mathematical point of view. Droop model is however sufficiently simple to allow a detailed mathematical analysis (Lange and Oyarzun, 1992; Bernard and Gouzé, 1995, 2002; Vatcheva et al., 2006), and link the model parameters to measurable quantities.

Property 1. *Droop model guarantees that internal quota stays between two bounds:*

$$Q_0 \leq q \leq Q_m \tag{3}$$

Where

$$Q_m = Q_0 + \frac{\rho_m}{\bar{\mu}} \tag{4}$$

represents the maximum cell quota obtained in conditions of non limiting nutrient. The growth rate is also bounded :

$$0 \leq \mu(q) \leq \mu_m = \frac{\rho_m}{Q_0\bar{\mu}+\rho_m}\bar{\mu} \tag{5}$$

where μ_m is the maximum growth rate reached in non limiting conditions.

Proof: See *e.g.* (Bernard and Gouzé, 1995).
As a corollary of this property, most of Droop model parameters can be straightforwardly identified from the measurements of the internal quota during nonlimited growth (for which $\mu(Q_m) = \mu_m$) and at the end of a batch phase, when growth rate becomes zero for a minimal value of the quota $q = Q_0$. The internal quota in nonlimited growth conditions (when $q = Q_m$) together with the maximum growth rate provides then the values of $\bar{\mu}$ and ρ_m:

$$\rho_m = \mu_m Q_m \text{ and } \bar{\mu} = \mu_m \frac{Q_m}{Q_m - Q_0} \tag{6}$$

Parameter K_s can be deduced (together with another estimate of ρ_m) from a batch experiment where the disappearance of inorganic nitrogen is measured together with algal biomass.

Droop model has been widely validated (Droop, 1983; Sciandra and Ramani, 1994; Bernard and Gouzé, 1999; Vatcheva et al., 2006). However, it cannot directly be used in the case of PBR for two main reasons:

- In its rough form it does not include the irradiance effect.
- It does not account for light gradient due to the cell density in the PBR

2. Improvement of Droop model to deal with light limitation

2.1. Inorganic carbon uptake rate

Droop model does not take irradiance into account. Including light is however not straightforward. A first approach consists in representing the light effect through $\bar{\mu} = \bar{\mu}(I)$ (Han, 2001):

$$\mu(q, I) = \bar{\mu}(I)(1 - \frac{Q_0}{q}) \tag{7}$$

where we use, depending on the species, two possible expressions for $\bar{\mu}(I)$. For the species that do not photoinhibit, we use a simple kinetic (Han, 2001):

$$\bar{\mu}^a(I) = \tilde{\mu}^a \frac{I}{I + K^a_{sI}} \tag{8}$$

Parameter K^a_{sI} refers to the half saturation coefficient with respect to light, and $\tilde{\mu}^a$ is the hypothetical maximal growth rate without photoinhibition.

This simple expression will be used as a first approximation for species whose photoinhibition is limited. With this simplified point of view the computation stays tractable and it leads to the model denoted ($\mathcal{S}^a$) . However, we will also consider the more complex model of Eilers and Peeters (1988, 1993):

$$\bar{\mu}^b(I) = \tilde{\mu} \frac{I}{I + K^b_{sI} + \frac{I^2}{K^b_{iI}}} \tag{9}$$

Here an inhibition coefficient K^b_{iI} is considered, together with parameter K^b_{sI}, they define the light intensity $I_{\text{opt}} = \sqrt{K^b_{sI} K^b_{iI}}$ for which $\bar{\mu}^b(I)$ is maximal. Parameter $\tilde{\mu}^b$ is the hypothetical growth rate at non limiting irradiance and without inhibition.

It is well known that, for eukaryotic microalgae, the initial slope of a photosynthesis irradiance (P-I) curve normalized with Chl *a* does not depend on the light at which cells have been photoadapted (MacIntyre et al., 2002). This can be observed on Figure 1 for the diatom *Skeletenonema costatum*. In mathematical terms, this property constraints the model in the sense that the parameter α^{Chl},

defined by the initial slope of the curve $\mu(I)/\theta$ has to be independent of the ratio $\theta = \text{Chl/x}$. Parameter α^{Chl} can be computed from equation (9):

$$\alpha^{\text{Chl}} = \frac{\tilde{\mu}}{\theta K_{sI}^b} \tag{10}$$

To ensure that α^{Chl} is a constant, it implies that K_{sI}^b has to be computed from θ as follows:

$$K_{sI}^b = K_{sI}^*/\theta \tag{11}$$

Indeed, with this expression, the initial slope of the inorganic carbon uptake rate normalized by chlorophyll is constant: $\alpha^{\text{Chl}} = \frac{\tilde{\mu}}{K_{sI}^*}$

A comparison of model given by equation (9) with the data of Anning et al. (2000) with the diatom *Skeletonema costatum* is presented figure 1. The data shows experiments where the cells have been photoadapted at a low irradiance ($I_L = 50\mu mol.m^{-2}.s^{-1}$) and at a high irradiance ($I_H = 1200\mu mol.m^{-2}.s^{-1}$). Model (9) together with equation (11) turns out to accurately represent these data.

When considering equation (9), we denote ($\mathcal{S}^b$) the corresponding model.

2.2. Inorganic nitrogen uptake rate

When including light effect in the growth rate, the maximum inorganic nitrogen uptake rate must be adapted to limit cell quota increase. Indeed, with Droop model, when keeping a constant maximum uptake rate, equation 4 becomes:

$$Q_m(I) = Q_0 + \frac{\rho_m}{\bar{\mu}(I)} \tag{12}$$

Then, during night periods, $\bar{\mu}(0) = 0$ and thus equation (12) would lead to an infinite maximal quota. Indeed, with such a formulation no growth occurs at night, so that the substrate can be indefinitely taken up into the cell without being consumed for growth. If an increase of the maximum cell quota in the absence of light is possible (Laws and Bannister, 1980), obviously it cannot become infinite.

We impose therefore, in line with Geider et al. (1998), that the uptake rate stops as cells become replete:

$$\rho(s,q) = \bar{\rho}\frac{s}{s+K_s}(1 - q/Q_l) \tag{13}$$

where parameter $Q_l > Q_0$ is the maximal internal quota in dark conditions.

2.3. Model synthesis

Finally we consider a respiration term. As in Geider et al. (1998), we assume that the rate of nitrogen loss (due both to mortality and excretion) is the same than the respiration rate.

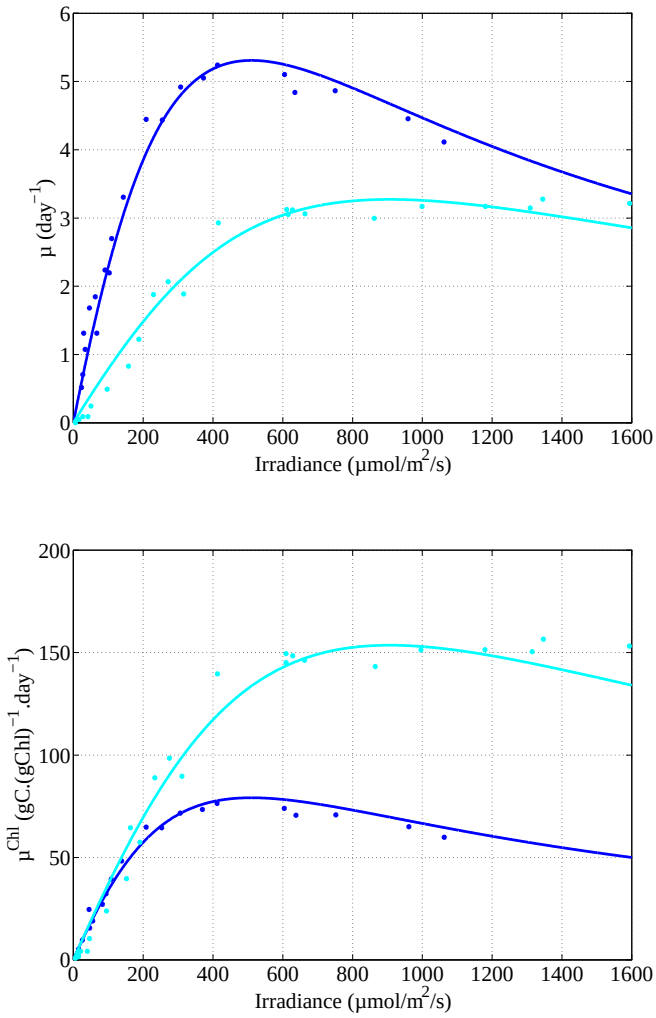

Figure 1: Model and data of the photosynthetic response of the diatom *Skeletenonema costatum* grown at low ($I_L = 50\mu mol.m^{-2}.s^{-1}$, dark points and lines) and at a high irradiance ($I_H = 1200\mu mol.m^{-2}.s^{-1}$, light grey points and lines) (Anning et al., 2000). The top graph is normalized with carbon and the lower graph is normalized by chlorophyll.

It leads to the following model including irradiance:

$$(\mathcal{S}^{a,b}) \begin{cases} \dot{s} = Ds_{in} - \bar{\rho}\frac{s}{s+K_s}(1 - q/Q_l)x - Ds \\ \dot{q} = \bar{\rho}\frac{s}{s+K_s}(1 - q/Q_l) - \bar{\mu}(I,\theta)(q - Q_0) \\ \dot{x} = \bar{\mu}(I,\theta)(1 - \frac{Q_0}{q})x - Dx - Rx \end{cases} \tag{14}$$

If $\bar{\mu}$ is represented with equation (8), it leads to model $(\mathcal{S}^a)$. If expression (9) is used for $\bar{\mu}$, we end up with model $(\mathcal{S}^b)$.

Now, with uptake rate (13), it is straightforward to show that the absence of light prevents growth, but that the maximum cell quota is lower than parameter Q_l:

Property 2. *The internal quota for models $(\mathcal{S}^a)$ and $(\mathcal{S}^b)$ stays between two bounds:*

$$Q_0 \leq q \leq Q_m(I) \leq Q_l \tag{15}$$

In model $(\mathcal{S}^a)$, where $\bar{\mu}$ does not depend on θ, the maximum quota, in nutrient replete conditions, can be explicitly computed: $Q_m(I) = \frac{\bar{\rho}+\bar{\mu}(I)Q_0}{\bar{\rho}+\bar{\mu}(I)Q_l}Q_l$. In these conditions, the associated maximum growth rate at irradiance I is now given by :

$$0 \leq \mu(q, I) \leq \mu_m(I) = \bar{\mu}(I)(1 - \frac{Q_0}{Q_m(I)}) \tag{16}$$

Proof: If $q = Q_l$, then $\dot{q} \leq 0$ so the nitrogen quota is bounded by Q_l.
Moreover, the quota equation in conditions of abundance of nutrients ($\bar{\rho}\frac{s}{s+K_s} \simeq \bar{\rho}$) for model $(\mathcal{S}^a)$ becomes:

$$\dot{q} = \bar{\rho}(1 - q/Q_l) - \bar{\mu}(I)(q - Q_0) = (\bar{\mu}(I) + \frac{\bar{\rho}}{Q_l})(Q_m(I) - q) \tag{17}$$

where

$$Q_m(I) = \frac{\bar{\rho} + \bar{\mu}(I)Q_0}{\bar{\rho} + \bar{\mu}(I)Q_l}Q_l \tag{18}$$

It is thus clear from (17) that q tends towards $Q_m(I)$ at a rate $(\bar{\mu}(I) + \frac{\bar{\rho}}{Q_l})$.

Note that $Q_m(I)$ as defined by equation (18) varies oppositely to $\bar{\mu}(I)$. It means that, for non-inhibiting irradiances, the maximum cell quota decreases with irradiance as observed by Laws and Bannister (1980) and Pawlowski (2004).

2.4. Relationship between chlorophyll and particulate nitrogen

The chlorophyll concentration must be represented in the model in order to predict the light field throughout the PBR. In a spirit of keeping the model very simple, we assume that chlorophyll is proportional to the cellular proteins, and thus to particulate nitrogen xq (Laws and Bannister, 1980; Pawlowski, 2004). More specifically, for a culture photoacclimated at an irradiance I^*, we have:

$$\mathrm{Chl} = \gamma(\mathrm{I}^\star)\mathrm{xq} \tag{19}$$

where

$$\gamma(I^\star) = \gamma_{max}\frac{k_{I^*}}{I^\star + k_{I^*}} \tag{20}$$

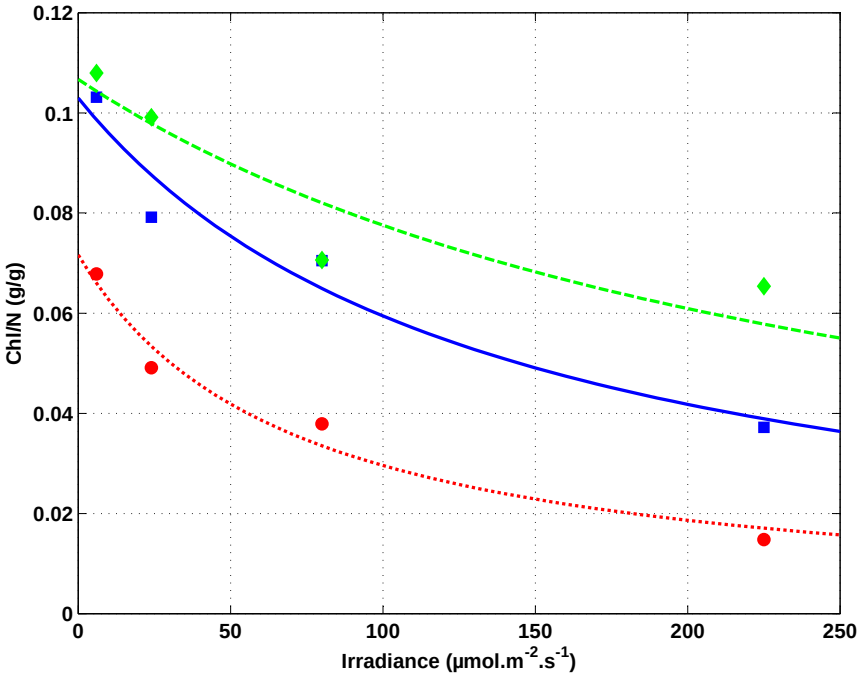

Figure 2: Chlorophyll *a* over particulate nitrogen for various light conditions under nutrient replete conditions for *Chaetoceros simplex* (blue line and square), *Phaeodactylum tricornutum* (red dash-dotted line and circle) and *Dunaliella tertiolecta* (green dashed line and diamond) (data from Thompson et al. (1990)).

This expression results from experimental observations of photoadapted cultures obtained at various irradiance and nitrogen conditions. Figure 2 presents three light limited data sets (Thompson et al., 1990) which support this relationship for batch cultures of *Chaetoceros simplex*, *Phaeodactylum tricornutum* and *Dunaliella tertiolecta*.Figure 3 shows data for continuous cultures of *Rhodomonas salina* at equilibrium, with various levels of nitrogen limitation (*i.e.* dilution rates) and various light intensities. The proposed relationship accurately represents the chlorophyll per unit of algal nitrogen.

One of the key originality of the proposed model is that we introduce a conceptual variable, denoted $I^\star$, which is the irradiance at which the cells are photoacclimated. Of course, for steady state cultures in a light homogeneous (low biomass density) PBR, this variable is exactly the irradiance I. For denser cultures at steady state it includes the effect of hydrodynamics through the light gradient which generates a succession of high (close to the lighten surfaces) and low irradiance (Pottier et al., 2005). After an irradiance shift from I_1 to I_2, since

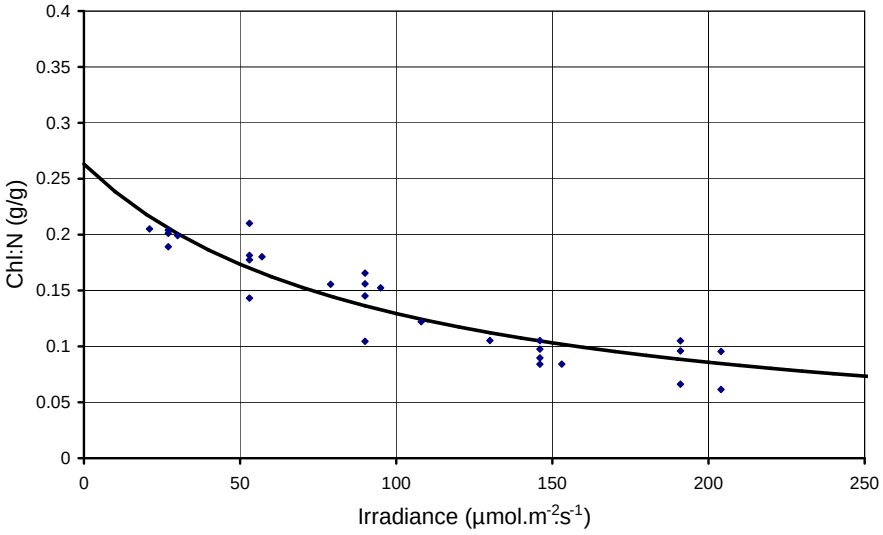

Figure 3: Representation of the ratio Chlorophyll *a* over particulate nitrogen for various light conditions for *Rhodomonas salina* with different levels of nitrogen limitation (data from Pawlowski (2004)).

photoacclimation is not instantaneous, the photoacclimation light $I^\star$ will move from I_1 to I_2, with a delay. To represent this light adaptation dynamics, we use the following formulation:

$$\dot{I}^\star = \delta\mu(q, I)(\bar{I} - I^\star) \tag{21}$$

where $\bar{I}$ is the average irradiance in the PBR. Nevertheless, a more subtle computation of $\bar{I}$ can be envisaged considering the hydrodynamics of the PBR. For sake of simplicity, we assume that the chlorophyll adaptation rate is proportional to the growth rate (with a factor δ). Note that this choice ensures that the adaptation rate stops during the night.

3. Dealing with light gradient in the PBR

3.1. Average light

We investigate here a simple representation of light attenuation inside a PBR of thickness L, due to high biomass. We consider a planar geometry with a light

source perpendicular to the PBR plane, so that irradiance distribution in the PBR can be represented with a good accuracy by a Beer-Lambert exponential decrease. Note that this approach can also describe the behavior of a high rate raceway pond. We assume that pigment concentrations are proportional to chlorophyll concentration (which is the main pigment), so that the light decrease rate is linearly correlated to chlorophyll concentration. When I_0 is the irradiance at the surface, we have thus, for a PBR where cells are photoacclimated at light $I^\star$:

$$I(z) = I_0 e^{-\xi z} \tag{22}$$

where the light attenuation coefficient ξ is linearly related to chlorophyll a: $\xi = a\mathrm{Chl} + \mathrm{b}$. As a consequence, from equation (19), we have: $\xi = a\gamma(I^\star)qx + b$.

This light attenuation coefficient is used to compute the optical depth $\lambda = \xi L$. λ is a key parameter of PBR performance as it reflects how efficiently light energy is absorbed.

$$\frac{I(L)}{I_0} = e^{-\lambda} \tag{23}$$

The average irradiance received by the cell culture between depth 0 and L is therefore:

$$\bar{I} = \frac{I_0}{L}\int_0^L e^{-\xi z} dz = \frac{I_0}{\lambda}[1 - e^{-\lambda}] \tag{24}$$

Note that this Beer-Lambert approximation could be improved by using more accurate radiative transfer models which would take the detailed pigment composition into account (Pottier et al., 2005; Pruvost et al., 2006), provided that we can predict this pigment composition at any time.

Remark: In order to get a more workable equation, we may replace (24) by a rational expression with equivalent behaviour:

$$\bar{I} \simeq I_0 \frac{K_g}{\lambda + K_g} \tag{25}$$

with $K_g = 1.25$. This expression is a good approximation of (24) since $\frac{1-e^{-x}}{x} \simeq \frac{K_g}{K_g+x}$.

3.2. Average growth rate

Now a key computation must be done to assess the average growth rate in the PBR. Indeed, Pottier et al. (2005) showed that an accurate way of estimating the

growth rate consists in computing the average value of $\bar{\mu}(I(z))$ through the light gradient:

$$\bar{\bar{\mu}}(I_0) = \frac{1}{L}\int_0^L \bar{\mu}(I(z))dz \tag{26}$$

Property 3. *The average growth rate is* $\mu(I_0, q, \xi) = \bar{\bar{\mu}}(I_0, \xi)(1 - \frac{Q_0}{q})$ *with, for model* ($\mathcal{S}^a$)*:*

$$\bar{\bar{\mu}}^a(I_0, \xi) = \tilde{\mu}\frac{1}{\lambda}\ln\left(\frac{I_0 + K_{sI}^a}{I_0 e^{-\lambda} + K_{sI}^a}\right) \tag{27}$$

and for model ($\mathcal{S}^b$)*, considering that* $K_{iI}^b < 2K_{sI}^b$*:*

$$\bar{\bar{\mu}}^b(I_0, \xi) = \tilde{\mu}\frac{2K_{iI}^b}{\lambda\sqrt{\Delta}}\arctan\left(\frac{I_0(1 - e^{-\lambda})\sqrt{\Delta}}{2I_0^2 e^{-\lambda} + I_0(1 + e^{-\lambda})K_{iI}^b + 2I_{\text{opt}}^2(\theta)}\right) \tag{28}$$

where $\Delta = 4I_{\text{opt}}^2(\theta) - K_{iI}^{b2}$*. The function* $\bar{\bar{\mu}}^b(I_0)$ *is an increasing function of* I_0 *up to an irradiance* $\tilde{I}_0 = I_{\text{opt}}(\theta)e^{\lambda/2}$*, and is then decreasing after* ($I_{\text{opt}}(\theta)$ *is the irradiance providing maximal rate of photosynthesis, as given by equation (9)).*

Proof: This results from straightforward computation based on the fact that, for a planar geometry:

$$\bar{\bar{\mu}}^b(I_0) = \frac{1}{L}\int_0^L \tilde{\mu}\frac{K_{iI}^b I_0 e^{-\xi z}}{K_{iI}^b I_0 e^{-\xi z} + I_{\text{opt}}^2(\theta) + I_0^2 e^{-2\xi z}}dz \tag{29}$$

with the variable change $v = I_0 e^{-\xi z}$, we get $dv = -\xi v dz$, and

$$\bar{\bar{\mu}}^b(I_0) = -\frac{\tilde{\mu}K_{iI}^b}{\lambda}\int_{I_0}^{I_0 e^{-\lambda}} \frac{1}{v^2 + K_{iI}^b v + I_{\text{opt}}^2(\theta)}dv = -\frac{2\tilde{\mu}K_{iI}^b}{\lambda\sqrt{\Delta}}\left[\arctan(\frac{2v + K_{iI}^b}{\sqrt{\Delta}})\right]_{I_0}^{I_0 e^{-\lambda}} \tag{30}$$

Remark: Property 3 shows that a PBR with high biomass or large thickness won't show any inhibition behaviour. Indeed, this is clear for model ($\mathcal{S}^a$) where $\bar{\bar{\mu}}^a$ is an increasing saturating function of I_0. But, even if we consider species with strong photoinhibition (case of model $\mathcal{S}^b$) the maximum of $\bar{\bar{\mu}}^b$ is reached at a value $\tilde{I}_0 = I_{\text{opt}}(\theta)e^{\lambda/2}$ which is much higher than $I_{\text{opt}}(\theta)$ when the optical depth λ is larger than 3 (*i.e.* when more than 95% of light is absorbed in the PBR). Figure 4 illustrate this, considering values of λ ranging from 0 (limit case where no shading effect occurs) to 10 (obtained when light is completely attenuated by a high biomass or a large reactor thickness). It results that the behaviour of high biomass density PBR can be approximated with a good accuracy with Michaelis-Menten type responses, and thus the PBR behaviour is equivalent to a $\mathcal{S}^a$ model. This can be explained by the fact that, for high density PBR, only the first few centimetres are photoinhibited, so that photoinhibition has a low weight in the averaging process.

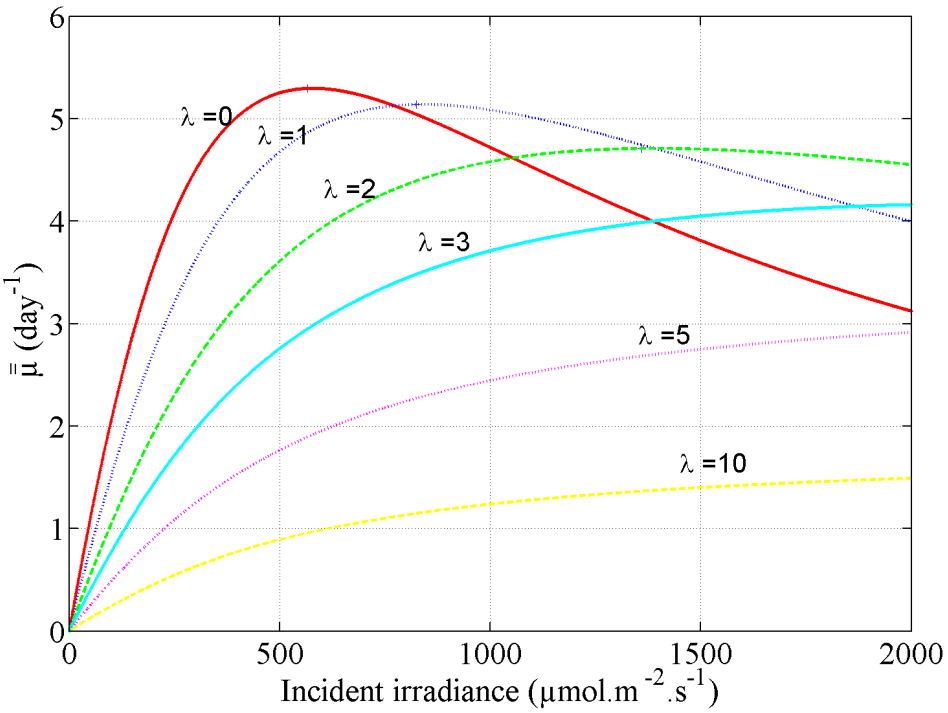

Figure 4: Average growth rate computed in the PBR with respect to influent light and optical depth λ.

4. Results and discussion

4.1. Synthesis: the nitrogen limited PBR model

Synthesising the developments of the previous sections, the resulting model in a light gradient field writes now, for an incident irradiance I_0:

$$(\mathcal{S}^{a,b}_{\text{PBR}}) \begin{cases} \dot{s} = Ds_{in} - \bar{\rho}\frac{s}{s+K_s}(1-q/Q_l)x - Ds \\ \dot{q} = \bar{\rho}\frac{s}{s+K_s}(1-q/Q_l) - \bar{\bar{\mu}}(I_0, I^\star, x, q)(q-Q_0) \\ \dot{x} = \bar{\bar{\mu}}(I_0, I^\star, x, q)(1-\frac{Q_0}{q})x - Dx - Rx \\ \dot{I}^\star = \bar{\bar{\mu}}(I_0, I^\star, x, q)(1-\frac{Q_0}{q})(\bar{I} - I^\star) \end{cases} \tag{31}$$

where the irradiance at which cells photoadapt can be, depending on the species, computed on the basis of the average irradiance $\bar{I} = I_0 \frac{K_g}{(a\gamma(I^\star)qx+b)L+K_g}$, or it can be computed from more subtle considerations, taking into account the PBR hydrodynamics.

The average growth function is given by equation (27) and (28) for models ($\mathcal{S}^a_{\text{PBR}}$) and ($\mathcal{S}^b_{\text{PBR}}$), respectively.

4.2. Model calibration

The way the model is designed makes its calibration rather straightforward. The idea is based on the fact that simpler models are easier to calibrate. The procedure thus consists in progressively improving the model accuracy by using the simple models calibration to initiate the identification of the more complex models, moving then from Droop model to the PBR model $\mathcal{S}^b_{\text{PBR}}$. The first step consists in calibrating the parameters of Droop model on the basis of Property 1. The observation of the nitrogen quota during phases of replete and depleted inorganic nitrogen in the culture gives an estimate of the minimal and maximal nitrogen quota of Droop model, and thus, using equations (4) and (6) together with an estimate of the (average) growth rate in conditions of nutrient repletion, we get parameters Q_0, ρ_m and $\bar{\mu}$. Parameter K_s is determined from additional uptake experiments. This first raw calibration of the Droop model is used as a first guess for the more detailed model parameters. Droop's parameter can now be seen as the average value of the detailed model. For example, the average value of $\bar{\bar{\mu}}()$ in the PBR model is $\bar{\mu}$ in Droop's model. The first guess of the PBR parameters are then chosen such that, taking into account the measured average light intensity and Chl:C ratio, we have:

$$\bar{\mu} = \frac{1}{T}\int_0^T \bar{\bar{\mu}}(I_0^\dagger, I^\star, x^\dagger, q^\dagger)d\tau \tag{32}$$

where the values with † are measurements. This approach, leads to a first sketch which generates simulation results improving Droop's predictions. A final refinement, where a least square quality criterion is minimised by Levenberg-Marquardt algorithm (function lsqcurvefit under Matlab®) produces the final values of the parameters.

Model is calibrated with the experimental data of Flynn et al. (1994) for *Isochrysis galbana* grown with ammonium in a batch PBR on a 12:12 light/dark cycle under incident illumination of 100 $\mu mol.m^{-2}.s^{-1}$. The resulting parameter values are given in table 1.

4.3. Model validation

Model simulations are shown on figure 5. The good adequation obtained with the experimental data illustrates the fact that the model calibration is rather straightforward. The model demonstrates a great ability to properly reproduce such data set. The simulations of particulate nitrogen seem to underestimate a bit the measured values. This results from a leak in the nitrogen balance, from the initial ammonium concentration to the final particulate nitrogen concentration.

Parameter	Value	Unit
$\tilde{\mu}$	1.7	day^{-1}
Q_0	0.050	gN. gC^{-1}
Q_l	0.25	gN.gC^{-1}
K^*_{sI}	1.4	$\mu\text{mol.m}^{-2}.s^{-1}$
K^b_{iI}	295	$\mu\text{mol.m}^{-2}.s^{-1}$
$\bar{\rho}$	0.073	$\text{gN.gC}^{-1}.\text{day}^{-1}$
K_s	0.0012	gN.m^{-3}
R	0.0081	day^{-1}
δ	1	–
γ_{max}	0.57	gChl.gN^{-1}
k_{I^*}	63	$\mu\text{mol.m}^{-2}.s^{-1}$
a	16.2	$\text{m}^2.\text{gChl}^{-1}$
b	0.087	m^{-1}

Table 1: Parameter values used for the simulation of the PBR model

This experimental imbalance in the nitrogen may also have impacted the accuracy on the chlorophyll *a*.

These results can be compared with the simulation results obtained by Smith and Yamanaka (2007) that use both biological models of Geider et al. (1998) and of Pahlow (2005), where the light distribution was added as an extra layer in the model. Our model prediction is of comparable quality, while it explicitly represents the coupling between microalgae physiology and light transfer properties on the PBR.

4.4. discussion

Light heterogeneity in the medium induces a complex photoacclimation process resulting from both a negative and a positive feedback. After an incident light shift, the biomass concentration increases and so do the pigments in the medium. It results in reducing the range of average light increase compared to the incident light shift. This negative feedback is completed by a positive feedback, since photoacclimation to a higher irradiance leads to a reduction of the pigment content and thus a higher light penetration. This shows that modelling is the only possibility to quantitatively describe the dynamics in a high density PBR. This is all the more crucial since microalgae are necessarily in a permanent dynamical regime induced by the daily light variations. As a consequence, such model is necessary to extrapolate from the cell characteristics to photobioreactor behaviour. It can also help in assessing and optimising the biomass productivity in outdoor conditions, which are the conditions for autotrophic biofuel production.

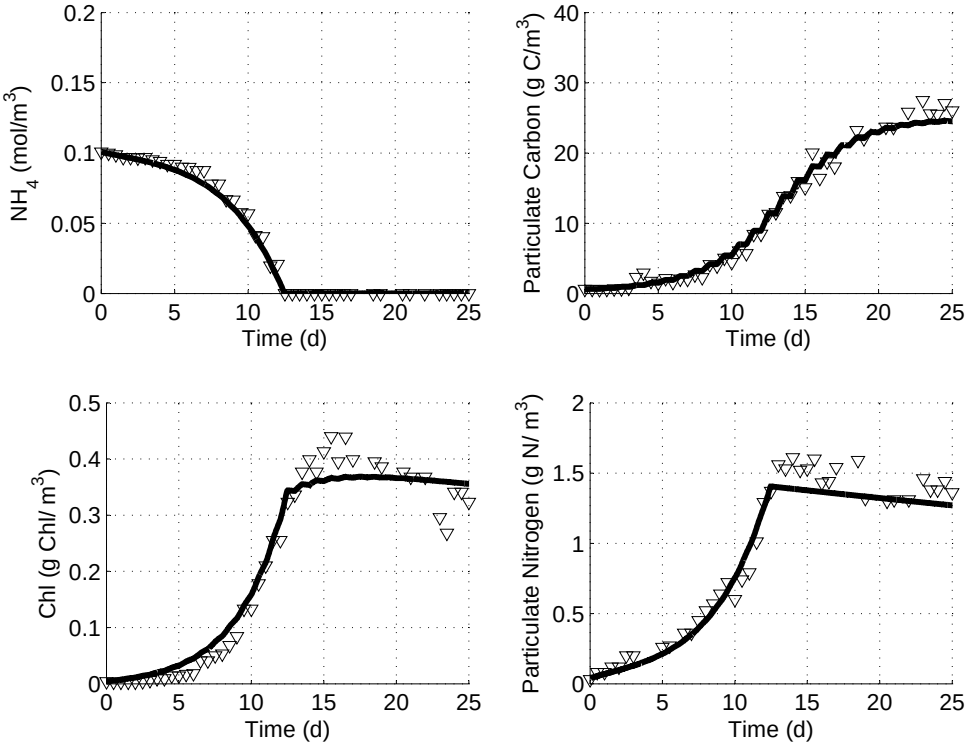

Figure 5: Simulation of the PBR model and comparison with experimental data from Flynn et al. (1994).

Beyond the prediction capacity of our model, under dynamical variations induced by the daily light variation, our approach explains a key point: for high density cultures, there is no apparent photoinhibition. This does not mean that algae do not photoinhibit, but it means that, because of averaging along the reactor depth, photoinhibition is not revealed by a standard production versus light intensity study. However photoinhibition must be avoided, since it results in a hidden loss of productivity that can be evaluated from the decreased apparent averaged maximum growth rate. Figure 4 also reveals that, for a given light intensity, there is an optimal optical depth that leads to the optimum average growth rate.

5. Conclusion

The proposed dynamical model integrates the light gradient in the PBR in order to represent the coupling between microalgal growth and radiative transfer

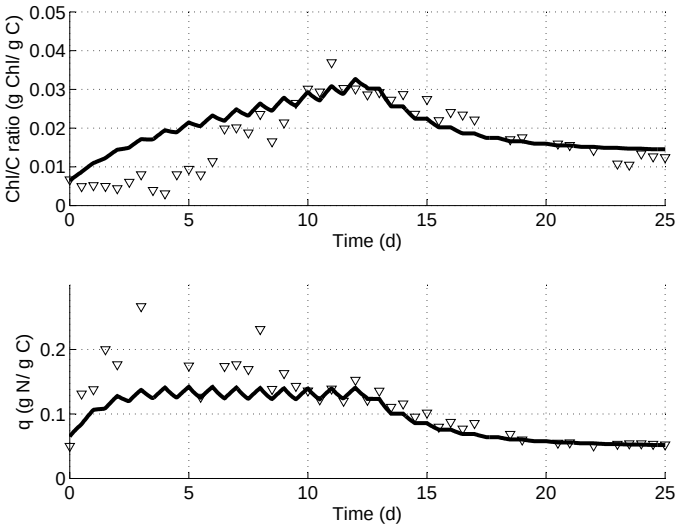

Figure 6: Simulation of the PBR model and comparison with experimental quota from Flynn et al. (1994).

properties. Dynamical photoacclimation to light variation is the key phenomenon which couples these two aspects.

When coupled with a lipid production model (Mairet et al., Submitted), this PBR model could predict the overall lipid productivity and guide the optimisation resulting from the trade-off between lipid content (enhanced by nitrogen deprivation) and growth (reduced by nitrogen deprivation)(Rodolfi et al., 2009). A lipid photobioreactor model is then the next step towards optimisation of lipid productivity under dynamical light regime.

Acknowledgements: This paper presents research results supported by the ANR-06-BIOE-014 Shamash project.

References

Anning, T., MacIntyre, H., Pratt, S., Sammes, P., Gibb, S., Geider, R., DEC 2000. Photoacclimation in the marine diatom Skeletonema costatum. Limnology and Oceanography 45 (8), 1807–1817.

Benemann, J., 1997. Co2 mitigation with microalgae systems. Energy Conversion and Management, 475–479.

Bernard, O., Gouzé, J. L., 1995. Transient Behavior of Biological Loop Models, with Application to the Droop Model. Mathematical Biosciences 127 (1), 19–43.

Bernard, O., Gouzé, J.-L., 1999. Nonlinear qualitative signal processing for biological systems: application to the algal growth in bioreactors. Math. Biosciences 157, 357–372.

Bernard, O., Gouzé, J.-L., 2002. Global qualitative behavior of a class of nonlinear biological systems: application to the qualitative validation of phytoplankton growth models. Artif. Intel. 136, 29–59.

Carvalho, A., Meireles, L., Malcata, F., 2006. Microalgal reactors: A review of enclosed system designs and performances. Biotechnology Progress 22(6), 1490–1506.

Chisti, Y., 2007. Biodiesel from microalgae. Biotechnology Advances 25, 294–306.

Droop, M. R., 1968. Vitamin B12 and marine ecology. IV. the kinetics of uptake growth and inhibition in *Monochrysis lutheri*. J. Mar. Biol. Assoc. 48 (3), 689–733.

Droop, M. R., 1983. 25 years of algal growth kinetics, a personal view. Botanica marina 16, 99–112.

Eilers, P., Peeters, J., 1988. A model for the relationship between light intensity and the rate of photosynthesis in phytoplankton. Ecological modelling 42 (3-4), 199–215.

Eilers, P., Peeters, J., SEP 1993. Dynamic behavior of a model for photosynthesis and photoinhibition. Ecological modelling 69 (1-2), 113–133.

Flynn, K., Davidson, K., Leftley, J., 1994. Carbon-nitrogen relations at whole-cell and free amino-acid levels, during batch growth of isochrysis galbanna (prymnesiophyceae) under conditions of alternating light and dark. Mar. Biol. 118, 229–237.

Franco-Lara, E., Havel, J., F, F., D, D. W.-B., 2006. Model-supported optimization of phototrophic growth in a stirred-tank photobioreactor. Biotech. Bioeng. 95, 1177–1187.

Geider, R., MacIntyre, H., Kana, T., 1996. A dynamic model of photoadaptation in phytoplankton. Limnol Oceanogr 41, 1–15.

Geider, R., MacIntyre, H., Kana, T., 1998. A dynamic regulatory model of phytoplanktonic acclimation to light, nutrients, and temperature. Limnol Oceanogr 43, 679–694.

Han, B., 2001. Photosynthesis-irradiance response at physiological level: A mechanistic model. J Theor Biol 213, 121–127.

Huntley, M., Redalje, D., 2007. Co2 mitigation et renewable oil from photosynthetic microbes: A new appraisal. Mitigation et Adaptation Strategies for Global Change 12, 573 – 608.

Lange, K., Oyarzun, F. J., 1992. The attractiveness of the Droop equations. Mathematical Biosciences 111, 261–278.

Laws, E., Bannister, T., 1980. Nutrient- and light-limited growth of thalassiosira fluviatilis in continuous culture, with implications for phytoplankton growth in the ocean. Limnol Oceanogr 25, 457–473.

MacIntyre, H., Kana, T., Anning, T., Geider, R., 2002. Photoacclimation of photosynthesis irradiance response curves and photosynthetic pigments in microalgae and cyanobacteria. Journal of Phycology 38 (1), 17–38.

Mairet, F., Bernard, O., Masci, P., Lacour, T., Sciandra, A., Submitted. Modelling neutral lipid production by the microalga *Isochrysis affinis galbana* under nitrogen limitation.

Metting, F., 1996. Biodiversity and application of microalgae. Journal of Industrial Microbiology & Biotechnology 17, 477 – 489.

Olaizola, M., 2003. Commercial development of microalgal biotechnology: from the test tube to the marketplace. Biomolecular Engineering 20, 459–466.

Pahlow, M., 2005. Linking chlorophyll-nutrient dynamics to the Redfield N : C ratio with a model of optimal phytoplankton growth. marine ecology-progress series 287, 33–43.

Pawlowski, L., 2004. Modélisation de l'incorporation du carbone photosynthétique en environnement marin contrôlé par ordinateur. Ph.D. thesis, Université Pierre et Marie Curie, Paris VI.

Pottier, L., Pruvost, J., Deremetz, J., Cornet, J.-F., Legrand, J., Dussap, C., 2005. A fully predictive model for one-dimensional light attenuation by chlamydomonas reinhardtii in a torus photobioreactor. Biotechnology and Bioengineering 91, 569–582.

Pruvost, J., Pottier, L., Legrand, J., 2006. Numerical investigation of hydrodynamic and mixing conditions in a torus photobioreactor. Chemical Engineering Science 61, 4476–4489.

Pruvost, J., Van Vooren, G., Cogne, G., Legrand, J., 2009. Investigation of biomass and lipids production with neochloris oleoabundans in photobioreactor. Biores. Technol. 100, 5988–5995.

Pulz, O., 2001. Photobioreactors: production systems for phototrophic microorganisms. Applied Microbiology et Biotechnology 57, 287–293.

Rodolfi, L., Zittelli, G. C., Bassi, N., Padovani, G., Biondi, N., Bonini, G., Tredici, M. R., JAN 1 2009. Microalgae for Oil: Strain Selection, Induction of Lipid Synthesis and Outdoor Mass Cultivation in a Low-Cost Photobioreactor. Biotechnol. Bioeng. 102 (1), 100–112.

Sciandra, A., Gostan, J., Collos, Y., Descolas-Gros, C., Leboulanger, C., Martin-Jézéquel, V., Denis, M., Lefèvre, D., C. Copin, C., Avril, B., 1997. Growth compensating phenomena in continuous cultures of *Dunaliella tertiolecta* limited simultaneously by light and nitrate. Limnol. Oceanogr. 46, 1325–1339.

Sciandra, A., Lazzara, L., Claustre, H., Babin, M., 2000. Responses of the growth rate, pigment composition and optical properties of cryptomonas sp. to light and nitrogen stresses. Mar. Ecol. Prog. Ser. 201, 107–120.

Sciandra, A., Ramani, P., 1994. The limitations of continuous cultures with low rates of medium renewal per cell. J. Exp. Mar. Biol. Ecol. 178, 1–15.

Sialve, B., Bernet, N., Bernard, O., 2009. Anaerobic digestion of microalgae as a necessary step to make microalgal biodiesel sustainable. Biotech. Advances 27 (4), 409–416.

Smith, S. L., Yamanaka, Y., 2007. Optimization-based model of multinutrient uptake kinetics. Limnology and Oceanography 52 (4), 1545–1558.

Spoehr, H. A., Milner, H. W., 1949. The chemical composition of *chlorella*: effect of environmental conditions. Plant Physiol. 24, 120 – 149.

Stramski, D., Sciandra, A., Claustre, H., 2002. Effects of temperature, nitrogen, and light limitation on the optical properties of the marine diatom thalassiosira pseudonana. Limnol. Oceanogr. 47, 392–403.

Suh, I., Lee, S., 2003. A light distribution model for an internally radiating photobioreactor. Biotech. Bioeng. 82, 180–189.

Thompson, P. A., Harrison, P. J., Whyte, J. N. C., 1990. Influence of irradiance on the fatty acid composition of phytoplankton. Journal of Phycology 26, 278–288.

Turpin, D., 1991. Effects of inorganic n availability on algal photosynthesis and carbon metabolism. J Phycol 27, 14–20.

Vatcheva, I., deJong, H., Bernard, O., Mars, N., 2006. Experiment selection for the discrimination of semi-quantitative models of dynamical systems. Artif. Intel. 170, 472–506.

Modelling lipid production in microalgae

Francis Mairet * **Olivier Bernard** * **Pierre Masci** *
Thomas Lacour ** **Antoine Sciandra** **

* *COMORE-INRIA, BP93, 06902 Sophia-Antipolis Cedex, France (e-mail: olivier.bernard@inria.fr).*
** *LOV, UMR 7093, BP28, 06234 Villefranche-sur-mer, France*

Abstract: Microalgae offer potentially great opportunities for producing biofuel. In order to optimize triglyceride production, this article proposes a dynamical model of microalgal lipid production. In this model, intracellular carbon is divided between a functional pool and two storage pools (sugars and neutral lipids). The various intracellular carbon flows between these pools lead to a complex dynamic with a strong discrepancy between accumulation and reuse of neutral lipids. This generates an hysteresis which has been observed experimentally. The model has been validated with experiments of *Isochrysis affinis galbana* (T. iso) culture under different nitrogen limitation conditions.

Keywords: phytoplankton, growth model, nitrogen starvation, neutral lipid, biofuel

1. INTRODUCTION

Various photosynthetic microorganisms (microalgae or cyanobacteria) have shown an ability to synthesize and accumulate considerable amounts of lipids [Chisti 2007]. Indeed, the photosynthetic yield of these microorganisms (abusively gathered under the name "microalgae") is higher than for terrestrial plants whose growth is limited by CO_2 availability. Its leads to algal biomass productivities of several tens of dry biomass tons per hectare and per year [Huntley and Redalje 2007]. When combined with a high neutral lipid content [Metting 1996], microalgae can potentially produce biofuel in a range of magnitude higher than for terrestrial plants. This potential has led some authors to consider that microalgae could be one of the main biofuel producers in the future [Huntley and Redalje 2007, Chisti 2007].

However, the culture of algae is not straightforward and suffers from many limitations [Pulz 2001, Carvalho et al. 2006]. For example, a nitrogen limitation increases the cell lipid content but it also strongly affects the growth rate. The lipid productivity, which is the consequence of these two factors, needs a trade off between biomass production and oil content.

The main objective of this work is to propose a new model for lipid production under nitrogen stress which will guide the research of an optimisation strategy. The model must thus find a trade off between realism, in order to accurately represent the key variables of the process, and simplicity so that it can be mathematically tractable and suitable to solve optimal control problems. The simplest model for describing growth of a population of microalgae limited by a nutrient (*e.g.* nitrogen or phosphorus) is the Droop model [Droop 1968, 1983]. This models assumes that the growth rate depends on the internal concentration of the limiting element. More accurate models have been proposed to deal with the coupling between nitrogen and carbon assimilation in various light conditions [Geider et al. 1998, Faugeras et al. 2004, Pahlow 2005]. However none of these models predicted the lipid concentration and, to our knowledge, the model which is presented in this work is the first dealing with neutral lipid production by microalgae. The main objective of this dynamical model is to identify conditions that optimise the lipid synthesis.

The article is structured as follows: after a material and methods section, the model assumptions are detailled and then the resulting model equations are presented. Then, we describe the calibration procedure and we compare the model with experimental data of a *Isochysis galbana* culture, with different nitrogen limitations. Finally, a section is devoted to the analysis of the model behavior.

2. MATERIAL AND METHODS

2.1 Culturing device

Cultures of *Isochrysis affinis galbana*, (clone T-iso) were grown in 5 l cylindrical vessels at constant temperature ($22.5°C$), ligth ($430 \pm 30\,\mu mol.m^{-2}.s^{-1}$ in the centre of the culture vessel) and pH (maintained at 8.0 by automatic injection of CO_2). The experiment consists in imposing nitrogen limitation through a succession of dilution rates changes followed by transient periods to reach the equilibrium. Finally, dilution was stopped to obtain a nitrogen starvation. Figure 1 presents the operating conditions.

2.2 Measurements

The following measurements were performed: nitrate concentrations (Technicon Auto-analyser), biovolumes (optical particle counter Hiac/Royco), concentrations of particulate carbon and nitrogen (CHN analyser, PerkinElmer), total carbohydrates concentrations (by the phenol method), and neutral lipid (column chromatography on silica gel, Extract-Clean, Alltech). A correlation between biovolume measurements and particulate carbon is used to convert

the biovolume measurements into particulate carbon. An imbalance in the total observed nitrogen concentration was punctually observed. We therefore excluded observations of particulate nitrogen for any time at which this nitrogen imbalance was greater than $0.3\,mgN/L$. An estimation of particulate nitrogen from the nitrogen balance is used in this case. Carbohydrates and neutral lipid measurements are converted in $g[C]$ using average values of conversion. For more details on the experiment protocol see Le Floc'h et al. [2002].

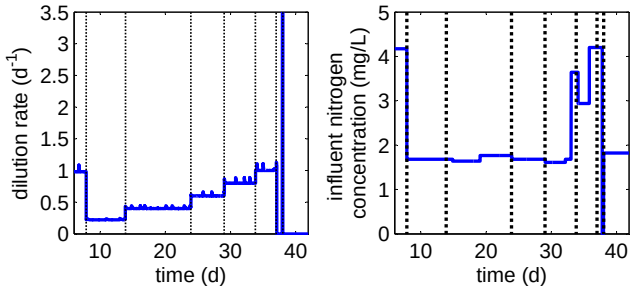

Fig. 1. Operating conditions for experiment with T-iso. Dilution rate variations impose various nitrogen limitations.

3. MODEL DESIGN

3.1 Variables and reaction network

Our objective is to propose a simple model which can support control approach an optimisation algorithm. It must therefore keep a minimal level of complexity to be mathematically tractable. We have therefore limited the number of variables to the most important ones. We focus on the growth of microalgae, whose biomass, in terms of organic carbon, is denoted x. These microalgae are limited by an inorganic nitrogen source (nitrate, denoted s).In line with Ross and Geider [2009], we consider that organic carbon can be split into functional and storage pools. The functional compartment (f) includes the biosynthetic apparatus (proteins and nucleic acids) and the stuctural material (membranes mainly made of glycolipids and phospholipids). Contrarily to Ross and Geider [2009], we add a new distinction: the storage pool is divided into a sugar reserve compartment (g) and a neutral lipid reserve compartment (l).

Nutrient uptake and biomass growth are known to be uncoupled processes for microalgae [Droop 1983, Geider et al. 1998] leading thus to variations in the internal quota of nutrient.

Nutrient is taken up by the microalgae to make cellular nitrogen (n) at rate $\rho(s)$. This flux of nitrogen can be summarized in the following macroscopic reaction which represents the mass flux between the inorganic and organic compounds:

$$s \xrightarrow{\rho(s)x} n \tag{1}$$

The absorption rate $\rho(s)$ is taken as Michaelis-Menten function:

$$\rho(s) = \rho_m \frac{s}{s + K_s} \tag{2}$$

whith K_s the half-saturation constant for the substrate and ρ_m the maximum uptake rate.

In line with Droop model philosophy, we consider that the specific growth rate μ, *i.e.* the net incorporation of CO_2 is an increasing function of the internal quota of nutrient ($q_n = \frac{n}{x}$). We assume that inorganic carbon is first incorporated in the pool of sugars g:

$$CO_2 \xrightarrow{\mu(q_n)x} g \tag{3}$$

This macroscopic reaction summarizes the set of reactions that occur in the dark phase of photosynthesis, and that lead, through the Calvin cycle to the production of carbohydrates such as glucose 6-phosphate. The mathematical expression for the specific growth rate μ is chosen using Droop model:

$$\mu(q_n) = \bar{\mu}(1 - \frac{Q_0}{q_n}) \tag{4}$$

where $\bar{\mu}$ and Q_0 represent the theoretical maximum growth rate and the minimum nitrogen quota allowing growth, respectively.

The sugar compartment g is then used in a second stage to synthesize the functional elements of the biomass f :

$$g \xrightarrow{\alpha\rho(s)x} f \tag{5}$$

This reaction corresponds to the synthesis of proteins and nucleic acids, which depends on nitrogen availability. We therefore consider as in Ross and Geider [2009] that the synthesis rate is proportional to the nitrogen assimilation rate .

The sugar compartment g is also used in a competitive pathway to synthesize neutral lipid (*i.e.* mainly triglycerides) :

$$g \xrightarrow{\beta q_n \mu(q_n)x} l \tag{6}$$

We assume that this rate of sugar mobilization depends on the photosynthesis rate $\mu(q_n)$, but that it is modulated by the nitrogen carbon. This assumption is based on the work of Sukenik and Livne [1991] who have observed the dependence of lipid production on the growth rate in T-iso cultures.

These neutral lipids are then mobilized to the production of functional carbon (mainly membranes):

$$l \xrightarrow{\gamma\rho(s)x} f \tag{7}$$

The rate of this reaction is assumed to be proportional to the synthesis of proteins and nucleic acids (reaction 5).

A representation of the carbon flows is given on Fig.2. Note that it is a rather strong simplification of the complex metabolism of the cell. Thus, reaction 6 can be decomposed in two steps with the formation of fatty acids as intermediate. These fatty acids can be used directly to synthetize structure (reaction 7). As "free" fatty acids can not be stored in the cell [Ohlrogge and Browse 1995, Guschina and Harwood 2009], neutral lipids are used to store or to

provide fatty acids when there is a disequilibrium between fatty acid synthesis and consumption [Thompson-Jr 1996]. Nevertheless, as fatty acid pool is of negligible size, we do not represent its dynamic in order to keep a low level of model complexity.

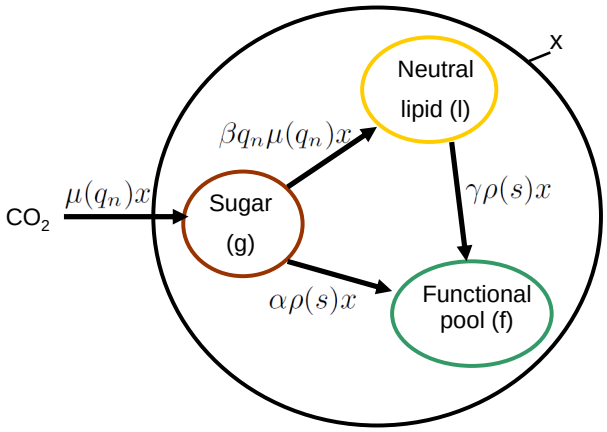

Fig. 2. Representation of the carbon flows. The dynamic of neutral lipids results from the unbalance between lipid synthesis and mobilization.

3.2 Model equations

Assuming that the main mass transfer of carbon and nitrogen can be summarized by the reactions (1) to (7), the time-varying evolution equations resulting from mass balances considerations [Bastin and Dochain 1990] in a continuously stirred homogeneous photobioreactor are given by:

$$\begin{cases} \dot{s} = Ds_{in} - \rho(s)x - Ds \\ \dot{n} = \rho(s)x - Dn \\ \dot{g} = (1 - \beta q_n)\mu(q_n)x - \alpha\rho(s)x - Dg \\ \dot{l} = \beta q_n \mu(q_n)x - \gamma\rho(s)x - Dl \\ \dot{f} = (\alpha + \gamma)\rho(s)x - Df \end{cases} \tag{8}$$

Where D is the dilution rate (ratio of the influent flow rate over the photobioreactor volume) and s_{in} the influent nitrate concentration.

From equations (8), we can deduce the dynamics of the quota of nitrogen q_n, the carbon biomass $x = c + g + l$, and the fractions of neutral lipid $q_l = l/x$ and functional carbon $q_f = f/x$, leading to the following set of equations:

$$\begin{cases} \dot{s} = Ds_{in} - \rho(s)x - Ds \\ \dot{q_n} = \rho(s) - \mu(q_n)q_n \\ \dot{x} = \mu(q_n)x - Dx \\ \dot{q_l} = (\beta q_n - q_l)\mu(q_n) - \gamma\rho(s) \\ \dot{q_f} = -q_f\mu(q_n) + (\alpha + \gamma)\rho(s) \end{cases} \tag{9}$$

It is worth noting that the first 3 equations of system (9) are *exactly* the Droop model [Droop 1968, 1983]. This model presents the advantage of being simple and having been extensively validated [Droop 1983, Sciandra and Ramani 1994, Bernard and Gouzé 1999]. The system has a cascade structure: the dynamics of the fractions q_l and q_f do not influence the kinetics of the biomass.

4. MODEL CALIBRATION

4.1 Parameter computation

First, we present some model properties that will be used to identify the parameter values. We take benefit of the Droop model which has been widely studied.

In the Droop model, it can be proved (see Bernard and Gouzé [1995]) that the nitrogen quota stays between two bounds:

$$Q_0 \leq q_n \leq Q_m \tag{10}$$

with

$$Q_m = Q_0 + \frac{\rho_m}{\bar{\mu}} \tag{11}$$

Q_m represents the maximum cell quota obtained in conditions of non limiting nutrients, and the minimum quota, Q_0, is obtained in batch conditions after nutrient depletion. Thus, we can deduce a maximal growth rate μ_m:

$$\mu_m = \mu(Q_m) = \bar{\mu}(1 - \frac{Q_0}{Q_m}) \tag{12}$$

This property will be used to compute $\bar{\mu}$, from the minimal and maximal nitrogen quota Q_0 and Q_m:

$$\bar{\mu} = \mu_m \frac{Q_m}{Q_m - Q_0} \tag{13}$$

In order to compute steady states for the fractions of neutral lipid q_l^* and functional carbon q_f^*, the dynamics of q_l and q_f in (9) can be rewritten:

$$\begin{cases} \dot{q_l} = [(\beta - \gamma)q_n - q_l]\,\mu(q_n) - \gamma\dot{q_n} \\ \dot{q_f} = [(\alpha + \gamma)q_n - q_f]\,\mu(q_n) + (\alpha + \gamma)\dot{q_n} \end{cases} \tag{14}$$

At steady state, as $\dot{q_n} = 0$, we obtain the following equilibrium:

$$\begin{cases} q_l^* = (\beta - \gamma){q_n}^* \\ q_f^* = (\alpha + \gamma){q_n}^* \end{cases} \tag{15}$$

The model predicts thus, at steady state, that neutral lipid and functional carbon quotas are proportional to the nitrogen quota. Steady state of the sugar fraction q_g^* is deduced from the relation $q_l + q_f + q_g = 1$:

$$q_g^* = 1 - (\beta + \alpha){q_n}^* \tag{16}$$

As both $q_l^*(q_n)$ and $q_f^*(q_n)$ are linear increasing functions, $q_g^*(q_n)$ is a linear decreasing function.

Parameters α, β and γ can then be computed from the previous equations, using steady state measurements.

4.2 Parameter estimation

We have decoupled the estimation into two groups of parameters: the Droop parameters (Q_0, $\bar{\mu}$, ρ_m, K_s) and the intracellular carbon flow parameters (α, β, and γ). The Droop parameters can be easily determined, on the basis of dedicated experimental conditions. Then, the carbon parameters are identified using steady state observations.

The minimal nitrogen quota Q_0 is obtained from the nitrogen quota measurement during nitrate starvation (at the end of the experiment). The maximum nitrogen quota Q_m and specific growth rate μ_m are estimated directly from the nitrogen quota measurements and the dilution rate during non-limited growth (see Fig. 3). The maximal absorption rate ρ_m and growth parameter $\bar{\mu}$ were obtained with relations (11) and (13). The half-saturation constant $K_s = 0.018\, mg[N]/L$ is taken from previous experiments (data not shown).

The second step of the calibration procedure concerns the intracellular carbon flow parameters. The data obtained at steady state for the several dilution rates are used to determine, thanks to equations (15), the parameters α, β, and γ. Using an estimation of the slopes of $q_l^*(q_n)$ and $q_f^*(q_n)$ lines, we obtain a system of two equations with three unknown parameters. We have therefore one freedom degree to fit the transient behavior of the model to the data using a minimization algorithm.

The results of the calibration are given in table 1.

Table 1. Parameters obtained by the calibration of the model

Parameter	Value
Minimal nitrogen quota Q_0	0.05 $mg[N].mg[C]^{-1}$
Maximal nitrogen quota Q_m	0.11 $mg[N].mg[C]^{-1}$
Maximal growth rate μ_m	1 d^{-1}
Protein synthesis coefficient α	2.9 $mg[C].mg[N]^{-1}$
Fatty acid synthesis coefficient β	3.75 $-$
Fatty acid mobilisation coefficient γ	2.0 $mg[C].mg[N]^{-1}$
Half-saturation constant K_s	0.018 $mg[N].L^{-1}$
Theoretical maximum growth rate $\bar{\mu}^\dagger$	1.83 d^{-1}
Maximal uptake rate $\rho_m{}^\dagger$	0.11 $mg[N].mg[C]^{-1}.d^{-1}$

† : Parameters computed from Q_0, Q_m and μ_m

5. SIMULATION AND COMPARISON WITH EXPERIMENTAL DATA

Continuous culture of T-iso is used in order to assess the ability of the model to reproduce experimental data. Results shown in Fig. 3 demonstrate that the model reproduces quite accurately the dynamics of s, q_n and x. This corroborates the fact that the Droop model has been widely validated [Droop 1983, Sciandra and Ramani 1994, Bernard and Gouzé 1999] for its aptitude to predict both biomass and remaining inorganic nitrogen. The simulated intracellular carbon distribution between sugar, neutral lipid and functional pool also accurately follows the experimental records (Fig. 4).

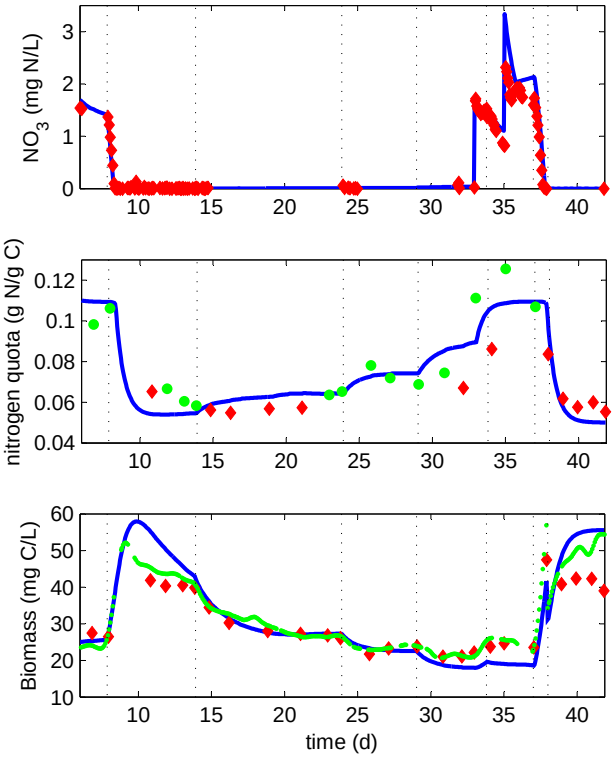

Fig. 3. Comparison of the Droop model with the data of T-iso culture under various nitrogen conditions. Nitrogen quota is directly measured (red diamond) or estimated from nitrogen balance (green circle). Carbon biomass is measured (red diamond) and deduced from biovolume measurements (green circle). Vertical lines indicate dilution rate changes.

6. ANALYSIS OF THE MODEL BEHAVIOR

In this section, we analyse the behavior of the model compared with the experimental data in order to explain the complex dynamic of neutral lipid quota.

6.1 Steady state

Equation (15) shows that the neutral lipid is proportional to the nitrogen quota in stabilized culture. This result is validated with the experimental data (see Fig. 5). The steady states obtained in chemostat mode through the various dilution rates indeed show that the lipid quota at equilibrium is proportional to the nitrogen quota.

6.2 Unbalanced conditions

Let us consider a situation where the cells are in a steady state given by a high nitrogen content q_{n1}^*. If the dilution rate is decreased, the cells should undergo a decrease of their nitrogen quota down to a value $q_{n2}^* < q_{n1}^*$. This means that, during this transient, we have $\dot{q_n} < 0$. Using equation of $\dot{q_l}$ in (14), the dynamic of $z = q_l - (\beta - \gamma)q_n$ is:

$$\dot{z} = -z\mu(q_n) - \beta\dot{q_n} \tag{17}$$

As z is initialy null, z remains nonnegative during this transient so that q_l is above the line of equation $q_l = (\beta -$

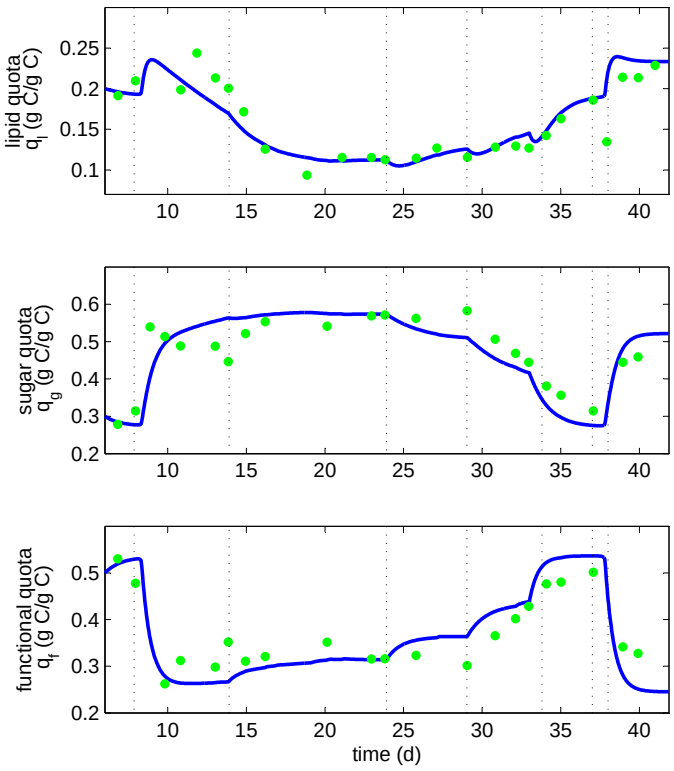

Fig. 4. Comparison of the lipid model with the data of T-iso culture under various nitrogen conditions. Evolution of the intracellular carbon quotas. Vertical lines indicate dilution rate changes.

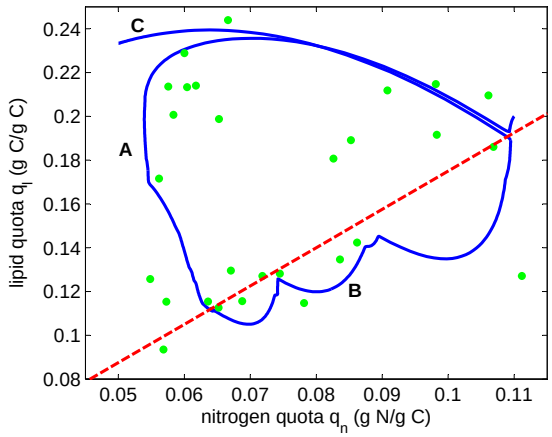

Fig. 5. The dependence of neutral lipid quota q_l on nitrogen quota q_n. Red dashed line represents model equilibrium line. A: transient decrease of q_n, B: transient increase of q_n, C: transient decrease of q_n until growth stops (nitrogen starvation).

$\gamma)q_n$, which is indeed the steady state line. Once the nitrogen quota has reached its steady state value, we have $\dot{q_n} = 0$. It follows that z tends toward zero and q_l finally reaches its steady state on the line $q_l^* = (\beta - \gamma){q_n}^*$.

Note that this behaviour is possible only since $\mu(q_n)$ is not zero, and is decreasing from $\mu(q_{n1})$ down to $\mu(q_{n2}) > 0$.

This transient behaviour of q_l is observed on Fig.4. During this transient, the neutral lipid mobilisation decreases faster than its synthesis which explains transient increase of neutral lipid quota.

6.3 Hysteresis behaviour

The same reasoning can describe the behaviour of the lipid content, when the internal nitrogen quota is increased (following for example an increase in the dilution rate). In such a case, we can show that q_l will increase under the line $q_l = (\beta - \gamma)q_n$. This behavior leads to a phenomenon of hysteresis experimentally observed: the trajectory between two steady states for an increase in nitrogen limitation is very different from this of a decrease in nitrogen limitation (see Fig. 5).

6.4 Nitrogen starvation

In a case of nitrogen starvation (*i.e.* $s = 0$), the steady state value of q_l can be computed, when q_n decreases from Q_m down to Q_0 as follows (see Appendix for details):

$$q_l^\dagger = Q_0 \left[(\beta - \gamma) + \beta \ln \left(\frac{Q_m}{Q_0} \right) \right] \tag{18}$$

If the parametric condition $\frac{\beta-\gamma}{\beta} < \frac{Q_0}{Q_m - Q_0} \ln\left(\frac{Q_m}{Q_0}\right)$ is verified, this expression shows that the final content of lipid after exhaustion of the nitrate is greater than $(\beta - \gamma)Q_m$, the maximum amount of lipid reached in balanced growth. With the computed parameters (Table 1), this condition is fulfilled. Nevertheless, it may be species dependent, meaning that for some species balanced growth may allow to reach higher lipid quota.
Nitrogen starvation at the end of the experiment confirms this result. A comparison between the nitrogen limitation at day 5 and the nitrogen starvation at day 38 is of particular interest. The model predicts that such a protocol should lead to radically different behaviour of neutral lipid fraction. In the nitrogen limitation, a new lower value of the lipid fraction should be reached after a transient increase, while the starvation should lead to an enhanced value of q_l, higher than the maximum obtained in balanced growth conditions. On the other side, the sugar fraction should increases in both situations. Fig. 4 and 5 show that these predictions are experimentally verified.

6.5 Consequences on neutral lipid productivity

This study emphasises that neutral lipid content at equilibrium is proportional to nitrogen quota. Therefore, it is worth noting that a continuous culture at low nitrogen quota leads to both a low growth rate and a low lipid fraction, and thus a weak productivity. However, a transient increase of lipid content is obtained when the nitrogen quota decreases (*i.e.* when there is a disequilibrium between carbon and nitrogen flows).
Finally, this study highlights the fact that the highest values of the neutral lipid content are obtained in two very different modes. Either after a nitrogen starvation,

or at maximum growth rate in non limiting conditions. This provides an hint to identify the optimal productivity conditions, which are probably a species dependent combination of these two working modes. The model simplicity will be the key point to make the optimisation study, from a mathematical point of view, tractable.

7. CONCLUSIONS

We have proposed a new model for neutral lipid production by microalgae. The strength of this model is to describe accurately both the steady state and the transient phases. The model catches the different dynamics encountered in various physiological conditions from low nitrogen limitation to starvation. The model, based on a Droop model principle, has a minimal degree of complexity so that it can be mathematical analysed. This models highlights and explains the phenomenon of hysteresis in neutral lipid production which has been experimentally verified.

The model must be assessed and validated with other microalgal species. This model will then be used to predict and optimize neutral lipid production in the perspective of large scale biofuel production. It may also endorse a model based closed loop control in order to on-line implement the optimal strategy [Mailleret et al. 2005].

REFERENCES

Bastin, G. and Dochain, D. (1990). *On-line estimation and adaptive control of bioreactors*. Elsevier, New York.

Bernard, O. and Gouzé, J.L. (1995). Transient Behavior of Biological Loop Models, with Application to the Droop Model. *Mathematical Biosciences*, 127(1), 19–43.

Bernard, O. and Gouzé, J.L. (1999). Nonlinear qualitative signal processing for biological systems: application to the algal growth in bioreactors. *Math. Biosciences*, 157, 357–372.

Carvalho, A., Meireles, L., and Malcata, F. (2006). Microalgal reactors: A review of enclosed system designs and performances. *Biotechnol Prog*, 22(6), 1490–1506.

Chisti, Y. (2007). Biodiesel from microalgae. *Biotechnology Advances*, 25, 294–306.

Droop, M.R. (1968). Vitamin B12 and marine ecology. IV. the kinetics of uptake growth and inhibition in *Monochrysis lutheri*. *J. Mar. Biol. Assoc.*, 48(3), 689–733.

Droop, M.R. (1983). 25 years of algal growth kinetics, a personal view. *Botanica marina*, 16, 99–112.

Faugeras, B., Bernard, O., Sciandra, A., and Levy, M. (2004). A mechanistic modelling and data assimilation approach to estimate the carbon/chlorophyll and carbon/nitrogen ratios in a coupled hydrodynamical-biological model. *Nonlinear Processes in Geophysics* , 11, 515–533.

Geider, R., MacIntyre, H., and Kana, T. (1998). "a dynamic regulatory model of phytoplanktonic acclimation to light, nutrients, and temperature. ". *Limnol Oceanogr*, 43, 679–694.

Guschina, I. and Harwood, J. (2009). *Algal Lipids and Effect of the Environment on their Biochemistry*. Springer New York.

Huntley, M. and Redalje, D. (2007). Co2 mitigation et renewable oil from photosynthetic microbes: A new appraisal. *Mitigation et Adaptation Strategies for Global Change*, 12, 573 – 608.

Le Floc'h, E., Malara, G., and Sciandra, A. (2002). An automatic device for in vivo absorption spectra acquisition in phytoplanktonic cultures: application to the study of photoadaptation to light and nutrient variations. *J. Applied Phycol.*, 14, 435–444.

Mailleret, L., Gouzé, J.L., and Bernard, O. (2005). Nonlinear control for algae growth models in the chemostat. *Bioprocess and Biosystem Engineering*, 27, 319–328.

Metting, F. (1996). Biodiversity and application of microalgae. *Journal of Industrial Microbiology & Biotechnology*, 17, 477 – 489.

Ohlrogge, J. and Browse, J. (1995). Lipid biosynthesis. *The Plant Cell*, 7, 957–9708.

Pahlow, M. (2005). Linking chlorophyllnutrient dynamics to the redfield n:c ratio with a model of optimal phytoplankton growth. *Mar Ecol Prog Ser*, 287, 33–43.

Pulz, O. (2001). Photobioreactors: production systems for phototrophic microorganisms. *Applied Microbiology et Biotechnology*, 57, 287–293.

Ross, O. and Geider, R. (2009). New cell-based model of photosynthesis and photo-acclimation: accumulation and mobilisation of energy reserves in phytoplankton. *Marine Ecology Progress Series*, 383, 53–71.

Sciandra, A. and Ramani, P. (1994). The limitations of continuous cultures with low rates of medium renewal per cell. *J. Exp. Mar. Biol. Ecol.*, 178, 1–15.

Sukenik, A. and Livne, A. (1991). Variations in lipid and fatty acid content in relation to acetyl coa carboxylase in the marine prymnesiophyte isochrysis galbana. *Plant Cell Physiol.*, 32, 371–378.

Thompson-Jr, G.A. (1996). Lipids and membrane function in green algae. *Biochimica et Biophysica Acta*, 1302, 17–45.

Appendix A. COMPUTATION OF FINAL LIPID QUOTA AFTER NITROGEN STARVATION

The dynamics of q_n and q_l, once external nitrate have been exhausted are:

$$\begin{cases} \dot{q_n} = -\mu(q_n)q_n \\ \\ \dot{q_l} = (\beta q_n - q_l)\mu(q_n) \end{cases} \tag{A.1}$$

Using these equations, the dynamic of $v = \frac{q_l}{q_n}$ is:

$$\dot{v} = \frac{q_n \dot{q_l} - q_l \dot{q_n}}{{q_n}^2} = -\frac{\beta}{q_n}\dot{q_n} \tag{A.2}$$

Integrating from t_1 to t_2, we obtain:

$$v_2 - v_1 = \int_{t_1}^{t_2} \dot{v}dt = \int_{q_{n1}}^{q_{n2}} -\frac{\beta}{q_n}dq = [-\beta \ln q_n]_{q_{n1}}^{q_{n2}} \tag{A.3}$$

Now consider a complete starvation from a non limited equilibrium,*i.e.* $q_{n1} = Q_m$, $q_{l1} = (\beta - \gamma)Q_m$, $q_{n2} = Q_0$ and $q_{l2} = q_l^\dagger$, the last expression becomes:

$$\frac{q_l^\dagger}{Q_0} - \frac{(\beta - \gamma)Q_m}{Q_m} = [-\beta \ln q_n]_{Q_m}^{Q_0} = \beta \ln \frac{Q_m}{Q_0} \tag{A.4}$$

From this equation, we can deduce the expression of $q_l^\dagger$.

Chapter 3

Model based productivity optimization

Productivity of a compound (biomass, oil, methane, ...) is the amount of this compound produced in the bioreactor per time unit (and possibly by reactor volume or surface). In this chapter, we focused on microalgae production, represented by the DPM model.

When we speak about productivity, it is important to say if we are speaking about volumetric productivity (grams per liter per day) or surface productivity (grams per square meters per day). When dealing with microalgae, we will be interested by surface productivity, as the sun delivers a given light energy per surface unit. What we want is to maximize the light energy converted into biomass per day.

When considering surface productivity, we consider a planar geometry with perpendicular light source. The depth of the culture will be W. We are interested in the quantity of microalgae per surface unit X, which is going to both use and attenuate light, and which can be computed with

$$X = xW$$

Based on the Droop Photobioreactor Model (presented in the last chapter), it is possible to compute analytically surface productivities in continuous (chemostat) culture.

In the papers presented here we answer rigorously the question "which controls ($D(t)$ and $s_{in}(t)$ values) induce maximal productivity?". For reaching this goal, our commands are the dilution rate D (input/output flow of water) and input substrate concentration s_{in}.

The first paper presents a study in a photobioreactor under constant light, at equilibrium. We consider the problem of surface productivity on a given production surface. The model is simplified by assuming that chlorophyll's photoadaptation dynamics reached its equilibrium.

The second paper proposes an optimization under day-night cycles. It uses Pontryagin's maximum principle. The complex mathematics involved led us to begin with volumetric productivity optimization, and with a simpler model assuming that microalgae are not substrate limited.

Microalgal biomass surface productivity optimization based on a photobioreactor model

Pierre Masci * **Frédéric Grognard** * **Olivier Bernard** *

* *INRIA- Project COMORE, 2004 route des lucioles, BP 93, 06902 Sophia Antipolis Cedex, FRANCE*
Tel: +33.4.92.38.78.72 (e-mail: pierre.masci@sophia.inria.fr, frederic.grognard@sophia.inria.fr, olivier.bernard@sophia.inria.fr).

Abstract: In this paper we predict and optimize the biomass surface productivity of microalgae in continuous culture under a constant light source. Surface biomass is identified as a key variable for assessing productivity: we provide both a mathematical and intuitive explanation. For reaching maximal productivities, biomass surface concentration must be such that growth at the culture bottom (assuming a planar geometry orthogonal to the light source) must be equal to respiration. Therefore the optimal biomass concentration depends both on the incident light and culture's depth. We then show how the chlorophyll/carbon ratio must also be carefully controlled to optimize light use in the photobioreactor. Finally, numerical results illustrate our theoretical approach.

Keywords: chemostat; microalgae; photobioreactor; model; light attenuation; productivity; biomass; optimization; continuous culture; bioenergy

1. INTRODUCTION

Microalgae cultures have recently received high attention in the frameworks of food supplements, pharmaceutic production (Spolaore et al., 2006), as well as CO_2 fixation and biofuel production (Huntley and Redalje, 2007; Chisti, 2007). Their high actual photosynthetic yield compared to terrestrial plants (whose growth is limited by CO_2 availability) leads to large potential algal biomass productions of several tens of tons per hectare and per year.

The objective of this paper is to give new insights in the optimization of microalgal biomass production. The key aspect when dealing with photobioreactor is the optimization of light use. The pigment concentration (mainly chlorophyll) affects the light distribution and use within the reactor, so that for too high biomass, light in the photobioreactor is strongly attenuated and growth is low. Moreover, in case of nitrogen depreciation (necessary to produce biofuel (Chisti, 2007)) the pigments are affected and decrease, which modifies light distribution.

In order to find a solution to this non intuitive optimization problem, analysis based on a modelling approach is required. In this paper, we base our approach on a simplified macroscopic photobioreactor model, dealing not only with light diffusion, but also with nitrogen use and nitrogen/carbon ratio variation. In order to perform this mathematical analysis we must use models that are simple so that they are mathematically tractable; we use a simplified version of the model proposed in (Bernard et al., 2009, Sub.). Our results are obtained at steady state, and we prove that these equilibria are achievable. From this model, it is shown mathematically that biomass surface concentration is the key parameter for surface productivity. Then global optimization is computed, and finally numerical results are presented.

The paper is structured as follows: first, we present the model dealing with both nitrogen limitation and light attenuation; then biomass concentration optimization is presented, followed by chlorophyll/carbon ratio optimization. A numerical result illustrates the approach. Finally, some ideas are given on how to choose the dilution rate in a continuous culture in order to maximize productivity.

2. A NEW DROOP PHOTOBIOREACTOR MODEL

2.1 Droop model presentation

We here focus on the growth of microalgae limited by inorganic nitrogen availability (provided by nitrate or ammonium), since such conditions are favourable for lipid production (Chisti, 2007) or other compounds such as astaxanthin (Aflalo et al., 2007). The Droop model (Droop, 1968, 1983) has been broadly used to take into account the ability of microalgae to uncouple substrate absorption and biomass (x) growth (Droop, 1968, 1983). The growth rate is assumed to depend on the internal quota (q) which, here, is the amount of intracellular nitrogen per biomass unit. This variable yield model writes thus:

$$\begin{cases} \dot{s} = Ds_{in} - \rho(s)x - Ds \\ \dot{q} = \rho(s) - \mu(q)q \\ \dot{x} = \mu(q)x - Dx \end{cases} \quad (1)$$

In this model the growth rate functions μ and absorption functions ρ are generally taken as Michaelis-Menten and

Droop functions:

$$\begin{aligned} \rho(s) &= \rho_m \frac{s}{s+K_s} \\ \mu(q) &= \bar{\mu}(1-\frac{Q_0}{q}) \end{aligned} \tag{2}$$

where ρ_m is the maximum uptake rate, K_s is the half saturation constant for substrate uptake, $\bar{\mu}$ is the hypothetical maximum growth rate (at infinite internal nitrogen quota) and Q_0 the minimal cell quota (below this level, no algal growth can take place).

It can be proved (Bernard and Gouzé, 1995) that the internal quota will stay between two bounds:

$$Q_0 \leq q \leq Q_m \tag{3}$$

Where $Q_m = Q_0 + \frac{\rho_m}{\bar{\mu}}$ represents the maximum cell quota obtained in conditions of non limiting nutrients.

The Droop model has been widely studied Bernard and Gouzé (1995, 2002) and validated (Sciandra and Ramani, 1994; Vatcheva et al., 2006). However, it cannot directly be used in the case of high density photobioreactors for two main reasons:

- In its rough form it does not include the effect of light intensity
- It does not account for the decrease of light due to the cell density

2.2 Adding light effect on growth

We first consider the case where light is homogeneous in the reactor, with an intensity I. In the next section we will consider the case with light attenuation in the reactor.

Light intensity has a direct effect on growth (photosynthesis), while nitrogen uptake can continue in the dark. Light can then be introduced into parameter $\bar{\mu} = \bar{\mu}(I)$ (Bernard et al., 2009, Sub.):

$$\mu(q,I) = \bar{\mu}(I)(1-\frac{Q_0}{q}) = \bar{\mu}\frac{I}{I+K_I}(1-\frac{Q_0}{q}) \tag{4}$$

where K_I is the light half saturation coefficient.

In order to prevent unrealistic quota increase in the dark, we use the down regulation mechanism proposed by Lehman et al. (1975):

$$\rho(s,q) = \rho_m \frac{s}{s+K_s}\frac{Q_l - q}{Q_l - Q_0} \tag{5}$$

with $Q_l > Q_0$: the uptake rate stops for replete cells $q = Q_l$.

We also add a constant respiration term r that applies to both nitrogen and carbon, so that the nitrogen/carbon ratio q is not affected:

$$\dot{x} = (\mu(q,I) - r - D)x$$

One can verify that the q equation does not change by adding this respiration term.

Finally, the model including light effect reads:

$$\begin{cases} \dot{s} = Ds_{in} - \rho_m \frac{s}{s+K_s}\frac{Q_l-q}{Q_l-Q_0}x - Ds \\ \\ \dot{q} = \rho_m \frac{s}{s+K_s}\frac{Q_l-q}{Q_l-Q_0} - \bar{\mu}\frac{I}{I+K_I}(q-Q_0) \\ \dot{x} = \bar{\mu}\frac{I}{I+K_I}(1-\frac{Q_0}{q})x - rx - Dx \end{cases} \tag{6}$$

In the next section, we will take into account the exponential light distribution within the reactor.

2.3 Light attenuation in the photobioreactor

Light is strongly attenuated by the biomass and its pigments in the photobioreactor. In this section we represent light distribution and its consequence on the growth rate. The biological and chemical concentrations are still assumed to be homogeneous within the photobioreactor.

We consider a planar geometry with perpendicular light source. For the sake of explanation simplicity we will consider a horizontal reactor and speak about "upper part" of the reactor on the side of incident light, and "reactor bottom" for the other side. However, our work is also valid for a vertical or diagonal geometry with perpendicular light source. The depth of the culture will be W.

At equilibrium, it has been shown (Bernard et al., 2009) that the chlorophyll concentration (Chl) is proportional to the nitrogen content:

$$Chl = \gamma(I^\star)qx$$

$\gamma(I^\star)$ is a chlorophyll to nitrogen ratio, depending on the light $I^\star$ at which the microalgae have been photoadapted. The photoadaptation mechanism is presented in Bernard et al. (Sub.), but it induces a significant complexity and will be neglected in this study. We thus consider that γ is a constant value which does not depend on light.

To model light attenuation we use a Beer-Lambert law, where the attenuation depends on the chlorophyll content:

$$I(q,xz) = I_0 e^{-a_i \gamma q x z} \tag{7}$$

where I_0 is the incident light, a_i is a light attenuation coefficient, and z is the depth, so that γqxz represents the chlorophyll per surface unit present above depth z.

From (7) we can compute the average irradiance received by the cell culture:

$$\begin{aligned} \bar{I} &= \frac{I_0}{W}\int_0^W e^{-a_i\gamma q x z}dz \\ &= \frac{I_0}{a_i\gamma q x W}\left(1-e^{-q_i\gamma q x W}\right) \end{aligned} \tag{8}$$

which decreases with γqx: this confirms the intuition that higher biomass or chlorophyll content leads to lower mean light in the reactor, due to stronger light attenuation.

In the reactor, growth rates vary with depth: in the upper part of the reactor, higher light causes higher growth than in the bottom part. The growth rate for a given depth z can be written:

$$\mu^z(q, I(q,xz)) = \bar{\mu}\frac{I(q,xz)}{I(q,xz)+K_I}(1-\frac{Q_0}{q}) \tag{9}$$

Then, we compute the mean growth rate in the reactor:

$$\mu(q,I_0,x) = \frac{1}{W}\int_0^W \mu^z(q,I(q,xz))dz$$

by the change of variable $\chi = xz$ it can be rewritten

$$\mu(q,I_0,x) = \frac{1}{xW}\int_0^{xW} \mu^z(q,I(q,\chi))d\chi \tag{10}$$

so that the mean growth rate depends on the surface biomass xW. It represents the total biomass present per

surface unit, and will be denoted $X = xW$. Finally, from (10), we compute the growth rate (now denoted $\mu(q, I_0, X)$ after a slight abuse of notation):

$$\mu(q, I_0, X) = \frac{\bar{\mu}(1-Q_0/q)}{a_i \gamma q X} \ln\left(\frac{I_0+K_I}{I_0 e^{-a_i \gamma q X}+K_I}\right) \quad (11)$$

which depends both on the surface biomass X and the nitrogen/carbon quota q, which is proportional to the chlorophyll/carbon quota at equilibrium. By construction μ is decreasing with X: the more surface biomass, the more light attenuation, so that mean growth rate in the reactor is lower. It is interesting to note that μ is increasing with q for low q values, and that it is decreasing with q for high q values: high chlorophyll concentrations lead to high light attenuation, so that mean growth in the reactor decreases.

It is also interesting to note that for a given q value, there is a maximal attainable biomass in the reactor, for which $\mu(q, I_0, X) = r$: if such a biomass is attained it cannot increase anymore due to respiration.

The simplified Droop Photobioreactor Model (DPM) is

$$\begin{cases} \dot{s} = Ds_{in} - \rho_m \frac{s}{s+K_s} \frac{Q_l - q}{Q_l - Q_0} x - Ds \\ \dot{q} = \rho_m \frac{s}{s+K_s} \frac{Q_l - q}{Q_l - Q_0} - \mu(q, I_0, X) q \\ \dot{x} = (\mu(q, I_0, X) - r - D)x \end{cases} \quad (12)$$

This model is a simplified version of the model presented by Bernard et al. (2009) when photoadaptation is neglected. It will be used in the rest of the paper.

3. OPTIMAL CONDITIONS FOR MAXIMIZING PRODUCTIVITY

3.1 Choosing surface biomass

With model (12), our aim is to compute and optimize biomass surface productivity (units: $mg[C]/m^2/day$):

$$P(q, I_0, X) = (\mu(q, I_0, X) - r)X \quad (13)$$

At equilibrium it is the product between dilution rate ($D = \mu(I_0, q, X) - r$) and surface biomass.

Important Remark: productivity is a function of the nitrogen/carbon quota q and surface biomass $X = xW$: according to this model a thin culture (W small) with high biomass concentration x is equivalent to a deep culture (W high) with low biomass concentration x, if they have the same surface biomass.

The reactor can be seen as a solar panel with an energy yield, and losses. The panel's parameter is X:

- A low X (low biomass and thin culture) indicates that most light is not absorbed by the culture: the panel has a low energy yield.
- A high X (high biomass and deep culture) indicates that in the culture's bottom there is very little light: most light is absorbed, but in the reactor's bottom there are only respiration losses.

Thus, we must choose the best X value to maximize the panel's efficiency P.

Theorem 1. For given I_0 and q, the optimal X surface biomass for maximizing productivity (13) is such that growth rate at depth W is equal to the respiration rate:

$$\mu^W(q, I(q, X_{opt})) = r \quad (14)$$

This optimal surface biomass concentration can thus be computed:

$$X_{opt}(q) = \frac{1}{a_i \gamma q} \ln\left(\frac{I_0}{K_I}\left(\frac{\tilde{\mu}(q)}{r} - 1\right)\right) \quad (15)$$

Proof: For a given biomass surface concentration X, productivity can be written from (13) and (10)

$$\begin{aligned} P(q, I_0, X) &= \int_0^X (\mu^z(q, I(q, \chi)) - r) d\chi \\ &= \int_0^{X_{opt}} (\mu^z - r) d\chi + \int_{X_{opt}}^X (\mu^z - r) d\chi \\ &= P(q, I_0, X_{opt}) + \int_{X_{opt}}^X (\mu^z - r) d\chi \end{aligned}$$

where the first term is the productivity $P(q, I_0, X_{opt})$ with X_{opt} chosen according to (14), and the second term is always negative because μ^z decreases with X:

- If X is lower than X^{opt}, then this term would "remove" microalgae that grow more than they respire: $\mu^z(q, I(q, \chi)) > r, \forall \chi < X^{opt}$.
- If X is higher than X^{opt}, then this term would "add" microalgae that respired more than they grow: $\mu^z(q, I(q, \chi)) < r, \forall \chi > X^{opt}$.

so that X_{opt} maximizes surface productivity.

It is then possible to compute this optimal surface biomass from (14), (9) and (7)

$$\tilde{\mu}(q) \frac{I_0 e^{-a_i \gamma q X_{opt}}}{I_0 e^{-a_i \gamma q X_{opt}} + K_I} = r$$

(with notation $\tilde{\mu}(q) = \bar{\mu}(1 - Q_0/q)$) we obtain

$$I_0 e^{-a_i \gamma q X_{opt}} = K_I \frac{r}{\tilde{\mu}(q) - r} \quad (16)$$

which gives the light intensity at depth W, and then leads to (15).

Since $X_{opt}(q)$ needs to be positive, it only exists for $q > \frac{I_0 \bar{\mu}}{I_0 \bar{\mu} - r(I_0 + K_I)} Q_0$, that is the minimal quota that ensures that growth can compensate respiration at the reactor's surface. □

3.2 Optimization with both surface biomass and nitrogen quota

We are then left with the choice of an optimal nitrogen/carbon value q, which can be controlled by adjusting D and s_{in} (see section 4).

- A low quota leads to low potential growth rate $\tilde{\mu}(q)$
- A high quota leads to high $\tilde{\mu}(q)$ potential growth rate, but also to higher light attenuation, so that the mean growth rate $\mu(I_0, q, X)$ in the reactor can be lower.

Thus, an optimal intermediate value must be found.

Theorem 2. There exists only one value q_{opt} maximizing P, provided that the following condition is satisfied:

$$I_0 > K_I \left[\frac{\bar{\mu}}{\bar{\mu} - 2r} e^{\frac{r^2}{\bar{\mu} - 2r}} - 1\right] \quad (17)$$

Important Remark: (17) is, in practice, always true since $I_0 \gg K_I$ and $\bar{\mu} \gg r$.

Proof: First, we compute the growth rate at optimal surface biomass concentration (15), from (11) and (16)

$$\mu(q, I_0, X_{opt}) = \tilde{\mu}(q) \frac{\ln\left((1 + \frac{I_0}{K_I})(1 - \frac{r}{\tilde{\mu}(q)})\right)}{a_i \gamma q X_{opt}(q)} \quad (18)$$

Then we compute the corresponding productivity

$$\begin{aligned} P(q, I_0, X_{opt}) &= (\mu(q, I_0, X_{opt}(q)) - r) X_{opt}(q) \\ &= \frac{\tilde{\mu}(q)}{a_i \gamma q} \ln\left((1 + \frac{I_0}{K_I})(1 - \frac{r}{\tilde{\mu}(q)})\right) \\ &\quad - \frac{r}{a_i \gamma q} \ln\left(\frac{I_0}{K_I}(\frac{\tilde{\mu}(q)}{r} - 1)\right) \end{aligned}$$

Its derivative with respect to q is then computed, to find the optimal q value:

$$\frac{\partial P(q, I_0, X_{opt})}{\partial q} = \frac{1}{a_i \gamma q^2} f(q)$$

with

$$\begin{aligned} f(q) =& \bar{\mu}(\frac{2Q_0}{q} - 1) \ln\left((1 + \frac{I_0}{K_I})(1 - \frac{r}{\tilde{\mu}(q)})\right) \\ &+ r \ln\left(\frac{I_0}{K_I}(\frac{\tilde{\mu}(q)}{r} - 1)\right) \end{aligned}$$

which can only be equal to zero for values of q higher than $2Q_0$, because both logarithms are positive by construction: the first one comes from the growth rate, and the second one from the optimal biomass surface concentration.

We can show that an extremum of P corresponds to a maximal productivity, and that it is unique, by demonstrating that when $\frac{\partial P(q, I_0, X_{opt})}{\partial q} = 0$ is achieved (equivalent to $f(q) = 0$), the second derivative $\frac{\partial^2 P(q, I_0, X_{opt})}{\partial q^2}$ is negative.

$$\frac{\partial^2 P(q, I_0, X_{opt})}{\partial q^2} = -\frac{r}{a_i \gamma q^3} f(q) + \frac{r}{a_i \gamma q^2} \frac{\partial f}{\partial q}(q)$$

When $f(q) = 0$, we know that $q > 2Q_0$, and that the sign of this second derivative is the sign of $\frac{\partial f}{\partial q}(q)$

$$\begin{aligned} \frac{\partial f}{\partial q}(q) = \frac{\bar{\mu}}{r} \frac{Q_0}{q^2} \Bigg[&\frac{r^2}{\tilde{\mu}(q) - r} - 2 \ln\left((1 + \frac{I_0}{K_I})(1 - \frac{r}{\tilde{\mu}(q)})\right) \\ &- (1 - \frac{2Q_0}{q}) \frac{r}{\tilde{\mu}(q) - r} \frac{\bar{\mu}}{\tilde{\mu}(q)} \Bigg] \end{aligned}$$

which should be negative when $f(q) = 0$, because the third term will be negative ($q > 2Q_0$ and $\tilde{\mu}(q) > r$), and the first term is small compared to the second one. Let us clarify precise conditions for $\frac{\partial f}{\partial q}(q) < 0$ to hold:

$$\frac{r^2}{\tilde{\mu}(q) - r} < 2 \ln\left((1 + \frac{I_0}{K_I})(1 - \frac{r}{\tilde{\mu}(q)})\right) \quad (19)$$

Starting from (19) and with

$$\mu(q) > \mu(2Q_0) = \frac{\bar{\mu}}{2}$$

we have that

$$\frac{r^2}{\tilde{\mu}(q) - r} < \frac{r^2}{\bar{\mu}/2 - r}$$

and also

$$1 - \frac{r}{\tilde{\mu}(q)} > 1 - \frac{2r}{\bar{\mu}}$$

so that (20) implies (19)

$$\frac{r^2}{\bar{\mu}/2 - r} < 2 \ln\left((1 + \frac{I_0}{K_I})(1 - \frac{2r}{\bar{\mu}})\right) \quad (20)$$

From this inequality, we can compute the condition (17) which shows that a "high enough" I_0 incident light ensures this unicity property. □

4. OPTIMAL CONTROL FOR A PHOTOBIOREACTOR

4.1 Choosing D and s_{in} to maximize productivity

Having identified optimal X_{opt} and q_{opt}, we now have to verify that an equilibrium with $X = X_{opt}$ and $q = q_{opt}$ can be achieved through an appropriated choice of $D^\star$ and $s^\star_{in}$. The $\dot{x} = 0$ equation imposes the choice of the dilution rate:

$$D^\star = \mu_{opt} - r$$

with

$$\mu_{opt} = \mu(q_{opt}, I_0, X_{opt}(q_{opt}))$$

$D^\star$ is positive since $\mu > \mu^z(q_{opt}, I(q_{opt}, X_{opt})) = r$ (see Theorem 1).

The equilibrium substrate concentration can then be computed from $\dot{q} = 0$:

$$\rho_m \frac{s}{s + K_s} \frac{Q_l - q_{opt}}{Q_l - Q_0} = \mu_{opt} q_{opt}$$

so that, at equilibrium:

$$s_{opt} = K_s \frac{\mu_{opt}(1 - Q_0/Q_l) q_{opt}}{\rho_m - (\rho_m / Q_l + \mu_{opt}(1 - Q_0/Q_l)) q_{opt}}$$

which must be positive: this point will be developed later.

Finally we obtain s_{in} from the Droop nitrogen mass balance equality (Bastin and Dochain, 1990)

$$s_{in} = s_{opt} + q_{opt} X_{opt} / W$$

which is the optimal input substrate value to maximize surface productivity.

4.2 Optimal equilibrium attainability

In some cases (depending on incident light and microalgal parameters) the computed s_{opt} is negative. This is caused by

$$\mu_{opt} q_{opt} > \rho_m \frac{Q_l - q_{opt}}{Q_l - Q_0} \quad (21)$$

so that the optimal q_{opt} quota cannot be attained under biomass surface concentration X_{opt} (see the $\dot{q}$ dynamics). In such cases, we must reformulate our optimization problem:

$$\begin{array}{ll} \max_{(q,X)} & (\mu(q, I_0, X) - r) X \\ \text{such that} & \mu(q, I_0, X) q \leq \rho_m \frac{Q_l - q}{Q_l - Q_0} \end{array} \quad (22)$$

Theorem 3. The solution of the optimization problem (22) is the one provided by Theorems 1 and 2 (q_{opt}, X_{opt}) or lies on the following constraint:

$$\mu(q, I_0, X) q = \rho_m \frac{Q_l - q}{Q_l - Q_0} \quad (23)$$

Proof: • If (q_{opt}, X_{opt}) is such that the constraint is valid, we have already demonstrated that this couple is optimal (see Figure 2 for a numerical example).

• If (q_{opt}, X_{opt}) does not verify the constraint (example on Figure 3), the closer from $X_{opt}(q)$ is X, the higher is P (see Theorem 1's demonstration). The optimal solution lies thus as close as possible to $X = X_{opt}(q)$, *i.e.* either on $X = X_{opt}(q)$ or on the constraint (23).

Let us denote C-curve the part of the $X = X_{opt}(q)$ curve that verifies the constraint.

Because $\mu(q, I_0, X)q$ is increasing with q and $\rho_m \frac{Q_l - q}{Q_l - Q_0}$ is decreasing with q, we know that any q value on the C-curve verifying the constraint is lower than q_{opt} (which is too high to verify the constraint). We also know from Theorem 2 that on the C-curve, the derivative of P with respect to q is positive for any $q < q_{opt}$. Because of that, on the C-curve, the maximal P is attained for the highest possible q: it is the q value lying both on the C-curve and constraint (23). This demonstrates that the optimal productivity will lie on the constraint.

In this last case s_{in} should be chosen infinite to have s infinite and $\rho(s) = \rho_m$, so that we can be on the constraint. The identification of the optimal (X, q) couple is then not straightforward, and this case will be the topic of further analysis. □

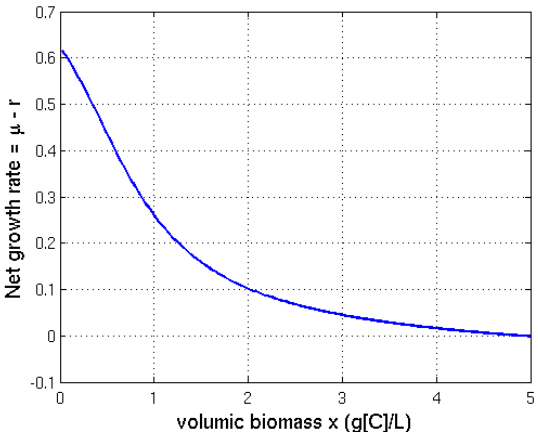

Fig. 1. Mean net growth rate $(\mu - r)$ in the reactor computed from (11), with $q = 0,1 g[N]/g[C]$ and $I_0 = 100\mu$ mol quanta. $m^{-2}s^{-1}$. It is affected by light attenuation, caused by high biomass concentration.

5. NUMERICAL RESULTS

In the previous sections we have determined that there is a unique optimal $(X_{opt}(q_{opt}), q_{opt})$ couple that maximizes the surface productivity P. In this section we illustrate this result with parameters for the microalgae *Isochrysis galbana*.

5.1 Microalgae parameters

The parameter values are taken from Bernard et al. (Sub.) to show productivity results predicted by the model for *I. galbana*. However, parameters K_I and γ (which may vary through photoacclimation) are computed from average values of the photoadaptation model in Bernard et al. (Sub.).

For all the simulations we use culture's depth $W = 0,1m$.

The growth rate predicted for such a strain is computed and plotted in Figure 1, for $q = 0.1 g[N]/g[C]$ and $I_0 = 100\mu$ mol quanta. $m^{-2}s^{-1}$. We see on this figure that because of respiration, there is a maximal biomass $x = 4.93 g[C]/L$ for which respiration is equal to growth $(\mu(X) - r = 0)$.

Table 1. Parameter values of the lipid model for *I.galbana* culture.

Parameter	Value	Unit
Q_0	0.05	$g[N].g[C]^{-1}$
Q_l	0.25	$g[N].g[C]^{-1}$
$\bar{\mu}$	1.7	d^{-1}
ρ_m	0.073	$g[N].g[C]^{-1}.d^{-1}$
K_s	0.0012	$g[N]/m^3$
r	0.07	day^{-1}
K_I	20	μ mol quanta. $m^{-2}s^{-1}$
a_i	16.2	m2/g[Chl]
γ	0.25	g[Chl]/g[N]

Condition (17) for the unicity of a maximum productivity is verified for $I_0 > 3,5\mu$ mol quanta. $m^{-2}s^{-1}$ which is small compared to incident light intensities ranging usually between 100μ mol quanta. $m^{-2}s^{-1}$ to 3000μ mol quanta. $m^{-2}s^{-1}$.

5.2 Productivity prediction

Productivity was computed with these parameters and with $I_0 = 100\mu$ mol quanta. $m^{-2}s^{-1}$ (Figure 2) and 2000μ mol quanta. $m^{-2}s^{-1}$ (Figure 3).

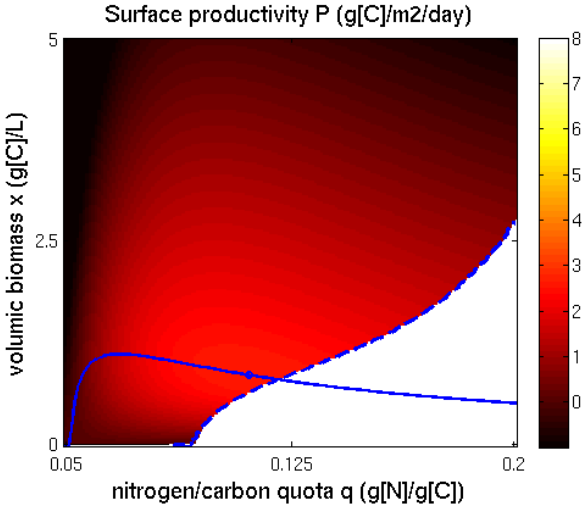

Fig. 2. Surface biomass productivity for $I_0 = 100\mu$ mol quanta. $m^{-2}s^{-1}$. The $X = X_{opt}(q)$ curve is represented by a solid line, and the optimal (q_{opt}, X_{opt}) couple is represented by a circle. Dotted line indicates constraint (23).

On Figure 2 we see that there is an optimal (q_{opt}, X_{opt}) couple which maximizes productivity. Note that, contrarily to the usually assumed hypothesis that higher nitrogen/carbon ratio leads to higher productivities, we see here that the optimal conditions do not correspond to nitrogen replete microalgae: for $X = X_{opt}$, $q > q_{opt}$ lead to suboptimal productivities. Thus, depending on the species and culture conditions, this result suggests that it could be advantageous to have slightly nitrogen limited microalgae, so that light attenuation by chlorophyll is weaker and light is used more efficiently in the photobioreactor.

In Figure 3 we see that the optimal (q_{opt}, X_{opt}) couple (*circle*) depends on the incident irradiance (it is not the same as in the previous figure), and that higher light intensities lead to higher productivities.

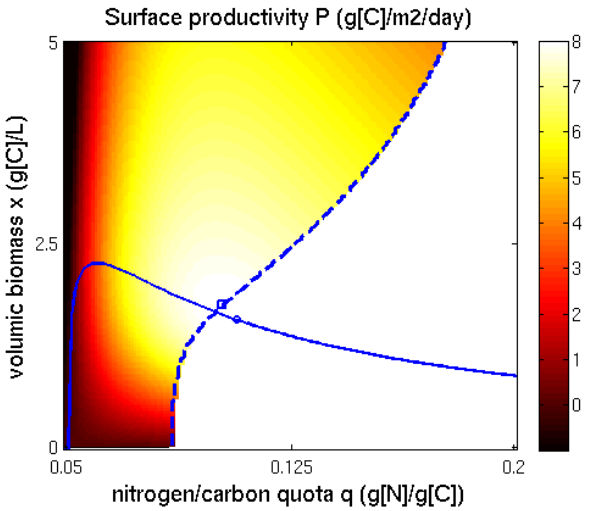

Fig. 3. Surface biomass productivity for $I_0 = 2000\mu$ mol quanta. $m^{-2}s^{-1}$. The $X = X_{opt}(q)$ curve is represented by a solid line, and the optimal (q_{opt}, X_{opt}) couple is represented by a circle. This optimal couple does not respect the constraint (dotted line) of the optimization problem (22). The real optimum (square) thus lies on the constraint.

Contrarily to the previous example, here the constraint of optimization problem (22) is not verified, so that the theoretical optimum cannot be attained: the real optimum (determined numerically) lies on the constraint, as predicted by Theorem 3.

6. CONCLUSION

In this paper we determined the optimal conditions for maximizing the biomass surface productivity, and redefined the optimization problem for the case where the optimal equilibrium is not attainable. The identified optimal conditions correspond to both optimal biomass surface concentration X_{opt} so that light is used optimally (section 3.1), and optimal nitrogen/carbon ratio. This work clearly follows the work of Cornet and Dussap (2009); Takache et al. (2009) who computed optimal biomass concentration from a light diffusion model (neglecting also photoacclimation) and experimentally validated the obtained productivities.

In order to get analytical results we have kept a trade-off between model simplicity to handle mathematical analysis, and model complexity to capture the main phenomena driving a photobioreactor's productivity: nitrogen absorption, growth depending both on the nitrogen/carbon quota and on the light attenuation induced by chlorophyll.

A key result shown by this approach is that slight nitrogen depreciation can enhance photobioreactor productivity. This is of particular importance since nitrogen limitation is known to stimulate lipids production. The model analysis also predicts that surface biomass $X = xW$ drives productivity, so that a thin reactor (low W) with dense biomass x or a deep reactor (high W) with low biomass concentration x should have the same productivity, if their surface biomass is the same. These results must now be verified with dedicated experiments.

ACKNOWLEDGEMENTS

This paper presents research results supported by the ANR-06-BIOE-014 Shamash project.

REFERENCES

Aflalo, C., Meshulam, Y., Zarka, A., and Boussiba, S. (2007). On the relative efficiency of two- vs. one-stage production of astaxanthin by the green alga *haematococcus pluvialis*. *Biotech. and Bioeng.*, 98(300-305).

Bastin, G. and Dochain, D. (1990). *On-line estimation and adaptive control of bioreactors*. Elsevier, Amsterdam.

Bernard, O. and Gouzé, J.L. (1995). Transient Behavior of Biological Loop Models, with Application to the Droop Model. *Mathematical Biosciences*, 127(1), 19–43.

Bernard, O. and Gouzé, J.L. (2002). Global qualitative behavior of a class of nonlinear biological systems: application to the qualitative validation of phytoplankton growth models. *Artif. Intel.*, 136, 29–59.

Bernard, O., Masci, P., Mairet, F., and Sciandra, A. (Sub.). A photobioreactor model in nitrogen limited conditions. *submitted*.

Bernard, O., Masci, P., and Sciandra, A. (2009). A photobioreactor model in nitrogen limited conditions. In *Proceedings of the Mathmod 09 conference*. Vienna, Austria.

Chisti, Y. (2007). Biodiesel from microalgae. *Biotechnology Advances*, 25, 294–306.

Cornet, J.F. and Dussap, C.G. (2009). A simple and reliable formula for assessment of maximum volumetric productivities in photobioreactors. *Biotechnol Prog*, 25(2), 424–435.

Droop, M. (1968). Vitamin B12 and marine ecology. IV. the kinetics of uptake growth and inhibition in *Monochrysis lutheri*. *J. Mar. Biol. Assoc.*, 48(3), 689–733.

Droop, M. (1983). 25 years of algal growth kinetics, a personal view. *Botanica marina*, 16, 99–112.

Huntley, M. and Redalje, D. (2007). Co2 mitigation and renewable oil from photosynthetic microbes: A new appraisal. *Mitigation et Adaptation Strategies for Global Change*, 12, 573 – 608.

Lehman, J.T., Botkin, D.B., and Likens, G. (1975). The assumptions and rationales of a computer model of phytoplankton population dynamics. *Limn. & Oceanogr.*, 20, 343–364.

Sciandra, A. and Ramani, P. (1994). The limitations of continuous cultures with low rates of medium renewal per cell. *J. Exp. Mar. Biol. Ecol.*, 178, 1–15.

Spolaore, P., Joannis-Cassan, C., Duran, E., and Isambert, A. (2006). Commercial applications of microalgae. *J. of Biosci. and Bioeng.*, 101(2), 87 – 96.

Takache, H., Christophe, G., Cornet, J.F., and Pruvost, J. (2009). Experimental and theoretical assessment of maximum productivities for the microalgae chlamydomonas reinhardtii in two different geometries of photobioreactors. *Biotechnol Prog*, 26(2), 431–440.

Vatcheva, I., deJong, H., Bernard, O., and Mars, N. (2006). Experiment selection for the discrimination of semi-quantitative models of dynamical systems. *Artif. Intel.*, 170, 472–506.

Optimization of a photobioreactor biomass production using natural light

Frédéric Grognard, Andrei Akhmetzhanov, Pierre Masci and Olivier Bernard

***Abstract*— We address the question of optimization of the biomass long term productivity in the framework of microalgal biomass production in photobioreactors under the influence of day/night cycles. For that, we propose a simple bioreactor model accounting for light attenuation in the reactor due to biomass density and obtain the control law that optimizes productivity over a single day through the application of Pontryagin's maximum principle, with the dilution rate being the control. An important constraint on the obtained solution is that the biomass in the reactor should be at the same level at the beginning and at the end of the day so that the same control can be applied everyday and optimizes the long term productivity. Several scenarios are possible depending on the microalgae's strain parameters and the maximal admissible value of the dilution rate: bang-bang or bang-singular-bang control or, if the growth rate of the algae is very strong in the presence of light, constant maximal dilution. A bifurcation diagram is presented to illustrate for which values of the parameters these different behaviors occur.**

I. INTRODUCTION

Microalgae have recently received more and more attention in the frameworks of CO_2 fixation and renewable energy [5], [2]. Their high actual photosynthetic yield compared to terrestrial plants (whose growth is limited by CO_2 availability) leads to large potential algal biomass productions in photobioreactors of several tens of tons per hectare and per year [2].

The objective of this paper is to develop an optimal control law that would maximize the photobioreactor yield, while taking into account that the light source (*i.e* the primary energy source) that will be used is the natural light. The light source is therefore periodic with a light phase (day) and a dark phase (night). In addition to this time-varying periodic light source, we will take the auto-shading in the photobioreactor into account: the pigment concentration (mainly chlorophyll) affects the light distribution and thus the biological activity within the reactor. As a consequence, for a too high biomass, light in the photobioreactor is strongly attenuated and growth is low.

It is therefore necessary to develop a model that takes both features into account in order to develop the control law, where the substrate concentration in the input (marginally) and the dilution rate (mainly) will be used. This model should not be too complicated in order to be tractable and should present the main features of the process. Since we want to develop a control strategy that will be used on the long run, we could choose an infinite time-horizon measure of the yield. However, we rather took advantage of the observation that, in the absence of a discount rate in the cost functional, the control should be identical everyday and force the state of the system to be identical at the beginning of the day and 24 hours later. We therefore opted for optimizing a cost over one day with the constraint that the initial and terminal state should be identical.

The paper is structured as follows: first, we present the model dealing with both substrate limitation, light attenuation and light periodicity; then biomass productivity optimization is presented in a constant light environment. The solution to the periodic light problem is then presented. Finally, numerical results are presented with a bifurcation analysis.

This work was supported by the ANR-06-BIOE-014 Shamash project.

The authors are with the COMORE project-team of INRIA Sophia Antipolis, BP 93, 06902 Sophia Antipolis Cedex, France, {frederic.grognard, andrei.akhmetzhanov, pierre.masci, olivier.bernard}@sophia.inria.fr

II. A PHOTOBIOREACTOR MODEL WITH LIGHT ATTENUATION

Micro-algae growth in a photobioreactor is often modelled through one of two models, the Monod model [9] or the Droop Model [3]. The latter is more accurate as it separates the process of substrate uptake and growth of the microalgae. The former gives a reasonable representation of reality by coupling growth and uptake, and is more convenient for building control laws since it is simpler. For sake of simplicity we will introduce the problem with the Monod model, but the presented results are similar with the Droop model when considering the working modes where nutrients are not limiting growth. The Monod model writes:

$$\left\{ \begin{array}{rcl} \frac{ds}{d\tau} & = & D(s_{in}-s) - k\nu(s)x \\ \frac{dx}{d\tau} & = & \nu(s)x - Dx \end{array} \right. \quad (1)$$

where s and x are the substrate and biomass concentrations in the medium, while D is the dilution rate, s_{in} is the substrate input concentration and k is the substrate/biomass yield coefficient. We will depart from this model in two directions. First, we introduce respiration by the microalgae: contrary to photosynthesis, this phenomeneon takes place with or without light; from a carbon point of view, it converts biomass into carbon dioxyde, so that we represent it as a $-\rho x$ term in the biomass dynamics. Secondly, under the hypothesis of an horizontal planar photobioreactor (or raceway) with vertical incoming light, we represent light attenuation following an exponential Beer-Lambert law where the attenuation at some depth z comes from the total biomass xz per surface unit contained in the layer of depth $[0, z]$:

$$I(xz) = I_0 e^{-axz} \quad (2)$$

where I_0 is the incident light and a is a light attenuation coefficient. In microalgae, as we proposed in (2) chlorophyll is mostly the cause of this shadow effect and, in model (1), it is best represented by a fixed portion of the biomass [1]. Finally, the light source variation will be introduced by taking a time-varying incident light $I_0(\tau)$. With such an hypothesis on the light intensity that reaches depth z, growth rates vary with depth: in the upper part of the reactor, higher light causes higher growth than in the bottom part. Supposing that light attenuation directly affects the maximum growth rate [4], the growth rate for a given depth z can then be written as

$$\nu_z(s, I(xz,\tau)) = \frac{\tilde{\nu} I(xz,\tau)}{I(xz,\tau)+K_I}\frac{s}{s+K_s}, \quad \text{with } I(xz,\tau) = I_0(\tau)e^{-axz}$$

Then, we can compute the mean growth rate in the reactor:

$$\nu(s, I_0(\tau), x) = \frac{1}{L}\int_0^L \nu_z(s, I(xz,\tau))dz$$

where L is the depth of the reactor and where we have supposed that, even though the growth rate is not homogeneous in the reactor due to the light attenuation, the concentrations of s and x are kept homogeneous through continuous reactor stirring. It is this average growth rate that will be used in the lumped model that we develop. We then have:

$$\begin{aligned}\nu(s, I_0(\tau), x) &= \frac{\tilde{\nu}}{L}\int_0^L \frac{I_0(\tau)e^{-axz}}{I_0(\tau)e^{-axz}+K_I}\,dz\frac{s}{s+K_s} \\ &= \frac{\tilde{\nu}}{axL}\ln\left(\frac{I_0(\tau)+K_I}{I_0(\tau)e^{-axL}+K_I}\right)\frac{s}{s+K_s}\end{aligned}$$

The system for which we want to build an optimal controller is therefore

$$\left\{\begin{array}{rcl}\frac{ds}{d\tau} &=& D(s_{in}-s) - k\frac{\tilde{\nu}}{axL}\ln\left(\frac{I_0(\tau)+K_I}{I_0(\tau)e^{-axL}+K_I}\right)\frac{s}{s+K_s}x \\ \frac{dx}{d\tau} &=& \frac{\tilde{\nu}}{axL}\ln\left(\frac{I_0(\tau)+K_I}{I_0(\tau)e^{-axL}+K_I}\right)\frac{s}{s+K_s}x - \rho x - Dx\end{array}\right. \tag{3}$$

However, since we want to maximize the productivity, it seems clear that the larger s the better, large values of s translating into large growth rates. The control s_{in} should then always be kept very large so as to always keep the substrate in the region where $\frac{s}{s+K_s} \approx 1$. We can then concentrate on the reduced model

$$\frac{dx}{d\tau} = \frac{\tilde{\nu}}{axL}\ln\frac{I_0(\tau)+K_I}{I_0(\tau)e^{-axL}+K_I}x - \rho x - Dx \tag{4}$$

which then encompasses all the relevant dynamics for the control problem.

In order to more precisely determine the model, we should now indicate what the varying light will be like. Classically, it is considered that daylight varies as the square of a sinusoidal function so that

$$I_0(\tau) = \left(\max\left\{\sin\left(\frac{2\pi\tau}{\mathcal{T}}\right), 0\right\}\right)^2$$

where $\mathcal{T}$ is the length of the day. The introduction of such a varying light would however render the computations analytically untractable. Therefore, we approximate the light source by a step function:

$$I_0(\tau) = \left\{\begin{array}{lll}\bar{I}_0, & 0 \le \tau < \bar{\mathcal{T}} & \text{— light phase} \\ 0, & \bar{\mathcal{T}} \le \tau < \mathcal{T} & \text{— dark phase}\end{array}\right.$$

In a model where the time-unit is the day, $\mathcal{T}$ will be equal to 1. In the following, we will consider $\bar{\mathcal{T}} = \frac{\mathcal{T}}{2}$, but this quantity obviously depends on the time of the year.

Finally, we consider a last simplification to the model: instead of considering that the biomass growth in the presence of light has the form $\frac{\tilde{\nu}}{aL}\ln\frac{\bar{I}_0+K_I}{I_0e^{-axL}+K_I}$, which is an increasing and bounded function, we replace it with another increasing bounded function $\frac{\bar{\nu}x}{k+x}$ and obtain the model

$$\frac{dx}{d\tau} = \frac{\nu(\tau)x}{\kappa+x} - \rho x - Dx$$

where $\nu(\tau) = \bar{\nu}$ during the light phase and 0 at night. It is possible to show that this simplified model is a good numerical approximation of the original model.

III. PRODUCTIVITY OPTIMIZATION

The productivity problems that we will consider in the sequel will be put in a framework where D is bounded, so that, $\forall t \ge 0$, $D(t) \in [0, D_{max}]$; such a bound makes sense in an optimal control framework since it prevents infinite values of the control, which might occur when harvesting the photobioreactor. In order to simplify notations, we then introduce the following change of time and variable $(t, y) = (D_{max}\tau, \frac{x}{k})$, which yields

$$\frac{dy}{dt} = \dot{y} = \frac{\mu(t)y}{1+y} - ry - uy \tag{5}$$

where $r = \frac{\rho}{D_{max}}$ and $u = \frac{D}{D_{max}} \in [0,1]$ is the new control. We also have $\mu(t) = \bar{\mu} = \frac{\bar{\nu}}{\kappa D_{max}}$ for $t \in [0, \bar{T}]$ and 0 for $t \in [\bar{T}, T]$ (with $\bar{T} = D_{max}\bar{\mathcal{T}}$ and $T = D_{max}\mathcal{T}$).

A. Productivity optimization in constant light environment

In a previous work [8], we have studied the productivity optimization of a microalgae photobioreactor with light-attenuation in the Droop framework with constant light. In that study, since we wanted to optimize the long-term productivity, we looked for the control values for D and s_{in} that optimized the instantaneous biomass output flow at equilibrium, that is

$$\max_u uy^*V$$

where V is the photobioreactor volume (assumed here to be constant). This study was complex because the shading was dependent on the internal substrate quota. In the present case, it will greatly simplify with s_{in} that does not need to be optimized. Indeed, for a given dilution u, the equilibrium of (5) in the presence of light is

$$y^* = \frac{\bar{\mu}}{r+u} - 1$$

which needs to be non-negative, so that $0 \le u \le \bar{\mu} - r$. The positivity of u imposes that $r \le \bar{\mu}$, that is the respiration

needs to be weaker than the maximal growth. For a given u, the productivity rate at equilibrium is then

$$\frac{\bar{\mu}uV}{r+u} - uV$$

whose optimum value is reached in

$$u_\sigma = \sqrt{\bar{\mu}r} - r \tag{6}$$

which is positive because $r \leq \bar{\mu}$ but requires

$$\bar{\mu} \leq \frac{(r+1)^2}{r} \tag{7}$$

to be smaller or equal to 1 (otherwise, the optimal dilution is $u = 1$). This yields the optimal productivity rate:

$$(\sqrt{\bar{\mu}} - \sqrt{r})^2 V$$

It is important to note that the equilibrium is then

$$y_\sigma = \sqrt{\frac{\bar{\mu}}{r}} - 1 \tag{8}$$

which maximizes the net production rate $\frac{\bar{\mu}y}{1+y} - ry = uy$. We will use this definition of y_σ even when it is not achievable with some $u_\sigma \leq 1$.

B. Productivity optimization in day/night environment

In an environment with varying light we cannot settle for an instanteneous productivity rate optimization since this equilibrium cannot be maintained during the night. In essence, we want to optimize the long term productivity of the photobioreactor, that is we want that, everyday, the same maximal amount is produced. The problem that we consider is therefore

$$\max_{u(t) \in [0,1]} \int_0^T u(t)Vy(t)dt$$

We then need to add constraints to the solution that we want to obtain; indeed, at the end of the day, we want to be able to start operating the photobioreactor in the same conditions for the next day. This then requires that we add the constraint

$$y(T) = y(0)$$

We therefore are faced with the following optimal control problem

$$\begin{aligned} \max_{u(t) \in [0,1]} \int_0^T & u(t)y(t)dt \\ \text{with} \quad & \dot{y} = \tfrac{\mu(t)y}{1+y} - ry - uy \\ & y(T) = y(0) \end{aligned} \tag{9}$$

1) Parameter constraints: In order to solve this problem, it is convenient to observe that $y(T) = y(0)$ cannot be achieved for large values of y even without considering optimality. Indeed, for all t, we have $\dot{y} < 0$ when $y(t) > \frac{\bar{\mu} - r}{r}$ independently of the choice of u; therefore, an initial condition such that $y(0) > \frac{\bar{\mu} - r}{r}$ cannot be considered since necessarily $y(T) < y(0)$ in that case. We then know that, for admissible initial conditions below that threshold, $y(t)$ will stay below this threshold for all times. It also implies that, whenever $u(t) = 0$ for such solution with $t \in [0, \bar{T})$, $\dot{y} > 0$ because $y(t)$ then tends toward $\frac{\bar{\mu}-r}{r}$;

We could make this bound stronger by noticing that, for a given $y(0)$, the largest value of $y(T)$ that can be achieved is reached by taking $u(t) = 0$ for all times; indeed, at any time, applying $u(t) > 0$ implies that $\dot{y}$ is smaller than if $u(t) = 0$ were applied. If the value of $y(T)$ corresponding to $u(t) = 0$ is smaller than $y(0)$, then the corresponding initial condition cannot be part of the optimal solution. Solving (5) with $u(t) = 0$ in the interval $[0, \bar{T}]$, by separating the variables yields

$$\frac{r \ln\left(\frac{y(\bar{T})}{y_0}\right) - \bar{\mu} \ln\left(\frac{\bar{\mu} - r(1 + y(\bar{T}))}{\bar{\mu} - r(1 + y_0)}\right)}{r(\bar{\mu} - r)} = \bar{T}$$

where we denoted $y(0)$ as y_0. Trivially, the integration of (5), for the dark period ($u(t) = 0$) on the interval $[\bar{T}, T]$, yields

$$y(T) = y(\bar{T})e^{-r(T-\bar{T})}$$

so that, introducing this equation in the previous one, we get

$$\frac{r \ln\left(\frac{y(T)e^{r(T-\bar{T})}}{y_0}\right) - \bar{\mu} \ln\left(\frac{\bar{\mu} - r(1 + y(T)e^{r(T-\bar{T})})}{\bar{\mu} - r(1 + y_0)}\right)}{r(\bar{\mu} - r)} = \bar{T}$$

The equality $y(T) = y_0$ is then achieved with $u(t) = 0$ when solving this last equation for y_0 with $y(T) = y_0$, which yields

$$y_{0max} = \frac{\bar{\mu} - r}{r} \frac{e^{\frac{r}{\bar{\mu}}(\bar{\mu}\bar{T} - rT)} - 1}{e^{\frac{rT}{\bar{\mu}}(\bar{\mu} - r)} - 1}$$

For larger values of y_0, we have $y(T) < y_0$ independently of the choice of $u(t)$; for smaller values of y_0, there exist control functions $u(t)$ that guarantee $y(T) = y_0$. The constraint $\mu > r$, which is necessary for growth to occur in the light phase guarantees that the first fraction and the denominator of the second one in y_{0max} are positive. We then need to add the constraint

$$\bar{\mu} > \frac{rT}{\bar{T}} \tag{10}$$

to ensure the positivity of y_{0max} and so the possibility of the existence of a solution to the optimal control problem (9). Note that, in the case where $\bar{T} = \frac{T}{2}$, this simply means that $\bar{\mu} > 2r$.

It is also interesting to see that, if a constant control $u(t) = 1$ is applied, a periodic solution is obtained for

$$y_{0min} = \frac{\bar{\mu} - r - 1}{r + 1} \frac{e^{\frac{r+1}{\bar{\mu}}(\bar{\mu}\bar{T} - (r+1)T)} - 1}{e^{\frac{(r+1)T}{\bar{\mu}}(\bar{\mu} - r - 1)} - 1}$$

which can be positive if $\bar{\mu} > \frac{(r+1)T}{\bar{T}}$. For any value of y_0 smaller than y_{0min}, any control law would force $y(T) > y_0$. As a consequence, y_0, solution of problem (9), should belong to the interval $[y_{0min}, y_{0max}]$.

2) Maximum principle: In order to solve problem (9), we will use Pontryagin's Maximum Principle (PMP, [10]) in looking for a control law maximizing the Hamiltonian

$$H(x,u,\lambda,t) \triangleq \left[\lambda\left(\left(\frac{\mu(t)}{1+y}-r\right)y-uy\right)+uy\right]$$

with the constraint

$$\left\{\begin{array}{rcl}\dot{y} &=& \frac{\mu(t)y}{1+y}-ry-uy\\ \dot{\lambda} &=& \lambda\left(-\frac{\mu(t)}{(1+y)^2}+r+u\right)-u\end{array}\right.$$

In addition, we should add the constraint

$$\lambda(T)=\lambda(0).$$

Indeed, the solution of the optimal control problem is independent of the reference initial time: defining $x(t) = x(t-T)$, $u(t) = u(t-T)$, and $\lambda(t) = \lambda(t-T)$ for values of t larger than T, we have that $x(t)$, $u(t)$ and therefore $\lambda(t)$ are unchanged if we consider the interval $[t_0, T+t_0]$ (for $0 < t_0 < T$) rather than $[0,T]$. Since $\lambda(t)$ is continuous inside the interval when considering the problem over $[t_0, T+t_0]$, it is continuous in time T and $\lambda(0) = \lambda(T)$ [6].

We see from the form of the Hamiltonian that

$$\frac{\partial H}{\partial u} = 1-\lambda$$

so that, when $\lambda > 1$, we have $u = 0$, when $\lambda < 1$, we have $u = 1$, and when $\lambda = 1$ over some time interval, intermediate singular control is applied.

In the sequel, we propose candidate solutions to the PMP by making various hypotheses on the value of $\lambda(0) = \lambda_0$.

Bang-bang with $\lambda_0 > 1$: With $\lambda_0 > 1$, we have $u = 0$ at times 0 and T. At any given time $0 \le t \le \bar{T}$ before the first switch, the solution of (5) yields

$$\frac{r\ln\left(\frac{y(t)}{y_0}\right)-\bar{\mu}\ln\left(\frac{\bar{\mu}-r(1+y(t))}{\bar{\mu}-r(1+y_0)}\right)}{r(\bar{\mu}-r)} = t \qquad (11)$$

and, as stated earlier, $y(t)$ is increasing because $y(0) < y_{0max} < \frac{\mu-r}{r}$. The constancy of the Hamiltonian during the light phase then imposes that

$$\lambda(t)y(t)\left(\frac{\bar{\mu}}{1+y(t)}-r\right) = \lambda_0 y_0\left(\frac{\bar{\mu}}{1+y_0}-r\right) \qquad (12)$$

for all times $t \in (0,\bar{T})$ such that $u(t) = 0$. A switch to 1 then needs to occur between time 0 and T (otherwise the payoff would be 0) and this switch cannot take place in the dark phase. Indeed, in that zone, as long as $u(t) = 0$, the λ dynamics are

$$\dot{\lambda} = r\lambda$$

with $\lambda(t) > 1$. The adjoint variable is therefore an increasing function in that region, and cannot go through $\lambda = 1$. We will use this impossibility of switch from 0 to 1 in the dark phase several times in the sequel.

For the solution that we study, a switch then needs to take place at time t_{01} in the $(0,\bar{T})$ interval and for $y(t_{01}) = y_{01}$ and $\lambda(t_{01}) = 1$ solutions of (11)-(12).

$$\frac{r\ln\left(\frac{y_{01}}{y_0}\right)-\bar{\mu}\ln\left(\frac{\bar{\mu}-r(1+y_{01})}{\bar{\mu}-r(1+y_0)}\right)}{r(\bar{\mu}-r)} = t_{01} \qquad (13)$$

$$y_{01}\left(\frac{\bar{\mu}}{1+y_{01}}-r\right) = \lambda_0 y_0\left(\frac{\bar{\mu}}{1+y_0}-r\right) \qquad (14)$$

Another constraint that appears at the switching instant from $u = 0$ to $u = 1$ is that $\dot{\lambda} < 0$, which amounts to $\frac{\bar{\mu}}{(1+y)^2} > r$ or $y < y_\sigma$ (see (8)). After time t_{01}, $y(t)$ then converges increasingly or decreasingly toward $\frac{\bar{\mu}-r-1}{r+1}$

Due to the constancy of the Hamiltonian, another switch can only take place at time $\tilde{t}$ before time $\bar{T}$ if

$$y(\tilde{t})\left(\frac{\bar{\mu}}{1+y(\tilde{t})}-r\right) = y_{01}\left(\frac{\bar{\mu}}{1+y_{01}}-r\right)$$

where we have used the fact that $\lambda(\tilde{t}) = \lambda(t_{01}) = 1$ at the switching instants. This can only happen for two values of $y(\tilde{t})$: $y(\tilde{t}) = y_{01}$ and another value $y(\tilde{t}) = \frac{\bar{\mu}}{1+y_{01}} - r$ which is larger than y_σ. Since $y(t)$ was converging to $\frac{\bar{\mu}-r-1}{r+1}$ with $u(t) = 1$, $y(\tilde{t})$ cannot go through y_{01} again unless $y_{01} = \frac{\bar{\mu}-r-1}{r+1}$. In this last case, by considering the $\dot{\lambda}$ dynamics, we see that another switch could only take place if $u(t) = 1$ solves the conditions for being a singular solution to the optimal control; this will be handled later. Generically, a single switch can then only take place inside the interval $(0,\bar{T})$.

The solution then reaches the time $\bar{T}$ with $(y(t),\lambda(t)) = (\bar{y},\bar{\lambda})$ that solve the same kind of equations as (11) and (12):

$$\frac{(r+1)\ln\left(\frac{\bar{y}}{y_{01}}\right)-\bar{\mu}\ln\left(\frac{\bar{\mu}-(r+1)(1+\bar{y})}{\bar{\mu}-(r+1)(1+y_{01})}\right)}{(r+1)(\bar{\mu}-r-1)} = \bar{T}-t_{01} \qquad (15)$$

$$\bar{\lambda}\bar{y}\left(\frac{\bar{\mu}}{1+\bar{y}}-r-1\right)+\bar{y} = y_{01}\left(\frac{\bar{\mu}}{1+y_{01}}-r\right) \qquad (16)$$

Since $\lambda(\bar{T}) < 1$ and $\lambda(T) > 1$, a switch from $u = 1$ to $u = 0$ then needs to take place inside the $(\bar{T},T)$ interval. With the dynamics being in the form

$$\dot{y} = -(r+1)y \qquad \dot{\lambda} = (r+1)\lambda - 1$$

another switch can only take place if $\bar{\lambda} > \frac{1}{r+1}$; otherwise λ cannot go through 1 again. The switching point (t_{10},y_{10}) is then characterized by

$$y_{10} = \bar{y}e^{-(r+1)(t_{10}-\bar{T})} \qquad (17)$$

$$\lambda(t_{10}) = 1 = \bar{\lambda}e^{(r+1)(t_{10}-\bar{T})} - \frac{e^{(r+1)(t_{10}-\bar{T})}-1}{r+1} \qquad (18)$$

After this switching, the dynamics become

$$\dot{y} = -ry \qquad \dot{\lambda} = r\lambda$$

so that no other switch can take place and these dynamics and the constraints $y(T) = y_0$ and $\lambda(T) = \lambda_0$ impose that

$$y_0 = y_{10}e^{-r(T-t_{10})} \qquad (19)$$

$$\lambda_0 = e^{r(T-t_{10})} \tag{20}$$

In the end, we have a system of 8 algebraic equations (13)-(20) with eight unknowns, which we solve numerically.

Even though, we were not able to lead this study analytically all the way to the end, we have shown the qualitative form of the solutions analytically. It is made of four phases:

- Growth with a closed photobioreactor until a sufficient biomass level is reached
- Maximal harvesting of the photobioreactor with simultaneous growth
- Maximal harvesting of the photobioreactor with no growth until a low level of biomass is reached
- Passive photobioreactor: no harvesting, no growth, only respiration

The first two phases take place in the presence of light, the other two in the dark. In phase 3, harvesting of as much biomass produced in the light phase as possible is continued while not going below the level where the residual biomass left is sufficient to efficiently start again the next day.

Bang-singular-bang with $\lambda_0 > 1$:

We will first look at what a singular arc could be. For that, we see that $\frac{\partial H}{\partial u} = 1 - \lambda$ should be 0 over a time interval and compute its time derivatives.

$$\frac{d}{dt}\left(\frac{\partial H}{\partial u}\right)_{|\lambda=1} = -\frac{\mu(t)}{(1+y)^2} + r$$

When $\mu(t) = 0$, that is in the dark phase, no singular arc is thus possible. When $\mu(t) = \bar{\mu}$, this derivative is equal to zero when $y = y_\sigma$ defined in (8). The singular control is then the control that maintains this equilibrium, that is $u_\sigma = \sqrt{\bar{\mu} r} - r$ defined in (6). This control is positive thanks to (10) but it is smaller or equal to 1 only if

$$\bar{\mu} \leq \frac{(r+1)^2}{r} \tag{21}$$

No singular control can exist otherwise. When a singular branch appears in the optimal solution, it is locally optimal because the second order Kelley condition

$$\frac{\partial}{\partial u}\left(\frac{d^2}{d\tau^2}\frac{\partial H}{\partial u}\right) = \frac{2\lambda\mu}{(1+y)^3} \geq 0$$

is satisfied on the singular arc [7].

The construction of the solution is very similar to that in the purely bang-bang case. Similarly, a switch needs to occur in the interval $(0, \bar{T})$. This switch can be from $u = 0$ to $u = 1$ or from $u = 0$ to $u = u_\sigma$ and should occur with $y \leq y_\sigma$ in order to have $\dot{\lambda} \leq 0$. In fact, if a switch first occurs to $u = 1$, an argument identical to the one in the previous section shows that no switch back to 0 can take place before $\bar{T}$; this same argument can in fact be used to show that no switch to $u = u_\sigma$ can take place either since: in both cases, λ should get back to 1, which we show to be impossible.

A switch from 0 to u_σ then takes place once $\lambda = 1$ at $(t_{0\sigma}, y_\sigma)$. Equations (11)-(12) can then be used to identify this switching instant:

$$\frac{r\ln\left(\frac{y_\sigma}{y_0}\right) - \bar{\mu}\ln\left(\frac{\bar{\mu} - r(1+y_\sigma)}{\bar{\mu} - r(1+y_0)}\right)}{r(\bar{\mu} - r)} = t_{0\sigma} \tag{22}$$

$$y_\sigma\left(\frac{\bar{\mu}}{1+y_\sigma} - r\right) = \lambda_0 y_0\left(\frac{\bar{\mu}}{1+y_0} - r\right) \tag{23}$$

From there, $\lambda(t) = 1$ and $y(t) = y_\sigma$ for some time. This could be until $t = \bar{T}$, followed directly by $u = 0$ in the dark phase but, more generically, the singular arc ends at time $t_{\sigma 1} < \bar{T}$, where a switch occurs toward $u = 1$. From then on, things are unchanged with respect to the bang-bang case. The equations that define the transitions from $t_{\sigma 1}$ to $\bar{T}$ are similar to (15) and (16):

$$\frac{(r+1)\ln\left(\frac{\bar{y}}{y_\sigma}\right) - \bar{\mu}\ln\left(\frac{\bar{\mu} - ((r+1)(1+\bar{y})}{\bar{\mu} - (r+1)(1+y_\sigma)}\right)}{(r+1)(\bar{\mu} - r - 1)} = \bar{T} - t_{\sigma 1} \tag{24}$$

$$\bar{\lambda}\bar{y}\left(\frac{\bar{\mu}}{1+\bar{y}} - r - 1\right) + \bar{y} = y_\sigma\left(\frac{\bar{\mu}}{1+y_\sigma} - r\right) \tag{25}$$

The remainder of the solution is unchanged with respect to the bang-bang one, so that we can compute the solution by solving system (17)-(20) and (22)-(25) of eight algebraic equations with eight unknown variables.

Again, the analytical approach has helped us identify the qualitative form of the optimal productivity solution. It now contains five phases:

- Growth with a closed photobioreactor until a sufficient biomass level is reached
- Maximal equilibrium productivity rate on the singular arc
- Maximal harvesting of the photobioreactor with simultaneous growth
- Maximal harvesting of the photobioreactor with no growth until a low level of biomass is reached
- Passive photobioreactor: no harvesting, no growth, only respiration

For this form of solution, we see that maximal instantaneous productivity is achieved during the whole second phase, when the singular solution occurs.

Solution with $\lambda_0 < 1$:

Such a solution would mean that harvesting takes place during the whole dark phase because no transition from $u = 0$ to $u = 1$ can take place in this phase, as we have already shown. Two possibilities then occur: either $u = 1$ all the time or switches from $u = 1$ to $u = 0$ or u_σ and then back to $u = 1$ take place in the interval $(0, \bar{T})$.

In the latter case, the first switch from $u = 1$ to $u = 0$ can only take place with $y > y_\sigma$ because of the constraint that $\dot{\lambda} > 0$ with $\lambda = 1$ at that moment. Then, when the control $u = 0$ is applied for some time, the solution $y(t)$ is increasing. We also have that the switch from $u = 0$ to $u = 1$ can only take place with $y < y_\sigma$ because of the constraint that $\dot{\lambda} < 0$ with $\lambda = 1$ at that moment. This is in contradiction with the fact that $y(t)$ was increasing from above y_σ.

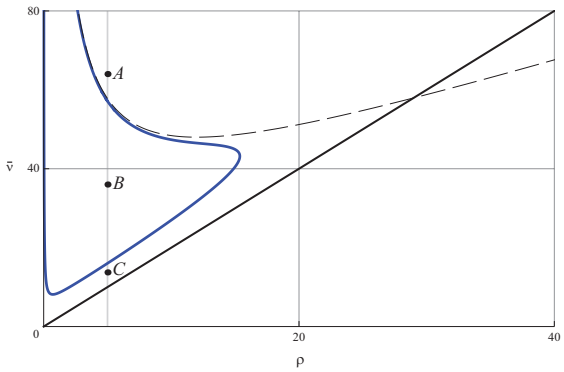

Fig. 1. Bifurcation picture for $D_{max} = 12$, $\kappa = 1$, $T = 1$, $\bar{T} = T/2$. The solid black line is $\bar{\nu} = \kappa\rho T/\bar{T}$ (see (10)), the dashed line is $\bar{\nu} = \kappa(\rho + D_{max})^2/\rho$ and it is related to (7). Optimal patterns for A, B and C are shown on Fig. 3

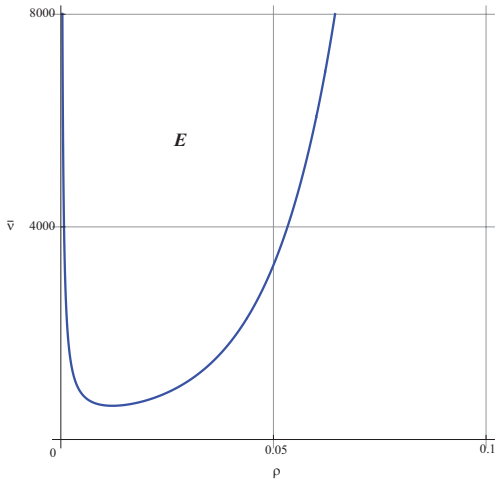

Fig. 2. The region E with optimal constant control $u = 1$. Below this region, this diagram is connected with Fig. 1

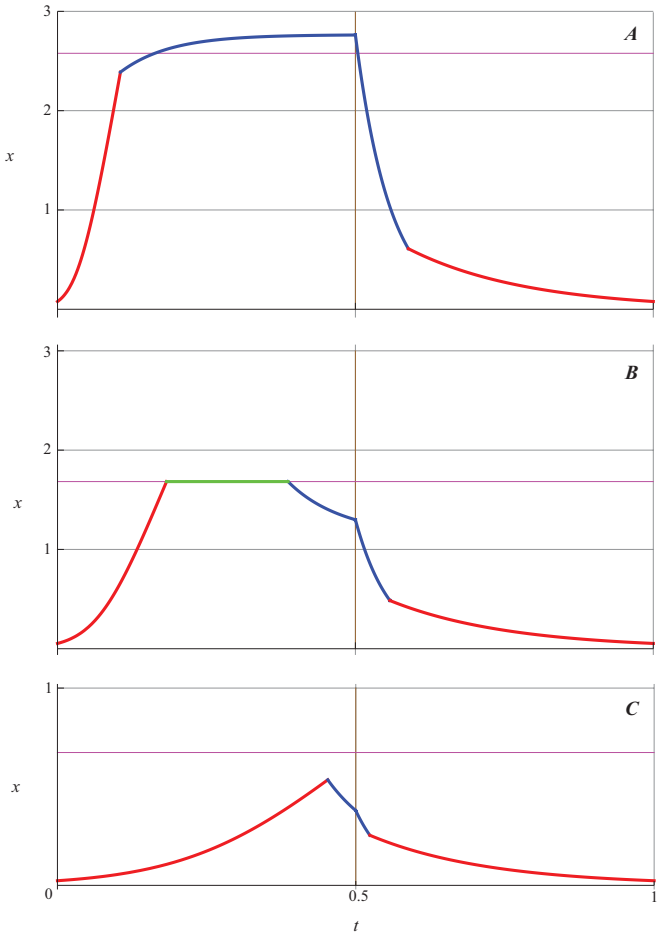

Fig. 3. Different optimal patterns: (A) $\bar{\nu} = 14$, (B) $\bar{\nu} = 36$, (C) $\bar{\nu} = 64$; $\rho = 5$, $D_{max} = 12$, $\kappa = 1$, $T = 1$, $\bar{T} = T/2$. Red: $u = 0$, Blue: $u = 1$, Green: intermediate control $u \in [0, 1]$. Magenta line indicates the level $x = \kappa y_\sigma$ (see (8))

We can also show that no strategy in the $(0, \bar{T})$ interval can have the form $u = 1 \to u_\sigma \to u = 0$ or 1. Indeed, in order to reach the singular arc with $u = 1$, a solution should be coming from above it. If the switch that takes place at the end of the singular phase is from u_σ to 0, $y(t)$ will increase and there should be a subsequent switch from 0 to 1 which is impossible with $y(t) > y_\sigma$. If the switch that takes place at the end of the singular phase is from u_σ to 1, $y(t)$ will decrease all the time between $t_{\sigma 1}$ and T, which is in contradiction with the fact that we had $y(0) > y_\sigma$.

The only potential optimal control in that family is therefore $u(t) = 1$ for all times. Using the expressions computed previously, this control can be a candidate optimal control law only if $y_0 = y_{0min}$ as we have seen earlier and the complete dynamics should satisfy:

$$\bar{\lambda}\bar{y}\left(\frac{\bar{\mu}}{1+\bar{y}} - r - 1\right) + \bar{y} = \lambda_0 y_0 \left(\frac{\bar{\mu}}{1+y_0} - r\right) \tag{26}$$

$$\bar{y} = y_0 e^{(r+1)(T-\bar{T})} \tag{27}$$

$$\lambda_0 = \bar{\lambda} e^{(r+1)(T-\bar{T})} - \frac{e^{(r+1)(T-\bar{T})} - 1}{r+1} \tag{28}$$

with $\lambda_0 < 1$ and $\bar{\lambda} < 1$.

IV. BIFURCATION ANALYSIS

In this section, we will consider fixed values of all parameters except of $\bar{\nu}$ and ρ. We build a bifurcation diagram for these two parameters by identifying in which region no solution is possible (where (10) is not satisfied, it is below the solid black line on Fig. 1), and where the optimal solution is bang-singular-bang (Fig. 1, inside the blue curve), bang-bang (Fig. 1, outside the blue curve and above the solid black line), and constant at value 1 (see Fig. 2). But the last case is only realized for extremely large values of $\bar{\nu}$. We see that the region where singular control can exist is smaller than what is defined by condition (21). This is due to the fact that, though the singular control is possible, there is not enough time for the control to reach that level (see Fig. 3(C)). For larger values of $\bar{\nu}$, no singular control is possible and the optimal solution in the light region goes toward the equilibrium corresponding to $u = 1$ (see Fig. 3(A)). In that case, as well as in the bang-singular-bang case, the solutions go to the optimal solution of the constant light problem (Fig. 3(B)).

V. CONCLUSIONS

We have shown that, because of the day-night constraint, the productivity rate cannot be as high as it could have been without it. However, when the maximal growth rate is sufficiently larger than the respiration rate, we manage to have a temporary phase where the productivity rate is at or near this level. The maximal harvesting at the end of the light phase and at the beginning of the dark phase minimizes the biomass during the dark phase and, consequently, the net respiration. If the maximal growth rate is very large, the optimal solution consists in constantly applying maximal control because the biomass that is built-up in the light phase needs to be harvested even during the night.

REFERENCES

[1] O. Bernard, P. Masci and A. Sciandra, "A photobioreactor model in nitrogen limited conditions", *in 6th Vienna International Conference on Mathematical Modelling MATHMOD 2009*, Vienna, Austria, 2009.

[2] Y. Chisti, Biodisel from microalgae. *Biotechnology Advances*, vol. 25, 2007, pp 294-306.

[3] M. Droop, Vitamin B12 and marine ecology. IV. the kinetics of uptake growth and inhibition in *Monochrysis lutheri*. *J. Mar. Biol. Assoc.*, vol. 48(3), 1968, pp 689-733.

[4] J. Huismann et al., Principles of the light-limited chemostat: theory and ecological applications. *Antonie van Leeuvenhoek*, vol. 81, 2002, pp 117-133.

[5] M. Huntley, D. Redalje, Co2 mitigation et renewable oil from photosynthetic microbes: A new appraisal. *Mitigation et Adaptation Strategies for Global Change*, vol. 12, 2007, pp 573-608.

[6] E.G. Gilbert, Optimal Periodic Control: a General Theory of Necessary Conditions. *SIAM J. Control and Optimization*, vol. 15(5), 1977, pp 717-746.

[7] A.A. Melikyan, *Generalized Characteristics of First Order PDEs: Applications in Optimal Control and Differential Games*. Birkhäuser, Boston; 1998.

[8] P. Masci, O. Bernard, F. Grognard, Microalgal biomass productivity optimization based on a photobioreactor model, *Computer Applications in Biotechnology*, 2010.

[9] J. Monod, *Recherches sur la Croissance des Culteres Bactériennes*. Herman, Paris; 1942.

[10] L.S. Pontryagin, V.G. Boltyansky, R.V. Gamkrelidze, E.F. Mishchenko, *Mathematical Theory of Optimal Processes*. Wiley-Interscience, New York; 1962.

[11] P. Spolaore, C. Joannis-Cassan, E. Duran, A. Isambert, Commercial applications of microalgae. *Journal of Bioscience and Bioengineering*, vol. 101(2), 2006, pp 87-96.

Chapter 4

Competition outcome prediction and control for selecting species of interest

Since Darwin's work, competition has become one of the main topics in ecology. In "On the Origin of Species by Means of Natural Selection, or the Preservation of Favoured Races in the Struggle for Life" [10], page 102, he was expressing the competitive exclusion principle quite clearly:

> *" Owing to the high geometrical rate of increase of all organic beings, each area is already fully stocked with inhabitants; and it follows from this, that as the favoured forms increase in number, so, generally, will the less favoured decrease and become rare. Rarity, as geology tells us, is the precursor to extinction. We can see that any form which is represented by few individuals will run a good chance of utter extinction, during great fluctuations in the nature of seasons, or from a temporary increase in the number of its enemies. But we may go further than this; for, as new forms are produced, unless we admit that specific forms can go on indefinitely increasing in number, many old forms must become extinct." "*

Darwin's work was an impressive demonstration of this principle, by the accumulation of a collection of examples.

Since then, many researchers have tried to apprehend this principle by different means. In 1934, Gause [17] opened the way for a methodology made of both mathematics and experiments:

> *" Experimental researches will enable us to understand the mechanism of the elementary process of the struggle for existence, and we can proceed to the next step: to express these process mathematically. As a result we shall obtain coefficients for the struggle for existence which can be exactly measured. "*

The theoretical result [1] in a competition between several species each represented by Monod model, states that in a pure competition for one limiting

nutrient in a chemostat, the species which needs the lower nutrient concentration to be at equilibrium will win the competition and exclude the others from the environment. A striking point about this result is that it permits to make predictions on the result of a competition, only by *a priori* knowledge of each species nutrient concentration at equilibrium in a monospecific chemostat. This latter can be determined in mono-specific chemostat cultures, so that the competition outcome can be predicted before the real competition experiment. This result was later extended to the more complex Droop competition model with several species, where the minimal nutrient subsistence concentration was also the criteria for winning the competition [25]. Based on these results, the pessimization principle of Adaptive dynamics states [12]:

> *" mutation and natural selection lead to a deterioration of the environmental condition, a Verlenderung. We end up with the worst of all possible environment (where the nutrient concentration is the lowest). "*

This result was validated experimentally by Hansen and Hubbel [22] with two bacterial species, by [44] with two microalgal species, and finally this theoretical behavior was also confirmed in a lake [43], where limitations by phosphate or silicate led to the winning of species with lowest phosphate or silicate equilibrium concentrations.

Meanwhile, theories where developed to explain the "paradox" of phytoplankton species coexistence, introduced by Hutchinson [27]:

> *" The problem that is presented by the phytoplankton is essentially how it is possible for a number of species to coexist in a relatively isotropic or unstructured environment all competing for the same sort of materials "*

Many explanations were found [46], among which biomass-dependence on growth, represented in the Contois model [9], which enables the coexistence of an indefinite number of species on one substrate [19, 32]. This result opens the way for new considerations, where the competitive exclusion and pessimization principles can be explored.

The first paper presented here generalizes the three previous theoretical competition results demonstrated on the Monod [1], Droop [41] and Contois [19] models. By studying a mixed competition with species represented by the three models (some Monod, some Droop, some Contois), we show how the pessimization principle can be revisited.

Then we explore another aspect of competition: instead of predicting competition, we propose new ways to control and modify its outcome. The experiments of Hansen and Hubbel [22] were not only a demonstration that mathematical models enable to predict the outcome of the struggle for existence, but that, by changing the dilution rate, it is possible to change the species that wins the competition, or even to force a coexistence between two species. Thus, it became possible to control competition in a chemostat by using the dilution rate. The second paper of this chapter gives new tracks in this direction, for a competition between species in the Droop model. By controlling the chemostat into a turbidostat mode (where biomass is kept constant), and by forcing the

substrate concentration to be periodic, we show that new competitive criteria arise.

The last paper applies the same methodology to anaerobic digestion for wastewater treatment and methane production, in the case of a reactor's start-up. Start-up in an anaerobic process is a long phase, during which more than 300 bacteria species settle the reactor and build a biofilm. Thus, the species favoured during start-up may have a strong impact on the ecosystem's performance. That is why we propose, using a previously developed model in two steps [6] (acidification and methanization), to control the competition during this phase in order to select the most efficient species.

MATHEMATICAL BIOSCIENCES
AND ENGINEERING
Volume **X**, Number **0X**, XX **200X**

http://www.mbejournal.org/

pp. **X–XX**

COMPETITION BETWEEN DIVERSE TYPES OF MICROORGANISMS : EXCLUSION AND COEXISTENCE

Pierre Masci[1], Frédéric Grognard[1], Eric Benoît[1,2], Olivier Bernard[1]

[1] INRIA Sophia-Antipolis - Team COMORE
2004 route des lucioles, BP 93, 06902 Sophia Antipolis

[2] Laboratoire MIA, Pôle Sciences et Technologie, Université de La Rochelle
Avenue Michel Crépeau, 17042 La Rochelle cedex 1

(Communicated by the associate editor name)

Abstract. Resource-based competition between microorganisms species in continuous culture has been studied extensively both experimentally and theoretically, mostly with Monod "constant yield", Droop "variable yield", and Contois "biomass dependent" models. In Monod or Droop model with N species, with one limiting substrate and under constant controls, the theoretical studies [1, 2, 3] indicated that competitive exclusion occurs: only one species wins the competition and displaces all the others. The winning species expected from theory is the one with the lowest "substrate subsistence concentration" $s^\star$, such that its corresponding equilibrium growth rate is equal to the dilution rate D. This theoretical result was validated experimentally with microalgae [4] and bacteria [5], and observed in a lake with microalgae [6]. On the contrary in Contois, theory [7] predicts coexistence between several species. In this paper we present a generalization of these results by studying a competition between several generalized Monod, Droop and Contois models, leading to a coexistence between several Contois species with the best Monod or Droop competitor, all the other Monod and Droop species being washed out. This demonstration is based mainly on the study of the substrate concentration's evolution caused by competition; it converges towards the lowest subsistence concentration $s^\star$, leading to three different types of competition outcome: 1. only the Monod / Droop best competitor excludes all other species; 2. only some Contois species coexist in the chemostat; 3. A coexistence between the best Monod / Droop species, with one or several Contois species.

1. Introduction.

1.1. The Competitive Exclusion Principle (CEP), an ecological and mathematical topic of interest.

"Complete competitors cannot coexist"

This is the formulation chosen by Hardin [8] to describe the Competitive Exclusion Principle (CEP). According to him, this ambiguous wording "is least likely to hide the fact that we still do not comprehend the exact limits of the principle". But still, a more precise formulation is given: if several non-interbreeding populations "do the same thing" (they occupy the same ecological niche in Elton's sense [9]) and if

2000 *Mathematics Subject Classification.* Primary: 92D40, 92D25, 34D23; Secondary: 34A34.
Key words and phrases. competition, competitive exclusion, droop, variable yield model, monod, ratio-dependent, biomass-dependent, microorganism, microalgae, phytoplankton.

they occupy the same geographic territory, then ultimately the most competitive species will completely displace the others, which will become extinct.

Darwin was already expressing this principle when he spoke about natural selection ([10] p.71 and 102). Scriven described and analyzed his work in these words: "Darwin's success lay in his empirical, case by case, demonstration that recognizable fitness was very often associated with survival. [...] Its great commitment and its profound illumination are to be found in its application to the lengthening past, not the distant future: in the tasks of explanation, not in those of prediction" [11].

Since the work of Darwin, men have tried to apprehend the limits of the principle in different context and by different means. The "paradox" of phytoplantkon species coexistence was introduced by Hutchinson [12]: "The problem that is presented by the phytoplankton is essentially how it is possible for a number of species to coexist in a relatively isotropic or unstructered environment all competing for the same sort of materials". The task we are interested in, in this paper, is a task of prediction: with the tools of mathematical modelization and analysis we consider the question "what are the mechanisms leading to competitive exclusion or coexistence, and to what competition outcome do they lead?". In the next sections we present how mathematical models have shown their appropriateness for predicting the outcome of competition, in the case of chemostat-controlled microcosms.

1.2. **The chemostat, a tool for studying the CEP in microcosms.** "Microbial systems are good models for understanding ecological processes at all scales of biological organization, from genes to ecosystems" [13]. The chemostat is a device which enables to grow microorganisms under highly controlled conditions. It consists of a vessel crossed by a flow of water, where nourishing nutrients are provided by the input flow, whereas both nutrients and microorganisms are evacuated by the output flow. To keep a constant volume in the vessel, these two flows are kept equal. In this paper we consider that the following conditions are imposed in the chemostat: the medium is well mixed (homogeneous); only one substrate is limiting for all the species, whose only (indirect) interaction is the substrate uptake; the environmental conditions (temperature, pH, light, ...) are kept constant, and so are the dilution rate D, corresponding to the input/output flow of water, and the input substrate concentration s_{in}. Figure 1 represents such a chemostat.

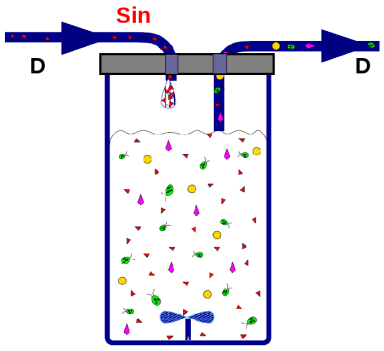

FIGURE 1. A chemostat, which enables to grow microorganisms under highly controlled conditions. The input/output flow of water is D, and the input substrate concentration is s_{in}

The chemostat has been used to study the CEP since the beginning of the XX^{th} century [14], and its experimental use has often been coupled with mathematical models [2].

1.3. **Simplistic mathematical models for microorganisms growth in a chemostat, and previous theoretical results on competition.**

1.3.1. *Substrate "S-model" (generalized Monod model).* To predict the growth of microorganisms species in a chemostat, Monod developed a first model [15], where the growth rates of the biomasses x_i ($i \in \{1, \cdots, N_x\}$ for a competition between N_x species) depend on the extracellular substrate concentration s. In the classical Monod model the growth rates $\alpha_i(s)$ are Michaelis-Menten functions

$$\alpha_i(s) = \frac{s}{s + K_i^s} \alpha_i^m$$

where α_i^m are the maximum growth rates in substrate replete conditions, and K_i^s are the half saturation constants. In this paper we consider a generalized Monod model called "S-model" (Substrate-model), by using the wider class of functions verifying Hypothesis 1.

Hypothesis 1. S-model:
$\alpha_i(s)$ are $\mathcal{C}^1$, increasing and bounded functions such that $\alpha_i(0) = 0$.

We note α_i^m the supremum of the growth rate:

$$\sup_{s \geq 0} \alpha_i(s) = \alpha_i^m > 0$$

The S-species dynamics write

$$\begin{array}{l} \dot{x}_i = (\alpha_i(s) - D) x_i \\ \text{with } s, x_i \in \mathbb{R}^+ \text{ for } i \in \{1, \cdots, N_x\} \text{ and } D \in \mathbb{R}_*^+. \end{array} \tag{1}$$

In this model the substrate uptake is proportional to the biomass growth for each species, so that the total substrate uptake per time unit will be $\sum_{i=1}^{N_x} \alpha_i(s) \frac{x_i}{a_i}$.

1.3.2. *Quota "Q-model" (generalized Droop model).* Some microorganisms, like phytoplankton species, are able to uncouple substrate uptake of nutrients from the growth associated to photosynthesis [16]. This capacity to store nutrients can provide a competitive advantage for the cells that can develop in situations where substrate and light (necessary for phytoplankton growth) are rarely available concomitantly. This behaviour results in varying intracellular nutrient quota: it is the proportion of assimilated substrate per unit of biomass z_k; it can be expressed for instance in mg[substrate]/mg[biomass]. Droop [17] developed a model where these internal quotas are represented by new dynamic variables q_k (denoted "cell quota"). The substrate uptake rates $\rho_k(s)$ are assumed to depend on the extracellular substrate while the biomass growth rates $\gamma_k(q_k)$ depend on the corresponding cell quota.

In the classical Droop model the functions have specified forms. Uptake rates are Michaelis-Menten functions (2) of the substrate concentration:

$$\rho_k(s) = \frac{s}{s + K_k^s} \rho_k^m \tag{2}$$

and the growth rates are Droop functions (3) of the cell quotas:

$$\gamma_k(q_k) = \begin{cases} \left(1 - \frac{Q_k^0}{q_k}\right)\bar{\gamma}_k & \text{if } q_k \geq Q_k^0 \\ 0 & \text{if } q_k < Q_k^0 \end{cases} \tag{3}$$

with ρ_k^m and $\bar{\gamma}_k$ the maximal uptake and growth rates; K_k^s represent the half saturation constants, and Q_k^0 the minimal cell quota. In this paper we consider the wider class of Q-models (Quotas models) verifying Hypothesis 2, so that it can encompass, among others, the classical Droop formulation [17] as well as the Caperon-Meyer model [18].

Hypothesis 2. Q-model:

- $\rho_k(s)$ are $\mathcal{C}^1$, increasing and bounded functions such that $\rho_k(0) = 0$
- $\gamma_k(q_k)$ are $\mathcal{C}^1$, increasing and bounded functions for $q_k > Q_k^0 > 0$. When $q_k \leq Q_k^0$, $\gamma_k(q_k) = 0$.

It directly ensues from Hypothesis 2 that $f_k(q_k) = \gamma_k(q_k)q_k$ are increasing functions (for $q_k > Q_k^0$) which are onto $\mathbb{R}_\star^+$, so that the inverse functions f_k^{-1} are defined on $\mathbb{R}_\star^+$.

We denote ρ_k^m and $\bar{\gamma}_k$ the supremal uptake and growth rates:

$$\begin{array}{l} \sup_{s\geq 0} \rho_k(s) = \rho_k^m > 0 \\ \sup_{q_k \geq Q_k^0} \gamma_k(q_k) = \bar{\gamma}_k > 0 \end{array}$$

The Q-species dynamics write

$$\begin{array}{l} \dot{q}_k = \rho_k(s) - f_k(q_k) \\ \dot{z}_k = (\gamma_k(q_k) - D)z_k \\ \text{with } s, q_k, z_k \in \mathbb{R}^+ \text{ for } k \in \{1, \cdots, N_z\} \text{ and } D \in \mathbb{R}_*^+. \end{array} \tag{4}$$

The substrate uptake per time unit is $\sum_{k=1}^{N_z} \rho_k(s)z_k$

This model has been experimentally shown to be better suited for micro-algae dynamic modelling than the Monod model ([19]) that implicitly supposes that the intracellular quota is simply proportional to the substrate concentration in the medium. The stability of the Q-model has been extensively studied in the monospecific case ([20, 21, 22]).

1.4. **Previous demonstrations of the CEP S- and Q-models.** The advantage of the S- and Q-models is that their relative simplicity allows a mathematical analysis. The analyses of the S-model with N_x competing species [1], and of the Droop model with 2 species [2] and then recently with N_z species [3] led to a confirmation of the CEP in the chemostat, and to a prediction on "who wins the competition", or "what criterion should a species optimize to be a good competitor". In both cases, we have

Theorem 1.1. *If environmental conditions are kept constant and the competition is not controlled (D and s_{in} remain constant) in a chemostat, then the species with lowest "substrate subsistence concentration" $s_i^{x\star}$ (or $s_k^{z\star}$), such that its corresponding equilibrium growth rate is equal to the dilution rate D, is the most competitive and displaces all the others.*

A striking point about this result is that it permits to make predictions on the result of a competition, only by *a priori* knowledge of the species substrate subsistence concentrations $s_i^{x\star}$ (or $s_k^{z\star}$). This latter can be determined in monospecific-culture chemostat, so that the competition outcome can be determined before competition

really occurs. Several experimental validations where carried out with microalgae [4] and bacteria [5]. This theoretical behaviour was also confirmed in a lake [6], where limitations by phosphate or silicate led to the winning of species with lowest phosphate or silicate subsistence concentrations.

1.4.1. *Substrate-Biomass "SB-model" (generalized Contois model).* In cases of intraspecific competition for space (spatial heterogeneity, flocculations/deflocculations phenomena [23]) or substrate, some bacterial or algal species have biomass-dependent growth rates. Contois model [24] represents such dynamics by using more complex growth functions where the growth rates depend not only on the substrate concentration, but also on the species biomass concentration y_j ($j \in \{1, \cdots, N_y\}$):

$$\beta_j(s, y_j) = \frac{s}{K_j^s y_j + s} \beta_j^m$$

In this paper we consider the wider class of "SB-model" (Substrate-Biomass model) verifying the following hypotheses:

Hypothesis 3. SB-model :
$\beta_j(s, y_j)$ are $\mathcal{C}^1$ functions on $\mathbb{R}^+ \times \mathbb{R}^+ \setminus \{(0,0)\}$, increasing and bounded functions of s (for $y_j > 0$), and decreasing functions of y_j (for $s_j > 0$) such that $\forall y_j \in \mathbb{R}_*^+$, $\beta_j(0, y_j) = 0$ and $\forall s \in \mathbb{R}^+$, $\lim_{y_j \to +\infty} \beta_j(s, y_j) = 0$

We also need to add the following technical hyposthesis, which is verified by the classical Contois function:

Hypothesis 4.

$$\frac{\partial}{\partial y_j} \left(\beta_j(s, y_j) y_j\right) > 0$$

We notice that the Contois growth function is undefined in $(0, 0)$, and that Hypothesis 3 has been built so that this property can (but does not have to) be retained by the generalized β function. All other properties imposed by Hypotheses 3 and 4 are satisfied by the original Contois growth-rate.

We denote $\beta_j^m(y_j)$ the supremal growth rates for biomass concentration y_j:

$$\sup_{s \geq 0} \beta_j(s, y_j) = \beta_j^m(y_j)$$

so that the SB-species dynamics write

$$\begin{array}{l} \dot{y}_j = (\beta_j(s, y_j) - D) y_j \\ \text{with } s, y_j \in \mathbb{R}^+ \text{ for } j \in \{1, \cdots, N_y\} \text{ and } D \in \mathbb{R}_*^+. \end{array} \tag{5}$$

In this model, like in the S-model, the substrate/biomass intracellular quotas b_j are supposed to be constant for each species, so that the substrate uptake rates are proportional to the growth rates with a factor $1/b_j$.

1.4.2. *Coexistence result for competition between SB-species.* Competition between several SB-species was studied [7] and led to a coexistence at equilibrium with the substrate at a level $s^{y\star}$ depending on the input substrate concentration s_{in} and the dilution rate D. The species share the available substrate. To be more precise we must define the "s_0-compliance" concept: s_0-compliant species are the species able to have a growth rate equal to the dilution rate D with a substrate concentration s_0. The results of [7] show that all the "$s^{y\star}$-compliant" species coexist in the reactor at equilibirum, and all the others are washed out, as they cannot grow fast enough with substrate concentration $s^{y\star}$.

Definition 1.2. A species x_i, y_j or z_k is s_0-compliant if it is able to reach a growth rate equal to the dilution rate D with a substrate concentration s_0.

1.4.3. *Competition and coexistence - towards a new paradigm.* Following these results an interrogation arises:

≪ What would be the result of a competition between "competitive" S- or Q-species, and "coexistive" SB-species? Competitive exclusion? Coexistence? ≫

The aim of this paper is to provide an answer to this question, and to give insight into the mechanisms forcing the outcome of such a competition. This answer leads to a broader view and understanding of competitive exclusion and coexistence mechanisms, following the words of Hardin [8]: "To assert the truth of the competitive exclusion principle is not to say that nature is and always must be, everywhere,"red in tooth and claw." Rather, it is to point out that *every* instance of apparent coexistence must be accounted for. Out of the study of all such instances will come a fuller knowledge of the many prosthetic devices of coexistence, each with its own costs and its own benefits."

1.5. **A generalized model for competition between several microorganisms species growing according to different kinetic models.** The generalized model for competition between all S-, Q- and SB-species is an aggregation of these models, which alltogether give the following substrate dynamics, subject to substrate input, output, and uptake rates:

$$\dot{s} = D(s_{in} - s) - \sum_{i=1}^{N_x} \alpha_i(s)\frac{x_i}{a_i} - \sum_{j=1}^{N_y} \beta_j(s, y_j)\frac{y_j}{b_j} - \sum_{k=1}^{N_z} \rho_k(s) z_k \tag{6}$$

The parameters related to the nutrient flow are the dilution rate $D > 0$ and the input substrate concentration $s_{in} > 0$, which are both assumed to be constant.

To simplify notations we can remark that this system can be normalized with $a_i = b_j = 1$, when considering the change of variables $\tilde{x}_i = \frac{x_i}{a_i}$ and $\tilde{y}_j = \frac{y_j}{b_j}$ (note that all the hypotheses are still satisfied). We obtain system (7) where variables x_i and y_j are now expressed in substrate units.

$$\begin{cases} \dot{s} = D(s_{in} - s) - \sum_{i=1}^{N_x} \alpha_i(s) x_i - \sum_{j=1}^{N_y} \beta_j(s, y_j) y_j - \sum_{k=1}^{N_z} \rho_k(s) z_k \\ \dot{x}_i = (\alpha_i(s) - D) x_i \\ \dot{y}_j = (\beta_j(s, y_j) - D) y_j \\ \dot{z}_k = (\gamma_k(q_k) - D) z_k \\ \dot{q}_k = \rho_k(s) - f_k(q_k) \end{cases}$$
$$\text{with} \quad f_k(q_k) = \gamma_k(q_k) q_k$$
$$\text{and } s, q_k \in \mathbb{R}^+, \quad s_{in}, D \in \mathbb{R}_*^+ \text{.and } x_i(0), y_j(0), z_k(0) \in \mathbb{R}_*^+ \text{ for } i \in \{1, \cdots, N_x\},$$
$$j \in \{1, \cdots, N_y\}, k \in \{1, \cdots, N_z\} \tag{7}$$

Note that the results obtained in this paper apply also on the simple S-only, Q-only, and SB-only competition models, or on a model with two of these three kind of species.

1.6. **Other coexistence mechanisms, and competition control.** This introduction wouldn't be complete without a short review of what has been done concerning other coexistive models, or the control of competition.

Following the question arised by Hutchinson [12] concerning the "paradox of the phytoplankton", a large amount of work has been done to explore the mechanisms that enable coexistence, mainly for models derived from the Monod model. It has been shown to occur in multi-resource models [25, 26], in case of non instantaneous growth [27], in some turbidity operating conditions [28], a crowding effect [29], or variable yield [30] (not in the Droop sense). [31] and [32] also presented several mechanisms which can mitigate the competition between microorganisms and promote coexistence.

In other papers ([33], [34] and [35]), controls were proposed to "struggle against the struggle for existence" (that is, to enable the coexistence of complete competitors). These controls indicate how to vary the environmental conditions in order to prevent the CEP from holding : some time varying or state-depending environmental conditions can enable coexistence. [36] propose a theoretical way of driving competition, that is, of choosing environmental conditions for which the competitiveness criterion changes.

2. **Mathematical preliminaries.**

2.1. **The variables are all bounded.** Throughout this paper we study the evolution of one solution of system (7) with initial condition $(s(0), x_1(0), \dots, x_{N_x}(0), y_1(0), \dots, y_{N_y}(0), q_1(0), \dots, q_{N_z}(0), z_1(0), \dots, z_{N_z}(0))$ where $x_i(0) > 0, y_j(0) > 0, z_k(0) > 0$. In this section we study the boundedness of the variables. First, the variables all stay in $\mathbb{R}^+$, as their dynamics are non negative when the variable is null.

Then we know that the biomasses remain positive:

Lemma 2.1.

$$\begin{aligned}
&\forall i \in \{1, \cdots, N_x\}, x_i(0) > 0 \Leftrightarrow \forall t, x_i(t) > 0\\
&\forall j \in \{1, \cdots, N_y\}, y_j(0) > 0 \Leftrightarrow \forall t, y_j(t) > 0\\
&\forall k \in \{1, \cdots, N_z\}, z_k(0) > 0 \Leftrightarrow \forall t, z_k(t) > 0
\end{aligned}$$

Proof. Because of the lower bounds on the dynamics ($\dot{x}_i > -Dx_i$ for the S-species for example), the biomasses are lower bounded by exponentials decreasing at a rate D:

$$\forall t, x_i(t) > x_i(0)e^{-Dt} > 0$$

□

Then, to upperbound the variables we define

$$M = s + \sum_{i=1}^{N_x} x_i + \sum_{j=1}^{N_y} y_j + \sum_{k=1}^{N_z} q_k z_k$$

the total concentration of intra and extracellular substrate in the chemostat. The computation of its dynamics gives

$$\dot{M} = D(s_{in} - M) \tag{8}$$

so that M converges exponentially towards s_{in}. This linear convergence implies the upper boundedness of M:

$$\forall t \geq 0, \quad M(t) \leq M^m = \max(M(0), s_{in})$$

Then s, x_i,y_j and $q_k z_k$ are also upper bounded:

$$\begin{array}{l} \forall t \geq 0, \quad s(t) \leq M(t) \leq M^m \\ \forall i \in \{1, \cdots, N_x\}, \forall t \geq 0, \quad x_i(t) \leq M(t) \leq M^m \\ \forall j \in \{1, \cdots, N_y\}, \forall t \geq 0, \quad y_j(t) \leq M(t) \leq M^m \\ \forall k \in \{1, \cdots, N_z\}, \forall t \geq 0, \quad q_k(t) z_k(t) \leq M(t) \leq M^m \end{array} \tag{9}$$

We are now interested in the boundedness of the Q-model's cell quotas q_k and biomasses z_k

Lemma 2.2. *$\forall k$, the q_k variables are upper bounded by* $\max(f_k^{-1}(\rho_k(M^m)), q_k(0))$

Proof. For any $q_k > f_k^{-1}(\rho_k(M^m))$ there is an upper bound on $\dot{q}_k$:

$$\dot{q}_k = \rho_k(s) - f_k(q_k) \leq \rho_k(s) - \rho_k(M^m) \leq 0$$

so that $s \leq M^m$ implies that q_k cannot increase if it is higher than $f_k^{-1}(\rho_k(M^m))$. □

Lemma 2.3. *$\forall k$, the z_k variables are upper bounded by*

$$z_k^m = \max\left(\frac{M^m}{\gamma_k^{-1}(D)}, z_k(0)\right) \tag{10}$$

with the convention that $\gamma_k^{-1}(D) = +\infty$ if $\bar{\gamma}_k \leq D$

Proof. As $q_k z_k$ is upper bounded by M^m, there is an upper bound on $\dot{z}_k$

$$\dot{z}_k = (\gamma_k(q_k) - D) z_k \leq \left(\gamma_k\left(\frac{M^m}{z_k}\right) - D\right) z_k$$

so that z_k cannot increase if it is larger than $\frac{M^m}{\gamma_k^{-1}(D)}$. □

Lemma 2.4. *After a finite time t_0 there exists a lower bound $\hat{s} > 0$ for s.*

Proof. With hypothesis 4, and as the biomasses are upper bounded, we see that $\dot{s}$ can be lower bounded

$$\dot{s} \geq D(s_{in} - s) - \sum_{i=1}^{N_x} \alpha_i(s) x_i^m - \sum_{j=1}^{N_y} \beta_j(s, y_j^m) y_j^m - \sum_{k=1}^{N_z} \rho_k(s) z_k^m = \phi(s)$$

where ϕ is a decreasing function of s, with $\phi(0) = D s_{in}$ and $\phi(s_{in}) < 0$. By continuity of the ϕ function, there exists a positive value $\hat{s} < s_{in}$ such that $\phi(\hat{s}) = D s_{in}/2$. The region where $s \geq \hat{s}$ is therefore positively invariant. Also s is increasing for any value lower than $\hat{s}$ with $\dot{s} \geq D s_{in}/2$ so that $s(t)$ reaches $\hat{s}$ after some finite time t_0. □

Remark 1. This lemma eliminates any problem that could have arisen from the problem of definition of $\beta_j(s, y_j)$ in $(0, 0)$. After the finite time t_0, no solution can approach this critical value anymore.

Lemma 2.5. *There exists a finite time $t_1 \geq 0$ such that for any time $t \geq t_1$, $q_k(t) \in (Q_k^0, Q_k^m)$ with $Q_k^m = f_k^{-1}(\rho_k^m)$.*

Proof. If $q_k(t) \geq Q_k^m$, then we have

$$\dot{q}_k \leq \rho_k(s) - f_k(Q_k^m) \leq \rho_k(M^m) - \rho_k^m < 0$$

for all $q_k \in [Q_k^m, q_k(0)]$, so that $q_k(t) < Q_k^m$ in finite time t_1 and for any $t \geq t_1$.

If $q_k(t) \leq Q_k^0$ with $t > t_0$ (defined in Lemma 2.4), then we have that

$$\dot{q}_k = \rho_k(s) \geq \rho_k(\hat{s}) > 0$$

for all $q_k \in [q_k(t_0), Q_k^0]$, so that $q_k(t) > Q_k^0$ in finite time t_1 and for any $t \geq t_1$. □

This lemma is biologically relevant since minimum and maximum cell quotas are indeed known characteritics of microalgae species. For the rest of this paper we will consider that all the q_k are in the (Q_k^0, Q_k^m) intervals.

Remark 2. In the classical case of Michaelis-Menten uptake rates (2) and Droop growth rates (3) we have:

$$Q_k^m = Q_k^0 + \frac{\rho_k^m}{\bar{\gamma}_k}$$

2.2. **From a "substrate" point of view... (How substrate concentration influences the system).** Since model (7) is of dimension $1 + N_x + N_y + 2N_z$, it is hard to handle directly. In this section we introduce functions which clarify how the q_k and y_j dynamics are influenced by s. This will enable us to focus on the substrate concentration evolution, and thus reduce the dimension in which the system needs to be analyzed.

2.2.1. *Internal cell quotas q_k are driven by the substrate concentration s.* It is convenient to introduce the functions

$$Q_k(s) = f_k^{-1}(\rho_k(s)) \tag{11}$$

and

$$S_k^z(q_k) = Q_k^{-1}(q_k) \tag{12}$$

With Hypothesis 2 it is easy to check that Q_k is defined, continuous, increasing from $(0, +\infty)$ to (Q_k^0, Q_k^m), so that S_k^z is also well defined, continuous and increasing from (Q_k^0, Q_k^m) to $(0, +\infty)$. The $\dot{q}_k$ equation can then be written

$$\dot{q}_k = f_k(Q_k(s)) - f_k(q_k) \tag{13}$$

or

$$\dot{q}_k = \rho_k(s) - \rho_k(S_k^z(q_k)) \tag{14}$$

Since $f_k(q_k)$ and $\rho_k(s)$ are increasing functions, we see how the dymanics of q_k is influenced by the sign of $Q_k(s) - q_k$ (or $s - S_k^z(q_k)$):

$$sign(\dot{q}_k) = sign(Q_k(s) - q_k) = sign(s - S_k^z(q_k)) \tag{15}$$

For a given constant substrate concentration s, the equilibrium value of q_k is $Q_k(s)$. Conversely, s must be equal to $S_k^z(q_k)$ for q_k to be at equilibirum.

Function Q_k realizes a mapping from the substrate axis to the cell quota axis. Functions S_k^z realizes a mapping from the cell quota axis to the substrate axis. An illustration of the cell quotas behaviour is presented in Figure 2.

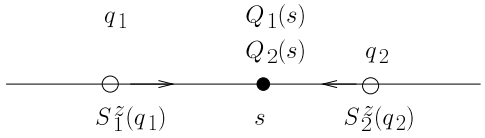

FIGURE 2. Two equivalent statements: "q_k goes towards $Q_k(s)$" and "$S_k^z(q_k)$ goes towards s" (see the sign Property (15)). The latter permits a one dimensional view of the s and q_k dynamics, on the substrate axis.

2.2.2. *How the biomasses y_j are driven by the substrate concentration s.* For the SB-species, it is also convenient to introduce functions $Y_j(s)$:

$$\begin{array}{l} \text{if } \beta_j(s,0) > D, \text{ then } Y_j(s) \text{ is defined by } \beta_j(s, Y_j(s)) = D \\ \text{if } \beta_j(s,0) \leq D, \text{ then } Y_j(s) = 0 \end{array} \tag{16}$$

and the inverse $S_j^y(y_j)$ functions:

$$\begin{array}{l} \forall y_j > 0, \left\{ \begin{array}{l} \text{if } \exists s_0 \text{ s.t. } \beta_j(s_0, y_j) > D, \text{ then } S_j^y(y_j) \text{ is defined by } \beta(S_j^y(y_j), y_j) = D \\ \text{else, } S_j^y(y_j) = +\infty \end{array} \right. \\ S_j^y(0) = \inf_{y_j>0} S_j^y(y_j) \end{array} \tag{17}$$

The values of s such that $Y_j(s) = 0$ correspond to values where the substrate is too low for y_j to survive (y_j is not s-compliant at these values). The values of y_j such that $S_j^y(y_j) = +\infty$ correspond to levels of biomass y_j that cannot be sustained independently of the substrate level.

With Hypothesis 3 it is easy to check that Y_j is defined, continuous, increasing from $\left(S_j^y(0), +\infty\right)$ to $\left(0, \sup_{s\geq 0} Y_j(s)\right)$, so that S_j^y is also well defined, continuous and increasing from $\left(0, \sup_{s\geq 0} Y_j(s)\right)$ to $\left(S_j^y(0), +\infty\right)$.

The $\dot{y}_j$ equation can then be written

$$\dot{y}_j = (\beta_j(s, y_j) - \beta_j(s, Y_j(s)))y_j \tag{18}$$

or

$$\dot{y}_j = (\beta_j(s, y_j) - \beta_j(S_j^y(y_j), y_j))y_j \tag{19}$$

Thus with y_j positivity (see Lemma 2.1) we see how the dymanics of y_j are influenced by the sign of $Y_j(s) - y_j$ (or $s - S_j^y(y_j)$):

$$sign(\dot{y}_j) = sign(Y_j(s) - y_j) = sign(s - S_j^y(y_j)) \tag{20}$$

For a given constant substrate concentration s, the equilibrium value of y_j is $Y_j(s)$. Conversely, s must be equal to $S_j^y(y_j)$ for y_j to be at equilibirum.

Function Y_j realizes a mapping from the substrate axis to the cell quota axis. Functions S_j^y realizes a mapping from the cell quota axis to the substrate axis. An illustration of the biomasses behaviour is presented in Figure 3.

Finally, with Figures 2 and 3 we obtain a one dimensional view of the s, q_k and y_j dynamics on the substrate axis. The demonstration presented in this paper ensues mainly from this one dimensional view of the system.

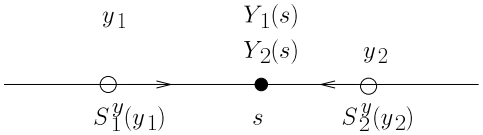

FIGURE 3. Two other equivalent statements: "y_j goes towards $Y_j(s)$" and "$S_j^y(y_j)$ goes towards s" (see the sign Property (20)). The latter permits a one dimensional view of the s and y_j dynamics, on the substrate axis.

2.3. The convergence of s is related to the convergence of q_k and y_j.

Lemma 2.6. *In system (7) the five following properties are equivalent for any* $s_0 > \min_j(S_j^y(0))$*:*

i) $\lim_{t\to+\infty} s(t) = s_0$
ii) $\forall i, \lim_{t\to+\infty} q_k(t) = Q_k(s_0)$
iii) $\exists i, \lim_{t\to+\infty} q_k(t) = Q_k(s_0)$
iv) $\forall j, \lim_{t\to+\infty} y_j(t) = Y_j(s_0)$
v) $\exists j, \lim_{t\to+\infty} y_j(t) = Y_j(s_0) > 0$

When $\lim_{t\to+\infty} s(t) = s_0 \leq \min_j(S_j^y(0))$*, all the* $q_k(t)$ *converge to* $Q_k(s_0)$ *and the* $y_j(t)$ *to* $Y_j(s_0) = 0$.

Proof. In the case $s_0 > \min_j(S_j^y(0))$ we successively demonstrate five implications.
$i \Rightarrow ii$ and $i \Rightarrow iv$: straightforward with the attraction (13) of q_k by $Q_k(s)$, and the attraction (18) of y_j by $Y_j(s)$. Note that $y_j(0)$ cannot be null (Lemma 2.1).
$ii \Rightarrow iii$ and $iv \Rightarrow v$: trivial implications.
$iii \Rightarrow i$ (and $v \Rightarrow i$): we equivalently demonstrate that the simultaneous convergence of q_k (resp. y_j) and non convergence of s lead to a contradiction.

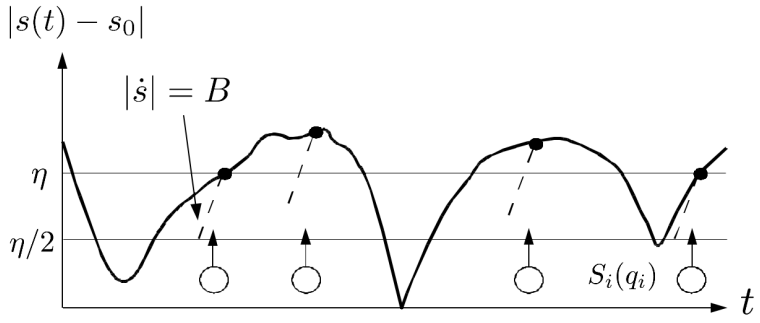

FIGURE 4. Visual explanation of the demonstration of Lemma 2.6. s is repeatedly escaping a η-interval around s_0 ($\bullet$). Because $|\dot{s}|$ is upper bounded by B, then s is out of the $\eta/2$-interval during non negligible time intervals (*dashed lines* represent $|\dot{s}| = B$). q_k (resp. y_j) is repeatedly attracted away from $Q_k(s_0)$ (resp. $Y_j(s_0)$) by $Q_k(s)$ (resp. $Y_j(s)$) (*arrows*)

If s does not converge towards s_0, it is repeatedly out of a $[s_0-\eta, s_0+\eta]$ interval, denoted η-interval:

$$\exists \eta > 0, \forall t > 0, \exists t^s > t, |s(t^s) - s_0| > \eta$$

In Figure 4, t^s time instants are represented by $\bullet$.

We can then use the upper-bounds (9) and (10) on s, x_i, y_j and z_k to show the boundedness of the s dynamics

$$D(s_{in} - M^m) - \sum_{i=1}^{N_x} \alpha_i^m x_i^m - \sum_{j=1}^{N_y} \beta_j^m(0) y_j^m - \sum_{k=1}^{N_z} \rho_k^m z_k^m \leq \dot{s} \leq D s_{in} \qquad (21)$$

so that

$$|\dot{s}| \leq B$$

with $B = \max\left(D s_{in}, -D(s_{in} - M^m) + \sum_{i=1}^{N_x} \alpha_i^m x_i^m + \sum_{j=1}^{N_y} \beta_j^m(0) y_j^m + \sum_{k=1}^{N_z} \rho_k^m z_k^m \right)$.

Then, every time s is out of the η-interval, it must also have been out of the $\eta/2$-interval during a time interval of minimal duration $A(\eta) = \frac{1}{B}\frac{\eta}{2}$. (For a visual explanation see the *dashed lines* of Figure 4, representing the increase caused by $|\dot{s}| = B$).

If for some t^s we have $s(t^s) \geq s_0 + \eta$, we then have that $s(t^s) \geq s_0 + \eta/2$ during the whole time-interval $[t^s - A(\eta), t^s]$. We can thus lower bound the dynamics of q_k (resp. y_j) during that time-interval:

$$\begin{aligned}
\dot{q}_k &= f_k(Q_k(s)) - f_k(q_k) \\
&> f_k(Q_k(s_0 + \eta/2)) - f_k(q_k) \\
&\text{and} \\
\dot{y}_j &> (\beta_j(s_0 + \eta/2, y_j) - D) y_j \\
&= (\beta_j(s_0 + \eta/2, y_j) - \beta_j(s_0 + \eta/2, Y_j(s_0 + \eta/2))) y_j
\end{aligned}$$

Now the convergence of q_k to $Q_k(s_0)$ (resp. y_j to $Y_j(s_0)$) is defined as

$$\forall \epsilon > 0, \exists t^q > 0, \forall t > t^q, |q_k(t) - Q_k(s_0)| < \epsilon (\text{resp. } |y_j(t) - Y_j(s_0)| < \epsilon) \qquad (22)$$

since we can pick ϵ such that $\epsilon < Q(s_0 + \eta/4) - Q(s_0)$ (resp. $\epsilon < \min(Y_j(s_0 + \eta/4) - Y_j(s_0), Y_j(s_0) - Y_j(s_0 - \eta/4))$), we then have, for $t > t_q$, that $q_k(t) < Q(s_0 + \eta/4)$ (resp. $Y_j(s_0 - \eta/4) < y_j(t) < Y_j(s_0 + \eta/4)$). Taking our t^s larger than the corresponding $t^q + A(\eta)$, we then have for all time $t \in [t^s - A(\eta), t^s]$

$$\begin{aligned}
\dot{q}_k &> f_k(Q_k(s_0 + \eta/2)) - (f_k(Q_k(s_0) + \epsilon)) \\
&> f_k(Q_k(s_0 + \eta/2)) - f_k(Q_k(s_0 + \eta/4)) = C^q(\eta) > 0 \\
&\text{and} \\
\dot{y}_j &> (\beta_j(s_0 + \eta/2, Y_j(s_0) + \epsilon) - \beta_j(s_0 + \eta/2, Y_j(s_0 + \eta/2))) y_j \\
&> (\beta_j(s_0 + \eta/2, Y_j(s_0 + \eta/4)) - \beta_j(s_0 + \eta/2, Y_j(s_0 + \eta/2))) y_j \\
&> (\beta_j(s_0 + \eta/2, Y_j(s_0 + \eta/4)) - \beta_j(s_0 + \eta/2, Y_j(s_0 + \eta/2))) Y_j(s_0 - \eta/4) \\
&= C^y(\eta) > 0
\end{aligned}$$

with $C^q(\eta) > 0$ since f_k is an increasing function of q_k, and $C^y(\eta) > 0$ since β_j is a decreasing function of y_j

We then define

$$C(\eta) = \min\left(C^q(\eta), C^y(\eta)\right)$$

If we then choose ϵ such that $\epsilon < \frac{C(\eta) \cdot A(\eta)}{2}$, then $|q_k(t^s) - q_k(t^s - A(\eta))| > 2\epsilon$ (resp. $|y_j(t^s) - y_j(t^s - A(\eta))| > 2\epsilon$), and we see that the increase of q_k (resp. y_j)

makes it eventually get out of the ϵ-interval around $Q_k(s_0)$ (resp. $Y_j(s_0)$). This is a contradiction, so that implication $iii \Rightarrow i$ (resp. $v \Rightarrow i$) holds.

Alternatively, if for some t^s we have $s(t^s) \leq s_0 - \eta$, then we can upper bound the dynamics of q_k (resp. y_j) during the $[t^s - A(\eta), t^s]$ time-interval:

$$\begin{array}{ll} \dot{q}_k & < f_k(Q_k(s_0 - \eta/2)) - f_k(q_k) \\ \text{and} & \\ \dot{y}_j & < (\beta_j(s_0 - \eta/2, y_j) - D)y_j \\ & = (\beta_j(s_0 - \eta/2, y_j) - \beta_j(s_0 - \eta/2, Y_j(s_0 - \eta/2)))y_j \end{array}$$

and the same arguments hold, with

$$\begin{array}{l} \dot{q}_k < f_k(Q_k(s_0 - \eta/2)) - f_k(Q_k(s_0) - \eta/4) = C(\eta) < 0 \\ \text{and} \\ \dot{y}_j < (\beta_j(s_0 - \eta/2, Y_j(s_0 - \eta/4)) - \beta_j(s_0 - \eta/2, Y_j(s_0 - \eta/2)))Y_j(s_0 + \eta/4) \\ = C(\eta) < 0 \end{array}$$

and finally $\epsilon < \frac{-C(\eta) \cdot A(\eta)}{2}$ which causes the contradiction. □

2.4. **The equilibria correspond to the substrate subsistence concentrations.** In this section we present the equilibria of the generalized competition model (7). The first equilibrium of this model corresponds to the extinction of all the microorganisms species:

$$E_0 = (s_{in}\ ,\ 0, \ldots, 0\ ,\ 0, \ldots, 0\ ,\ 0, \ldots, 0\ ,\ Q_1(s_{in}), \ldots, Q_N(s_{in}))$$

This equilibrium is globally attractive if the input substrate concentration s_{in} is not high enough for the species' growth to compensate their withdrawal of the chemostat by the output flow D, that is if $\forall i, \alpha_i(s_{in}) \leq D$ and $\forall j, \beta_j(s_{in}, 0) \leq D$ and $\forall k, \gamma_k(Q_k(s_{in})) \leq D$ (proof of this result is easy and we omit it; for getting a clear idea of the demonstration, see [1] and [2] for the S-only and Q-only cases). We suppose that we are not in this situation through the following hypothesis:

Hypothesis 5. We assume that one of the following condition is satisfied:

- $\exists i, \alpha_i(s_{in}) > D$
- $\exists j, \beta_j(s_{in}, 0) > D$
- $\exists k, \gamma_k(Q_k(s_{in})) > D$

This guarantees that, at least for one of the families of species, there exists some index i, j, k and some associated unique $s_i^{x\star}, s_j^{y\star}, s_k^{z\star} < s_{in}$ (denoted "subsistence concentration") such that

$$\begin{array}{l} \alpha_i(s_i^{x\star}) = D \\ \beta_j(s_j^{y\star}, Y_j(s_j^{y\star})) = D \quad \text{with} \quad s_j^{y\star} + Y_j(s_j^{y\star}) = s_{in} \\ \gamma_k(Q_k(s_k^{z\star})) = D \end{array}$$

Note that in the SB-model, there exists an infinity of $s \in [S_j^y(0), s_{in})$ verifying $\beta_j(s, Y_j(s)) = D$. The value $s_j^{y\star}$ is then the substrate concentration required for having species j remaining alone in the chemostat at equilibrium. It has to satisfy $s_j^{y\star} + Y_j(s_j^{y\star}) = s_{in}$ because of (8) that imposes $M = s + y_j = s_{in}$ at equilibrium.

$$\begin{array}{l} 0 < s^{x\star} = s_1^{x\star} < s_2^{x\star} < \ldots < s_{n_x}^{x\star} \leq s_{in} \\ 0 < S_1^y(0) < S_2^y(0) < \ldots < S_{n_y}^y(0) \leq s_{in} \\ 0 < s^{z\star} = s_1^{z\star} < s_2^{z\star} < ... < s_{n_z}^{z\star} \leq s_{in} \\ \text{with } \forall (i,j,k) \in (\{1,...,n_x\},\{1,...,n_y\},\{1,...,n_z\}),\ s_i^{x\star} \neq S_j^y(0) \neq s_k^{z\star} \end{array} \tag{23}$$

where n_x, n_y and n_z are the number or S-, SB- and Q-species having a subsistence concentration smaller than s_{in} for the given D; all other species cannot be positive at equilibrium. Hypothesis 5 implies that at least one of n_x, n_y and n_z is non-zero. We denote $s^{x\star}$ and $s^{z\star}$ the lowest S- and Q- substrate subsistence concentrations. We also denote $s^{y\star}$ the substrate concentration that there would be at equilibrium if there were only SB-species in the chemostat (see [7]); since it needs to satisfy (8), it requires

$$s^{y\star} + \sum_{j=1}^{n_y} Y_j(s^{y\star}) = s_{in}$$

Though the sum of $Y_j(s^{y\star})$ spans all the relevant indices, some species might have $Y_j(s^{y\star}) = 0$ because they have $s^{y\star} < S_j^y(0) < s_{in}$. If some n_x, n_y or n_z is zero, we set the corresponding $s^{x\star}$, $s^{y\star}$ or $s^{z\star}$ to s_{in} because none of the species from their family can survive at a substrate concentration lower than s_{in}, which is the higher admissible concentration.

In the previous competitive exclusion studies [1, 2, 7] these quantities were of primer importance, as they directed the result of competition. Here we show that the competition outcome is strongly linked to

$$s^\star = \min(s^{x\star}, s^{y\star}, s^{z\star})$$

which is the lowest of all subsistence concentrations. Hypothesis 5 implies that $s^\star < s_{in}$.

We do not consider the case where two subsistence concentrations are equal, because we suppose that the biological parameters of each species are different. In his broad historical review about competitive exclusion [8] Hardin wrote: "no two things or processes in a real world are precisely equal. In a competition for substrate, no difference in growth rate or subsistence quota can be so slight as to be neglected".

Hypothesis 6. $\forall (i,j,k) \in (\{1,...,n_x\},\{1,...,n_y\},\{1,...,n_z\}),\ s_i^{x\star} \neq S_j^y(0) \neq s_k^{z\star}$

The subsistence concentrations and $Y_j(s)$ functions are presented in Figure 5. In this figure, we see that no S- or Q-model species can coexist at equilibrium because s cannot simultaneously be equal to $s_i^{x\star}$ and $s_k^{z\star}$. On the contrary, SB-species verifying Hypothesis 5 can support different s value at equilibrium (between $S_j^y(0)$ and s_{in}), so that there exist equilibria where one S- or Q-model species coexist with one or several SB-species (see Figure 5 for a graphical explanation). On those equilibria, only the SB-species verifying

$$S_j^y(0) < s_i^{x\star} \quad (\text{resp. } S_j^y(0) < s_k^{z\star}) \tag{24}$$

can coexist as they can be at equilibrium at the subsistence concentration of the S-model (resp. Q-model) species, by having a biomass equal to $Y_j(s_i^{x\star})$ (resp. $Y_j(s_k^{x\star})$).

For these considerations, we can enunciate the following proposition which does not need to be proved:

Lemma 2.7. *For a given s_0 substrate concentration, we have*

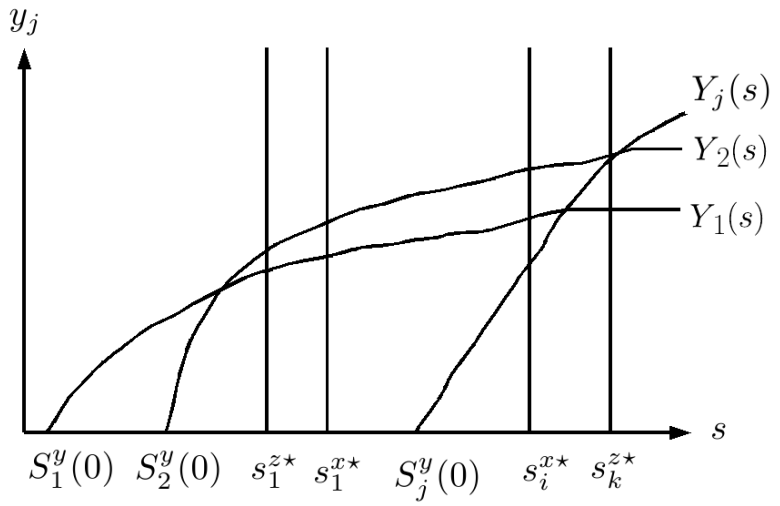

FIGURE 5. Subsistence concentrations of the S-model ($s_i^{x\star}$) and Q-model ($s_k^{z\star}$) species, and equilibrium biomass $Y_j(s)$ of the SB-species, which enable these species to have a growth rate equal to the dilution rate D, and thus to be at equilibrium. We see that S- and Q-model species cannot coexist at equilibrium because they have only one fixed subsistence concentration, and s cannot be simultaneously equal to several of these concentrations. On the contrary, SB-species can coexist with others at equilibrium because they can have a growth equal to D for any $s \in [S_j^y(0), s_{in})$, by adjusting their biomass concentration to $Y_j(s)$ (see definition (16))

- *x_i is s_0-compliant if $s_i^{x*} = s_0$;*
- *y_j is s_0-compliant is $S_j(0) < s_0$;*
- *z_k is s_0-compliant if $s_k^{z*} = s_0$*

It ensues that, for the corresponding SB-species we have

$$Y_j(s_0) > 0$$

which means that they can be at positive equilibrium under dilution rate D and substrate concentration s_0. Thus, the $s^\star$-compliant species are:

- only the $s^\star$-compliant SB-species, if $s^\star = s^{y\star}$
- x_1 and all the $s^\star$-compliant SB-species, if $s^\star = s^{x\star}$
- z_1 and all the $s^\star$-compliant SB-species, if $s^\star = s^{z\star}$

We now present all these equilibria and their stability in S-, SB- and Q-only substrate competitions.

2.5. **S-only equilibria.**

$E_i^x = (s_i^{x\star}\ ,\ 0, \ldots, x_i^\star, \ldots, 0\ ,\ 0, \ldots, 0\ ,\ 0, \ldots, 0\ ,\ Q_1(s_i^{x\star}), \ldots, Q_{N_z}(s_i^{x\star}))$
with $x_i^\star = s_{in} - s_i^{x\star}$

each of these S-only equilibria corresponds to the winning of competition by S-species i; such an equilibrium only exists for $i \in \{0, \cdots, n_x\}$ (all other species

cannot survive at a substrate level lower than S_{in} fot the given D). In a competition between several S-species, eqilibrium E_1^x (with lowest substrate subsistence concentration $s_1^{x\star}$) is asymptotically globally stable, while all the others are unstable [1].

2.6. **Q-only equilibria.**

$$E_k^z = (s_k^{z\star}\ ,\ 0,\dots,0\ ,\ 0,\dots,0\ ,\ 0,\dots,z_k^\star,\dots,0\ ,\ Q_1(s_k^{z\star}),\dots,Q_{N_z}(s_k^{z\star}))$$
$$\text{with}\ \ z_k^\star = \frac{s_{in}-s_k^{z\star}}{Q_k(s_k^{z\star})}$$

Similarly to S-only equilibria, each of these Q-only equilibria corerspond to the winning of competition by Q-species k; such an equilibrium only exists for $k \in \{0,\cdots,n_z\}$. In a competition between several Q-species, eqilibrium E_1^z (with lowest substrate subsistence concentration $s_1^{z\star}$) is asymptotically globally stable, while all the others are unstable [2].

2.7. **SB-only equilibria.** We denominate G a subset of $\{1,\cdots,n_y\}$ representing any SB-species coexistence. For example if we want to speak about species 1, 5 and 7 coexistence, then we use $G = \{1,5,7\}$. We then define E_G^y the equilibrium where these species coexist. It is composed by

- $s_G^{y\star}$ such that $s_G^{y\star} + \sum_{j\in G} Y_j(s_G^{y\star}) = s_{in}$ because of (8)
- $\forall j \in G, y_j = Y_j(s^{y\star})$
- for any other j, $y_j = 0$
- $\forall i \in \{1,\cdots,N_x\}, x_i = 0$
- $\forall k \in \{1,\cdots,N_z\}, z_k = 0$
- $\forall k \in \{1,\cdots,N_z\}), q_k = Q_k(s_G^{y\star})$

there exist many E_G^y equilibria, corresponding to all the possible G subset. The globally asymptotically stable equilibrium of a competition with only SB-species is given by the choice $G = \{1,\cdots,n_y\}$ [7]. Note that some of the G species can have a null biomass on these equilibria, as $Y_j(s_G^{y\star})$ might be null for some $j \in G$. Therefore $E_{G_1}^y$ and $E_{G_2}^y$ with $G_1 \neq G_2$ are not necessarily different.

We must here introduce a technical hypothesis which will be useful later to prove hyperbolicity of the equilibria.

Hypothesis 7. For all G and all j : $S_j(0) \neq s_G^{y\star}$

2.8. **Coexistence equilibria.** As previously said in this section, there also exist equilibria where one of the S- or Q-species coexist with several $s_i^{x\star}$- or $s_k^{z\star}$-compliant SB-species. For a coexistence with S-species we denote them $E_{i,G}^{(x,y)\star}$. They are composed of:

- $s = s_i^{x\star}$
- $\forall j \in G, y_j = Y_j(s_i^{x\star})$
- for any other j, $y_j = 0$
- $\forall l \neq i, x_l = 0$
- $\forall k \in \{1,\cdots,N_z\}, z_k = 0$
- $\forall k \in \{1,\cdots,N_z\}, q_k = Q_k(s_i^{x\star})$
- $x_i = s_{in} - s_i^{x\star} - \sum_{j\in G} Y_j(s_i^{x\star})$ (this value will be denoted $\bar{x}_i^G$)

Similarly, for a coexistence with Q-species we denote them $E_{k,G}^{(z,y)\star}$. They are composed of:

- $s = s_k^{z\star}$
- $\forall j \in G, y_j = Y_j(s_k^{z\star})$

- for any other j, $y_j = 0$
- $\forall i \in \{1, \cdots, N_x\}, x_i = 0$
- $\forall l \neq k, z_l = 0$
- $\forall l \in \{1, \cdots, N_z\}, q_l = Q_l(s_k^{z\star})$
- $z_k = \frac{s_{in} - s_k^{z\star} - \sum_{j \in G} Y_j(s_k^{z\star})}{Q_k(s_k^{z\star})}$ (this value will be denoted $\bar{z}_k^G$)

To our knowledge, these equilibria have never been studied until now.

Note that some of these equilibria might be reduntant with S- or Q-only equilibria, if all the SB-species represented by G are not $s_i^{x\star}$- or $s_k^{z\star}$-compliant. Note also that all those equilibria do not necessarily exist in the non-negative orthant. Indeed, $\bar{x}_i^G$ and $\bar{z}_k^G$ can be negative, depending on s_{in} and on the substrate subsistence concentrations. These equilibria with negative components will not be studied any further since we only consider initial conditions in the positive orthant, which is invariant. In the sequel, we will denote E an equilibrium of (7) which belongs to an unspecified class.

We will now show that if $s = s^\star$ at equilibrium, there exists a positive equilibrium containing all $s^\star$-compliant species.

Lemma 2.8.

- *If* $s^\star = s^{x\star}$ *then* $E^{(x,y)\star}_{1,\{1,\cdots,n_y\}}$ *is in the positive orthant.*
- *If* $s^\star = s^{y\star}$ *then* $E^{y\star}_{\{1,\cdots,n_y\}}$ *is in the positive orthant.*
- *If* $s^\star = s^{z\star}$ *then* $E^{(z,y)\star}_{1,\{1,\cdots,n_y\}}$ *is in the positive orthant.*

Proof.
- If $s^\star = s^{x\star}$, then all $y_j = Y_j(s^{x\star}) \geq 0$ at equilibrium and $s^{y\star} + \sum_{j=1}^{n_y} Y_j(s^{y\star}) = s_{in}$ implies that $s^{x\star} + \sum_{j=1}^{n_y} Y_j(s^{x\star}) < s_{in}$ since $s^{x\star} < s^{y\star}$ and $Y_j(s)$ is non-decreasing. It directly follows that $x_1^\star = s_{in} - s^{x\star} - \sum_j^{n_y} Y_j(s^{x\star}) > 0$.
- If $s^\star = s^{y\star}$, then all x_i and z_k are zero at equilibrium and all $y_j = Y_j(s^{y\star}) \geq 0$
- If $s^\star = s^{z\star}$, then all $y_j = Y_j(s^{z\star}) \geq 0$ at equilibrium and $s^{y\star} + \sum_{j=1}^{n_y} Y_j(s^{y\star}) = s_{in}$ implies that $s^{z\star} + \sum_{j=1}^{n_y} Y_j(s^{z\star}) < s_{in}$ since $s^{z\star} < s^{y\star}$. It directly follows that $z_1^\star = \frac{s_{in} - s^{z\star} - \sum_j^{n_z} Y_j(s^{z\star})}{Q_k(s^{z\star})} > 0$.

□

We call $E^\star$ the equilibrium with all $s^\star$-compliant species remaining in the chemostat, while all the others are excluded. Depending on the species subsistence concentrations, $E^\star$ can be one of the previously presented equilibria:

- if $s^\star = s^{y\star}$ then $E^\star = E^{y\star}_{\{1,\cdots,n_y\}}$: only the $s^\star$-compliant SB-species remain in the chemostat.
- if $s^\star = s^{x\star}$ then $E^\star = E^{(x,y)\star}_{1,\{1,\cdots,n_y\}}$: the best S-species (lowest $s_i^{x\star}$) remains in the chemostat with all the $s_i^{x\star}$-compliant SB-species.
- if $s^\star = s^{z\star}$ then $E^\star = E^{(z,y)\star}_{1,\{1,\cdots,n_y\}}$: the best Q-species (lowest $s_k^{z\star}$) remains in the chemostat with all the $s_k^{z\star}$-compliant SB-species.

In the next section, we present an important global stability result for this equilibrium.

3. **Statement and demonstration of the Main Theorem: competitive exclusion or coexistence in the generalized competition model.** This theorem

states that all the $s^\star$-compliant species (those who can be at equilibrium with substrate subistence concentration $s^\star$, which is the lowest of all $s^{x\star}.s^{y\star}, s^{z\star}$) coexist in the chemostat at equilibrium, while all the others are excluded.

Main Theorem. *In the generalized competition model (7), if Hypotheses 1–7 hold, then all the solutions of the system, having $x_i(0), y_j(0), z_k(0) > 0$ for all s^*-compliant species, converge asymptotically towards equilibrium $E^\star$.*

Structure of the proof: In a first step we reduce system (7) to the mass balance surface. Then we present a non decreasing lower bound $L(t)$ for $s(t)$, and use it to demonstrate that s converges towards $s^\star$. Finally only the s^*-compliant species have a large enough substrate concentration to remain in the chemostat, so that all other S-, Q-, and SB-model species are washed out. The final step consists in showing that the convergence result that we showed on the mass-balance surface can be extended to the whole non-negative orthant.

Remark 3. It is not restrictive to consider $x_i(0), y_j(0), z_k(0) > 0$ for the solutions of the system since species with null initial condition can be ignored, so that we can then consider a smaller dimensional system.

3.1. **Step 1: we consider the system on the mass balance surface and in the region where $q_k \in (Q_k^0, Q_k^m)$ for all $k \in \{1, ..., N_z\}$.** Lemma 2.5 indicates that q_k reaches (Q_k^0, Q_k^m) in finite time, and in (8) we showed that the total concentration of intra and extracellular substrate in the chemostat M converges to s_{in}.

We denote "Σ", the generalized competition model (7) on the mass balance surface defined by

$$M = s + \sum_{i=1}^{N_x} x_i + \sum_{j=1}^{N_y} y_j + \sum_{k=1}^{N_z} q_k z_k = s_{in} \tag{25}$$

For the remainder of the demonstration we will study system Σ, and we will later show that its asymptotic convergence towards an equilibrium has the same behaviour as the initial model (7). While studying system Σ, we will however retain all the states of the original system and the expressions of the equilibria; Σ is then defined by the addition of the invariant constraint (25).

3.2. **Step 2: we propose a non decreasing lower bound $L(t)$ for s.** The main obstacle for the demonstration of the Main Theorem was the possibility that s would repeatedly be lower than $s^\star$ and repeatedly be higher than $s_n^\star = \max(s_{n_x}^{x*}, s_{n_z}^{z*})$, which would generate an oscillating behaviour. In order to eliminate this possibility we build a non decreasing lower bound for s, which converges towards $s_1^\star$. We now present such a lower bound, which will be used to show that s converges to $s^\star$ in the next sections.

Lemma 3.1. *In system Σ*

$$L(t) = \min\left(\min_k(S_k^z(q_k(t))), \min_j(S_j^y(y_j(t)), s^\star, s(t)\right)$$

is a non decreasing lower bound for s

Proof. We know that the right derivative of L is the derivative of one of the function which realizes the minimum. In four cases we show that this right derivative is non negative.

- Case 1: If $S_k^z(q_k(t))$ realizes the minimum then its derivative is non negative, because $S_k^z(q_k)$ goes towards s (see (15)).
- Case 2: If $S_j^y(y_j(t))$ realizes the minimum then its derivative is non negative, because $S_j^y(s)$ goes towards s (see (20)).
- Case 3: If $s(t)$ realizes the minimum then we examine its dynamics $\dot{s}$ for system Σ (*i.e.* on the mass balance equilibrium manifold). We replace s_{in} by $s + \sum_i x_i + \sum_j y_j + \sum_k q_k z_k$:

$$\dot{s} = \sum_i (D - \alpha_i(s))x_i + \sum_j (D - \beta_j(s, y_j))y_j + \sum_k \left(Dq_k - \rho_k(s)\right) z_k$$

which is equivalent to, from the definition (11) of $Q_k(s)$:

$$\dot{s} = \sum_i (D - \alpha_i(s))x_i + \sum_j (D - \beta_j(s, y_j))y_j + \sum_k \left(Dq_k - \gamma_k(Q_k(s))Q_k(s)\right) z_k$$

Then
  - for all i, $s \leq s^\star$ gives us $\alpha_i(s) \leq D$, so that the first sum is non negative;
  - for all j, $s \leq S_j^y(y_j))$ gives us $\beta_j(s, y_j) \leq \beta_j(S_j^y(y_j), y_j) = D)$, so that the second sum is non negative;
  - for all k, $s \leq S_k^z(q_k)$ gives us $Q_k(s) \leq q_k$, and $s \leq s^\star$ gives us $\gamma_k(Q_k(s)) \leq \gamma_k(Q_k(s_k^{z\star})) = D$ so that the third sum is also non negative.

  Finally we obtain
$$\dot{s} \geq 0$$
- Case 4: If $s^\star$ realizes the minimum, we know that its right derivative is null and thus non negative.

□

3.3. **Step 3: we demonstrate that s converges towards $s^\star$.**

Lemma 3.2. *In system* Σ
$$\lim_{t \to +\infty} s(t) = s^\star$$

Proof. We first show, by contradiction, that the substrate concentration $s(t)$ cannot converge towards any constant value other than $s^\star$. Suppose the reverse hypothesis, *i.e.* $\lim_{t\to+\infty} s(t) = \bar{s} \neq s^\star$. Through Lemma 2.6, we then have that $\lim_{t\to+\infty} q_k(t) = Q_k(\bar{s})$ and $\lim_{t\to+\infty} y_j(t) = Y_j(\bar{s})$.

If $\bar{s} < s^\star$,

- $\alpha_i(\bar{s}) < D$ for all i so that all x_i go to 0
- $\gamma_k(Q_k(\bar{s})) < D$ for all k implies that all z_k go to 0

So that we have a contradiction with mass balance equilibrium (25), as the total substrate (in the medium + in the biomasses) at equilibrium $\bar{s} + \sum_{j=1}^{N_y} Y_j(\bar{s})$ will be lower than $s^{y\star} + \sum_{j=1}^{N_y} Y_j(s^{y\star}) = s_{in}$.

If $\bar{s} > s^\star$ we must consider three cases:

- if $s^\star = s_1^{x\star}$ then $\alpha_i(\bar{s}) > D$ implies that x_1 diverges to $+\infty$, which is in contradiction with the boundedness shown in (9).
- if $s^\star = s_1^{z\star}$ then $\gamma_1(Q_1(\bar{s})) > D$ implies that z_1 diverges to $+\infty$, which is in contradiction with the boundedness shown in (10).
- if $s^\star = s^{y\star}$ then we have a contradiction with mass balance equilibrium (25), because $\bar{s} + \sum_{j=1}^{N_y} Y_j(\bar{s})$ will be higher than $s^{y\star} + \sum_{j=1}^{N_y} Y_j(s^{y\star}) \leq s_{in}$.

Hence the impossibility of convergence of s towards any $\bar{s}$ other that $s^\star$ is proven.
We now demonstrate the lemma by contradiction. We assume that

$$s \text{ does not converge towards } s^\star$$

which, from the previous remark means that s does not converge to any constant value.

Remark 4. As s does not converge towards $s^\star$, we know that the q_k do not converge towards $Q_k(s^\star)$ (see Lemma 2.6)

We consider two cases, which both lead to a contradiction, on the basis of a reasoning which is close to the demonstration developed to prove Lemma 2.6.

• Case *a*: L attains $s^\star$ in finite time
In Appendix A we show that a contradiction occurs.
Idea : s cannot stay higher than $s^\star$ without converging to $s^\star$, because this would cause x_1 or z_1 to diverge, or $s + \sum_{j=1}^{N_y} Y_j(s)$ to be always higher than s_{in} without converging to s_{in}.
• Case *b*: L never attains $s^\star$
See Appendix B.
Idea : If s did not converge to $s^\star$, the non decrease of L and its attraction by s would cause it to reach $s^\star$.

In both cases we found a contradiction, so that the proof of Lemma 3.2 is complete.

□

3.4. **Step 4: all the $s^\star$-compliant species remain in the chemostat, while the others are excluded.** In this section we show that, as s converges towards $s^\star$ in model Σ, all the S- and Q-species with substrate subsistence concentration higher than $s^\star$ are washed out of the chemostat because their growth $\alpha_i(s)$ or $\gamma_k(q_k)$ cannot stay high enough to compensate the output dilution rate D. Finally, all the $s^\star$-compliant species able to be at equilibrium with a substrate concentration $s^\star$ remain in the chemostat.

Lemma 3.3. *In system Σ all the solutions with positive initial conditions for the s^*-compliant species converge to $E^\star$.*

Proof. For all the x_i and z_k species such that $\alpha_i(s^\star) < D$ and $\gamma_k(Q_k(s^\star)) < D$, it is straigthforward that the convergence of s to $s^\star$ will cause their biomass to converge to 0. If $s^\star = s^{y\star}$, then this is true for all the S- and Q-species.

For all the $s^\star$-compliant SB-species, we have from Lemma 2.6 that their biomass will tend to $Y_j(s^\star)$, which is positive for the $s^\star$-compliant species and null for all the others.

Finally, if $s^\star = s^{x\star}$ or $s^\star = s^{z\star}$, then we have through the mass balance equilibrium (25) that the S- or Q-species whose subsistence concentration is $s^\star$ will have its biomass converge to $s_{in} - s^\star - \sum_{j=1}^{N_{z1}^y} Y_j(s^\star)$: all the substrate which is not present in the medium or in the SB-biomasses is used by the best S- or Q-competitor. □

3.5. **Step 5: convergence of the solutions for model Σ implies convergence for model (7).** In order to extend the convergence result to the full model and thus prove our Main Theorem, we apply a classical theorem for asymptotically autonomous system [37, 2].

Lemma 3.4. *All solutions of system (7) with positive initial conditions for the s^*-compliant species converge to E^* defined in section 2.7.*

Remark 5. While, up to here, we simply had considered Σ as the same system as (7), in the same dimension, except that it was restricted to (25), we will now equivalently explicitely include (25) into system (7) to obtain Σ in the form of a system that has one dimension less than (7) by omitting the s coordinate. Since both representations of Σ are equivalent, the previously proven stability results are still valid in the new representation, with the exception that convergence takes place towards equilibria directly derived from these presented in sections 2.5-2.8 by omitting the s coordinate. These new equilibria are differentiated from the original ones by adding a $\tilde{}$, so that an arbitrary equilibrium is denoted $\tilde{E}$.

Proof. System Σ can be written as follows :

$$\begin{cases} \dot{x}_i = \left(\alpha_i\left(s_{in} - \sum_{l=1}^{N_x} x_l - \sum_{m=1}^{N_y} y_m - \sum_{r=1}^{N_z} q_r z_r\right) - D\right) x_i \\ \dot{y}_j = \left(\beta_j\left(s_{in} - \sum_{l=1}^{N_x} x_l - \sum_{m=1}^{N_y} y_m - \sum_{r=1}^{N_z} q_r z_r, y_j\right) - D\right) y_j \\ \dot{z}_k = (\gamma_k(q_k) - D) z_k \\ \dot{q}_k = \rho_k\left(s_{in} - \sum_{l=1}^{N_x} x_l - \sum_{m=1}^{N_y} y_m - \sum_{r=1}^{N_z} q_r z_r\right) - f_k(q_k) \\ \text{for } i \in \{1, \cdots, N_x\}, j \in \{1, \cdots, N_y\}, k \in \{1, \cdots, N_z\} \end{cases} \tag{26}$$

where the s state has been removed compared to (7). In order to recover model (7), we should add the equation

$$\dot{M} = D(s_{in} - M)$$

which we interconnect with (26) by replacing every s_{in} in (26) with M. It is this interconnection that we will now study.

In the first part of the proof, we will show that every solution of (7) converges to an equilibrium E. We will then show by induction that all the solutions that do not converge to E^* have an initial condition with some $x_i = 0$, $y_j = 0$ or $z_k = 0$ for some s^*-compliant species. Thus, all the solutions with $x_i \neq 0, y_j \neq 0, z_k \neq 0$ for the s^*-compliant species converge to E^*.

For that, we will use Theorem F.1 from [2]. We will therefore first compute the stable manifolds of all equilibria of Σ:

- The stable manifold of $\tilde{E}^*$ is of dimension $N_x + N_y + 2N_z$. It is constituted of all the initial conditions which verify $x_i(0), y_j(0), z_k(0) > 0$ for s^*-compliant species and $x_i(0), y_j(0), z_k(0) \geq 0$ for all other species, as well as $q_k \geq 0$ for all k (see Lemma 3.3).
- The stable manifold of $\tilde{E}_0$ is of dimension $N_x - n_x + N_y - n_y + 2N_z - n_z$. It is constitued of all the initial conditions which verify $x_1(0) = \ldots = x_{n_x}(0) = 0$, $y_1(0) = \ldots = y_{n_y}(0) = 0$ and $z_1(0) = \ldots = z_{n_z}(0) = 0$. The only species that can be present at the initial condition are those that cannot survive for the given D and s_{in}. Indeed, if any $x_i(0) > 0$ for $i \leq n_x$ (or similar $y_j(0) > 0$ or $z_k(0) > 0$), one can apply Lemma 3.3. to the reduced order system containing these species to show that convergence does not take place

towards $\tilde{E}_0$. Conversely, any initial condition with $x_1(0) = \ldots = x_{n_x}(0) = 0$, $y_1(0) = \ldots = y_{n_y}(0) = 0$ and $z_1(0) = \ldots = z_{n_x}(0) = 0$ generates a solution that goes to $\tilde{E}_0$ since for the other species we have:
  - $\dot{x}_i < (\alpha_i(s_{in}) - D)x_i$, with $\alpha_i(s_{in}) - D < 0$ for all $i > n_x$ because of the definition of n_x presented in (23);
  - $\dot{y}_j < (\beta_j(s_{in}, y_j) - D)y_j$, with $\beta_j(s_{in}, 0) - D < 0$ for all $j > n_y$, because of the definition of n_y;
  - $\dot{z}_k < (\gamma_k(Q_k(s_{in})) - D)z_k$, with $\gamma_k(Q_k(s_{in})) - D) < 0$ for all $k > n_z$ because of the definition of n_z.
- The dimension of the stable manifold of any other $\tilde{E}$ can be computed from Lemma 3.3. To an equilibrium $\tilde{E}$ corresponds a substrate value $\tilde{s}$ ($> s^*$ by definition of s^*). Lemma 3.3 indicates that solutions of Σ converge towards an equilibrium corresponding to $\tilde{s}$, if there is no smaller subsistance concentration corresponding to a species present in the system (for S- and Q species) and if all S-, Q- and SB-species that are $\tilde{s}$-compliant are present in the corresponding equilibrium. The stable manifold of $\tilde{E}$ must therefore be constrained to initial conditions that verify $x_i(0) = 0$, $y_j(0) = 0$ and $z_k(0) = 0$ for all species that are s-compliant for some $s \leq \tilde{s}$ and that are not positive in $\tilde{E}$. Having set all these values to zero, it is indeed clear that $\tilde{s}$ is the $s^\star$ as defined in Lemma 3.3 of the reduced order system (without the aforementionned x_i, y_j and z_k coordinates). All solutions defined in Lemma 3.3 of this system then converge to $\tilde{E}$, which justifies our definition of the stable manifold of $\tilde{E}$. Its dimension is $N_x + N_y + 2N_z - n_{\tilde{E},\tilde{s}}$, where $n_{\tilde{E},\tilde{s}}$ is the number of s-compliant species (for some $s \leq \tilde{s}$) that are not present in $\tilde{E}$.

Through Lemma 3.3, we have in fact shown that all solutions of Σ in the non-negative orthant converge to an equilibrium. Indeed, for a given initial condition, either it belongs to the stable manifold of $\tilde{E}_0$ or, eliminating from the system all species that are null at the initial time necessarily sets it in a form where Lemma 3.3 can be applied (which shows convergence to an equilibrium).

The dimension of the stable manifold of any equilibrium E will therefore be the one of $\tilde{E}$ plus 1. The hypotheses of Theorem F.1 from [2] are indeed all verified:

- The whole system (7) is bounded (see section 2.1)
- The equilibria of system Σ are hyperbolic (see Appendix C.2-C.6).
- There are no cycles of equilibria in system Σ. Indeed, if we analyze the potential transition between two equilibria, both equilibria must belong to the same face, so that convergence takes place to the one corresponding to the smallest value of s. A potential sequence of equilibria would then be characterized by a decreasing value of s at each equilibrium, which prevents it from cycling.

We can then conclude from this theorem that all solutions of (7) tend to an equilibrium. We are then left with checking to what equilibrium they tend.

Before continuing this proof, we need to detail $n_{\tilde{E},\tilde{s}}$. In the case of $\tilde{E} = \tilde{E}^*$ and $\tilde{s} = s^*$, we have $n_{\tilde{E},\tilde{s}} = 0$ (by definition, all s^*-compliant species are present in E^* and there is no other species that is compliant for smaller values of s). Otherwise, we necessarily have $n_{\tilde{E},\tilde{s}} > 0$. Indeed, we know that $\tilde{s} > s^*$, so that all species present in E^* are compliant for some $s < \tilde{s}$; as such, in order to have $n_{\tilde{E},\tilde{s}} = 0$, $\tilde{E}$ would need to at least contain all species that are present in $\tilde{E}^*$. In such a case no

S and Q species can be present in $\tilde{E}^*$ (otherwise, it could not be present in $\tilde{E}$ also for a different value of s). Defining J the set of SB-species that are present in E^* and writing (25) for E^* then yields

$$M = s^* + \sum_{j \in J} Y_j(s^*) = s_{in}$$

Equality (25) should also be valid in $\tilde{s} > s^*$ so that

$$s_{in} = \tilde{s} + \sum_{i=1}^{N_x} x_i + \sum_{j=1}^{N_y} y_j + \sum_{k=1}^{N_z} q_k z_k > \tilde{s} + \sum_{j \in J} Y_j(\tilde{s}) > s_{in}$$

where we have the last inequality (which leads to a contradiction) because $Y_j(s)$ is an increasing function. We can then conclude that, for all $\tilde{E} \neq \tilde{E}^*$, $n_{\tilde{E},\tilde{s}} > 0$, and at least one $s^\star$-compliant species species must be null.

In order to check to what equilibrium solutions of (7) tend, we use an induction argument, by supposing that our Main Theorem has been proven up to $N-1$ species, which we use for the proof for N species. Along with the fact that the stability result is trivial for 1 species (classical Monod model, [2], classical Droop model, [21] and generalized Contois model, [7]), this will conclude our proof.

Let us consider a system of N species with equilibrium E^* as defined earlier. This equilibrium contains positive species (which are $s^\star$-compliant) and null species (which are not $s^\star$-compliant).

Imposing, for one of the not $s^\star$-compliant species, $x_i = 0$ (or $y_j = 0$ or $z_k = 0$) for the initial condition, sets us in the framework where we have $N-1$ species present in the system. Also, since this species did not belong to the positive ones in $E^\star$, its absence does not change anything into which equilibrium is the one corresponding to the smallest subsistance concentration, which remains $E^\star$. We can then apply the induction hypothesis, which indicates that all such initial conditions initiate solutions that converge to $E^\star$ (as long as the $s^\star$-compliant species have positive initial condition).

Studying now the equilibrium E_0, we know from the beginning of the proof that its stable manifold is of dimension $N_x - n_x + N_y - n_y + 2N_z - n_z + 1$. As was done for Σ, it is directly apparent that any initial condition with $x_1(0) = \ldots = x_{n_x}(0) = 0$, $y_1(0) = \ldots = y_{n_y}(0) = 0$ and $z_1(0) = \ldots = z_{n_x}(0) = 0$ generates a solution that has all species exponentially go to zero. Finally, the analysis of the $\dot{s}$ equation shows that it has the form $\dot{s} = D(s_{in} - s) - F(t)$ with $F(t)$ exponentially going to zero so that s goes to s_{in} and all such solutions go to E_0.

We can now consider all the other equilibria. Let an equilibrium E corresponding to a substrate concentration $\tilde{s}$ ($> s^*$ by definition). As we have seen in our analysis of Σ, the stable manifold of the corresponding $\tilde{E}$ is of dimension $N_x + N_y + 2N_z - n_{\tilde{E},\tilde{s}}$, so that the stable manifold of E is of dimension $N_x + N_y + 2N_z - n_{\tilde{E},\tilde{s}} + 1$. Let us set ourselfes in the situation where all $n_{\tilde{E},\tilde{s}}$ species are set to zero at the initial time and all others are positive. We can then consider the system with only the remaining $N_x + N_y + 2N_z - n_{\tilde{E},\tilde{s}}$ positive species and the substrate. We have seen that, in this case, all solutions of the corresponding reduced order Σ go to $\tilde{E}$ which means that $\tilde{s}$ is the "s^*" defined in Lemma 3.4 for the reduced order system. Since the reduced order system contains less than N species because $n_{\tilde{E},\tilde{s}} > 0$, we conclude that all solutions of the full system (7) that have zero initial condition for all $n_{\tilde{E},\tilde{s}}$ species and positive values for all $N_x + N_y + 2N_z - n_{\tilde{E},\tilde{s}}$ others converge to $\tilde{E}$. We have then

exhibited an invariant manifold of dimension $N_x + N_y + 2N_z - n_{\tilde{E},\tilde{s}} + 1$ for which all solutions go to E; this corresponds to the predicted dimension of the stable manifoldof E. No solution with some of the $n_{\tilde{E},\tilde{s}}$ species positive (among which there is at least on s^*-compliant species) at the initial time can then converge to E.

This completes the proof of our Main Theorem since all solutions go to an equilibrium and we have exhibited the stable manifold of all equilibria other than E^*. These manifolds cannot go into the region where x_i, y_j or $z_k > 0$ for all $s*-compliant$ species because at least one of them is in the corresponding $n_{\tilde{E},\tilde{s}}$-set. All initial conditions in the region where x_i, y_j or $z_k > 0$ for all $s*-compliant$ species therefore generate solutions that go to E^*. □

4. **Discussion: How D and s_{in} both determine competition outcome.** In S- and Q-only competitions, the outcome of competition is mainly determined by D, which fixes the $s_i^{x\star}$ and $s_k^{z\star}$ S- and Q-substrate subsistence concentrations; the role of s_{in} is to allow the best competitor (already determined by the value of D) to settle the reactor, or to cause it to be washed out with all the others. On the contrary in SB-only competition, both controls have important roles: D fixes the $Y_j(s)$ functions, while s_{in} determines the equilibrium, where $s^{y\star} + \sum_j Y_j(s^{y\star}) = s_{in}$. With a low enough s_{in}, only few SB-species will settle the chemostat ($s^{y\star}$ being low in this case, there will be few $s^{y\star}$-compliant species, with non-null $Y_j(s^{y\star})$), whereas a high enough s_{in} can enable all SB-species to coexist.

Finally, in a mixed S-Q-SB-competition the dilution rate D fixes all the S- and Q-substrate subsistence concentrations $s_i^{x\star}$ and $s_k^{z\star}$, as well as the $Y_j(s)$ functions, while the input substrate concentration s_{in} selects the species remaining in the reactor, by limiting the available nutrients, and thus the biomasses present in the reactor at equilibrium. Figure 6 gives an example between three competitors.

On this figure the $s^{x\star}$ and $s^{z\star}$ values and the $Y(s)$ function are fixed by D. Here $s_1^{z\star}$ is lower than $s_1^{x\star}$, so that the S-species will be outcompeted and washed out. Then the value of s_{in} determines wether

1. no species remain at equilibrium
2. only the SB-species remains at equilibrium, as there is not enough input substrate to feed both SB- and Q-species: because $s^{y\star} + Y(s^{y\star}) = s_{in}$ and $s_{in} < s^{z\star} + Y(s^{z\star})$, we know that $s^{y\star} < s^{z\star}$, so that $s^\star = s^{y\star}$, and only the SB-species remains in the reactor.
3. both the SB- and Q-species remain in the chemostat: here $s_{in} > s^{z\star} + Y(s^{z\star})$ and $s_{in} = s^{y\star} + Y(s^{y\star})$ give $s^{y\star} > s^{z\star}$, so that $s^\star = s^{z\star}$ and the Q-species remains in the reactor, coexisting with the $s^{z\star}$-compliant SB-species.

In this last case D has fixed the $s^{z\star}$ substrate equilibrium value and the $Y(s)$ function, and at equilibrium the total substrate in the chemostat, equal to s_{in}, will be composed of

- the substrate in the medium $s^{z\star}$ (which is fixed by D and does not depend on s_{in});
- the SB-species internal substrate $Y(s^{z\star})$ (which is also fixed by D only);
- the Q-species internal substrate $Q(s^{z\star}))z^\star = s_{in} - Y(s^{z\star}) - s^{z\star}$, which depends on s_{in}.

By going from left to right in Figure 6, starting with $s_{in} = 0$, it is possible to imagine the input substrate concentration increase, thus enabeling more and more substrate $s = s_{in}$ at equilibrium (zone 1). Then in zone 2 the SB-species is present

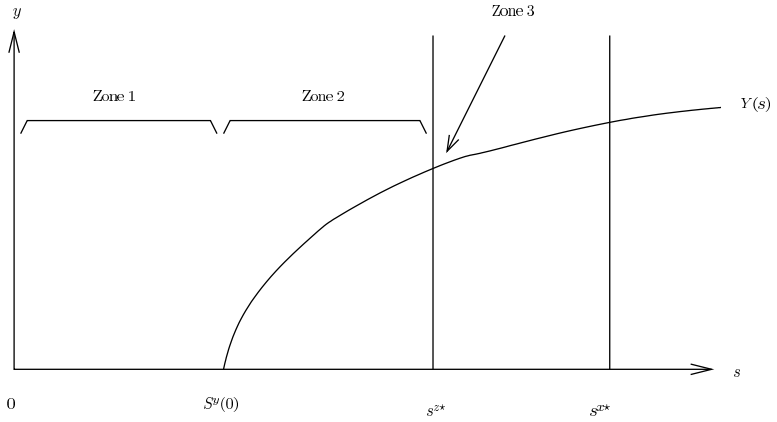

FIGURE 6. Mixed S-SB-Q-competition outcome depends both on the dilution rate D and input substrate concentration s_{in}. The solid lines represent the influence of D, which fixes the subsistence concentrations of one S-model ($s^{x\star}$) and Q-model ($s^{z\star}$) species, and the equilibrium biomass $Y(s)$ of one SB-species. As the S-species has a too high subsistence concentration $s^{x\star} > s^{z\star}$ it will be outcompeted and excluded. The three numerated zones represent the influence of s_{in}. *Zone 1* ($s_{in} \leq S^y(0)$) : no species remain at equilibrium. *Zone 2* ($S^y(0) < s_{in} \leq s^{z\star} + Y(s^{z\star})$) : only the SB-species remains at equilibrium. *Zone 3* ($s_{in} > s^{z\star} + Y(s^{z\star})$) : the SB- and Q-species coexist.

at equilibrium, and as s_{in} increases, more and more biomass $Y(s)$ is present at equilibrium. Finally $Y(s^{z\star})$ is the maximal biomass for which the SB-species needs less substrate at equilibrium than the Q-species to have a growth rate equal to D. After that it has to coexist with the Q-species: when s_{in} increases higher than $s^{z\star} + Y(s^{z\star})$ it enables more and more Q-biomass $z^\star$, while keeping substrate concentration $s = s^{z\star}$ and SB-biomass $y = Y(s^{z\star})$.

5. **Conclusion.** In this paper a demonstration was given for the outcome of competition between generalized Monod "constant yield" (S-model), Contois "biomass dependent" (SB-model) and Droop "variable yield" (Q-model) models. Three scenarios are possible, depending both on the dilution rate D and input substrate concentration s_{in} (see discussion for precisions):

- only the best S- or Q-competitor remains in the chemostat;
- only some SB-species coexist at equilibrium;
- a new equilibrium (never studied before) is attained, where the best S- or Q-competitor coexists with all the $s^\star$-compliant SB-species.

The demonstration explains how the state variables evolve, and its originality for the study of pure substrate competition model can be summed up in three points. First, we chose to study the substrate evolution instead of ignoring it after the classical mass balance equilibrium transformation $s = s_{in} - \sum_i x_i - \sum_j y_j - \sum_k q_k z_k$. Then, the definition of the S_j^y and S_k^z functions enabled to gather most information on the substrate axis: instead of having separate information on $1 + N_x + N_y + 2N_z$

axes we obtained a one dimensional view on these dynamics (Figure 2 and 3), where all the $S_j^y(y_j)$ and $S_k^z(q_k)$ go towards s. We have thus turned a complex $1 + N_x + N_y + 2N_z$ dimensional problem into a simpler one: "how do s and the $S_j^y(y_j)$ and $S_k^z(q_k)$ behave on the substrate axis, and what are the consequences for the biomasses?".
Finally the definition of the non decreasing lower bound $L(t)$ (section 3.2) and its convergence towards $s^\star$ (section 3.3) were the last steps for this demonstration to emerge.

Monod and Droop-only pure competitions for substrate lead to the "survival of the fittest", the fittest being the species with lowest substrate requirement $s^\star$. On the contrary, Contois-only competition lead to a coexistence equilibrium, because biomass dependence gives SB-species the capability to remain at equilibrium for different substrate concentrations in the range $[S_j^y(0), s_{in})$ (see Figure 5). Monod and Droop species are mutually exclusive, which leads to the pessimization principle of adaptative dynamics [38] : "mutation and natural selection lead to a deterioration of the environmental condition, a Verlenderung. We end up with the worst of all possible environment." On the contrary Contois species are coexistence-compliant thanks to biomass dependence, which nuances the pessimization principle: "some species could live in worse environments ($s = \min_j(S_j^y(0))$ being the worse one) but if there is enough substrate for other species, they can coexist." (see Figure 6 and discussion)

Since the introduction of the concept of evolution, with its link to competitive exclusion [8] and the "paradox of phytoplankton" [12] modelling has tried to apprehend competition, and to predict or control it. Our contribution in this framework was to extend the results proven in the N-species Monod model, N-species Droop model and N-species Contois model, where the outcome of competition was predicted and explained with mathematical arguments, accompanied by ecological interpretations.

Appendix A. Step 3 - Case *a*: L attains $s^\star$ in finite time.

In this case

- if $s^\star = s_1^{z\star}$ we consider Figure 7 where L attains $s^\star$ after a finite time t^L:

$$\forall t \geq t^L, L(t) = s_1^\star$$

Substep 3a.1: after a finite time larger than t^L, q_1 is repeatedly higher than $Q_1(s^\star) + \theta$. Since $\min_i(S_k^z(q_k)) \geq L$, we know that

$$\forall t > t^L, q_1(t) \geq Q_1(s^\star)$$

As s does not converge to $s^\star$, we also know from Lemma 2.6 that q_1 does not converge towards $Q_1(s^\star)$:

$$\exists \theta > 0, \forall t > 0, \exists t^q > t, |q_1(t^q) - Q_1(s^\star)| > \theta$$

Those two facts imply that the repeated exits of $q_1(t)$ from the θ-interval around $Q_1(s^\star)$ take place above $Q_1(s^\star)$ for any $t^q > t^L$, so that, in that case, we have $q_1(t^q) > Q_1(s^\star) + \theta$. In Figure 7, such t^q time instants are represented by $\bullet$.

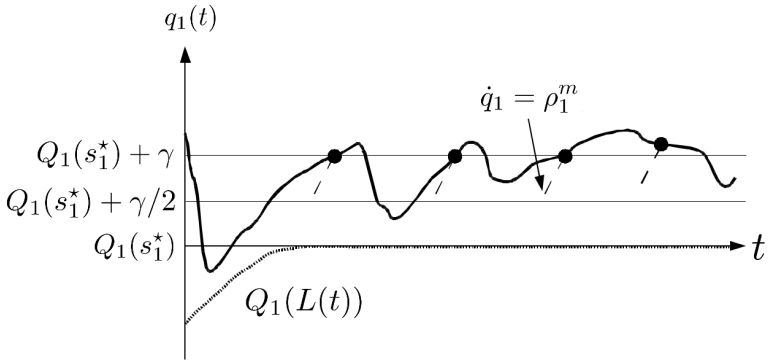

FIGURE 7. Visual explanation of the demonstration of Lemma 3.2 - Case 1: L attains $s^\star$ in finite time t^L (Q-model). *i*) q_1 is repeatedly higher than $Q_1(s^\star) + \theta$ (•). *ii*) Because $\dot{q}_1$ is upper bounded by ρ_1^m, so that q_1 is higher than $Q_1(s^\star) + \theta/2$ during non negligible time intervals (*dashed lines* represent $\dot{q}_1 = \rho_1^m$). Thus z_1 diverges, which is a contradiction.

Substep 3a.2: q_1 is higher than $Q_1(s^\star) + \theta/2$ during non negligible time intervals. Since the q_1-dynamics are upper bounded with

$$\dot{q}_1 \leq \rho_1^m$$

we know that every time q_1 is higher than $Q_1(s^\star) + \theta$, it has been higher than $Q_1(s^\star) + \theta/2$ during a time interval of minimal duration $A(\theta) = \frac{\theta}{2\rho_1^m}$. On Figure 7, $\dot{q}_1 = \rho_1^m$ is represented by the *dashed lines*.

Substep 3a.3: then z_1 diverges, which is impossible. From time t^L on, we have that $q_1 \geq Q_1(s^\star) \Rightarrow \gamma_1(q_1) \geq D$, so that $z_1(t)$ is non decreasing. During each of the time interval where q_1 is higher than $Q_1(s^\star) + \theta/2$, the increase of z_1 is lower bounded by

$$\dot{z}_1 = \gamma_1(Q_1(s^\star) + \theta/2) - D = C(\theta) > 0$$

so that every t^q time we have

$$z_1(t^q) - z_1(t^q - A(\theta)) > C(\theta)A(\theta)$$

As such increases occurs repeatedly, and as z_1 is non decreasing, z_1 diverges. This is a contradiction because z_1 is upper bounded (see (10)).

- if $s^\star = s_1^{x\star}$ then the non convergence of s to $s^\star$, and the fact that $s \geq s^\star$ will cause s to be non negligibly "away" from $s^\star$, so that x_1 will diverge, causing a contradiction with (9). This is exactly the same demonstration as above (in the case $s^\star = s_1^{z\star}$) without needing the q_k study.
- if $s^\star = s^{y\star}$ then $s + \sum_{j=1}^{N_y} Y_j(s)$ will always be higher than $s_{in} = s^{y\star} + \sum_{j=1}^{N_y} Y_j(s^{y\star})$ without converging to s_{in}, which is in contradiction with (25).

Appendix B. **Step 3 - Case** *b***:** L **never attains** $s^\star$**.** In this case $L(t)$ converges towards a value $\hat{L} \in (0, s^\star]$, because it is non decreasing and bounded in $[0, s^\star]$, so that

$$\forall \epsilon > 0, \exists t^L(\epsilon) > 0, \forall t > t^L(\epsilon), |L(t) - \hat{L}| < \epsilon$$

We consider the neighborhood of $\hat{L}$ in Figure 8.

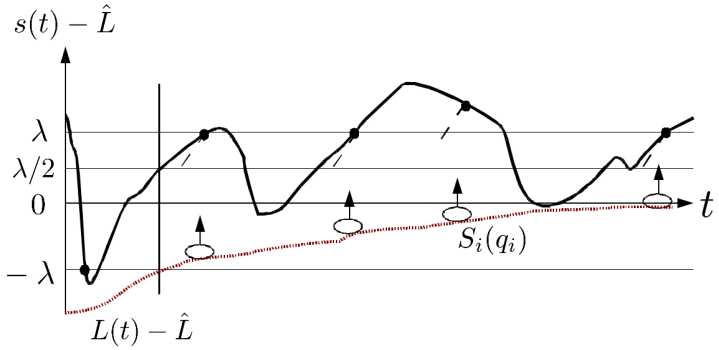

FIGURE 8. Visual explanation of the demonstration of Lemma 3.2 - Case 2: L never attains $s^\star$. *i)* s is repeatedly higher than $\hat{L} + \lambda$ (•). *ii)* $\dot{s}$ is upper bounded by Ds_{in}, so that s is higher than $\hat{L} + \lambda/2$ during non negligible time intervals (*dashed lines* represent $\dot{s} = Ds_{in}$) *iii)* during such a time intervals $L = \min_k(S_k^z(q_k))$ (or $\min_j(S_j^y(y_j))$) is increasing non negligibly towards s, so that L cannot both converge towards $\hat{L}$ and stay lower than $\hat{L}$ during the whole time interval: there is a contradiction.

Substep 3b.1: after a finite time, s *is repeatedly higher than* $\hat{L} + \lambda$. Since, from the beginning of the proof of Lemma 3.2, we know that s does not converge to any constant value, hence not to $\hat{L}$,

$$\exists \lambda > 0, \forall t > 0, \exists t^s > t, |s(t^s) - \hat{L}| > \lambda$$

Since L is increasing and converges to $\hat{L}$, it reaches $\hat{L} - \lambda$ in finite time $t^L(\lambda)$. After this finite time, s is higher than $\hat{L} + \lambda$ on every t^s time instants, which are represented by • in Figure 8.

Substep 3b.2: s *is higher than* $\hat{L} + \lambda/2$ *during non negligible time intervals.* Because of the boundedness of $\dot{s}$

$$\dot{s} \leq Ds_{in}$$

every time s is higher than $\hat{L} + \lambda$, it has been higher than $\hat{L} + \lambda/2$ during a non negligible time interval of minimal duration $A(\lambda) = \frac{\lambda}{2Ds_{in}}$. On Figure 8 the case $\dot{s} = Ds_{in}$ is represented by *dashed lines*.

Substep 3b.3: $L = \min_k(S_k^z(q_k))$ (or $\min_j(S_j^y(y_j))$) is increasing non negligibly towards s, so that L cannot both converge towards $\hat{L}$ and stay lower than $\hat{L}$ during the whole time interval: there is a contradiction. Like in previous proofs, we are interested in what happens during the $[t^s - A(\lambda), t^s]$ time-interval, with $t^s - A(\lambda) > t^L(\epsilon)$ (for some $\epsilon < \lambda$). Since, during this time-interval, $s(t) > \hat{L} + \lambda/2$ and $L < \hat{L}$, we know that there exists a k such that $L(t^s) = S_k^z(q_k(t^s)) < \hat{L}$, or a j such that $L(t^s) = S_j^y(y_j(t^s)) < \hat{L}$.

For both this step (3b.3) we choose to first only present arguments for the case $L(t^s) = \min_k(S_k^z(q_k))$; almost similar arguments for the case $L(t^s) = \min_j(S_j^y(y_j))$ will then be briefly presented.

- if $L(t^s) = \min_k(S_k^z(q_k))$, then during the whole considered time-interval, as $S_k^z(q_k)$ was increasing, we know that

$$\hat{L} - \epsilon < L \leq S_k^z(q_k) \leq S_k^z(q_k(t^s)) < \hat{L} \tag{27}$$

  so that $Q_k(\hat{L} - \epsilon) < q_k(t) < Q_k(\hat{L})$. For the k species, the dynamics of q_k can then be lower bounded:

$$\dot{q}_k \geq \rho_k(\hat{L} + \lambda/2) - f_k(Q_k(\hat{L}))$$

  and then

$$\dot{q}_k \geq \rho_k(\hat{L} + \lambda/2) - \rho_k(\hat{L}) = G_k(\lambda)$$

  positive, so that the increase of q_k during the $[t^s - A(\lambda), t^s]$ time-interval is also lower bounded:

$$q_k(t^s) - q_k(t^s - A(\lambda)) \geq G_k(\lambda)A(\lambda) = H_k(\lambda)$$

  Since $Q_k = S_k^{z^{-1}}$ is locally Lipschitz with constant K (because $f_k' > 0$), we have

$$\begin{aligned} q_k(t^s) - q_k(t^s - A(\lambda)) &= Q_k(S_k^z(q_k(t^s))) - Q_k(S_k^z(q_k(t^s - A(\lambda)))) \\ &< K\left[S_k^z(q_k(t^s)) - S_k^z(q_k(t^s - A(\lambda)))\right] \end{aligned}$$

  so that the corresponding increase of $S_k^z(q_k)$ is lower bounded with

$$S_k^z(q_k(t^s)) - S_k^z(q_k(t^s - A(\lambda))) \quad \geq \tfrac{1}{K}H_k(\lambda)$$

  and then

$$S_k^z(q_k(t^s - A(\lambda))) < \hat{L} - \frac{1}{K}H_k(\lambda)$$

  which implies the same higher bound for L:

$$L(t^s - A(\lambda)) < \hat{L} - \frac{1}{K}H_k(\lambda)$$

  By choosing $\epsilon < \frac{1}{K}H_k(\lambda)$, this inequality is contradictory with (27) so that Case 2 is not possible
- if $L(t^s) = \min_j(S_j^y(y_j))$, then the same arguments can be developped for the j species, with a lower bound $G_j(\lambda)$ on the y_j dynamics:

$$G_j(\lambda) = \beta_j(\hat{L} + \lambda/2, Y_j(\hat{L})) - \beta_j(\hat{L}, Y_j(\hat{L})) > 0$$

  and then an increase of variable y_j at least equal to $H_j(\lambda) = G_j(\lambda)A(\lambda)$ followed by a non negligible increase of L

$$L(t^s - A(\lambda)) < \hat{L} - \frac{1}{K}H_j(\lambda)$$

because Y_j is locally Lipschitz. Finally a contradiction also occurs when $\epsilon < \frac{1}{K} H_j(\lambda)$:

$$L(t^s - A(\lambda)) < \hat{L} - \epsilon$$

Appendix C. **Computation of system Σ Jacobian Matrix and eigenvalues for all the equilibria.** Computation of the Jacobian Matrix of system Σ, with $s = s_{in} - \sum_{i=1}^{N_x} x_i - \sum_{j=1}^{N_y} y_j - \sum_{k=1}^{N_z} q_k z_k$.

$$\begin{pmatrix} J^{xx} & J^{xy} & J^{xz} & J^{xq} \\ J^{yx} & J^{yy} & J^{yz} & J^{yq} \\ J^{zx} & J^{zy} & J^{zz} & J^{zq} \\ J^{qx} & J^{qy} & J^{qz} & J^{qq} \end{pmatrix}$$

where

$$\begin{array}{l}
J^{xx}_{ii} = \alpha_i(s) - D - \frac{\partial \alpha_i}{\partial s} x_i \quad \text{and} \quad \forall l \neq i, J^{xx}_{il} = -\frac{\partial \alpha_i}{\partial s} x_i \\
J^{xy}_{ij} = -\frac{\partial \alpha_i}{\partial s} x_i \\
J^{xz}_{ik} = -\frac{\partial \alpha_i}{\partial s} x_i q_k \\
J^{xq}_{ik} = -\frac{\partial \alpha_i}{\partial s} x_i z_k \\
\text{and} \\
J^{yx}_{ji} = -\frac{\partial \beta_j}{\partial s} y_j \\
J^{yy}_{jj} = \beta_j(s, y_j) - D + \frac{\partial \beta_j}{\partial y_j} y_j - \frac{\partial \beta_j}{\partial s} y_j \quad \text{and} \quad \forall l \neq j, J^{yy}_{jl} = -\frac{\partial \beta_j}{\partial s} y_j \\
J^{yz}_{jk} = -\frac{\partial \beta_j}{\partial s} y_j q_k \\
J^{yq}_{jk} = -\frac{\partial \beta_j}{\partial s} y_j z_k \\
\text{and} \\
J^{zx}_{ki} = 0 \\
J^{zy}_{kj} = 0 \\
J^{zz}_{kk} = \gamma_k(q_k) - D \quad \text{and} \quad \forall l \neq k, J^{zz}_{kl} = 0 \\
J^{zq}_{kk} = \frac{\partial \gamma_k}{\partial q_k} z_k \quad \text{and} \quad \forall l \neq k, J^{zq}_{kl} = 0 \\
\text{and} \\
J^{qx}_{ki} = -\frac{\partial \rho_k}{\partial s} \\
J^{qy}_{kj} = -\frac{\partial \rho_k}{\partial s} \\
J^{qz}_{kl} = -\frac{\partial \rho_k}{\partial s} q_l \\
J^{qq}_{kk} = -\frac{\partial \rho_k}{\partial s} z_k - \frac{\partial f_k}{\partial q_k} \quad \text{and} \quad \forall l \neq k, J^{qq}_{kl} = -\frac{\partial \rho_k}{\partial s} z_l
\end{array}$$

Fortunately for eigenvalue computations, at equilibria the null biomasses will simplify the matrix:

- when $x_i = 0$, then the whole i^{th} line gives eigenvalue $\alpha_i(s) - D$ (denoted "x_i-eigenvalue") and can be deleted, as well as the $i^{th} column$;
- when $y_j = 0$ then the whole $N_x + j^{th}$ line gives eigenvalue $\beta_j(s, y_j) - D$ (denoted "y_j-eigenvalue") and can be deleted, as well as the $N_x + j^{th}$ corresponding column;
- when $z_k = 0$ then the whole $N_x + N_y + k^{th}$ line gives eigenvalue $\gamma_k(q_k) - D$ (denoted "z_k-eigenvalue") and can be deleted, as well as the $N_x + N_y + k^{th}$ column; in a second step, the whole $N_x + N_y + N_z + k^{th}$ column can also be deleted and gives eigenvalue $\frac{-\partial f_k}{\partial q_k}$ (denoted "q_k-eigenvalue"), as well as the $N_x + N_y + N_z + k^{th}$ line.

C.1. **Complete washout equilibrium.** With this in hand, we see that for equilibrium $\tilde{E}_0$ ($x_i = y_j = z_k = 0$) the Jacobian matrix is triangular, so that the eigenvalues lay on the diagonal. They are:

- $\alpha_i(s_{in}) - D$
- $\beta_j(s_{in}, 0) - D$
- $\gamma_k(Q_k(s_{in})) - D$
- $-\frac{\partial f_k}{\partial q_k}$ (negatives)

We denote n_x, n_y, n_z the number of S-, SB- and Q- species verifying the inequalities of Hypothesis 5, and thus having the possibility to be at equilibrium with a positive biomass, under controls D and s_{in}. Each of these species has a positive corresponding eigenvalue on this equilibrium, so that equilibirum $\tilde{E}_0$ has $n_x + n_y + n_z$ positive eigenvalues, and $N_x - n_x + N_y - n_y + 2N_z - n_z$ negative eigenvalues.

C.2. **S-only equilibria.** For equilibrium E_i^x we get all the previously cited x-,y-, z-and q-eigenvalues:

- $\alpha_l(s_i^{x\star}) - D$ whose signs are the same as $sign(s_i^{x\star} - s_l^{x\star})$
- $\beta_j(s_i^{x\star}, 0) - D$ which are positive if the j^{th} species is $s_i^{x\star}$-compliant, or negative else;
- $\gamma_k(Q_k(s_i^{x\star})) - D$ whose signs are the same as $sign(s_i^{x\star} - s_k^{z\star})$
- $\frac{-\partial f_k}{\partial q_k}$ which are all negative

and the remaining eigenvalue corresponds to the positive x_i-only dynamics:

$$\dot{x}_i = (\alpha_i(s_{in} - x_i) - D)x_i$$

which yields the eigenvalue $-\frac{\partial \alpha_i}{\partial s} x_i^\star$ for S-species i. Each S- or Q-species with a substrate subsistence concentration $s_l^{x\star}$ or $s_k^{z\star}$ lower than $s_i^{x\star}$ gives a positive eigenvalue. Among all the E_i^x equilibria, only E_1^x is stable if and only if $s^\star = s_1^{x\star} < s_1^{z\star}$, and if all the SB-species are not $s_1^{x\star}$-compliant.

C.3. **Q-only equilibria.** For Equilibrium E_k^z we get all the

- x-eigenvalues whose signs are the sign of $sign(s_k^{z\star} - s_i^{x\star})$;
- y-eigenvalues: as previously, y-eigenvalues are positive if the corresponding SB-species is $s_k^{z\star}$-compliant and negative else;
- z_l-eigenvalues whose signs are the sign of $sign(s_k^{z\star} - s_l^{z\star})$;
- q_l-eigenvalues for all $l \neq k$ (negative);

and the remaining eigenvalues correspond to the positive (z_k, q_k)-only dynamics:

$$\left\{ \begin{array}{rcl} \dot{z}_k & = & (\gamma_k(q_k) - D)z_k \\ \dot{q}_k & = & \rho_k(s_{in} - q_k z_k) - f_k(q_k) \end{array} \right.$$

and we obtain the following resulting matrix:

$$\left(\begin{array}{cc} 0 & \frac{\partial \gamma_k}{\partial q_k} z_k \\ -\frac{\partial \rho_k}{\partial s} q_k & -\frac{\partial \rho_k}{\partial s} z_k - \frac{\partial f_k}{\partial q_k} \end{array} \right)$$

which has negative trace and positive determinant, so that its two eigenvalues are real negative. Just like before, each S- or Q-species with a substrate subsistence concentration $s_i^{x\star}$ or $s_l^{z\star}$ lower than $s_k^{z\star}$ gives a positive eigenvalue. Among all the E_k^z equilibria, only E_1^z is stable if and only if $s^\star = s_1^{z\star} < s_1^{x\star}$, and if all the SB-species are not $s_1^{z\star}$-compliant.

C.4. **SB-only equilibria.** Now let us consider the E_G^y equilibria for which all $j \in G$ (where G represents a subset of $\{1, \dots, N_y\}$) SB-species coexist in the chemostat under substrate concentration $s_G^{y\star}$, while all the S- and Q-species are washed out. $s_G^{y\star}$ is defined by $s_G^{y\star} + \sum_{j\in G} Y_j(s_G^{y\star}) = s_{in}$. Note that some of the G species can have a null biomass on these equilibria, as $Y_j(s_G^{y\star})$ might be null for some $j \in G$.

This gives all the

- x-eigenvalues whose sign are the same as the signs of $s_i^{x\star} - s_G^{y\star}$;
- z-eigenvalues whose sign are the same as the signs of $s_k^{z\star} - s_G^{y\star}$;
- q-eigenvalues (negative).

All the y_j species who are not included in G give negative eigenvalues if they are not $s_G^{y\star}$-compliant, and positive eigenvalues else; their eigenvalues cannot be null because of technical hypothesis 7. All the y_j species who are included in G but have a null biomass $Y_j(s_G^{y\star})$ on the E_G^y equilibrium give negative eigenvalues. Now let us study the remaining matrix J_G^{yy} which is composed of all the $j \in G$ lines of J^{yy}, for which $Y_j(s_G^{y\star}) > 0$, and thus $\beta_j(s_G^{y\star}, Y_j(s_G^{y\star})) = D$:

$$\dot{y}_j = \left(\beta_j(s - \sum_l y_l, y_j) - D\right) y_j$$

which yields the Jacobian matrix:

$$J_G^{yy} = \begin{pmatrix} -a_1 - b_1 & \dots & -a_1 & \dots & -a_1 \\ \vdots & \ddots & \vdots & & \vdots \\ -a_j & \dots & -a_j - b_j & \dots & -a_j \\ \vdots & & \vdots & \ddots & \vdots \\ -a_n & \dots & -a_n & \dots & -a_n - b_n \end{pmatrix}$$

with $a_j = \frac{\partial \beta_j}{\partial s} Y_j(s_G^{y\star}) > 0$ and $b_j = -\frac{\partial \beta_j}{\partial y_j} Y_j(s_G^{y\star}) > 0$.

Let us show that this matrix has only real negative eigenvalues, by using the definition of an eigenvalue $\lambda = (A + Bi)$, where $A \in \mathbb{R}$ is the real part and $B \in \mathbb{R}$ the imaginary part:

$$J_G^{yy} \cdot \begin{pmatrix} y_1 \\ \vdots \\ y_n \end{pmatrix} = (A + Bi) \begin{pmatrix} y_1 \\ \vdots \\ y_n \end{pmatrix} \tag{28}$$

We obtain n equations:

$$-b_j y_j - a_j \sum_l y_l = (A + Bi) y_j$$

and thus

$$(A + Bi + b_j) y_j = -a_j \sum_l y_l \tag{29}$$

If we have $A + Bi + b_j = 0$ for some j, then $B = 0$ and $A = -b_j < 0$ so that we have a negative eigenvalue.
Else, isolating y_j yields

$$y_j = \frac{-a_j \sum_l y_l}{b_j + A + Bi}$$

Summing over j, we obtain

$$\sum_j y_j = \sum_j \left(\frac{-a_j \sum_l y_l}{b_j + A + Bi} \right)$$

Now if $\sum_j y_j = 0$, since some y_j must be different of 0, (29) yields, for that j, that $A + Bi + b_j = 0$ so that again $B = 0$ and $A = -b_j < 0$.
Else, simplifying the sums of y_l and y_j, this yields

$$\begin{array}{rcl} 1 & = & \sum_j \left(\frac{-a_j}{b_j + A + Bi} \right) \\ & = & \sum_j \left(\frac{-a_j (b_j + A - Bi)}{(b_j + A)^2 + B^2} \right) \\ & = & \sum_j \left(\frac{-a_j (b_j + A)}{(b_j + A)^2 + B^2} \right) + i \sum_j \left(\frac{a_j B)}{(b_j + A)^2 + B^2} \right) \end{array}$$

Since the left-hand-side is real, the imaginary part of the right-hand side must be zero, which imposes $B = 0$. For thr right-hand-side to be positive, at least one of the $b_j + A$ must be negative, which translates into $\min_j (b_j + A) < 0$ and

$$A < -\min_j b_j < 0$$

We conclude from this that all eigenvalues of this matrix are real negative.

Finally, an E_G^y equilibrium is stable if and only if all the SB-species not contained in G are not $s_G^{y\star}$-compliant (this is equivalent to saying that $s_G^{y\star} = s^{y\star}$, with $s^{y\star} = s^{y\star}_{\{1,\ldots,N_y\}}$), and if $s^\star = s^{y\star}$.

C.5. **S-coexistive equilibria.** In this section we consider equilibria $E_{i,G}^{(x,y)}$ where S-species x_i coexists with the SB-species in G, a subset of $\{1, \ldots, N_y\}$, under substrate concentration $s_i^{x\star}$.

We obtain here all the

- x_l-eigenvalues ($l \neq i$) whose signs are the signs of $s_i^{x\star} - s_l^{x\star}$;
- z-eigenvalues whose sign is the sign of $s_i^{x\star} - s_k^{z\star}$;
- q-eigenvalues (negative);

y_j-eigenvalues with j not in G are positive if y_j is $s_i^{x\star}$-compliant and negative else; y_j-eigenvalues with j in G but have a null biomass $Y_j(s_i^{x\star})$ give negative eigenvalues. For the remaining SB-species, and species x_i, we obtain the following system:

$$\left\{ \begin{array}{rcl} \dot{x}_i & = & (\alpha_i(s_{in} - x_i - \sum_l y_l) - D)\, x_i \\ \dot{y}_j & = & (\beta_j(s_{in} - x_i - \sum_l y_l, y_j) - D)\, y_j \end{array} \right.$$

and the Jacobian matrix:

$$\begin{pmatrix} -a_0 & -a_0 & \ldots & -a_0 & \ldots & -a_0 \\ -a_1 & -a_1 - b_1 & \ldots & -a_1 & \ldots & -a_1 \\ \vdots & \vdots & \ddots & \vdots & & \vdots \\ -a_j & -a_j & \ldots & -a_j - b_j & \ldots & -a_j \\ \vdots & \vdots & & \vdots & \ddots & \vdots \\ -a_n & -a_n & \ldots & -a_n & \ldots & -a_n - b_n \end{pmatrix}$$

with $a_0 = \frac{\partial \alpha_i}{\partial s} x_i^\star > 0$, $a_j = \frac{\partial \beta_j}{\partial s} Y_j(s_i^{x\star}) > 0$ and $b_j = -\frac{\partial \beta_j}{\partial y_j} Y_j(s_i^{x\star}) > 0$ (for $j \in \{1, \cdots, n\}$). This matrix has exactly the same form has the one considered on Appendix C.4. The only difference being that the there is no "b_0" in the first element

of the matrix. Defining a $b_0 = 0$, we can then conclude that all eigenvalues are real and negative because, following the development of Appendix C.4, we obtain

$$A < -\min_j b_j = 0$$

Finally, only equilibrium $E^{(x,y)}_{1,\{1,\dots,N_y\}}$ can be stable if and only if $s^\star = s_1^{x\star}$.

C.6. **Q-coexistive equilibria.** In this section we consider equilibria $E^{(z,y)}_{k,G}$ where Q-species z_k coexists with the SB-species in G, a subset of $\{1,\dots,N_y\}$, under substrate concentration $s_k^{z\star}$.

We obtain here all the

- x-eigenvalues whose signs are the signs of $s_k^{z\star} - s_i^{x\star}$;
- z_l-eigenvalues ($l \neq j$) whose sign are the signs of $s_k^{z\star} - s_l^{z\star}$;
- q-eigenvalues (negative);

y_j-eigenvalues with j not in G are positive if y_j is $s_k^{z\star}$-compliant and negative else; y_j-eigenvalues with j in G but have a null biomass $Y_j(s_k^{z\star})$ give negative eigenvalues. For the remaining SB-species, and species z_k, we obtain the following model

$$\left\{\begin{array}{lcl} \dot{y}_j &=& (\beta_j(s_{in} - \sum_l y_l - q_k z_k, y_j) - D)y_j \\ \dot{z}_k &=& (\gamma_k(q_k) - D)z_k \\ \dot{q}_k &=& \rho_k(s_{in} - \sum_l y_l - q_k z_k) - f_k(q_k) \end{array}\right.$$

and, swapping the last two equations and using $f_k(q_k) = \gamma_k(q_k)q_k$, we get the Jacobian matrix:

$$\begin{pmatrix} -a_1 - b_1 & \dots & -a_1 & \dots & -a_1 & -a_1 z_k & -a_1 q_k \\ \vdots & \ddots & \vdots & & \vdots & \vdots & \vdots \\ -a_j & \dots & -a_j - b_j & \dots & -a_j & -a_j z_k & -a_j q_k \\ \vdots & & \vdots & \ddots & \vdots & \vdots & \\ -a_n & \dots & -a_n & \dots & -a_n - b_n & -a_n z_k & -a_n q_k \\ -a_{n+1} & \dots & -a_{n+1} & \dots & -a_{n+1} & -a_{n+1} z_k - b_{n+1} q_k - \gamma & -a_{n+1} q_k \\ 0 & \dots & 0 & \dots & 0 & b_{n+1} z_k & 0 \end{pmatrix}$$

with $a_j = \frac{\partial \beta_j}{\partial s} Y_j(s_k^{z\star}) > 0$ and $b_j = -\frac{\partial \beta_j}{\partial y_j} Y_j(s_k^{z\star}) > 0$ for $j \in \{1, \cdots, n\}$, with $a_{n+1} = \frac{\partial \rho_k}{\partial s}$ and $b_{n+1} = \frac{\partial \gamma_k}{\partial q_k}$. By using the definition of eigenvalue $\lambda = (A + Bi)$ (see (28)) we follow a similar path to that of Appendix C.4, we show that the eigenvalues are real and negative.

Finally, only equilibrium $E^{(z,y)}_{1,\{1,\dots,N_y\}}$ can be stable if and only if $s^\star = s_1^{z\star}$.

Remark 6. The same work can be done for the whole system (7), where the eigenvalues are the same, plus the $-D$ eigenvalue which arises from mass balance dynamics (8).

REFERENCES

[1] R. Armstrong, R. McGehee, Competitive exclusion, American Naturalist 115 (1980) 151.
[2] H. Smith, P. Waltman, The theory of the chemostat. Dynamics of microbial competition, Cambridge Studies in Mathematical Biology. Cambridge University Press, 1995.
[3] S. Hsu, T. Hsu, Competitive exclusion of microbial species for a single-nutrient with internal storage, SIAM Journal on Applied Mathematics 68 (6) (2008) 1600–1617.
[4] D. Tilman, R. Sterner, Invasions of equilibria: tests of resource competition using two species of algae, Oecologia 61 (2) (1984) 197–200.

[5] S. Hansen, S. Hubell, Single-nutrient microbial competition: qualitative agreement between experimental and theoretically forecast outcomes, Science 207 (4438) (1980) 1491–1493.
[6] D. Tilman, Resource competition between plankton algae: An experimental and theoretical approach., Ecology 58 (22) (1977) 338–348.
[7] F. Grognard, F. Mazenc, A. Rapaport, Polytopic lyapunov functions for persistence analysis of competing species, Discrete and Continuous Dynamical Systems-Series B 8 (1) (2007) 73–93.
[8] G. Hardin, The competitive exclusion principle, Science 131 (3409) (1960) 1292–1297.
[9] C. Elton, Animal Ecology, Sidgwick & Jackson, LTD. London, 1927.
[10] C. Darwin, On the Origin of Species by Means of Natural Selection, or the Preservation of Favoured Races in the Struggle for Life, John Murray, 1859.
[11] M. Scriven, Explanation and prediction in evolutionnary theory, Science 130 (3374) (1959) 477–482.
[12] G. E. Hutchinson, The paradox of the plankton, The American Naturalist 95 (1961) 137.
[13] C. Jessup, S. Forde, B. Bohannan, Microbial experimental systems in ecology, Advances in Ecological Research 37 (2005) 273–306.
[14] G. Gause, The Struggle for Existence, Williams and Wilkins, Baltimore, 1934.
[15] J. Monod, Reserches sur la croissance des cultures bacteriennes, Paris: Herrmann et Cie.
[16] A. Sciandra, P. Ramani, The steady states of continuous cultures with low rates of medium renewal per cell, J. Exp. Mar. Biol. Ecol. 178 (1994) 1–15.
[17] M. Droop, Vitamin b_{12} and marine ecology, J. Mar. Biol Assoc. U.K. 48 (1968) 689–733.
[18] J. Caperon, J. Meyer, Nitrogen-limited growth of marine phytoplankton. i. changes in population characteristics with steady-state growth rate, Deep-Sea Res. 19 (1972) 601–618.
[19] I. Vatcheva, H. deJong, O. Bernard, N. Mars, Experiment selection for the discrimination of semi-quantitative models of dynamical systems, Artif. Intel. 170 (2006) 472–506.
[20] K. Lange, F. J. Oyarzun, The attractiveness of the Droop equations, Mathematical Biosciences 111 (1992) 261–278.
[21] F. J. Oyarzun, K. Lange, The attractiveness of the Droop equations. II: Generic uptake and growth functions, Mathematical Biosciences 121 (1994) 127–139.
[22] O. Bernard, J.-L. Gouzé, Transient behavior of biological loop models, with application to the Droop model, Mathematical Biosciences 127 (1) (1995) 19–43.
[23] B. Haegeman, C. Lobry, J. Harmand, Modeling bacteria flocculation as density-dependent growth, AICHE JOURNAL 53 (2) (2007) 535–539.
[24] D. Contois, Kinetics of bacterial growth: relationship between population density and specific growth rate of continuous cultures., J Gen Microbiol. (1959) 40–50.
[25] J. Leon, D. Tumpson, Competition between two species of two complementary or substitutable resources, J. Theor. Biol. 50 (1975) 185–201.
[26] S. Hsu, K. Cheng, S. Hubbel, Exploitative competition of micro-organisms for two complementary nutrients in continuous culture, SIAM J. Appl. Math. 41 (1981) 422–444.
[27] H. Freedman, J. So, P. Waltman, Coexistence in a model of competition in the chemostat incorporating discrete delays, SIAM J. Appl. Math. 49 (1989) 859–870.
[28] P. de Leenheer, H. Smith, Feedback control for the chemostat, J. Math. Biol. 46 (2003) 48–70.
[29] P. de Leenheer, D. Angeli, A. Sontag, A feedback perspective for chemostat models with crowding effects, in: Positive Systems, Vol. 294 of Lecture Notes in Control and Inform. Sci, Springer-Verlag, 2003, pp. 167–174.
[30] J. Arino, S. Pilyugin, G. Wolkowicz, Considerations on yield, nutrient uptake, cellular growth, and competition in chemostat models, Canadian Applied Math Quarterly 11 ((2003) [2005]) 107–142.
[31] J. B. Wilson, Mechanisms of species coexistence: twelve explanations for the hutchinson's 'paradox of the phytoplankton': evidence from new zealand plant communities, New Zealand journal of Ecology 17–42 (1990) 137.
[32] A. Fredrickson, G. Stephanopoulos, Microbial competition, Science 213 (1981) 972–979.
[33] J. Gouzé, G. Robledo, Feedback control for nonmonotone competition models in the chemostat, Nonlinear Analysis: Real World Applications (2005) 671–690.
[34] P. de Leenheer, B. Li, H. Smith, Competition in the chemostat : some remarks, Canadian applied mathematics quarterly 11 (2) (2003) 229–247.
[35] N. Rao, E. Roxin, Controled growth of competing species, Journal on Applied Mathematics 50 (3) (1990) 853–864.
[36] P. Masci, O. Bernard, F. Grognard, Continuous selection of the fastest growing species in the chemostat, in: Proceedings of the IFAC conference, Seoul, Korea, 2008, pp. 9707–9712.

[37] H. R. Thieme, Convergence results and a Poicaré-Bendixson trichotomy for asymptotically autonomous differential equations, Journal of Mathematical Biology 30 (7) (1992) 755–763.
[38] O. Diekmann, A beginner's guide to adaptive dynamics, Banach Center Publ. (2003) 47–86.

Received September 2006; revised February 2007.

E-mail address: pierre.masci@sophia.inria.fr
E-mail address: frederic.grognard@sophia.inria.fr, eric.benoit@univ-lr.fr, olivier.bernard@sophia.inria.fr

Continuous Selection of the Fastest Growing Species in the Chemostat

Pierre Masci, Olivier Bernard, and Frédéric Grognard

INRIA- Project COMORE, 2004 route des lucioles, BP 93, 06902 Sophia Antipolis Cedex, FRANCE
Tel : 0033.4.92.38.71.85; e-mail : pierre.masci@sophia.inria.fr, olivier.bernard@sophia.inria.fr, frederic.grognard@sophia.inria.fr

Abstract: This paper proposes control laws for the continuous culture of microorganisms, which make it possible to select species which maximize a criterion. In particular, by controlling the dilution rate and the input substrate concentration, the species with the fastest growth rate in chosen environmental conditions can be selected.
In a first step a control is proposed for Monod and Droop models in order to achieve periodic substrate stresses, and a closed loop control is proposed to regulate the total biomass concentration. We show that this biomass regulation causes the selection of the fastest growing species if the system has a periodic behavior, and derive new selection criteria. Finally, the method is simulated using the Droop model for selecting species which maximize these criteria.

Keywords: chemostat; microorganisms; competition; selection

1. INTRODUCTION

The chemostat is an open bioreactor where a microorganism can grow in suboptimal conditions of substrate limitation. The chemostat model supports several ecological theories (Jessup et al. [2005]) that were then extrapolated and tested in real life. Among these theories, the competition theory is one of the most famous. It states that if n competing species are introduced in a chemostat, generically (in the adequate working modes) only one species will stay in the chemostat, while the $n-1$ other will disappear. This principle was validated with real experiments in Hansen and Hubell [1980] where the species that "wins" the competition could be predicted; it was the one that could grow at a constant rate (equal to the dilution rate as detailed further on) with the smallest amount of limiting substrate s^*. This theoretical result could be used to select among a blend of species, the ones of interest. This idea has been used for diverse applications, such as Directed Evolution for strain improvement (see the reviews of Dykhuizen and Hartl [1983], Zelder and Hauer [2000] and Percival Zhang et al. [2006]). By adjusting a particular stress such as an inhibitor's concentration, a substrate limitation, or the dilution rate, it can lead to the isolation of species with optimal yield. This is of particular importance since it is a rather simple way of making a particular species emerge within a population. However, in most biotechnological applications, the selection criterion based on the idea of "optimal yield" is not appropriate. A selection that would e.g. select the microorganism with the highest growth potential would be preferable, especially if one wants to identify organisms that grow in hostile conditions. More generally, the objective of this paper is to propose new selection criteria. For this, the chemostat is not run in open loop, but a control law is proposed to run the system in closed loop. We show how the competition outcome is modified and we propose new criteria that could be used for species separation.

The paper is structured as follows. In a first part we recall two classical models of microorganisms in the chemostat, and the classical competition principle. Then we propose control laws to generate periodic substrate stresses, and to put the chemostat into a turbidostat mode. In the third part we show that this last control causes the selection of the fastest growing species if the system has a periodic behavior, and infer new selection criteria. A simulation example illustrates the benefit of the approach and shows how three species can be separated on this principle.

2. SHORT REVIEW OF COMPETITION ON A SINGLE SUBSTRATE IN THE CHEMOSTAT

2.1 Basic model for microorganisms in the chemostat

Monod model is the basic model for describing microorganisms growth on a single substrate in a chemostat.

$$\begin{cases} \dot{s} = D(s_{in} - s) - \sum_{i=1}^{N} \frac{1}{y_i}\mu_i(s)x_i \\ \dot{x_i} = (\mu_i(s) - D)x_i \end{cases} \quad (1)$$

where s stands for the substrate concentration in the chemostat, s_{in} its input concentration, and x_i the ith species biomass concentration. The μ_i functions represent the growth rates of these species, and the y_i constants are their substrate conversion yields. D is the input/output dilution rate. We control the system with s_{in} and D.

In this model the growth rate functions μ_i are taken as positive monotonic increasing functions

$$s_a < s_b \Leftrightarrow \mu_i(s_a) < \mu_i(s_b) \quad (2)$$

They are bounded by their supremum values μ_{m_i} :

$$\mu_i(s) < \mu_{m_i} \quad \text{and} \quad \lim_{s\to+\infty} \mu_i(s) = \mu_{m_i} \tag{3}$$

2.2 Variable yield model

Droop model (Droop [1968]) is more complex, it describes the internal substrate storage q of the microorganisms :

$$\begin{cases} \dot{s} = D(s_{in} - s) - \sum_{i=1}^{N} \rho_i(s) x_i \\ \dot{q}_i = \rho_i(s) - \mu_i(q_i) q_i \\ \dot{x}_i = (\mu_i(q_i) - D) x_i \end{cases} \tag{4}$$

In this model the ρ_i functions represent the substrate absorption rates, while the μ_i functions represent the growth rates. These functions are positive monotonic increasing functions. They are upper-bounded by the supremum values ρ_{m_i} and $\bar{\mu}_i$. The minimum absorption and growth rate are $\rho_i(0) = 0$ and $\mu_i(q_i) = 0$ for $q_i \in [0, K_{q_i}]$.

Internal substrate storage behavior : For each fixed substrate concentration s, the $\dot{q}_i$ equation indicates that q_i goes toward $Q_i(s)$, defined as the unique solution of

$$\mu_i(Q_i(s)) Q_i(s) = \rho_i(s) \tag{5}$$

The uniqueness of $Q_i(s)$ and its attractivity for a fixed s are straightforward since $\mu_i(q_i)q_i$ is increasing in q_i.

Let us define the maximum internal substrate storage

$$Q_{m_i} = \lim_{s\to+\infty} Q_i(s) \tag{6}$$

Q_{m_i} is thus the solution of $\mu_i(Q_{m_i}) Q_{m_i} = \rho_{m_i}$.

$Q_i(s)$ is bounded in $[K_{q_i}, Q_{m_i}]$, and K_{q_i} and Q_{m_i} are lower and upper-bounds for q_i along the solutions of (4). Indeed for $q_i(t) = K_{q_i}$ (resp. $q_i(t) = Q_{m_i}$) then $\dot{q}_i \geq 0$ (resp. $\dot{q}_i \leq 0$), so that the interval $[K_{q_i}, Q_{m_i}]$ is invariant for q_i. The fact that there is a minimum and a maximum internal substrate storage for each species is biologically relevant.

Corresponding to the maximum internal substrate storage, there is a maximum growth rate μ_{m_i} for each species

$$\mu_{m_i} = \mu_i(Q_{m_i}) \tag{7}$$

2.3 The Competitive Exclusion Principle (CEP)

Under constant D and s_{in}, for some x_i species, there exists a substrate concentration $s_i^\star$ for which the growth rate μ_i at equilibrium is equal to the dilution rate D :

$$\begin{array}{l} \mu_i(s_i^\star) = D \quad \text{in the Monod model} \\ \mu_i(Q_i(s_i^\star)) = D \quad \text{in the Droop model} \end{array} \tag{8}$$

If this substrate concentration does not exist for a given species, it means that $\mu_i(s)$ or $\mu_i(Q_i(s)) < D \quad \forall s$, and the species will be washed out of the chemostat. If $\mu_i(s_{in})$ or $\mu_i(Q_i(s_{in})) < D$ for a particular species, that species will also be washed out of the chemostat because we will have $s(t) < s_{in}$ after some finite time t_0, and then $\mu_i(s(t))$ or $\mu_i(Q_i(s(t))) < D$ for all $t > t_0$.

With no loss of generality, we order the species so that their $s_i^\star$ satisfy : $s_1^\star < s_2^\star < ... < s_N^\star$.

Hypothesis 1. $s_1^\star < s_{in}$ and $x_1(0) > 0$

The CEP stipulates that in a chemostat with single substrate growth limitation, constant controls D and s_{in}, and under hypothesis 1, only species 1 stays in the chemostat:

$$\begin{array}{l} \lim_{t\to+\infty} x_1(t) > 0 \\ \forall i \in [2, N], \lim_{t\to+\infty} x_i(t) = 0 \end{array} \tag{9}$$

Criterion 2. CEP's Competitiveness Criterion
Under hypothesis 1, the species with smallest $s_i^\star$, who needs less substrate than the others for obtaining an equilibrium growth rate $\mu_i(s)$ or $\mu_i(Q_i(s))$ equal to the dilution rate D, wins the competition and excludes all others from the chemostat.

Proof : A demonstration can be found in Smith and Waltman [1995] for the Monod model with N species and for the Droop model with 2 species. It has been validated with several species (Hansen and Hubell [1980] - Ducobu et al. [1998]). □

The CEP is crucial for the understanding of natural ecosystems. Some authors (Li and Smith [2003] - Hesseler et al. [2006] - Lobry and Harmand [2006]) developped alternative models for which the CEP is not verified, in order to explore some coexistence cases.

Motivations for this work
Some works have already been done to control the competition in the chemostat, generally to enable the coexistence of several species (Rao and Roxin [1990] - de Leenheer et al. [2003] - Gouzé and Robledo [2005]). Here we aim at finding controls which change the result of the competition keeping a single species. More precisely, we want to select species of interest who maximize a criterion other than the smallest $s_i^\star$, by imposing a periodic behavior to the system.

Bernard et al. [1996] have studied the effect of periodic substrate stresses, which is a realistic ecological situation. In section 3.1 we propose controls which permit to reproduce such stresses, and in section 4.3 we show that this can cause a new selection criterion.

3. CONTROLS FOR SELECTING SPECIES

3.1 Periodic substrate stresses

We propose an approach for the generation of periodic substrate stresses. It consists in periodically imposing a phase of rising substrate concentration, followed by a phase of falling substrate concentration. The reference period is $T = t_{rise} + t_{fall}$.

Rising phase during time t_{rise}
We choose s_{in} to obtain the dynamics $\dot{s} = \lambda(s_M - s)$:

$$s_{in} = s + \frac{1}{D}\left(\lambda(s_M - s) + \sum_{i=1}^{N} \rho_i(s) x_i\right) \tag{10}$$

Control s_{in} is positive because $s_M > s$.

We obtain $s(t) = s_M(1 - e^{-\lambda t})$ with $s(0) = 0$

Notice that $\sum_{i=1}^{N} \rho_i(s) x_i$ is generally not available from measurements so that an observer may be built.

Falling phase during time t_{fall}
Let us define the total biomass concentration $X_T = \sum_{i=1}^{N} x_i$. We choose s_{in} such that $\dot{s} = -\gamma\phi(s)$.

$$s_{in} = s + \frac{1}{D}\left(X_T\left(\sum_{i=1}^{N}\frac{x_i}{X_T}\rho_i(s)\right) - \gamma\phi(s)\right) \tag{11}$$

For s_{in} to be positive, we need $X_T\sum_{i=1}^{N}\frac{x_i}{X_T}\rho_i(s) \geq \gamma\phi(s)$. Since $\sum_{i=1}^{N}\frac{x_i}{X_T}\rho_i(s)$ is a convex combination of the $\rho_i(s)$, we have for all $s : X_T\sum_{i=1}^{N}\frac{x_i}{X_T}\rho_i(s) \geq X_T \min_i \rho_i(s)$. Then $\phi(s) \leq \min_i \rho_i(s)$ for $s \in [0, s_M]$ and $\gamma \leq X_T$ are sufficient conditions for the positivity of s_{in}.

If γ is high enough and t_{fall} is long enough, $s(kT)$ can reasonably be considered null, which ensures the periodicity of $s(t)$ when periodically imposing control (10) followed by (11).

Periodic substrate stresses cause periodic growth rates
In this subsection we show that periodic $s(t)$ causes periodic $q_i(t)$, and thus periodic growth rates $\mu_i(q_i(t))$.

Let us remind

$$\dot{q}_i = \rho_i(s) - \mu_i(q_i)q_i \tag{12}$$

Lemma 3. Under any T-periodic $s(t)$, there exists a unique periodic solution $\bar{q}_i(t)$ to (12). This solution is attractive for any initial condition $q_i(0)$ inside $[K_{q_i}, Q_{m_i}]$

Proof : First we demonstrate that $\bar{q}_i(t)$ exists. Then we prove its attractivity.

As the q_i-attractive $Q_i(s)$ is bounded in $[K_{q_i}, Q_{m_i}]$, initial condition $q_i(0) = K_{q_i}$ causes $q_i(T) \geq q_i(0)$, and $q_i(0) = Q_{m_i}$ causes $q_i(T) \leq q_i(0)$. Thus by continuity of $q_i(T)$ with regard to the initial condition, there exists an initial condition $q_i(0) = \bar{q}_i(0)$ in $[K_{q_i}, Q_{m_i}]$ such that $\bar{q}_i(T) = \bar{q}_i(0)$ and q_i is T-periodic under controls (10) and (11)

For the attractivity, $V_i(t) = |q_i(t) - \bar{q}_i(t)|$ is decreasing along the solutions : $\dot{V}_i(t) = sign(q_i(t) - \bar{q}_i(t))(\dot{q}_i(t) - \dot{\bar{q}}_i(t)) < 0$ because $sign(\dot{q}_i - \dot{\bar{q}}_i) = sign(-\mu_i(q_i)q_i + \mu_i(\bar{q}_i)\bar{q}_i) = -sign(q_i - \bar{q}_i)$. V_i being a Lyapunov function converging to zero, $\lim_{t\to+\infty} q_i(t) = \bar{q}_i(t)$. □

Therefore, under controls (10) and (11) q_i converges towards a T-periodic behavior, and so does $\mu_i(q_i(t))$. We will see in section 4.3 that this periodic behavior, caused by the periodic stresses, can lead to a new selection criterion.

3.2 Regulation of the total biomass concentration

To achieve the effective selection of one species, X_T must be lower bounded so that at least one microorganisms species remains in the chemostat, and it must be upper bounded to avoid saturation of the chemostat by microorganisms. That is why we propose a control D to obtain the dynamics

$$\dot{X}_T = D(X_T^\star - X_T) \tag{13}$$

so that X_T converges towards a chosen concentration $X_T^\star$.

In both models this leads us to $\sum_{i=1}^{N}\mu_i(.)x_i - DX_T = D(X_T^\star - X_T)$ and

$$D = \sum_{i=1}^{N}\frac{x_i}{X_T^\star}\mu_i(.) \tag{14}$$

For the positivity of (11) we need $\gamma \leq X_T$. It is now possible to choose $\gamma \leq min(X_T^\star, X_T(0))$.

Implementation : In practice $\sum_{i=1}^{N}\mu_i(.)x_i$ is often an indicator of the microorganisms activity that can be measured through the evolution of influent and effluent gas composition and flow rate. For example in the case of anaerobic digestion, this would be the CH_4 flow rate; in the case of microalgae, this would be the O_2 production (or CO_2 uptake).

Remark : It is also possible to regulate $K_T = \sum_{i=1}^{N} k_i x_i$ with k_i coefficients who can represent turbidity coefficients. This is what is approximatively done in a particular family of chemostat, the turbidostat.

4. SELECTION OF THE FASTEST GROWING SPECIES

4.1 Selection theorem in the X_T-regulated chemostat

We have shown how to obtain periodic growth rates, and regulated X_T. In this section we will suppose that these controls or others are applied to the system so that X_T is bounded in a fixed positive interval $[X_0, X_m]$, and the growth rates are T_i-periodic functions $\mu_i(t)$.
Hypothesis 4. X_T is bounded in $[X_0, X_m]$ with $X_0 > 0$, and the $\mu_i(t)$ are T_i-periodic functions.

We use the following notation for the mean growth of the species :

$$\mu_{mean_i} = \frac{1}{T_i}\int_0^{T_i}\mu_i(t)dt \tag{15}$$

Hypothesis 5. Let us assume that
$\exists j \in [1; N]$ such that $\mu_{mean_j} > \mu_{mean_i} \quad \forall i \neq j$

Theorem 6. Selection Theorem for any periodic behavior
Under hypotheses 4 and 5, species j with highest mean growth μ_{mean_j} is selected and excludes all others.

Proof : We denote $d_i = \ln\left(\frac{x_j}{x_i}\right)$.With $\dot{x}_i = (\mu_i - D)x_i$ we obtain $\dot{d}_i(t) = \frac{\dot{x}_j(t)}{x_j(t)} - \frac{\dot{x}_i(t)}{x_i(t)} = \mu_j(t) - \mu_i(t)$ and

$$d_i(t) = d_i(0) + \int_0^t \mu_j(\tau)d\tau - \int_0^t \mu_i(\tau)d\tau$$

We then use the following notations :

$$\begin{array}{l} p_i(t) = \dfrac{t - \mathrm{mod}(t, T_i)}{T_i} \\ r_i(t) = \mathrm{mod}(t, T_i) \\ t = p_i(t)T_i + r_i(t) \end{array} \tag{16}$$

where $p_i(t)$ is the number of T_i-periods for species i until time t. which leads us to

$$\int_0^t \dot{d}_i(\tau)d\tau = p_j(t)\int_0^{T_j}\mu_j(\tau)d\tau - p_i(t)\int_0^{T_i}\mu_i(\tau)d\tau + R_i^j(t)$$
$$= p_j(t)\left(\int_0^{T_j}\mu_j(\tau)d\tau - \frac{p_i(t)}{p_j(t)}\int_0^{T_i}\mu_i(\tau)d\tau\right) + R_i^j(t)$$
$$= p_j(t)\left(T_j\mu_{mean_j} - \frac{p_i(t)}{p_j(t)}T_i\mu_{mean_i}\right) + R_i^j(t)$$

with notation $R_i^j(t) = \int_0^{r_j(t)}\mu_j(\tau)d\tau - \int_0^{r_i(t)}\mu_i(\tau)d\tau$.
Since $\frac{p_i(t)}{p_j(t)} = \frac{t-\mathrm{mod}(t,T_i)}{t-\mathrm{mod}(t,T_j)}\frac{T_j}{T_i}$, $\lim_{t\to+\infty}\frac{p_i(t)}{p_j(t)} = \frac{T_j}{T_i}$ and $\lim_{t\to+\infty} d_i(t) = d_i(0)+p_j(t)T_j\left(\mu_{mean_j}-\mu_{mean_i}\right)+R_i^j(t)$. Then as $d_i(0)$ and $R_i^j(t)$ are bounded, $\lim_{t\to+\infty} d_i(t) = +\infty$ because $\lim_{t\to+\infty} p_i(t) = +\infty$ and $\mu_{mean_j} > \mu_{mean_i}$.

Thus $\lim_{t\to+\infty}\frac{x_j(t)}{x_i(t)} = +\infty$ and, as x_j is upper bounded by the upper-bound on X_T, then $\lim_{t\to+\infty} x_i(t) = 0$. As X_T is also lower bounded by $X_0 > 0$, then $\liminf_{t\to+\infty} x_j(t) \geq X_0 > 0$ and the proof is complete. □

4.2 Selection of the species with highest μ_{m_i}

We have shown that it is possible to select a species with fastest mean growth in given environmental conditions. Here we determine conditions for selecting the species with highest μ_{m_i}. Bennett and Boraas [1988] have realized such a selection by using a turbidostat culture.

Criterion 7. μ_{m_i} Selection Criterion
With a bounded total biomass concentration X_T, and with $\mu_i(t) \approx \mu_{m_i} \quad \forall t$, the species with highest μ_{m_i} is selected

Proof : The demonstration of Criterion 7 is the same as for Theorem 6, with $\mu_{mean_i} = \mu_{m_i}$. □

Implementation : In order to have $\mu_i(t) \approx \mu_{m_i}$, we regulate s at a large value s_0 (so that $\mu_i(s_0)$ or $\mu_i(Q_i(s_0)) \approx \mu_{m_i}$) by imposing $\dot{s} = D(s_0 - s)$ which is achieved through $s_{in} = s_0 + \frac{1}{D}\sum_{i=1}^N \rho_i(s)x_i$.

Remark : From a practical point of view, as $\sum_{i=1}^N \rho_i(s)x_i$ is not always measurable, we have imagined a simpler way to realize $\mu_i(s)$ or $\mu_i(Q_i(s)) \approx \mu_{m_i}$: with a high constant s_{in} and a small $X_T^\star$ we have $\dot{s} \approx D(s_{in} - s)$ and the substrate concentration will converge close to s_{in}, which is chosen high enough to have $\mu_i(s_{in})$ or $\mu_i(Q_i(s_{in})) \approx \mu_{m_i}$.

4.3 Periodic stresses and new selection criterion

In this section we present the results that we obtained with controls (10), (11), and the Selection Theorem 6.

Functions used for the study
We have used Michaelis-Menten absorption rates $\rho_i(s)$ and Droop growth rates $\mu_i(q_i)$:

$$\rho_i(s) = \rho_{m_i}\frac{s}{s+K_{s_i}}$$
$$\mu_i(q_i) = \bar{\mu}_i\left(1 - \frac{K_{q_i}}{q_i}\right) \qquad (17)$$

Rectangular shaped stresses
With functions (17) and controls (10) and (11), we have obtained pseudo-rectangular shaped stresses of Figure 1.

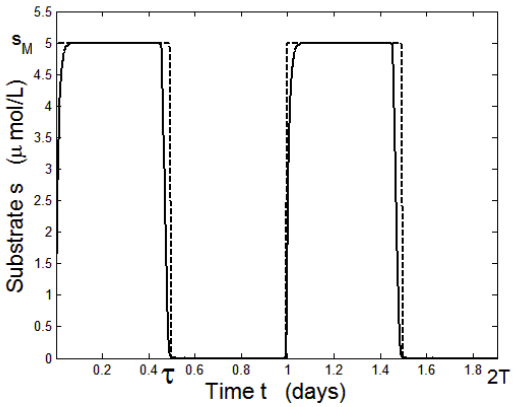

Fig. 1. Pseudo-rectangular shaped regular periodic stresses

The way to approach this regular rectangular shape as much as possible is described in section 5.

It is then reasonable (with $s_M \gg K_{s_i}$ such that $\rho_i(s_M) \approx \rho_{m_i}$) to approximate the stresses by (18)

$$\rho_i(s(t)) = \begin{cases} \rho_{m_i} & \text{if } \mathrm{mod}(t,T) \leq \tau \\ 0 & \text{if } \mathrm{mod}(t,T) > \tau \end{cases} \qquad (18)$$

The ratio τ/T is the proportion of time the microorganisms are fed, and $(T-\tau)/T$ is the proportion of time during which they are stressed.

Determination of a new selection criterion
Under control (18) we have calculated the periodic behavior of the internal substrate storage $\bar{q}_i(t)$ presented in Appendix A, with $\lim_{t\to+\infty} q_i(t) = \bar{q}_i(t)$ (see Lemma 3)

We have then calculated :

$$\mu_{mean_i} = \frac{1}{T}\frac{\mu_{m_i}}{\bar{\mu}_i}\ln\left(1 + \frac{Q_{m_i}/K_{q_i}}{\frac{1}{e^{\bar{\mu}_i\tau}-1} + \frac{Q_{m_i}/K_{q_i}-1}{e^{\bar{\mu}_i T}-1}}\right) \qquad (19)$$

This criterion can be simplified in the specific case where τ is small compared to T :

Hypothesis 8. $\tau/T \ll \frac{1}{Q_{m_i}/K_{q_i}-1}$ and $\tau \ll \frac{1}{\bar{\mu}_i \cdot Q_{m_i}/K_{q_i}}$

Criterion 9. Selection Criterion under periodic stresses
Under control (18) and hypothesis 8, the species with highest $\frac{T}{\tau}\mu_{mean_i} \approx \mu_{m_i}\frac{Q_{m_i}}{K_{q_i}}$ is selected.

where $\frac{Q_{m_i}}{K_{q_i}}$ represents the capacity of the species to increase its internal substrate storage.

Consequently, periodic stresses with a small τ make it possible to select a species which can both grow fast and increase significantly its internal substrate storage.

5. SIMULATIONS WITH THREE SPECIES

These simulations have been carried out on the Droop model (4) with control (14) so that the total biomass concentration converges toward $X_T^\star$.

We have used (17) with the parameters of Table 1 for the species, whose values come from Vatcheva et al. [2006].

species	1	2	3
K_s $(\mu mol/L)$	0.01	0.15	0.10
ρ_m $(10^{-9} \cdot (\mu mol/(\mu m)^3)/day)$	9	14	8
K_q $(10^{-9} \cdot \mu mol/(\mu m)^3)$	1.5	5	2
$\bar{\mu}$ $(1/day)$	1.5	6	3
μ_m $(1/day)$	1.2	1.91	1.71
$\mu_m \cdot Q_m/K_q$ $(1/day)$	6	2.8	4

Table 1. Parameter values of the species

5.1 Selection of the highest μ_{m_i} with a X_T-regulation

For this simulation we have chosen a large s_{in} and a small $X_T^\star$ to ensure a large s, and thus we meet the conditions of Criterion 7 ($s_{in} = 10\mu mol/L$, $X_T^\star = 1 \cdot 10^9 \cdot (\mu m)^3/L$)

Figure 2 shows the result of the simulation, where species 2 with highest μ_{m_i} excludes all others.

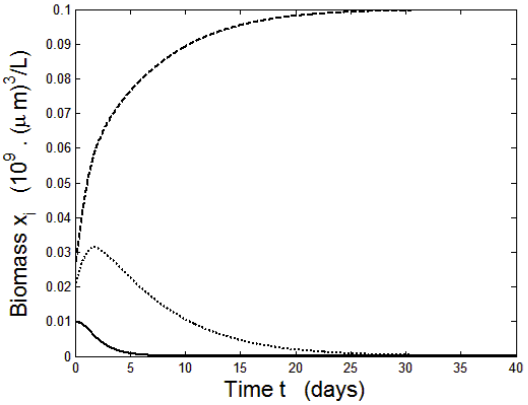

Fig. 2. Selection of the species with highest μ_{m_i}
Lines & species : *Solid*-1, *Dashed*-2, *Dotted*-3

5.2 Selection under periodic substrate stresses

For these simulations we have used controls (10) and (11) with $T = 1$ day, and $s_M \gg K_{s_i}$ so that $\rho_i(s_M) \approx \rho_{m_i}$ ($s_M = 5\mu mol/L$)

Approaching rectangular shaped stresses
We chose a high λ so that s rises fast ($\lambda = 1000$). In the presence of perturbations, λ should not be taken that high, in order to avoid amplifying them.
For a fast fall we have chosen a high $X_T^\star$, and a $X_T(0)$ close to $X_T^\star$ (this can be achieved by using control (14) long enough before starting the s_{in} control), which allowed us to choose a high $\gamma \leq min(X_T^\star, X_T(0))$:
$X_T^\star = 400 \cdot 10^9(\mu m)^3/L)$, $X_T(0) = 220 \cdot 10^9(\mu m)^3/L$, $\gamma = 100 \cdot 10^9(\mu m)^3/L$.
We also used $\phi(s) = \rho_{m_\phi} \frac{s}{s+K_{s_\phi}}$ with $\rho_{m_\phi} = 5 \cdot 10^9 \mu mol/(\mu m)^3 < \rho_{m_i}$ and $K_{s_\phi} = 1\mu mol/L > K_{s_i}$ so that $\phi(s) < \rho_i(s) \quad \forall i \in \{1, ..., N\}, \forall s$.
The method to obtain s_M-phases with duration τ is presented in Appendix B.

Selecting a species by choosing a τ value
Figure 3 shows that different species can be selected with different environmental condition τ, because for each species i here (see Table 1 for their parameter values), there exists a τ value such that μ_{mean_i} is higher than the other species' mean growth.

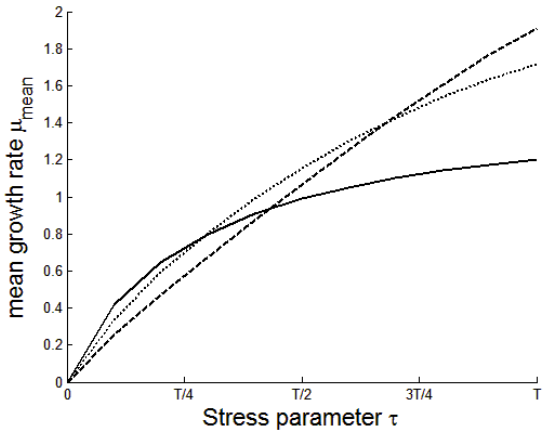

Fig. 3. $\mu_{mean_i}(\tau)$ for the three species. The species with highest μ_{mean_i} will be selected. It is thus possible to select each of the three species, by using different τ
Lines & species : *Solid*-1, *Dashed*-2, *Dotted*-3

Finally, Figure 4 illustrates the possibility of selecting any of the three species by choosing an adequate τ.

6. CONCLUSION

This work shows that it is in theory possible to select species exhibiting a desired feature in the chemostat : under turbidostat-like control in constant or periodic conditions, the species with the fastest mean growth rate is selected. We have proposed two possible applications : the selection of a species that can grow faster than any other, and the selection of a species which can both grow fast and increase its internal substrate storage.

This method makes it possible to select quite easily a species for its study or culture. It could be used to identify species which grow in hostile conditions, to amplify and verify the presence of a species in a medium, to determine conditions which permit a species to be resistant to invaders, to select a species which is interesting for a specific biotechnological objective, or to improve strains by directed evolution. The selection criterion, which is the maximum mean growth rate in chosen environmental conditions, seems very promising.

This work could be extended by using other controls such as an inhibitor's concentration. This would lead to other selection criteria.

REFERENCES

WN Bennett and ME Boraas. Isolation of a fast-growing strain of the rotifer brachionus calyciflorus pallas using turbidostat culture. *Aquaculture(Amsterdam)*, 73(1-4): 27–36, 1988.

O. Bernard, G. Malara, and A. Sciandra. The effects of a controlled fluctuating nutrient environment on continuous cultures of phytoplankton monitored by a computer. *J. Exp. Mar. Biol. Ecol*, 197:263–278, 1996.

P. de Leenheer, B. Li, and H.L. Smith. Competition in the chemostat : some remarks. *Canadian applied mathematics quarterly*, 11(2):229–247, 2003.

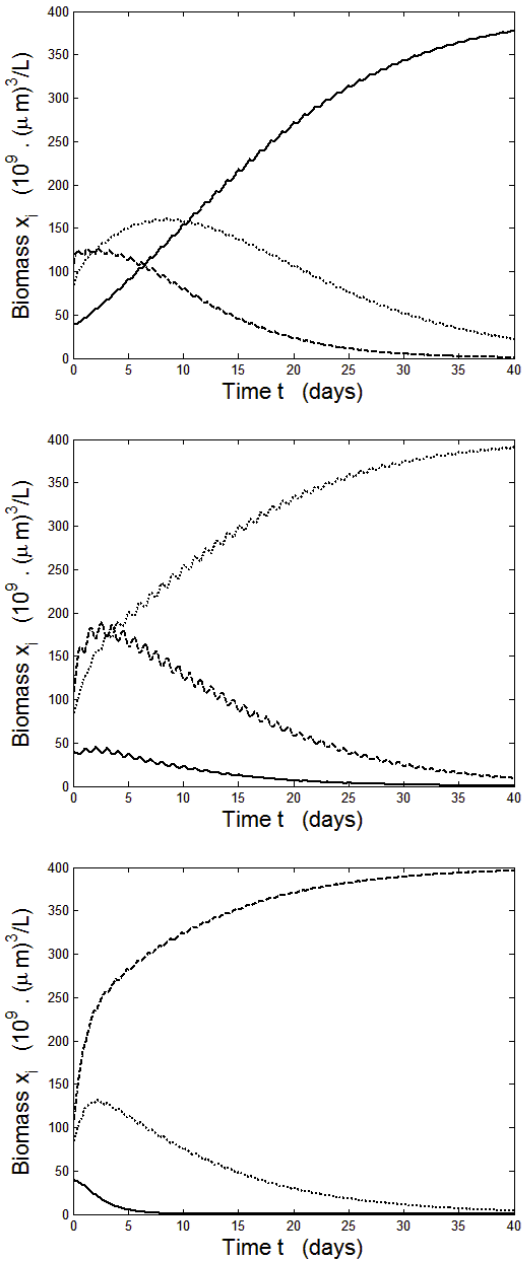

Fig. 4. Simulations of selections in the Droop model, under controls (14), (10) and (11).
top : $\tau = 0.1T$, *middle* : $\tau = 0.5T$, *bottom* : $\tau = 0.9T$
Lines & species : *Solid*-1, *Dashed*-2, *Dotted*-3

M.R. Droop. Vitamin b_{12} and marine ecology. *J. Mar. Biol Assoc. U.K.*, 48:689–733, 1968.

H. Ducobu, J. Huisman, R.R. Jonker, and L.R. Mur. Competition between a prochlorophyte and a cyanobacterium under various phosphorus regimes: Comparison with the droop model. *Journal of Phycology*, 34(3):467–476, 1998.

DE Dykhuizen and DL Hartl. Selection in chemostats. *Microbiological reviews. Baltimore*, 47(2):150–168, 1983.

J. Gouzé and G. Robledo. Feedback control for nonmonotone competition models in the chemostat. *Nonlinear Analysis: Real World Applications*, pages 671–690, 2005.

S.R. Hansen and S.P. Hubell. Single-nutrient microbial competition: qualitative agreement between experimental and theoretically forecast outcomes. *Science*, 207 (4438):1491–1493, 1980.

J. Hesseler, J.K. Schmidt, U. Reichl, and D. Flockerzi. Coexistence in the chemostat as a result of metabolic by-products. *Journal of Mathematical Biology*, 53(4): 556–584, 2006.

C.M. Jessup, S.E. Forde, and B.J.M. Bohannan. Microbial Experimental Systems in Ecology. *Adv Ecol Res*, 37: 273–307, 2005.

B.T. Li and H.L. Smith. Periodic coexistence of four species competing for three essential resources. *Mathematical Biosciences*, 184(2):115–135, 2003.

C. Lobry and J. Harmand. A new hypothesis to explain the coexistence of n species in the presence of a single resource. *Comptes Rendus Biologies*, 329(1):40–46, 2006.

Y.H. Percival Zhang, M.E. Himmel, and J.R. Mielenz. Outlook for cellulase improvement: Screening and selection strategies. *Biotechnology Advances*, 24(5):452–481, 2006.

N.S. Rao and E.O. Roxin. Controled growth of competing species. *Journal on Applied Mathematics*, 50(3):853–864, 1990.

H.L. Smith and P. Waltman. *The theory of the chemostat. Dynamics of microbial competition*. Cambridge Studies in Mathematical Biology. Cambridge University Press, 1995.

I. Vatcheva, H. de Jong, O. Bernard, and N. J.I. Mars. Experiment selection for the discrimination of semi-quantitative models of dynamical systems. *Artificial Intelligence*, 170(4-5):472–506, 2006.

O. Zelder and B.; Hauer. Environmentally directed mutations and their impact on industrial biotransformation and fermentation processes. *Current Opinion in Microbiology*, 3:248–251, 2000.

Appendix A. PERIODIC INTERNAL SUBSTRATE STORAGE CAUSED BY PERIODIC STRESSES (18)

We have demonstrated that (A.1) is the unique solution of (12) under periodic substrate stresses (18)

$$\bar{q}_i(t) = \begin{cases} Q_{m_i}\left(1 - e^{-\bar{\mu}_i t}\right) + \bar{q}_i(0)e^{-\bar{\mu}_i t} \text{ if } \mathrm{mod}(t,T) \leq \tau \\ K_{q_i}\left(1 - e^{-\bar{\mu}_i (t-\tau)}\right) + \bar{q}_i(\tau)e^{-\bar{\mu}_i (t-\tau)} \text{ else} \end{cases}$$

$$\begin{aligned} &\text{with } \bar{q}_i(0) = Q_{m_i} - (Q_{m_i} - K_{q_i})\frac{1 - e^{-\bar{\mu}_i (T-\tau)}}{1 - e^{-\bar{\mu}_i T}} \\ &\text{and } \bar{q}(\tau) = K_{q_i} + (Q_{m_i} - K_{q_i})\frac{1 - e^{-\bar{\mu}_i \tau}}{1 - e^{-\bar{\mu}_i T}} \end{aligned} \quad \text{(A.1)}$$

Appendix B. OBTAINING τ FOR (18)

To obtain regular stresses (18), we need to predict τ_{fall}, the time needed, starting from $s = s_M$, to obtain $s = s_0$ where s is negligeable ($s_0 = 0.005\mu mol/L$).
$\frac{ds}{dt} = -\gamma\phi(s) = \gamma\rho_{m_\phi}\frac{s}{s+K_{s_\phi}}$ leads us to $dt = -\frac{1}{\gamma\rho_{m_\phi}}(1 + \frac{K_{s_\phi}}{s})ds$ and to $\tau_{fall} = \frac{1}{\gamma\rho_{m_\phi}}\left(s_M - s_0 + K_{s_\phi}\ln\left(\frac{s_M}{s_0}\right)\right)$. If the stresses are rectangular shaped ($s \approx s_M$ during most of the time interval $[0, t_{rise}]$), it is thus possible to choose t_{rise} so that $\tau = t_{rise} + \tau_{fall}$, and to approach control (18).

ACKNOWLEDGEMENTS

This work was financed and carried out as part of the ANR - 06 - BIO E - 014 - 06 project.

Driving competition in a complex ecosystem: application to anaerobic digestion

P. Masci, O. Bernard, F. Grognard, E. Latrille and J.-B. Sorba and J.P. Steyer

Abstract— **Anaerobic digestion is a wastewater treatment process where bacteria degrade an organic substrate and produce methane, which can be used as a biofuel. The first task when starting up an anaerobic digester is the increase of its microbial population. It is a delicate phase, which is still not well understood, and its influence on the digester's future performance is not well known. During this phase, we show that a competition between the various species occurs and finally some species become dominant. In this paper, extending the competitive exclusion principle, we propose to drive the competition during this start-up phase, by regulating the volatile fatty acids concentration, with the aim of selecting species with good performance in the standard operating mode of the process. This new "selective" start-up strategy should lead to more efficient ecosystems.**

Keywords: Anaerobic digestion; Bioreactors;Biological systems; Competition; Selection; Directed Evolution

I. Introduction and motivation

Anaerobic digestion is a more and more widely used bioprocess for wastewater treatment. This complex ecosystem involves several hundreds of bacterial and achaeal species [1] that progressively degrade organic matter into methane and CO_2. It has many advantages compared to the more widespread activated sludge process: it can handle concentrated substrates, produces few sludge, and methane can be recovered and used as a biofuel. However this process is difficult to manage since the steady state associated to the operating mode is not globally stable [2]. As a corollary, the start-up of the digester is a long and risky phase [3] during which the digester loading is progressively increased in order to let the bacterial population adapt, grow and settle the reactor. Reactor start-up is then a long procedure (from one month to almost one year) that is essential to achieve a high treatment capacity at steady-state [4], and therefore this phase should be better understood and controlled.

Despite its key role, this phase did not receive so far much attention, perhaps because it is quite difficult to properly characterise since biomass measurements are not available. In [5], it was shown that disturbing the microbial community in a "bang bang" like approach leads to better diversity and thus improves the bioprocess when facing a toxicant.

In this paper, we propose a new model for the start-up phase, including biodiversity. We assume that, at the beginning, N species are competing for the substrate. We show that, depending on the way the digester is started up, some populations will be enhanced and will preferentially remain in the digester. The underlying idea relies on the competitive exclusion principle, which has been theoretically studied and experimentally demonstrated in various conditions [6], [7]. We exploit the idea proposed in [8] to drive the competition during the start-up phase, by regulating the volatile fatty acids (VFA) concentration around a fixed value, which is determined by the normal operating mode of the digester. By doing so, we act upon the ecosystem in order to enhance the process efficiency. Also, bacterial biomass extinction, which is one of the main risks of the start-up phase, is avoided, and the obtained ecosystem presents an interesting steadiness property. Simulations and a first experiment are presented for supporting this start-up strategy.

II. Process modelling

A. Presentation of the model

We propose here a simple macroscopic model (derived from [9]) in order to be able to handle the involved mathematics. We assume that, in a first acidogenesis step, the dissolved organic substrate, of concentration s_1, is degraded by a population made of N_a species of acidogenic bacteria (y_j, with $j \in [1; N_a]$) into volatile fatty acids (VFA, denoted s_2). The growth rate of these bacteria is $\gamma_j(s_1)$:

$$k_1\, s_1 \xrightarrow{\gamma_j(s_1) y_j} y_j + k_2\, s_2 + k_5\, \mathrm{CO_2}$$

where k_1, k_2 and k_5 are pseudo-stoichiometric coefficients which represent the transfer from substrate to acidogenic biomass, VFA and CO_2. They are assumed to be constant between the various acidogenic species.

In a second step (methanogenesis), the VFA are degraded into CH_4 and CO_2 by N_m methanogenic archaeabacteria (x_i, with $i \in [1; N_m]$) with growth rate $\mu_i(s_2)$:

$$k_3\, s_2 \xrightarrow{\mu_i(s_2) x_i} x_i + k_4\, \mathrm{CH_4} + k_6\, \mathrm{CO_2}$$

P. Masci, O. Bernard and F. Grognard are with INRIA Sophia Antipolis, 2004 route des lucioles, BP 93, 06902 Sophia Antipolis, France olivier.bernard@inria.fr

J.B. Sorba, E. Latrille and J.P. Steyer are with LBE, UR050, INRA, Avenue des étangs 11100 Narbonne, France

where k_3, k_4 and k_6 represent the transfer from substrate to methanogenic biomass, methane and CO_2. They are also assumed to be constant between all the methanogenic species.

We assume that the concentrations are perfectly distributed throughout the reactor, and the dilution rate for the dissolved components is D. Since a part of the bacteria are attached on a fixed biofilm within the digester, the dilution rate for the y_j and x_i biomasses are $\beta_j D$ and $\alpha_i D$ (*i.e.* the biomasses have a retention time $1/(\beta_j D)$ or $1/(\alpha_i D)$). The dynamical mass-balance model in a continuous stirred tank reactor is then straightforwardly derived [10], [9]:

$$\left\{\begin{array}{lcl} \dot{s}_1 &=& D(s_1^{in}-s_1)-k_1\sum_{j=1}^{N_a}\gamma_j(s_1)y_j \\ \dot{y}_j &=& \gamma_j(s_1)y_j-\beta_j D y_j \\ \dot{s}_2 &=& D(s_2^{in}-s_2)+k_2\sum_{j=1}^{N_a}\gamma_j(s_1)y_j \\ && -k_3\sum_{i=1}^{N_m}\mu_i(s_2)x_i \\ \dot{x}_i &=& \mu_i(s_2)x_i-\alpha_i D x_i \\ q_m &=& k_4\sum_{i=1}^{N_m}\mu_i(s_2)x_i \end{array}\right. \quad (1)$$

where s_1^{in} and s_2^{in} are respectively the concentration of the influent organic substrate and influent VFA, and q_m is the methane flow rate.

We consider a Monod kinetics (2) for the growth rate of acidogenic bacteria

$$\gamma_j(s_1)=\bar{\gamma}_j\frac{s_1}{s_1+h_j^1} \quad (2)$$

and an Haldane function (3) for the methanogenesis, to represent the possible inhibition by an accumulation of VFA [9]:

$$\mu_i(s_2)=\bar{\mu}_i\frac{s_2}{s_2+h_i^2+(s_2/h_i^{2*})^2} \quad (3)$$

where $\bar{\gamma}$ is the maximal growth rate of the acidogenic bacteria and $\bar{\mu}$ is the potential maximum growth rates of the methanogenic bacteria, h_j^1 and h_i^2 the half-saturation constants associated to substrates s_1 and s_2, and h_i^{2*} the inhibition constants associated to substrate s_2.

III. The "selective" start-up strategy

A. Standard start-up strategy

The main danger during the start-up phase is imposing too high a dilution rate D, such that the VFA concentration becomes high and inhibitory, and all the methanogenic biomasses are washed out of the digester (see [2] for a study of the two stable equilibria attraction bassins, in the mono-specific case). In order to avoid such a dramatic scenario, the plant operator often starts the digester with a very low dilution rate. Under such a control, the outcome of competition between bacterial species can be predicted in the case where $\forall j \in \{1,\cdots,N_a\}, \beta_j=\beta$ and $\forall i \in \{1,\cdots,N_m\}, \alpha_i=\alpha$ for some $\alpha,\beta>0$.

Any acidogenic species whose maximum growth rate $\bar{\gamma}_j$ is lower than the dilution rate βD will be excluded from the digester, because for such a species $\dot{y}_j<-K_j y_j$, with $K_j=-\bar{\gamma}_j+\beta D>0$, and then $y_j(t)<y_j(0)e^{-K_j t}$ tends to zero. The same exclusion applies for all methanogenic species such that $\max_{s_2}\mu_i(s_2)<\alpha D$.

For the other acidogenic species, it is possible to define equilibrium substrate concentration s_{1j}^* such that

$$\gamma_j(s_{1j}^*)=\beta D$$

where the s_{1j}^* concentration depends on D:

$$\frac{\partial}{\partial D}s_{1j}^*\geq 0$$

For the other methanogenic species, it is possible to define s_{2i}^* and $s_{2i}^\dagger\geq s_{2i}^*$ such that

$$\mu_i(s_{2i}^*)=\mu_i(s_{2i}^\dagger)=\alpha D$$

where the s_{2i}^* and $s_{2i}^\dagger$ concentrations depend on D:

$$\frac{\partial}{\partial D}s_{2i}^*\geq 0 \text{ and } \frac{\partial}{\partial D}s_{2i}^\dagger\leq 0$$

In order to prove the next property, we can then define a dilution rate D^* low enough such that:

$$\min_i(s_{2i}^\dagger)=\max_i(s_{2i}^*)$$

and, for any $S>0$, there exists $D^S<D^*$ such that $\forall D<D^S$,

$$\min_i(s_{2i}^\dagger)>S>\max_i(s_{2i}^*) \quad (4)$$

The following property determines the outcome of the competition when the dilution is small enough and when there is enough substrate in the input to avoid the straightforward wash-out of all species:

Property: If $\forall j,\beta_j=\beta$, $\forall i,\alpha_i=\alpha$, the dilution satisfies $D<D^*$, and $s_1^{in}>\min_j(s_{1j}^*)$ then

- the species with lowest s_{1j}^* is selected among all acidogenic species (with $lim_{t\to\infty}y_j=y_j^*$),

if, moreover, $S=s_2^{in}+\frac{k_2}{k_1}(s_1^{in}-s_{1j}^\star)$ satisfies (4)

- the species with lowest s_{2i}^* is selected among all the methanogenic species.

Proof : Under such a constant low dilution rate, the theory of competitive exclusion predicts (with Monod-like growth functions) that the most efficient species for the growth βD, i.e. the acidogenic species with lowest s_{1j}^*, is selected [6]. This is also true with Haldane-like growth functions when (4) is satisfied [11]: the methanogenic species with lowest s_{2i}^* wins the competition. □

Then if a constant dilution rate $D<D^*$ is imposed, two independent selection processes occur, which do not depend on the s_1^{in} and s_2^{in} input concentrations. Note that the trait which is optimized is the lowest substrate requirement, and that it is not possible to choose the s_{1j}^*

and s_{2i}^* concentrations: selection occurs but it is not controlled. That is a major problem of this start-up strategy: species which would grow fast in the standard operating mode can be washed out; uncontrolled competition can lead to the selection of species with low growth rate in the standard operating mode, thus slowing the pollution removal process.

We propose an alternative strategy which permits to control the competition and select the most efficient species in the standard operating mode.

B. Objective of the proposed strategy

A reasonable objective for an anaerobic digester is to consume the pollutant substrate and obtain a constant VFA output concentration $\bar{s}_2$ (VFA is necessary for the process, but it is also a pollutant), with the highest possible dilution rate D, which corresponds to the wastewater treatment rate.

The objective of the strategy that we want to explore is to preserve and select the species whose equilibrium $\mu_i(\bar{s}_2)/\alpha_i$ (denoted "relative growth rate") is maximal, thus optimizing the wastewater treatment rate (at equilibrium $D = \mu_i(\bar{s}_2)/\alpha_i$). More than that, we propose to drive this selection since the beginning of the start-up phase, which may have a positive impact on the biofilm composition, thus resulting in better performances. For achieving this goal we regulate s_2 and show that it leads to the desired competition outcome.

C. Control design for the regulation of s_2

Here we assume that a control strategy has been set-up which ensures the convergence of s_2 towards the setpoint $\bar{s}_2 < s_2^{in}$. Because of space limitation, we won't detail the considered control law, nor prove its convergence. However we refer the reader to other works aiming at the substrates regulation in an anaerobic digestion process [10], [12], [13]. In the sequel, the used controller is presented and its convergence is shown on a real plant.

D. Selection of archaeal species with maximal $\mu_i(s_2)/\alpha_i$

The principle of driving the competition for selecting species or individuals which maximize a chosen criterion is presented in [8], where a general law is given for this selection, and specific selection criteria are given for Monod and Droop models. This theory can also be adapted and applied to system (1) if the VFA concentration is regulated to a constant value.

Main Theorem : In system (1), if a controller achieves the regulation of s_2 to $\bar{s}_2 < s_2^{in}$, then the methanogenic species x_k with highest relative growth rate $\mu_k(\bar{s}_2)/\alpha_k$ is selected and all the others are excluded.

Proof In a first step we will prove that the regulation of s_2 to $\bar{s}_2 < s_2^{in}$ leads to the boundedness of the total methanogenic biomass $\sum_{i=1}^{N_m} x_i(t)$ (denoted $X_T(t)$) in $[X_0; X_m]$ with $X_0 > 0$. Therefore the total methanogenic biomass X_T cannot diverge, and its complete washout cannot occur (at least one methanogenic species will remain in the chemostat). In a second step, we will show that the difference in relative velocity between species lead to the survival of only one species, with maximal relative growth rate.

First, s_2 regulation causes the total methanogenic biomass boundedness. Indeed, defining the variable $z = s_1 + \frac{k_1}{k_2}s_2 + \frac{k_3 k_1}{k_2}X_T$ and $z^{in} = s_1^{in} + \frac{k_1}{k_2}s_2^{in}$, we have

$$\dot{z} = Dz^{in} - Ds_1 - \frac{k_1}{k_2}Ds_2 - D\frac{k_3 k_1}{k_2}\sum_i \alpha_i x_i$$

so that

$$D(z^{in} - z) \leq \dot{z} \leq D(z^{in} - \alpha z) \tag{5}$$

where $\alpha = \min_i \alpha_i$. We directly conclude that an upperbound on X_T is deduced from an upperbound on z, so that

$$X_m = \frac{k_2}{k_3 k_1}\max\left(\frac{z^{in}}{\alpha}, z(0)\right)$$

We can deduce from this upperbound that $\int_0^\infty D(\tau)d\tau$ is unbounded. Indeed, if it was not the case and knowing that s_2 converges to $\bar{s}_2$, any $\dot{x}_i$ equation aymptotically yields

$$\dot{x}_i = (\mu(\bar{s}_2) - D(\tau))x_i$$

whose solution is unbounded when the aforementionned integral is bounded, which is in contradiction with the existence of X_m.

Also, the unboundedness of $\int_0^\infty D(\tau)d\tau$ and (5) yield $\liminf_{t\to\infty} z \geq z^{in}$, so that, having $lim_{t\to\infty} s_2 = \bar{s}_2$ and using the fact that $s_1(t) \leq s_1^{in}$ for all times

$$\liminf_{t\to\infty} X_T \geq \frac{1}{k_3}(s_2^{in} - \bar{s}_2)$$

so that there is a lower-bound X_0 on X_T.

Secondly, X_T being lower and upper bounded, let us show that the difference in relative growth rates between the species lead to competitive exclusion. We denote x_k the species with maximal $\mu_k(\bar{s}_2)/\alpha_k$, such that $\mu_k(\bar{s}_2)/\alpha_k > \mu_i(\bar{s}_2)/\alpha_i, \forall i \neq k$ and t_s a time such that $\mu_k(s_2(t))/\alpha_k > \mu_i(s_2(t))/\alpha_i, \forall i \neq k, \forall t \geq t_s$. Let us define

$$r_i = \ln\left(\frac{x_k^{1/\alpha_k}}{x_i^{1/\alpha_i}}\right)$$

which leads to

$$\dot{r}_i(t) = \frac{\dot{x}_k}{\alpha_k x_k} - \frac{\dot{x}_i}{\alpha_i x_i} = \frac{\mu_k(s_2(t))}{\alpha_k} - \frac{\mu_i(s_2(t))}{\alpha_i} > 0$$

for all $t \geq t_s$. Then $r_i(t)$ will increase, so that $\lim_{t\to+\infty} r_i(t) = +\infty$. This means that the ratio $\frac{x_k^{1/\alpha_k}}{x_i^{1/\alpha_i}}$ will tend to infinity.

As x_k is upper bounded by X_m, it cannot diverge, which implies that

$$\lim_{t\to+\infty} x_i(t) = 0, \forall i \neq k$$

As x_k is also lower bounded by X_0, then

$$\liminf_{t\to+\infty} x_k(t) > 0$$

and we obtain that only methanogenic species x_k is not excluded from the chemostat. □

Thus, if one can regulate the VFA concentration s_2 so that it remains constant at a given $\bar{s}_2$ value, then the selection of the species with maximal relative growth rate $\mu_k(\bar{s}_2)/\alpha_k$ will occur, thus shaping the ecosystem and optimizing the wastewater treatment rate at equilibrium $D = \mu_k(\bar{s}_2)/\alpha_k$.

IV. Simulations

Even though, as previously said, several hundreds of microbial species are present in anaerobic digesters, we have simulated system (1) with only 3 acidogenic species and 4 methanogenic species to keep the system understandable. Species-specific parameters are taken from [9] with $\pm 50\%$ values. The substrate and VFA inputs were $s_1^{in} = 5g/L$ and $s_2^{in} = 5mmol/L$. The relative growth functions $\mu_i(s_2)/\alpha_i$ of the various methanogenic species is presented in Fig. 1. Species 1 grows better with low VFA concentration, species 3 grows faster under high VFA concentration, and species 2 is better for medium ones. Species 4 is less efficient than the others for any VFA concentration, so that it should be excluded whatever the start-up strategy.

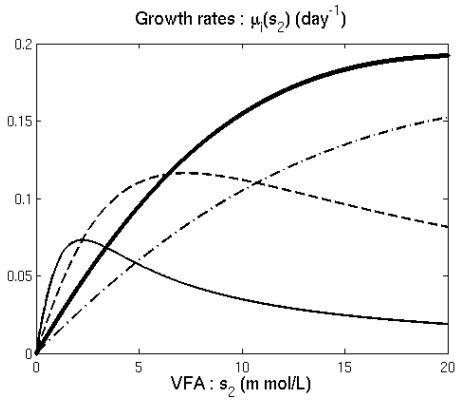

Fig. 1. Relative growth functions $\mu_i(s_2)/\alpha_i$ of the 4 methanogenic species used in simulation. Species 1 (*Solid*), species 2 (*Dashed*), species 3 (*Thick*), species 4 (*Dashdot*)

A. Interest of the "selective" start-up strategy

In this section we show the interest of the selective start-up strategy, by comparing it with two other strategies.

The first strategy is the *standard start-up strategy* where D is chosen low ($D = 0.05$) to avoid bacterial wash out. The result is presented in Fig. 2, where we can see that species 1, which grows slowly for high VFA concentrations, is selected. The digester was started safely but the obtained ecosystem is such that the digester's performance will not be optimal.

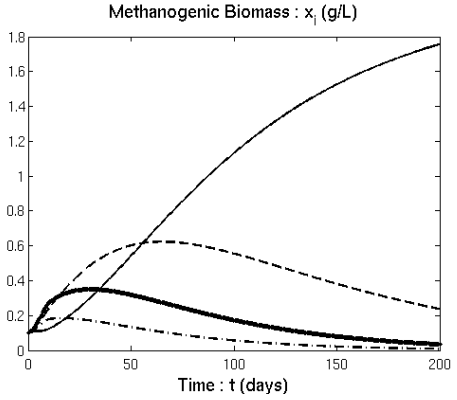

Fig. 2. Standard start-up strategy with low $D = 0.05$, to avoid archaeal washout. This strategy leads to the selection of species 1, which is not optimal for VFA concentrations higher than $2mmol/L$ (see Fig. 1)

The second strategy is the *selective start-up strategy* where the species which grows faster at VFA concentration $\bar{s}_2$ is favored. In Fig. 3 we use a controller to regulate s_2 to $\bar{s}_2 = 3mmol/L$, and species 2 is selected. We see on Fig. 1 that it is the most efficient species at this concentration.

For this strategy we used the following pseudo-linearizing

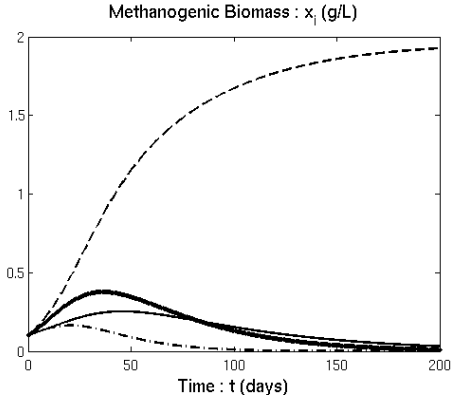

Fig. 3. Selective start-up strategy : species 2, which is the most efficient under VFA concentration $\bar{s}_2 = 3mmol/L$, is selected.

controller

$$D = \frac{\lambda_1(\bar{s}_2 - s_2) + \frac{k_3}{k_4} q_m}{s_2^{in} - s_2} + \lambda_2 \int_0^t (\bar{s}_2 - s_2(\tau))d\tau \quad (6)$$

(λ_1 and λ_2 are two gains) where the non-measured acidogenic activity is replaced by a PI correction.

The last one is a *naive start-up strategy* where the value of D is constant and equal to $\mu_2(\bar{s}_2)$. The objective of this strategy is to obtain the same result as in the selective strategy, but the simulation of Fig. 4 shows that it leads to process failure: the VFA were accumulated such that they became inhibitory ($\approx 100mmol/L$), and the methanogenic biomasses were washed out.

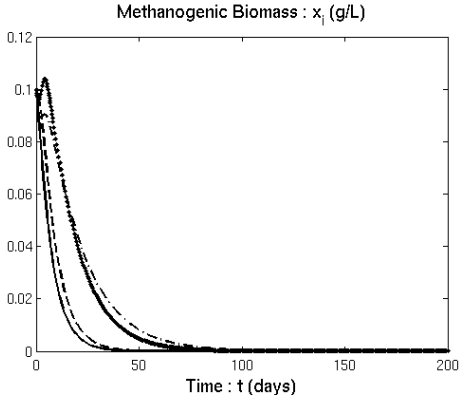

Fig. 4. Naive start-up strategy : by choosing D high ($D = \mu_2(\bar{s}_2)$) since the beginning of start-up, the methanogenic biomasses became inhibited and were washed out.

These simulations show that the selective start-up strategy avoids bacterial extinction, while selecting efficient species for the digester in the standard operating mode.

B. Selecting a population optimal for a given VFA concentration

Let us suppose now that we want an anaerobic digester whose VFA concentration in the standard operating mode is $\tilde{s}_2 = 8mmol/L$. Using linearizing controller (6) to regulate s_2 to $\tilde{s}_2$, we obtain the simulation of Fig. 5 where species 3 (the most appropriate at concentration $8mmol/L$) is selected.

This simulation emphasizes that depending on the digester VFA concentration in the standard operating mode, different species should be selected during the start-up phase, so that the obtained ecosystem will be more efficient.

C. The selective process consolidates the ecosystem

On Fig. 6 we can see that the dilution rate, during the $\tilde{s}_2$ selective start-up, rises until selection occurs and then becomes almost constant and equal to $\mu_2(\tilde{s}_2)/\alpha_i$. Then, after time $t = 100days$, the controller is turned off and the dilution rate is kept constant with no consequence for the digester, as the VFA concentration stays almost constant: the ecosystem is settled and composed of the most efficient population in the standard operating mode, such that it became naturally stable around the desired

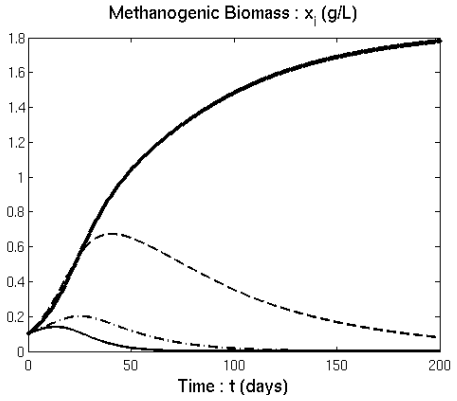

Fig. 5. Start-up selection, under the closed loop control, of species which maximize $\mu_2(\tilde{s}_2)/\alpha_i$, with $\tilde{s}_2 = 8mmol/L$. Depending on the VFA concentration in the standard operating mode, different populations should be selected to optimize the process.

equilibrium ($s_2 = \tilde{s}_2$). This result is of great importance and must be verified experimentally : the selective start-up strategy gives birth to a stable ecosystem involving bacterial species such that the natural steady state is exactly the requested one, without needing a control feedback anymore.

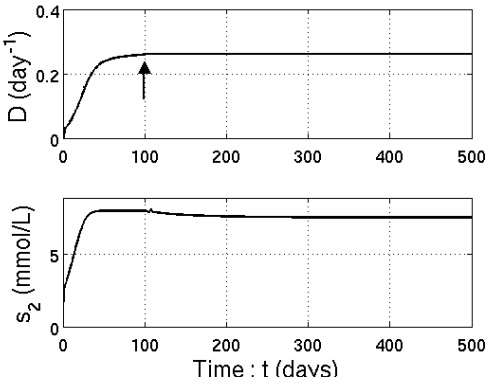

Fig. 6. The dilution rate (*top*) in the $\tilde{s}_2$ experiment was kept constant after time $t = 100days$ with negligible consequence on the VFA concentration (*bottom*), showing that selection leads naturally to a consolidated ecosystem where the desired equilibrium ($s_2 = \tilde{s}_2$) is stable.

V. Application to a real anaerobic digester start-up phase

In order to verify the proposed selection principle and to assess the effect of a controller that regulates the VFA during the start-up phase, experiments have been carried out at the LBE-INRA Laboratory in Narbonne (France).

A. Experiment design

The process is an up-flow anaerobic fixed bed reactor with a useful volume of 0.548 m3. The reactor is highly

instrumented and many variables were measured during the experiments [9]. More details about the process and evaluation of its on-line instrumentation are available in [14].

B. Experimental results and discussion

Control (6) was applied, with command $\bar{s}_2 = 4$ g/L, and control parameters $k_3 = 116.5$ mmol/g, $k_4 = 453$ mmol/g, $\lambda_1 = 12$ day^{-1} and $\lambda_2 = 0.05$ mmol^{-1} day^{-1} . The experimental results are presented in Fig. (7).

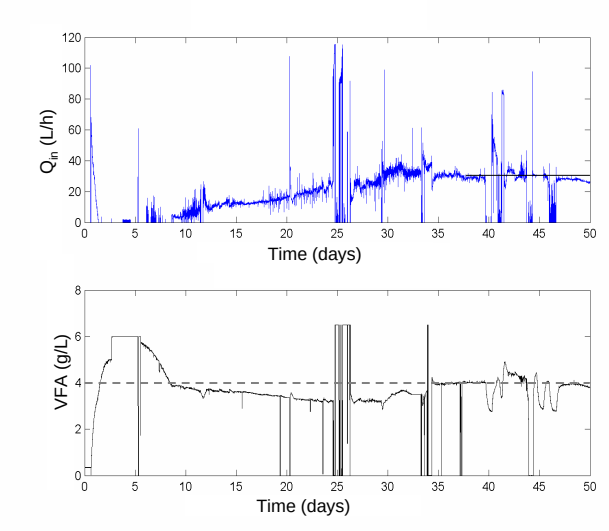

Fig. 7. Start-up experiment where s_2 is regulated at $\bar{s}_2 = 4g/L$. The influent flow rate ($Q_{in} = D/V$) and the VFA concentration are plotted.

We can see on this figure that our control objective was attained : the VFA concentration was well driven towards $\bar{s}_2$ despite many disturbances related to failures and disturbances in the process. It is worth noting that the more the ecosystem is selected, the more efficient the regulation. At the end, when the interesting species have probably been selected in the digester, the regulation is more and more efficient.

Finally, the proposed strategy enabled us to reach a high dilution rate $D = 0.78$ while avoiding start-up failure.

VI. CONCLUSIONS

We proposed a start-up strategy for an anaerobic digester, whose aim is to influence the structure of the ecosystem, so that the obtained ecosystem in the end of start-up will be optimal for a given VFA concentration. For implementing such a selective process, we drive the competition by regulating the VFA concentration at a fixed value. We showed how the obtained ecosystem should also be consolidated because of the selection that occurs during the start-up phase.

According to model (1), a control law was proposed and a mathematical demonstration was given for predicting the competition outcome. Simulations were used to verify and explain the utility of the method, and a real experiment was presented where the start-up strategy was tested.

We emphasize that the aim of this strategy is not to minimize the start-up duration, but rather to build an efficient ecosystem. This kind of start-up strategy, where the objective is to act on the bacterial community's structure for optimizing a particular process, was never (to our knowledge) proposed before for anaerobic digestion. Further investigations in this direction are presently performed.

VII. ACKNOWLEDGMENTS

This work was carried out with support provided by the CODA ARC project funded by the INRIA.

REFERENCES

[1] C. Delbès, R. Moletta, and J.-J. Godon, "Bacterial and archaeal 16s rdna and 16s rrna dynamics during an acetate crisis in an anaerobic digestor ecosystem," *FEMS Microbiology Ecology*, vol. 35, pp. 19–26, 2001.

[2] J. Hess and O. Bernard, "Design and study of a risk management criterion for an unstable anaerobic wastewater treatment process," *J. Process. Contr.*, vol. 18, pp. 71–79, 2008.

[3] K.-Y. how.and Y. Wang, S.-F. Foong, and J.-H.Tay, "Accelerated start-up and enhanced granulation in upflow anaerobic sludge blanket reactors," *Water Research*, vol. 28, pp. 2293–2304, 2004.

[4] S. Michaud, N. Bernet, P. Buffiére, M. Roustan, and R. Moletta, "Methane yield as a monitoring parameter for the strat-up of anaerobic fixed film reactors," *Water Research*, vol. 36, pp. 1385–1391, 2002.

[5] J. S. I. Ramirez, E.I.P. Volcke, "Modeling and monitoring of microbial diversity in ecosystems - application to biological wastewater treatment processes," in *Proceedings of the IFAC conference*. Seoul, Korea, 2008.

[6] H. L. Smith and P. Waltman, *The theory of the chemostat: dynamics of microbial competition*. Cambridge University Press, 1995.

[7] S. R. Hansen and S. P. Hubbell, "Single-nutrient microbial competition," *Science*, vol. 207, no. 28, pp. 1491–1493, 1980.

[8] P. Masci, F. Grognard, and O. Bernard., "Continuous selection of the fastest growing species in the chemostat," in *Proceedings of the IFAC conference*. Seoul, Korea, 2008.

[9] O. Bernard, Z. Hadj-Sadok, D. Dochain, A. Genovesi, and J.-P. Steyer, "Dynamical model development and parameter identification for an anaerobic wastewater treatment process," *Biotech.Bioeng.*, vol. 75, pp. 424–438, 2001.

[10] G. Bastin and D. Dochain, *On-line estimation and adaptive control of bioreactors*. Amsterdam: Elsevier, 1990.

[11] G. Wolkowicz and L. Zhiqi, "Global show, k.-y.; wang, y.; foong, s.-f.; tay, j.-h. accelerated start-up and enhanced granulation in upflow anaerobic sludge blanket reactors. water research 2004, 38, 2293–2304.dynamics of a mathematical model of competition in the chemostat: General response functions and differential death rates," *SIAM Journal of Applied Mathematics*, vol. 52, pp. 222–233, 1992.

[12] O. Bernard, Z. Hadj-Sadok, M. Pengov, and D. Dochain, "Modelling, monitoring and control of anaerobic digestion processes," *Journal A.*, vol. 41, pp. 82–88, 2000.

[13] L. Mailleret, O. Bernard, and J.-P. Steyer, "Robust nonlinear adaptive control for bioreactors with unknown kinetics," *Automatica*, vol. 40:8, pp. 365–383, 2004.

[14] J. P. Steyer, J. C. Bouvier, T. Conte, P. Gras, and P. Sousbie, "Evaluation of a four year experience with a fully instrumented anaerobic digestion process," *Water Science and Technology*, vol. 45, pp. 495–502, 2002.

Chapter 5

Conclusion

Microbial ecosystems play key roles in our biosphere: they highly contribute to harvest light energy from the sun and to recycle nutrients. They should therefore be better understood, both for a better apprehension of natural ecosystems but also for developing cleaner biotechnologies. The implications of the ecosystems studied in this thesis are multiple:

- microalgal and anaerobic ecosystems both play an important role in global warming since they respectively consume CO_2 and produce CH_4. Thus, they should be better understood and models must quantify the associated carbon and energy fluxes.
- some microalgae, like spirulina, can be eaten and are great potential sources of proteins, vitamins and minerals [42];
- some microalgae produce pharmaceutics and neutraceutics [38];
- some others produce oil which can be used as a biofuel, and high productivities seem possible [8];
- anaerobic bacteria can clean wastewater, and degrade low biodegradable substrates,
- methanogenic bacteria produce methane which is also a renewable biofuel.

Our first step to better apprehend these ecosystems was to develop models for microalgae populations in photobioreactors (chapter 2.1). The model needed to include enough ingredients to reproduce the main process behavior, but had to be kept simple enough to be validable, identifiable, and to be mathematically tractable. Our model represents nutrients absorption and storage. This is a key issue for biofuel production since nitrogen influences lipids synthesis (see our lipid synthesis model in [33]). It also represents light attenuation and respiration which are crucial when biomass concentration is high, which is often the case in real bioprocesses. The last ingredients are photoinhibition (high light intensities inhibit growth) and photoacclimation (Chl/C ratio variations depending on the received light) which is important when light or biomass vary in the photobioreactor. While representing all these phenomena, the model stays relatively simple, based on only four dynamical equations representing nitrogen in the medium, biomass, internal nitrogen quota, and chlorophyll evolutions.

A parameter calibration procedure is proposed and used to validate the model on a dataset. Analytical results demonstrate that high density cultures, when subject to photoinhibition under strong light, show no apparent photoinhibition, as only the little proportion of microalgae near the reactor's incident surface are photoinhibited. This explains why photoinhibition is not always observed in high density cultures. However, photoinhibition induces a hidden loss that must be considered and, if possible, avoided.

With a variant of this model, where photoadaptation was assumed to be at equilibrium, we proceeded to an optimization of biomass surface productivity at equilibrium (chapter 3.1). We showed that a key parameter is surface biomass X: the photobioreactor acts like a solar panel where surface biomass enables to gather light energy, but causes energy losses by respiration. An optimal surface biomass is derived, as well as an optimal nitrogen/carbon quota. The result is counter-intuitive, as it states that depending on the microalgal species parameters, it might be optimal to grow microalgae in nutrient limited conditions. Indeed, for a fixed high biomass, higher nitrogen/carbon ratio correspond to higher chlorophyll concentration and thus strong light attenuation, causing lower growth rate.

Productivity is the result of many biological and physical interacting phenomena, the most important of which are represented in the DPM model. That is why the productivity is a complex combination of several model parameters. This results enables to compare microalgal species productivity, which can be computed directly from their parameters.

As microalgae must be grown into natural light for biofuel production (for high value products they are sometimes grown under artificial light), they encounter day-night light variations. In the case of nutrient profusion (chapter 3.2), we show that several optimal control scenarii must be applied for optimizing volumetric productivity, depending on the microalgal species parameters: bang-bang, bang-singular-bang control, or constant maximal dilution if the microalgal growth rate is very high.

Finally we gave some key results for competition study and control. The analysis of mixed competition between several Monod, Droop and Contois species (section 4.1) introduces a new paradigm for competition, where both competitive exclusion or coexistence can happen, depending on both species parameters and controls. Thus in this paradigm, neither competitive exclusion nor coexistence are the rule; one or the other can happen, depending on the species and environmental conditions. More precisely, in some cases the most competitive Monod or Droop species wins the competition alone. In other cases one or several Contois species are able to coexist with or without the best Monod or Droop competitor. The pessimization principle of Adaptive dynamics, based on the competitive exclusion principle, is contradicted by this result: instead of leaving the environment with the worst (lowest) possible substrate concentration, we see that some Contois-species could live in worse environments, but if there is more substrate than the minimal concentration they need, then some other species can coexist. This is due to the fact that higher input substrate concentration induces higher equilibrium biomass, and thus higher equilibrium substrate concentration needed to have growth rate $\beta(s, x)$ equal to the dilution rate D.

Then (section 4.2) we demonstrate rigorously that in the periodic turbidostat, the species with highest mean growth rate wins the competition. This gives us the possibility to control competition in order to select species with diverse characteristics. In particular, we prove that in the classical turbidostat (nutrient replete conditions), the species with highest maximum growth rate is selected. In the pulsed turbidostat we show that the selected species maximizes a criterion which is a trade-off between high maximum growth rate (μ^m), and high potential increase of its internal substrate storage (Q^m/Q^0). These applications had already been validated in three previous distinct experiments concerning different types of microorganisms (zooplankton [4], yeast [18], and microalgae [20]).

We extended this methodology to the more complex anaerobic ecosystem during its start-up phase (chapter 4.3), in order to favour an efficient biofilm which would maximize the wastewater treatment rate. This should also increase the methane production rate.

This work is a whole that can be continued in each of these three directions: modelling, optimization, competition study and control.

The DPM and lipid synthesis models must be confronted with experiments, in order to be validated or improved. In particular, the simulated result that photoinhibition is not perceptible but present in high density cultures should be validated by a devoted experiment.

The optimization result, that for some microalgal population parameters, nitrogen limited cultures could have higher biomass productivities than nitrogen replete ones, should also be explored experimentally. Many optimization research remains to be done under day-night cycles with non-nitrogen replete culture, as well as for lipids production maximization. Some factors, like temperature or pH, could also be added to the DPM model in order to explore their effect on productivity. Much work and experiments remain to be done in this direction.

For competition theory, it would be interesting to validate the mixed competition result, by doing an experiment with Monod/Droop species and Contois species and verifying if the diverse competitive exclusion and coexistence outcomes can be produced and precisely controlled.

Then, the proposed selection procedures in microalgal and methanogenic bacteria ecosystems should be tested both on the short term (validation of the predicted outcome of competition), and on the long run: to see if species / biofilms with improved characteristics can be selected with these methods. Such results would gives some hope for alternative techniques to GMO organisms, in order to improve ecosystem's efficiency. This method could also be used to identify species which grow in hostile conditions, to amplify and verify the presence of a species in a medium, or to determine conditions which permit a species to be resistant to invaders. The selection criterion, which is the maximum mean growth rate in chosen environmental conditions, seems very promising and can take different forms depending on the imposed environmental conditions: this work could be extended by using other controls such as an inhibitor's concentration, or light in the case of microalgae. This would lead to new selection criteria.

We stress again that many factors should be taken into account for choosing a microalgal species that maximizes surface productivity: microalgal resistance to temperature shifts or to predation, and the various effects of the local environment affecting growth of a specific microalgal species. For this purpose, models including additional factors, like temperature or pH, must be developed and explored analytically. The steps of modelling, optimization and competition prediction and control must then be revisited with these new factors. We hope to have participated in creating solid bases for the undertaking of such a long term task.

Both the competition prediction and controls works presented here show the beauty of mathematics. We have highlighted the ability of mathematical modelling for giving ecological insight in a very general sense: the same equations and methodologies enable to successfully describe different ecosystems, from microalgae to bacteria and yeast.

Conclusion

Les écosystèmes microbiens jouent un rôle clé dans notre biosphère: ils contribuent significativement à intégrer l'énergie lumineuse du soleil au cycle de la vie, et à recycler les éléments nutritifs. Ils devraient donc être mieux compris, à la fois pour une meilleure appréhension des écosystèmes naturels, mais également pour le développement de biotechnologies propres. Les implications des écosystèmes étudiés dans cette thèse sont multiples:

- les écosystèmes de microalgues et de digestion anaérobie jouent un rôle important dans le réchauffement climatique, car les premiers consomment du CO_2 et les seconds produisent du CH_4. Ainsi, les modèles doivent quantifier les flux de carbone et d'énergie;
- certaines microalgues, comme la spiruline, peuvent être consommées et sont potentiellement de grandes sources de protéines, vitamines et minéraux [42];
- certaines microalgues produisent des composés chimiques utilisés dans des produits pharmaceutiques et nutraceutique [38];
- d'autres produisent de l'huile qui peut être utilisée comme biocarburant, et des productivités élevées semblent possibles [8];
- les bactéries anaérobies peuvent nettoyer les eaux usées, et dégrader des substrats faiblement biodégradables,
- les bactéries méthanogènes produisent du méthane qui est un biocarburant renouvelable.

Notre premier pas pour mieux appréhender ces écosystèmes a été de développer des modèles de population de microalgues en photobioréacteur (chapitre 2.1), le modèle "DPM" (Droop Photobioreactor Model). Le modèle devait inclure les ingrédients clés permettant de reproduire les comportements principaux du procédé, mais devait aussi être assez simple pour être validable, identifiable, et mathématiquement analysable. Notre modèle représente l'absorption et le stockage des nutriments. Il s'agit d'une question clé pour la production de biocarburants, puisque la synthèse de lipides est influencée par la disponibilité en azote dans le milieu (voir la construction du modèle de synthèse des lipides au chapitre 2.2). Il représente également l'atténuation de la lumière et l'influence de la respiration qui sont essentiels lorsque la concentration de la biomasse est élevée, ce qui est souvent le cas dans les bioprocédés réels. Les derniers ingrédients sont la photoinhibition (les fortes intensités lumineuses inhibent la

croissance) et la photoacclimation (variations du rapport Chl / C en fonction de la lumière reçue), qui sont importants quand la lumière ou la biomasse varient dans le photobioréacteur. Tout en représentant tous ces phénomènes, le modèle reste relativement simple, basé sur seulement quatre équations dynamiques représentant l'évolution de l'azote dans le milieu, de la biomasse, du quota d'azote interne, et de la chlorophylle.

Une procédure de calibration des paramètres est proposée et utilisée pour valider le modèle sur un ensemble de données. Les résultats des analyses démontrent que les cultures à haute densité, lorsqu'elles sont soumises à la photoinhibition sous une forte lumière, ne montrent pas de photoinhibition apparente, puisque seule la petite proportion de microalgues proches de la surface d'incidence du réacteur sont photoinhibées. Cela explique pourquoi la photoinhibition n'est pas toujours observée dans les cultures à haute densité. Toutefois, la photoinhibition induit une perte cachée qui doit être examinée et, si possible, évitée.

À partir de données expérimentales obtenues au LOV, nous avons ensuite construit un modèle qui reproduit fidèlement les évolutions des taux de lipides et de sucres (chapitre 2.2).

Avec une variante de notre modèle DPM, où la photoadaptation était à l'équilibre, nous avons procédé à une optimisation de la productivité surfacique de la biomasse à l'équilibre (chapitre 3.1). Nous avons montré qu'un paramètre clé est la biomasse surfacique X : le photobioréacteur agit comme un panneau solaire où la biomasse permet d'exploiter l'énergie lumineuse mais provoque des pertes d'énergie par respiration. Une biomasse surfacique et un quota interne azote/carbone optimaux sont calculés. Le résultat est contre-intuitif, car il indique que, selon les paramètres de l'espèce de microalgues considérée, il pourrait être optimal de faire pousser les microalgues dans des conditions limitées en azote. En effet, pour une biomasse fixée élevée, un fort rapport azote/carbone correspond à une forte concentration en chlorophylle et donc une plus forte atténuation de la lumière, provoquant un taux de croissance plus faible.

La productivité est le résultat de nombreux phénomènes biologiques et physiques qui interagissent, et dont les plus importants sont représentés dans le modèle DPM. C'est pourquoi la productivité est une combinaison complexe de plusieurs paramètres du modèle. On peut donc comparer la productivité de différentes espèces de microalgues, en la calculant directement à partir de leurs paramètres.

Comme les microalgues doivent être cultivées sous lumière naturelle pour la production de biocarburants (les microalgues qui synthétisent des composants à haute valeur ajoutée sont parfois cultivées sous lumière artificielle), elles subissent les variations jour-nuit de la lumière. Dans le cas d'une profusion en éléments nutritifs (chapitre 3.2), nous montrons que plusieurs scénarios de contrôle optimal peuvent être appliqué pour optimiser la productivité volumétrique, selon les paramètres de l'espèce de microalgues considérée : bang - bang, bang - arc singulier - bang, ou taux de dilution maximal si le taux de croissance des microalgues est très élevé.

Enfin, nous avons donné quelques résultats clés pour l'étude et le contrôle de la compétition. L'analyse de la compétition mixte entre plusieurs espèces représentées par les modèles de Monod, Droop et Contois (section 4.1) introduit

un nouveau paradigme de la compétition, où exclusion compétitive et coexistence peuvent tous deux survenir, en fonction des paramètres des espèces et des contrôles utilisés. Ainsi, dans ce paradigme, ni l'exclusion compétitive ni la coexistence ne sont la règle; l'un ou l'autre peut se produire, selon les espèces en compétition et les conditions environnementales. Plus précisément, dans certains cas, la plus compétitive des espèces de Monod et de Droop remporte seule la compétition. Dans d'autres cas une ou plusieurs espèces de Contois sont capables de coexister avec ou sans le meilleur des concurrents de Monod et Droop. Le "Pessimization principle" de la Dynamique Adaptative, basé sur le principe de l'exclusion compétitive, est contredit par ce résultat : au lieu de laisser l'environnement avec la pire (la plus basse) concentration du substrat possible, nous voyons que certaines espèces de Contois pourraient vivre dans de pires environnements, mais s'il y a plus de substrat que la concentration minimale dont ils ont besoin, alors d'autres espèces peuvent coexister. Cela est dû au fait qu'une concentration plus élevée de substrat en entrée provoque une biomasse à l'équilibre plus élevée, et donc une concentration plus élevée de substrat à l'équilibre pour avoir un taux de croissance $\beta(s, x)$ égal au taux de dilution D.

Ensuite (section 4.2) nous avons démontré de façon rigoureuse que dans un turbidostat périodique, l'espèce avec le taux de croissance moyen le plus élevé gagne la compétition. Cela nous donne la possibilité de contrôler la compétition afin de sélectionner des espèces présentant diverses caractéristiques. En particulier, nous avons montré que dans le turbidostat classique (profusion d'éléments nutritifs), l'espèce avec le taux de croissance maximal le plus élevé est sélectionnée. Dans le turbidostat pulsé nous avons montré que l'espèce sélectionnée maximise un critère qui est un compromis entre un taux de croissance maximal élevé (μ^m), et une forte augmentation potentielle de son stock interne de nutriment (Q^m/Q^0). Ces applications avaient déjà été validées dans trois expériences distinctes précédentes portant sur différents types de micro-organismes (zooplancton [4], levure [18], et les microalgues [20]).

Nous avons étendu cette méthodologie à l'écosystème plus complexe de la digestion anaérobie au cours de sa phase de démarrage (chapitre 4.3), afin de favoriser un biofilm efficace qui permettrait de maximiser la vitesse de traitement des eaux usées. Cela devrait également augmenter le taux de production de méthane.

Ce travail est un tout qui peut être poursuivi dans chacune de ces trois directions : modélisation, optimisation, étude et contrôle de la compétition.

Les modèles DPM et de synthèse de lipides doivent être confrontés à d'avantage d'expériences, afin d'être validés ou améliorés. En particulier, le résultat simulé que la photoinhibition n'est pas perceptible, mais présente dans les cultures à haute densité, devrait être validé par une expérience dédiée.

Le résultat d'optimisation, stipulant que pour certains paramètres de la population de microalgues, des cultures limitées en azote pourraient avoir des productivités de biomasse supérieures à celles qui ne sont pas limitées, devrait également être étudié expérimentalement. Beaucoup reste à faire pour l'optimisation en cycles jour-nuit avec des cultures non limitées en azote, ainsi que pour la maximisation de la production de lipides. Certains facteurs, comme la température ou le pH, peuvent également être ajoutés au modèle DPM afin d'explorer leurs effets sur la productivité. Beaucoup de travail et d'expériences restent à faire

dans cette direction.

Pour la théorie de la compétition, il serait intéressant de valider le résultat de la compétition mixte, en faisant une expérience avec des espèces représentées par les modèles de Monod, de Droop, et de Contois, et de vérifier si exclusion compétitive et coexistence peuvent tous deux être obtenus et contrôlés avec précision.

Ensuite, les procédures de sélection proposées pour les écosystèmes de microalgues, et de bactéries méthanogènes, devraient être testées à la fois sur le court terme (validation de la prédiction du résultat de la compétition), et sur le long terme : pour voir si des populations aux caractéristiques améliorées peuvent être sélectionnés avec ces méthodes. De tels résultats donnent un espoir pour améliorer l'efficacité de ces écosystèmes sans avoir recours aux OGM. Cette méthode pourrait également être utilisée pour identifier les espèces qui poussent dans des conditions hostiles, pour amplifier et vérifier la présence d'une espèce dans un milieu, ou pour déterminer les conditions qui permettent à une espèce de résister aux envahisseurs. Le critère de sélection, qui est le taux de croissance moyen maximal dans des conditions environnementales données, semble très prometteur et peut prendre différentes formes selon les conditions imposées à l'environnement : ce travail pourrait être étendu à l'aide d'autres contrôles tels que la concentration d'un inhibiteur, ou la lumière dans le cas de microalgues. Cela conduirait à de nouveaux critères de sélection.

Nous soulignons à nouveau que de nombreux facteurs doivent être pris en compte pour le choix d'espèces de microalgues qui maximisent la productivité surfacique : la résistance des microalgues aux variations de température ou à la prédation, et les divers effets de l'environnement local qui affectent la croissance d'une espèce particulière de microalgues. Dans ce but, des modèles incluant d'autres facteurs, comme la température ou le pH, doivent être développés et étudiés analytiquement. Les étapes de modélisation, d'optimisation et de prédiction et contrôle de la compétition devront alors être revisitées avec ces nouveaux facteurs. Nous espérons avoir participé à la création de bases solides pour la réalisation de cette longue tâche.

Les résultats sur la prédiction de l'issue de la compétition et son contrôle montrent la beauté des mathématiques. Nous avons mis en évidence la capacité de la modélisation mathématique à développer la compréhension écologique dans un sens très général : les mêmes équations et méthodes permettent de décrire avec succès des écosystèmes différents, des microalgues jusqu'aux bactéries et aux levures.

Bibliography

[1] R. Armstrong & R. McGehee – "Competitive exclusion", *American Naturalist* **115** (1980), p. 151.

[2] J. E. Bailey & D. F. Ollis – *Biochemical engineering fundamentals*, McGraw-Hill, 1986.

[3] J. Benemann – "Co2 mitigation with microalgae systems", *Energy Conversion and Management* (1997), p. 475–479.

[4] W. Bennett & M. Boraas – "Isolation of a fast-growing strain of the rotifer brachionus calyciflorus pallas using turbidostat culture", *Aquaculture(Amsterdam)* **73** (1988), no. 1-4, p. 27–36.

[5] B. C. Benson & K. A. Rusch – "Investigation of the light dynamics and their impact on algal growth rate in a hydraulically integrated serial turbidostat algal reactor (histar)", *Aquacultural engineering* **35** (2006), p. 122–134.

[6] O. Bernard, Z. Hadj-Sadok, D. Dochain, A. Genovesi & J.-P. Steyer – "Dynamical model development and parameter identification for an anaerobic wastewater treatment process", *Biotech.Bioeng.* (2001), no. 75, p. 424–438.

[7] J.-P. Cadoret & O. Bernard – "La production de biocarburants lipidique avec des microalgues: promesses et défis", *Journal de la socété de biologie* **202** (2008), p. 201–211.

[8] Y. Chisti – "Biodiesel from microalgae", *Biotechnology Advances* **25** (2007), p. 294–306.

[9] D. Contois – "Kinetics of bacterial growth: relationship between population density and specific growth rate of continuous cultures.", *J Gen Microbiol.* (1959), p. 40–50.

[10] C. Darwin – *On the origin of species by means of natural selection, or the preservation of favoured races in the struggle for life*, John Murray, 1859.

[11] C. Delbès, R. Moletta & J.-J. Godon – "Bacterial and archaeal 16s rdna and 16s rrna dynamics during an acetate crisis in an anaerobic digestor ecosystem", *FEMS Microbiology Ecology* **35** (2001), p. 19–26.

[12] O. Diekmann – "A beginner's guide to adaptive dynamics", *Banach Center Publ.* (2003), p. 47–86.

[13] M. Droop – "Vitamin b_{12} and marine ecology", *J. Mar. Biol Assoc. U.K.* **48** (1968), p. 689–733.

[14] D. Dykhuizen & D. Hartl – "Selection in chemostats.", *Microbiological reviews. Baltimore* **47** (1983), no. 2, p. 150–168.

[15] B. Ewing, S. Goldfinger, A. Oursler, A. Reed, D. Moore & M.Wackernagel. – *The ecological footprint atlas 2009.*, 2009.

[16] P. G. Falkowski & J. A. Raven – *Aquatic photosynthesis*, Blackwell Science, 2007.

[17] G. Gause – *The struggle for existence*, Williams and Wilkins, Baltimore, 1934.

[18] P. Groeneveld, A. Stouthamer & H. Westerhoff – "Super life - how and why 'cell selection' leads to the fastest-growing eukaryote", *FEBS Journal* **276** (2008), p. 254–270.

[19] F. Grognard, F. Mazenc & A. Rapaport – "Polytopic lyapunov functions for persistence analysis of competing species", *Discrete and Continuous Dynamical Systems-Series B* **8** (2007), no. 1, p. 73–93.

[20] J. Grover – "Dynamics of competition among microalgae in variable environments: experiment tests of alternative models", *Oikos* **62** (1991), p. 231–243.

[21] B. Haegeman, C. Lobry & J. Harmand – "Modeling bacteria flocculation as density-dependent growth", *AICHE JOURNAL* **53** (2007), no. 2, p. 535–539 (English).

[22] S. Hansen & S. Hubell – "Single-nutrient microbial competition: qualitative agreement between experimental and theoretically forecast outcomes", *Science* **207** (1980), no. 4438, p. 1491–1493.

[23] G. Hardin – "The competitive exclusion principle", *Science* **131** (1960), no. 3409, p. 1292–1297.

[24] G. P. Harris – *Phytoplankton ecology*, Chapman and hall, 1986.

[25] S. Hsu & T. Hsu – "Competitive exclusion of microbial species for a single-nutrient with internal storage", *SIAM Journal on Applied Mathematics* **68** (2008), no. 6, p. 1600–1617.

[26] M. Huntley & D. Redalje – "Co2 mitigation et renewable oil from photosynthetic microbes: A new appraisal", *Mitigation et Adaptation Strategies for Global Change* **12** (2007), p. 573 – 608.

[27] G. E. Hutchinson – "The paradox of the plankton", *The American Naturalist* **95** (1961), p. 137.

[28] A. Jacquard – *Le compte à rebours a-t-il commencé ?*, Stock, 2009.

[29] C. Jessup, S. Forde & B. Bohannan – "Microbial experimental systems in ecology", *Advances in Ecological Research* **37** (2005), p. 273–306.

[30] T. Lacour – "Influence du statut azoté et du cycle lumineux diurne sur le métabolisme lipidique d'isochrysis sp. (haptophyceae).", Thèse, Université de la méditerranée (Aix-Marseille 2), 2010.

[31] C. Lobry & J. Harmand – "A new hypothesis to explain the coexistence of n species in the presence of a single resource", *Comptes Rendus Biologies* **329** (2006), no. 1, p. 40–46.

[32] C. Lobry, F. Mazenc & A. Rapaport – "Persistence in ecological models of competition for a single resource", *Comptes Rendus Mathematique* **340** (2005), no. 3, p. 199–204.

[33] F. Mairet, O. Bernard, P. Masci, T. Lacour & A. Sciandra – "Modelling lipid prduction in microalgae", in *Proceedings of the CAB conference*, 2010.

[34] M. G. Malea, F. Ancíen, M. C. J.M. Fernández & E. Molina – "Continuous production of green cells of *haematococcus pluvialis*: Modeling of the irradiance effect", *Enzyme and microbial technology* **38** (2006), p. 981–989.

[35] F. Mazenc & Z.-P. Jiang – "Persistence and time-varying nonlinear controllers for a chemostat with many species", *Dynamics of Continuous, Discrete and Impulsive Systems* (2010), p. to appear.

[36] J. Monod – "Recherches sur la croissance des cultures bacteriennes", *Paris: Herrmann et Cie* (1942).

[37] Y. Percival Zhang, M. Himmel & J. Mielenz – "Outlook for cellulase improvement: Screening and selection strategies", *Biotechnology Advances* **24** (2006), no. 5, p. 452–481.

[38] O. Pulz – "Photobioreactors: production systems for phototrophic microorganisms", *Applied Microbiology et Biotechnology* **57** (2001), p. 287–293.

[39] O. N. Ross & R. J. Geider – "New cell-based model of photosynthesis and photo-acclimatation: accummulation and mobilisation of energy reserves in phytoplankton", *Marine ecology progress series* **383** (2009), p. 53–71.

[40] F. C. Rubio, F. G. Camacho, J. F. Sevilla, Y. Chisti & E. M. Grima – "A mechanistic model of photosynthesis in microalgae", *Biotechnology and Bioengineering* **81** (2003), no. 4, p. 459–473.

[41] H. Smith & P. Waltman – *The theory of the chemostat. dynamics of microbial competition*, Cambridge Studies in Mathematical Biology. Cambridge University Press, 1995.

[42] P. Spolaore, C. Joannis-Cassan, E. Duran & A. Isambert – "Commercial applications of microalgae", *Journal of Bioscience and Bioengineering* **101** (2006), no. 2, p. 87 – 96.

[43] D. Tilman – "Resource competition between plankton algae: An experimental and theoretical approach.", *Ecology* **58** (1977), no. 22, p. 338–348.

[44] D. Tilman & R. Sterner – "Invasions of equilibria: tests of resource competition using two species of algae", *Oecologia* **61** (1984), no. 2, p. 197–200.

[45] M. Wackernagel & W. Rees – "Perceptual and structural barriers to investing in natural capital: Economics from an ecological footprint perspective", *Ecol. Econom.* **20** (1997), no. 1, p. 3–24.

[46] J. B. Wilson – "Mechanisms of species coexistence: twelve explanations for the hutchinson's 'paradox of the phytoplankton': evidence from new zealand plant communities", *New Zealand journal of Ecology* **17–42** (1990), p. 137.

[47] O. Zelder & B. Hauer – "Environmentally directed mutations and their impact on industrial biotransformation and fermentation processes", *Current Opinion in Microbiology* **3** (2000), p. 248–251.

List of publications

Olivier Bernard, Pierre Masci, Francis Mairet and Antoine Sciandra, *A photobioreactor model in nitrogen limited conditions*, submitted to Biotechnology & Bioengineering

Pierre Masci, Frédéric Grognard, Eric Benoît, Olivier Bernard, *Competition between diverse types of microorganisms : exclusion and coexistence*, submitted to Mathematical Biosciences and Engineering

Pierre Masci and Olivier Bernard and Frédéric Grognard, *Continuous Selection of the Fastest Growing Species in the Chemostat*, 2008, Proceedings of the IFAC conference (p. 9707-9712)

Olivier Bernard and Pierre Masci and Antoine Sciandra, *A photobioreactor model in nitrogen limited conditions*, 2009, Proceedings of the Mathmod 09 conference

P. Masci and O. Bernard and F. Grognard and E. Latrille and J.-B. Sorba and J.P. Steyer, *Driving competition in a complex ecosystem : application to anaerobic digestion*, 2009, Proceedings of the ECC conference

F. Mairet, O. Bernard, P. Masci, T. Lacour, A. Sciandra, *Modelling lipid production in microalgae*, 2010, Proceedings of the CAB conference

Pierre Masci, Olivier Bernard, Frédéric Grognard, *Microalgal biomass surface productivity optimization based on a photobioreactor model*, 2010, Proceedings of the CAB conference

Frédéric Grognard, Andrei Akhmetzhanov, Pierre Masci and Olivier Bernard, *Optimization of a photobioreactor biomass production using natural light*, 2010, CDC10 conference

Confidential deliverables for the ANR-06-BIOE-014 Shamash project

Pierre Masci, Olivier Bernard, Frédéric Grognard, Bruno Sialve, *Etude théorique des conditions de croissance permettant la sélection continue d'espèces maximisant la production d'huiles*, 2008

Pierre Masci, Olivier Bernard, Frédéric Grognard, *Development of dynamical models to predict lipid production and accumulation in microalgal cultures*, 2008

Olivier Bernard, Pierre Masci, Frédéric Grognard, Francis Mairet, *Premier rapport sur les stratégies théoriques de limitation et de stress maximisant la productivité lipidique*, 2008

Olivier Bernard, Pierre Masci, Frédéric Grognard, Francis Mairet, *Second report on stress or limitation strategies to maximize oil surface productivity*, 2009

Résumé

Des biocarburants alternatifs, utilisant des écosystèmes microbiens, sont actuellement étudiés dans le but de limiter la consommation non raisonnée de ressources énergétiques et le rejet de gaz à effet de serre, qui modifient le climat. Dans cette thèse, nous avons considéré des bioréacteurs à base de microalgues oléagineuses, et des écosystèmes bactériens anaérobies qui décomposent des déchets et produisent du méthane. Ces travaux avaient pour objectif de mieux comprendre ces procédés et d'en améliorer les performances. Nous avons tout d'abord modélisé et étudié des cultures de microalgues en photobioréacteurs, dans lesquels les pigments algaux induisent une forte atténuation lumineuse. Pour les écosystèmes bactériens, nous avons utilisé un modèle précédemment développé. A l'aide de ces modèles et de leur analyse mathématique rigoureuse, nous avons proposé des stratégies pour optimiser leur productivité. Ensuite, l'étude de la sélection naturelle entre plusieurs espèces de microorganismes dans ces deux écosystèmes a permis de prédire quelles espèces remportent la compétition. Et finalement nous avons montré comment il est possible, dans chaque écosystème, de contrôler la compétition pour diriger la sélection naturelle, de façon à avantager des espèces ayant des caractéristiques permettant une performance accrue.

Abstract

Some alternative biofuels, produced by microbial ecosystems, are presently studied with the aim of limiting the unreasoned resource consumption of energetic resources, and greenhouse gases emissions which modify the climate. In this thesis we have considered bioreactors based on oleaginous microalgae, and on anaerobic bacterial ecosystems which degrade wastes and produce methane. The aims of these works were to better understand these processes and to improve their performances. First we have developed and studied models of microalgal cultures in photobioreactors, in which algal pigments cause strong light attenuation. For anaerobic digestion we have used an existing model. By rigorous mathematical analysis of these models, we propose strategies for optimizing their productivity. Then the study of natural selection between several microbial species, in these two ecosystems, leads to the prediction of the species which wins the competition. And finally we showed how it is possible in each ecosystem to control competition and drive natural selection, in order to advantage species with efficient characteristics, inducing better performances.